Novel DOTA-α-melanocyte-stimulating hormone analogs for melanoma targeting: the impact of dimerization, carbohydration and negative charges on the in vivo biodistribution

Inauguraldissertation

zur
Erlangung der Würde eines Doktors der Philosophie
vorgelegt der
Philosophisch-Naturwissenschaftlichen Fakultät
der Universität Basel

von

Jean-Philippe Bapst
aus La Roche (FR) und Pont-la-Ville (FR), Schweiz

Basel, 2008

Genehmigt von der Philosophisch-Naturwissenschaftlichen Fakultät

auf Antrag von

Prof. Dr. Alex N. Eberle

Prof. Dr. P. August Schubiger

Prof. Dr. med. Peter Itin

Prof. Dr. Hans-Peter Hauri
Dekan

Basel, 24.06.2008

"La clef de toutes les sciences est sans contredit le point d'interrogation ;

nous devons la plupart des grandes découvertes au comment ?

Et la sagesse dans la vie consiste peut-être à se demander,

à tout propos, pourquoi ?"

Honoré de Balzac

To my family...

Table of contents

Abbreviations

AcOH	Acetic acid	GABA	γ-aminobutyric acid
ACTH	Adrenocorticotropic hormone	Gal	Galactose
ADH	Antidiuretic hormone	GDP	Guanosine diphosphate
AGE	Advance glycation end product	GF	Growth factor
AGRP	Agouti-related protein	Glc	Glucose
All	Allyl	GPCR	G protein-coupled receptor
ASIP	Agouti signaling protein	GTP	Guanosine triphosphate
ATP	Adenosine triphosphate	GVHD	Graft-versus-host disease
AUC	Area under the curve	HATU	2-(7-Aza-1H-benzotriazole-1-yl)-1,1,3,3-tetramethyluronium hexafluorophosphate
BSA	Bovine serum albumin		
*t*Bu	*t*-Butyl	HOAt	1-Hydroxy-7-Azabenzotriazole
cAMP	Cyclic 3',5'-adenosine monophosphate	HOBt	1-Hydroxybenzotriazol
CNS	Central nervous system	HPLC	High performance liquid chromatography
COSY	Correlation spectroscopy	HSQC	Heteronuclear single quantum coherence
CPTA	4-(1,4,8,11-tetraazacyclotetradec-1-yl)-methyl benzoic acid tetrahydrochloride	HSV	Herpes simplex virus
		HuMAb	Humanized monoclonal antibodies
CRH	Corticotropin releasing hormone	HUVEC	Human umbilical vein endothelial cells
CTLA	Cytotoxic T lymphocyte-associated protein	IC_{50}	half maximal inhibitory concentration of a substance
DCC	Dicyclohexylcarbodiimide		
DCM	Dichloromethane	ICAM	Intercellular adhesion molecule
DHI	Dihydroxyindole	IFN	Interferon
DHICA	5,6-dihydroxyindole-2-carboxylic acid	IL	Interleukin
DIPEA	*N,N*-Diisopropylethylamine	IP	Inositol phosphate
DMF	*N,N*-Dimethylformamide	iv	Intravenous
DOPA	Dihydroxyphenylalanine	LD_{50}	Median lethal dose
DOTA	1,4,7,10-tetraazacyclododecane-1,4,7,10-tetraacetic acid	LH	Luteinizing hormone
		LPH	Lipotropic hormone
DTPA	Diethylenetriaminepentaacetic acid	MC1R	Melanocortin type 1 receptor
DTT	Dithiothreitol	MEM	Modified Eagle's medium
EC_{50}	Effective concentration producing a 50% response	MBM	Mouse binding medium
		MeOH	Methanol
ECM	Extracellular matrix	MMP	Matrix metalloproteinase
EDTA	Ethylenediaminetetraacetic acid	MS	Mass spectrometry
EP	Endorphin	MSH	Melanocyte-stimulating hormone
FDA	American Food and Drug Administration	Mtr	Maltotriose
FDG	Fluorodeoxyglucose	NAT	*N*-acetyltransferase
Fmoc	Fluorenylmethyloxycarbonyl	Nle	Norleucine
FSH	Follicle-stimulating hormone		

NMR	Nuclear magnetic resonance
NO	Nitric oxide
NOTA	1,4,7-triazacyclononane-1,4,7-triacetic acid
NPY	Neuropeptide Y
PBS	Phosphate-buffered saline
PEG	Polyethylene glycol
PET	Positron emission tomography
PIP	Phosphatidylinositol phosphate
PK	Protein kinase
PNS	Peripheral nervous system
POMC	Pro-opiomelanocortin
RER	Rough endoplasmic reticulum
RGD	Arginyl-glycyl-aspartic acid
ROS	Reactive oxygen species
RP	Reversed-phase
SAR	Structure-activity relationship
sc	Subcutaneous
SEM	Standard error of the mean
SPECT	Single photon emission computed tomography
TBTU	O-(Benzotriazol-1-yl)-N,N,N',N'-tetramethyl-uronium tetrafluoroborate
TETA	Triethylenetetraamine
TFA	Trifluoroacetic acid
TFE	Trifluoroethanol
TLC	Thin-layer chromatography
TM	Transmembrane domain
TMS	Trimethylsilane
TNF	Tumor necrosis factor
TRP	Tyrosinase-related protein
Trt	Trityl
TSH	Thyroid-stimulating hormone
UV	Ultraviolet
VEGF	Vascular endothelial growth factor
VIS	Visible light
VM	Vasculogenic mimicry

Abstract

Various epidemiological surveys have recently demonstrated that the incidence and mortality rates of cutaneous malignant melanoma are still increasing in western countries. Incidence rates have dramatically increased during the last 70 years, raising from 1:1,500 in 1935 to 1:68 in 2002. Although its morbidity rates in certain population groups have slightly declined lately, it remains the most common malignancy among young adults. Malignant melanoma represents 5% of all skin cancers, but 71% of all skin cancer deaths in Caucasian populations. Unless primary melanoma tumors are detected early enough and adequate surgery can be performed, the prognosis of the disease is very poor, particularly, because of its high metastasizing potential and the difficulty to detect and to treat either the primary or the secondary lesions.

Ionizing radiation is one of the major means to kill tumor cells in patients suffering from cancer. Specific targeting of radioisotopes to the surface of cancer cells, with the purpose of exposing them to *in situ* generated radiation, was initially studied with antibodies as vehicles. Radiopeptides for targeting began to interest radiochemists and nuclear oncologists later, when structural peptide analogues with excellent biostability and bioactivity became available; in addition, these analogues carried suitable chemical groups for incorporation of a variety of different isotopes. The idea, however, to apply radioactive peptides to receptor-mediated targeting of tumor cells dates back to the early 1970s, when peptide hormone receptors (i.e. binding sites) had been identified on cell membranes. Radiopeptides are attractive tools for cancer diagnosis and therapy because a variety of human tumors overexpress surface receptors for regulatory peptides or peptide hormones. The best examples illustrating the rationale of this strategy are radiolabeled somatostatin (SST) analogs, which are commercially available (OctreoScan® and OctreoTher®) and routinely used in clinics to image or even treat neuroendocrine tumors and tumors of the nervous system expressing SST receptors.

Melanocortin type 1 receptors (MC1R) are overexpressed at the surface of melanoma cells. The hormone α-MSH is the native ligand of MC1R, and α-MSH analogs bind with great affinity as well. Therefore, α-MSH derivatives with improved *in vivo* stability and behavior and bearing chelates able to incorporate various radionuclides have been developed. Nevertheless, the side-effects of nonspecific retention in the kidneys limits the therapeutic efficacy of most radiopeptides, as nephrotoxicity is the dose-limiting factor. Simultaneously, diagnosis of tumors localized in the renal region can be markedly compromised.

Elevated renal uptake and prolonged retention of radiolabeled antibody fragments and peptides in this and other organs represent a major issue for the therapeutic application of such agents. Over recent years, one of the focuses of research has therefore been to find new methods to reduce renal uptake. Several strategies have been investigated without sufficient success. Whether variations in the net charge of the peptide itself, use of chelator complexes other than DOTA, study of different isotopes, the position of the

chelator complexes in the peptide molecule or of various regulating elements within the peptide sequence such as, e.g., cyclization of the peptide, none of these approaches resulted in substantial satisfaction. Therefore, new strategies are needed to potentially solve the kidney uptake issue, or at least to improve the ratio between tumor uptake and kidney uptake of radioactivity.

Dimerization of peptides has been studied in the field of MSH derivatives since 1977, when several MSH molecules (up to 300) were attached to the tobacco mosaic virus (TMV), yielding a complex that displayed a 1,500-fold higher potency than α-MSH. Other dimeric α-MSH derivative synthesized later showed increased *in vitro* affinity. Finally, various dimeric ACTH derivatives displayed increased potencies compared to their monomeric equivalents. Thus, this approach was tempting to test new dimeric peptides derived from known efficient sequences, taking latest findings about peptide sequences and key structural elements into account. The idea was not to hit simultaneously two receptors, but to increase the concentration of the binding motif in the vicinity of the receptor in order to potentially improve tumor uptake of the peptides *in vivo*. Three dimeric peptides were successfully synthesized, labeled with ^{111}In and tested, and although they exhibited excellent receptor binding affinities in the subnanomolar range and good internalization properties, the *in vivo* data did not match the expectations. Indeed, no increase in tumor uptake could be observed, and the dimeric derivatives suffered from very high kidney uptake, making them unsuitable for diagnostic or therapeutic purposes.

A new type of ^{111}In-labeled α-MSH glycopeptide analogs was then investigated. Glycopeptides were initially introduced to improve drug delivery to target tissues, either by taking advantage of specific uptake mechanisms or by enhancing the bioavailability of peptides. Glycopeptides were shown to exhibit prolonged effects (glycosylated enkephalin peptides) due to better delivery to the target tissue, enhanced renal peptide uptake from blood (glycosylated Arg^8-vasopressin), an improved stability toward enzymatic degradation *in vivo*, or a better intestinal absorption, thus enhancing the bioavailability of the peptides. Other effects of glycation on peptide properties appeared later, including higher or lower accumulation in the proximal tubules of the renal cortex, depending on the coupled sugar. Structure-activity relationship studies could describe structural features to exploit or avoid in order to target the kidney. It was observed that the affinity of peptides for kidney membrane cells could be modulated by attaching different types of sugars to the molecules, and this led to systematic SAR studies confirming the observations. Other studies also mention that after carbohydration of somatostatin derivatives, a switch in the excretion way could be observed. It appeared that the glycopeptides tended to exhibit a switch from the hepato-biliary towards the renal excretion way, without affecting the uptake in targeted tissues.

This was the basis for the development of carbohydrated α-MSH derivatives in this thesis. Six glycated α-MSH derivatives, based on the sequence of DOTA-NAPamide (one of the peptides exhibiting the best pharmacokinetic profile to date) were synthesized and tested. Various carbohydrate moieties were coupled at different positions along the peptide sequence, in order to determine the influence of the type of sugar or its position on the *in vitro* and *in vivo properties* of α-MSH analogs. Competitive binding assays displayed results in accordance with the data obtained for the reference peptide, indicating that carbohydration does

not affect target receptor affinity. Biodistribution experiments with melanoma-bearing mice delivered interesting results. While C-terminal glycation enhanced kidney uptake and retention time, side-chain-glycation seemed only to increase kidney uptake. The N-terminal end, on the other hand, is apparently the best position for carbohydration. Indeed, two of the three peptides displayed promising results. Introduction of a galactose moiety was particularly favorable, as it delivered a better tumor-to-kidney ratio of the area under the curve (4-48h) than the reference peptide DOTA-NAPamide. Thus, carbohydration was shown to exhibit a high impact on the pharmacokinetics of α-MSH analogs. Some major tendencies on the biological characteristics after glycation could be drawn, and a new candidate with good potential as lead for further derivation could be developed.

Finally, novel analogs of negatively charged α-MSH were investigated in this work. It has been shown in the past that the surface of tubular cells is negatively charged and that anionic molecules are excreted more easily than cationic molecules, probably because of repulsive electrostatic effects. Therefore, derivatives carrying an overall negative charge were synthesized and tested. One of them bore two negatively-charged D-Asp and the chelate at its C-terminal end, in order to enhance the renal excretion of a potential metabolite. The peptide yielded poor results, both *in vitro* and *in vivo*. Affinity of the peptide for the receptor was lost. In another peptide, DOTA was coupled over a Gly-spacer to a phosphorylated Tyr located at the N-terminal end of the peptide. While the new derivative displayed average results *in vitro*, its *in vivo* data were excellent. Indeed, an even better tumor-to-kidney ratio of the area under the curve (4-48h) than DOTA-Gal-NAPamide was reached, delivering the best linear ^{111}In-labeled α-MSH analog to date.

Although this study encompasses only a limited panel of derivatives from each group of peptides investigated, some important trends for the development of further derivatives could be established. Complete sets of *in vitro* and *in vivo* data were collected for all the peptides, providing valuable information for the elucidation of structural features required to improve the pharmacokinetic behavior of peptides for targeting the MC1R. Two new lead candidates provided excellent data; they could be further optimized by combining features of both of them. Indeed, no linear ^{111}In-labeled α-MSH analog exhibited such interesting tumor-to-kidney ratios as DOTA-Gal-NAPamide and DOTA-phospho-MSH$_{2-9}$ to date.

1 Introduction

1.1 MSH and skin

The skin is the largest organ of the body, and its first line of defense against heat, sunlight, injury and infection through various pathogens. In addition to its ability to communicate internal physiological information, like the presence of fever, the skin also reacts to external stimuli, such as sun exposure, toxins, and even psychological stimuli. From poison indication and warning, to the "cold sweats" and "goosebumps", the skin is a constant and dynamic interface between the body and its environment. It also helps to regulate the temperature and the water and electrolyte contents of the body. Additionally, it helps to protect the underlying organs and muscles. Skin also contains various sensory organs or receptors and contributes to the synthesis of vitamins B and D. Finally, the skin is involved in breathing and gas exchange processes.
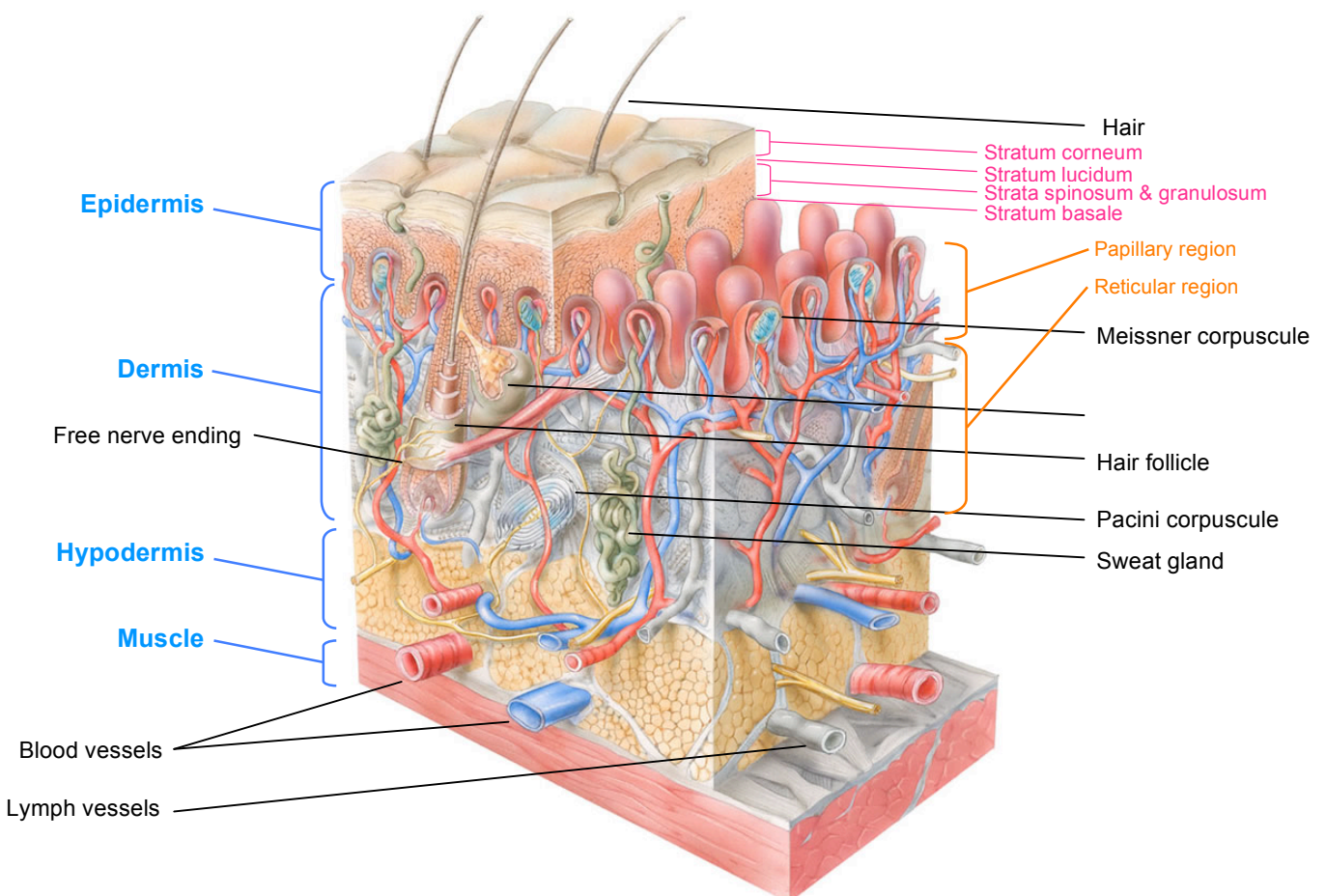
Figure 1: Anatomy of the skin (modified from H. Leonhardt, Histologie, Zytologie und Mikroanatomie des Menschen, Thieme Verlag 1990).

The skin has an average surface of about 1.5-2 m^2, and to the greater extent it is 2-3 mm thick. It consists of three main layers, subdivided into several others. These layers are differentiated by their respective amounts of hair follicles, pigmentation, cell formation, gland makeup, and blood supply. Moreover, these layers are present in the two general types of skin, thin and hairy, and thick and hairless. The former is more prevalent on the body, while the latter is found on parts of the body that are used heavily and experience extreme friction, like the palm and the heel. Underneath the dermis lies subcutaneous tissue, or hypodermis.

Figure 1 describes the anatomy of the skin, and its major components can be easily observed. The epidermis represents the outermost layer and is subdivided into 5 sublayers. Under the epidermis lies the dermis, which is divided into two regions. Finally, the hypodermis, which is not really part of the skin, but more an important component of the whole integumentary system, is responsible for the attachment of the skin to muscles and bones, and for the blood supply to the skin.

- Epidermis: - *stratum corneum*
                     - *stratum lucidum*
                     - *stratum granulosum*
                     - *stratum spinosum*
                     - *stratum basale*

- Dermis: - papillary dermis
                     - reticular dermis

- Hypodermis: - subcutaneous tissue

In the epidermis, our main region of interest, cells called keratinocytes are formed through mitosis in the innermost layer (*stratum basale*). They move up the various *strata* changing shape and composition as they go through the process of differentiation, fill themselves with keratin (from whence their name is derived), develop into cornocytes and die due to lack of blood supply. The epidermis contains no blood vessels, and only the lower cell layers are nourished by diffusion from blood capillaries reaching the upper layers of the dermis. Therefore, cells die as they differentiate and move up the *strata* towards the *stratum corneum*, consisting of dead cells that will detach in a process called desquamation. The whole process is called keratinization and takes place within weeks. The outermost sublayer of the epidermis, *stratum corneum*, consists of 25 to 30 layers of dead cells, and this keratinized layer is responsible for sparing body hydration and protection against harmful chemicals and pathogens.

Langerhans cells represent around 3 to 8% of the epidermal cells. They belong to the group of T-lymphocyte antigen-presenting dendritic cells, and are trans-epithelial. They are particularly scattered between the keratinocytes of the *stratum spinosum* of the epidermis. E-cadherin probably plays an important role in their adhesion to keratinocytes. Langerhans cells are known to initiate and spread immune

responses against antigens on the skin surface. Their role is to capture exo-antigens via endosomes, to process them and to re-express them on the surface with class II molecules of the MHC (major histocompatibility complex)[295]. After catching the antigen, activated Langerhans cells leave the epidermis and head for the satellite lymph nodes where they present antigenic determinants to T-lymphocytes.
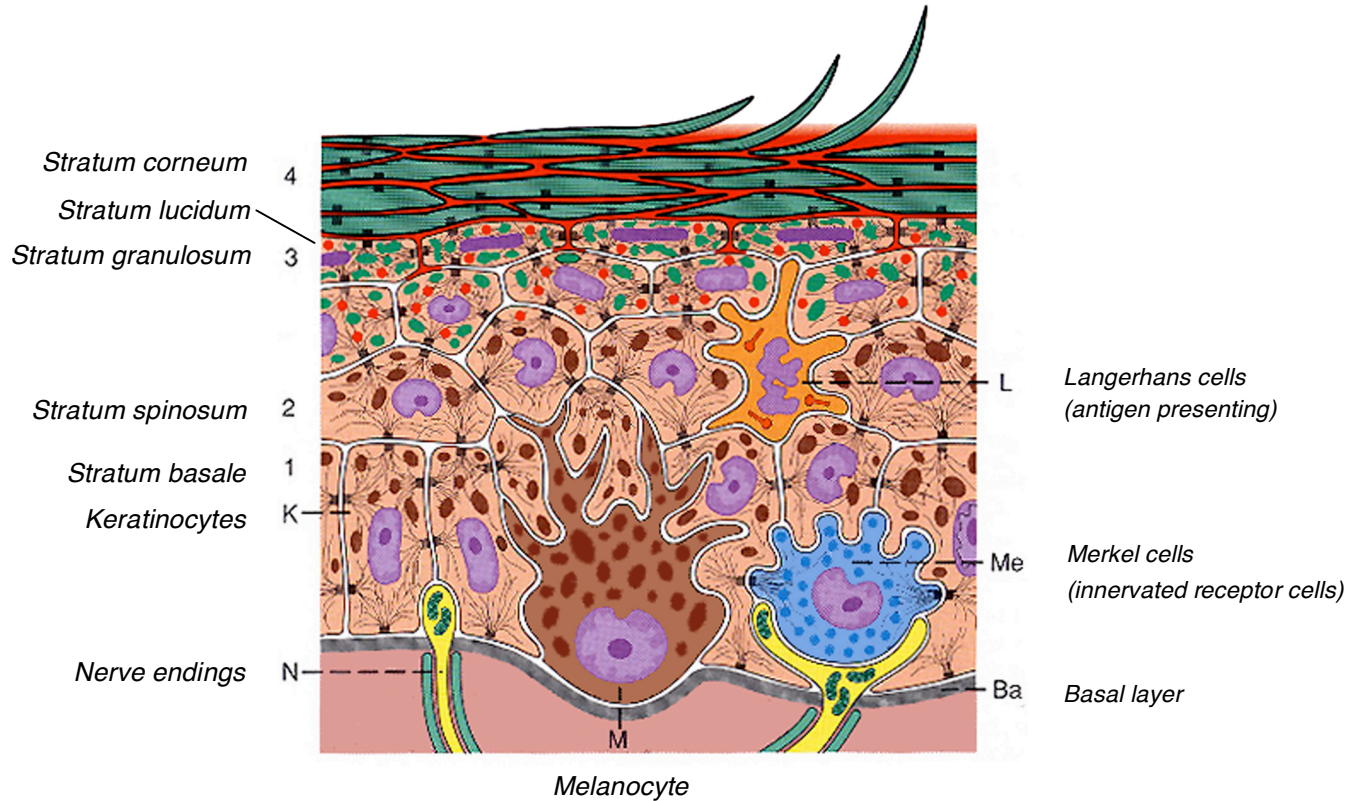
Figure 2: Detailed view of the epidermis (from Sobotta Lehrbuch Histologie, 2nd edition (2006), Urban & Fischer, München)

Melanocytes are the cells mainly responsible for skin pigmentation, and therefore will be of major interest in this work. There are typically between 1000 and 2500 melanocytes per square millimeter of skin. Although their size can vary, melanocytes typically measure 7 micrometers in length. Melanocytes can be found at many locations throughout the body. In the skin they are usually associated with the hair follicle, and in some mammals (including humans), they are found in the basal layer (*stratum basale*) of the interfollicular epidermis as well. Mature melanocytes form long dendritic processes that ramify around the neighboring keratinocytes. Each melanocyte typically makes contact with about 30 to 40 keratinocytes and forms the so-called epidermal melanin unit, described later in this work (**1.2.2**). Melanin is transferred from those melanocytes to the keratinocytes, where it contributes to the determination of skin color and helps protecting the skin against the damaging UV radiation[278].

α-Melanocyte-stimulating hormone (α-MSH) is the native ligand of melanocortin receptors type 1 (MC1R), which are located at the surface of melanocytes and induce signals triggering melanogenesis. α-MSH is

generated by post-translational enzymatic cleavage of the precursor molecule proopiomelanocortin (POMC), which occurs primarily in the pituitary gland (=hypophysis)[87], in both the anterior and the intermediate lobe. α-MSH itself is produced in the intermediate lobe, located between the adenohypophysis (anterior lobe) and the neurohypophysis (posterior lobe). Although it is mainly located in the hypophysis, POMC and production of POMC-derived peptides is not confined to this organ. It was shown in several studies that POMC-derived peptides could be detected in significant levels in various tissues, such as lymphocytes and monocytes, and more particularly in the skin (Langerhans cells)[36]. α-MSH was isolated from the skin of various species (including humans), and it was proven that this α-MSH could not be pituitary-derived. In the skin, it is usually produced by melanocytes, but was also shown to be produced by keratinocytes[269]. POMC expression could also be detected in the dermis *in vitro*. Human papilla cells (regulating hair follicle activity) also exhibited immunoreactivity for ACTH, α-MSH and β-endorphin, and expressed both the MC1R and the MC4R. Additionally, immunoreactivity for both receptors could be detected in human dermal papilla cells *in situ*. The data collected in this study suggest a regulatory role of α-MSH within the dermal papilla. Deregulation of the system may lead to abnormal immune and inflammatory responses of the hair follicle, and could have an implication in inflammatory forms of alopecia[41].

Other components of the skin comprise the so-called appendages. These are usually located in the dermis (see **Figure 1**). Sweat glands, for example, are distributed almost over the whole body at a density of approximately 400 glands/cm^2. Their function is to decrease skin temperature by secreting a nearly isotonic solution. Hair follicles extend from less than 1 mm into the dermis to more than 3 mm into the hypodermis. The average density is about 40-50/cm^2, which is less than the density of sweat glands, but their average surface area may be larger. A sebaceous gland is associated with each hair follicle. The ducts of sebaceous glands join the hair follicles approximately 0.5 mm below the surface of the skin. In the initial diffusion state, hair follicles are one of the most important sites for percutaneous penetration. The inner root sheath surrounding the hair shaft presents an opportunity for molecules to diffuse along the hair follicle. This compartment is filled with sebum, which does not form a barrier to diffusion. When a steady diffusion state has been reached, diffusion through the stratum corneum becomes the dominant pathway[66].

Sebaceous glands are found in all regions of the body except on the palms of the hands and sole of the feet. They are connected with a duct to the hair follicle where they deliver the sebum. The sebum is composed primarily of triglycerides and free fatty acids with fewer amounts of squalene and waxes. It is generally accepted that sebum does not participate in the barrier function of the skin. Among these appendages, the sebaceous glands are of great interest, as MC1R expression was detected both *in vitro* and *in situ* in human sebocytes[40], and as α-MSH has long been known to target the sebaceous gland as well. By modulating interleukin-8 secretion[307], α-MSH is thought to modulate the inflammatory response in the pilosebaceous unit.

1.2 Melanocytes, epidermal melanin unit and melanogenesis

In order to understand the process of normal physiologic pigment production or of its disorders such as hyper- and hypopigmentation, an appreciation of the structure and functions of melanocytes, briefly described in the previous chapter, is required.

1.2.1 Melanocytes

Histologically, melanocytes are derived from the neural crest. During embryogenesis, they migrate from the lateral ridges of the neural plate as the ridges join to form the neural tube. During further development, presumptive melanocytes (undifferentiated melanoblasts) migrate to various sites including the skin, where they proliferate and then differentiate into melanin-producing cells[239]. The uveal tract of the eye (choroids, ciliary body and iris), the leptomeninges (the two innermost membranes of the meninges) and the inner ear (cochlea) constitute additional sites of melanocyte migration. In the inner ear, melanocytes play a role in developing the ability to hear. Thus, the lack of migration or survival of melanocytes in the inner ear, the iris, and parts of the forehead and extremities may explain the expression of congenital deafness, heterochromia irides (two differently colored irises), and patches of leukoderma (synonym of vitiligo: an auto-immune disorder in which the body destroys its own melanocytes) in patients with Waardenburg syndrome (rare disorder resulting from an autosomal dominant mutation involving disorders in the neural crest-derived tissue).

During embryogenesis, melanin-producing melanocytes are found diffusely spread throughout the dermis. With the help of the monoclonal antibody HMB-45, melanoblasts have been identified in human fetal skin at approximately 7 weeks of gestation[147]. After 10 weeks, they appear for the first time in the head and neck region. They then become numerous between the 12th and the 14th week of fetal development[104]. These dermal melanocytes disappear after birth either by migration to the epidermal tissues or through cell death (given the difference in the absolute numbers of cells in the dermis and in the epidermis), except in three anatomic locations: the head and neck, the dorsal part of the distal extremities, and the presacral area[337]. In addition, these three sites coincide with the most common sites for dermal melanocytoses and dermal melanocytomas (blue nevi).

As mentioned earlier, the basal layer of the hair matrix and the outer root sheath of hair follicles are also main migration destinations of melanocytes. Cells located in the matrix produce melanin, whereas melanocytes of the outer root sheath usually are amelanotic, and therefore more difficult to identify. It is also thought that there are two populations of melanocytes, one in the hair follicle and one in the interfollicular epidermis[308]. Based on clinical observations and antigen expression, the latter seems to be more sensitive to the destructive effect of vitiligo. Melanocytes usually reside in the basal layer of the epidermis, where they will remain during their whole life. They allow their dendrites to make contact with keratinocytes, building the epidermal melanin unit described later in **1.2.2**.

Under normal conditions, it is more the level of activity of the melanocytes than their number that determines the degree of pigmentation of the skin[44]. Although some regional variations occur in the density of epidermal melanocytes, their amount remains more or less equal even in different skin types and ethnic groups. Normally, their density in the genital region lies around 1500 melanocytes/mm^2 and is higher than on the back (~900/mm^2). Usually the number of melanocytes in humans varies from about 900 to 2800 per cm^2, and there are smaller differences between individuals when the same anatomic part is examined. Therefore, skin pigmentation is considered to depend on the level of melanogenic activity and the transfer of melanin to the neighboring keratinocytes. Hence, even people suffering from the most severe form of oculo-cutaneous albinism show normal amounts and densities of epidermal melanocytes. Several factors contribute to the melanogenic activity of the cells, including specific characteristics of the melanosomes (e.g. diameter), the organelle where melanin is synthesized, as well as constitutive and stimulated levels of activity of enzymes involved in the melanin synthesis. These enzymes are influenced by receptor-mediated interactions with extracellular ligands, e.g. α-melanocyte-stimulating hormone (α-MSH), that will be described later on.

1.2.2 Epidermal melanin unit

The function of melanocytes in mammalian skin is to form and maintain dendrites, to synthesize and mature melanosomes and to secrete these into keratinocytes with which they are associated. In the human epidermis, each melanocyte secretes melanosomes to approximately 36 keratinocytes, forming an *epidermal melanin unit*. The epidermal melanin unit is the structural and functional unit allowing a color adaptation. Skin and hair pigmentation is clearly related to the amount of melanin contained in the keratinocytes. Several sequential processes can be distinguished[233,278].

1. Formation of structural proteins and the enzyme tyrosinase, and their assembly in the melanosomes;
2. Melanization of the melanosomes through enzymatic oxidation of tyrosine to melanin;
3. Migration of the melanosomes from the perikaryon into the dendrites of the melanocytes;
4. Transfer of the melanosomes to the keratinocytes;
5. Incorporation of melanosomes by the keratinocytes either as single particles or as melanosome complexes;
6. Degradation of the protein matrix of melanosomes within keratinocytes.

These processes are described in the following figure:
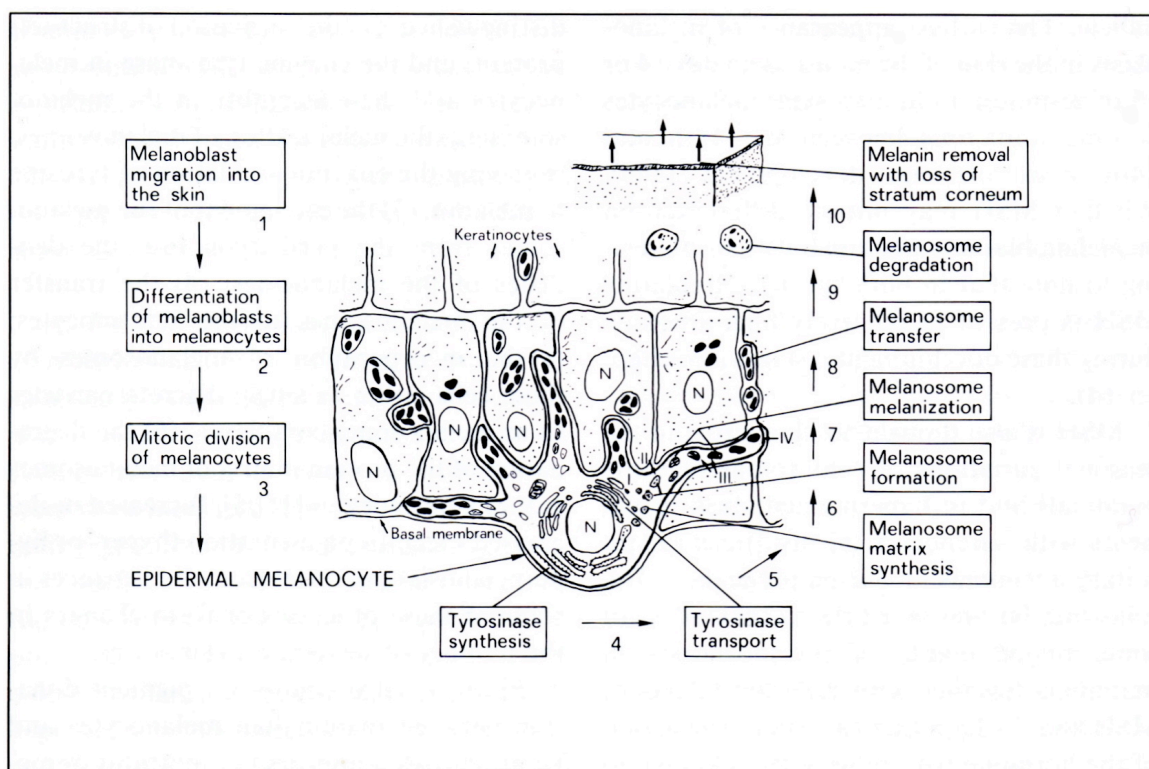
Figure 3: Epidermal Melanin Unit in human skin and process involved in melanogenesis (from A.N. Eberle, The Melanotropins. 1988, Karger Verlag, Basel)[87].

1-3: Steps in melanocyte development. 4-10: Stages in melanin formation (tyrosinase is synthesized by RER and then transported to Golgi). Abnormalities in pigmentation may be caused by a defect at any of these steps. I-IV: The four stages of melanosome development as differentiated by electron microscopy: I = Large spherical, membrane limited vesicle formed by fusion of tyrosinase-containing Golgi-vesicle and RER-derived vesicle; no melanin deposition. II = Oval; obvious matrix in the form of parallel longitudinal filaments; minimal deposition of melanin; high tyrosinase activity. III = Oval; moderate deposition of melanin; high tyrosinase activity. IV = Oval; heavy deposition of melanin; electron-opaque; minimal tyrosinase activity.

1.2.3 Melanogenesis

Melanogenesis is the process leading to the synthesis of two chemically distinct kinds of melanin: the lighter yellow-red phaeomelanins and the darker brown-black eumelanins. The type of melanin produced is also important for the level of skin pigmentation, and it is recognized that both types of melanin are synthesized in human melanocytes[152]. Phaeomelanin is the major type of melanin in red hair and also predominates in skin types I and II. Humans with red hair will tend to produce more pheomelanin in hair and skin and/or have a reduced ability to produce eumelanin, thus explaining the lack of tanning and higher sensitivity to harmful UV-radiation[315]. Eumelanin is present in larger amounts in individuals with darker skin and hair (types III and IV). Eumelanin provides a better protection against damaging UV radiation.

The process of skin pigmentation can be divided into two components. The first is the pigmentation genetically determined in the absence of stimulatory influences, affecting, e.g., the level of pigmentation of parts of the body normally not UV-radiation exposed. It is called "constitutive pigmentation". The second is

the level of pigmentation (or tanning) occurring in response to stimuli like UV-radiation or even, to a certain degree, hormones, and is called "facultative pigmentation". These external stimuli are converted into intracellular messenger molecules that then affect melanogenesis.

Following a single exposure to UV irradiation, an increase in the size of melanocytes can be observed, along with an increase in tyrosinase activity[44]. Repeated exposures to UV irradiation lead to an increase in the number of stage IV melanosomes transferred to keratinocytes, as well as an increase in the number of active melanocytes. Density of melanocytes is roughly twofold higher in the chronically exposed (e.g. the upper outer arm) than in the non-sun-exposed (e.g. the upper inner arm) skin at all ages[127]. An *immediate pigmentary darkening* occurs within minutes after UVA exposure, and fades away after 6-8 hours. It is more easily observed in darker skin types, and therefore is thought to illustrate oxidation of pre-existing melanin or melanin precursors. A new pigment production (via an increase in tyrosinase activity) happens and becomes visible 48-72 hours after exposure to UVB and UVA radiation. It is called *delayed tanning*. The majority of red-haired individuals are unable to develop a tan after UV exposure. Dysfunctional MC1-R on their melanocytes can partly explain this inability. This phenomenon, along with the production of free oxygen radicals following the UV irradiation of phaeomelanins, probably contributes to the increased incidence of both cutaneous melanoma and nonmelanoma skin cancers in red-haired persons[45].

The synthesis of melanin takes place in the melanosomes, organelles located in the cytoplasm of melanocytes and that are closely related to lysosomes. Indeed, in the same way the cell is protected from proenzymes and proteinases contained in the lysosomes, melanosomes home the melanogenesis process in order to protect the inner part of the cell against various harmful melanin precursors (e.g. phenols, quinines, catechols) generated during melanogenesis, and able to oxidize lipid membranes[99]. The melanosomes contain matrix proteins, which form a scaffold to deposit the melanin itself, and enzymes that regulate the biosynthesis of melanin (e.g. tyrosinase). Many of these enzymes are glycoproteins, requiring carbohydrate ligand binding in order to gain full function[141]. For example, after synthesis and release of pre-tyrosinase in the lumen of the rough endoplasmic reticulum (RER), the enzyme migrates via the smooth surface membrane to the Golgi apparatus where terminal carbohydrates, such as sialic acid, are bound. Then it joins the matrix proteins to form the melanosomes. Targeting enzymes to the plasma membrane via intracytoplasmic organelles requires "helper"-proteins. The adaptor protein 3 (AP3) carries this function, and is involved in the budding of vesicles from the trans Golgi network, and therefore plays a role in the melanosome formation[141].

After tyrosinase is transported to the Golgi apparatus and the melanosome matrix is synthesized, the maturation process of the melanocytes reaches its final stages. The melanization of the melanosome occurs in several steps. Tyrosinase activity reaches a peak and then decreases as melanization of melanosomes increases. As soon as melanin is deposited, the melanosomes migrate via microtubules into the dendrites of the melanocyte for the transfer into the neighboring keratinocytes. Microtubules and the motor proteins kinesin and dynein are involved in the movement. Within the dendrites, a specialized myosin protein is contributing to the process by forming a bridge between the actin cytoskeleton beneath the

plasma membrane and the organelle itself, each end of the myosin connecting both structures together[140,141].
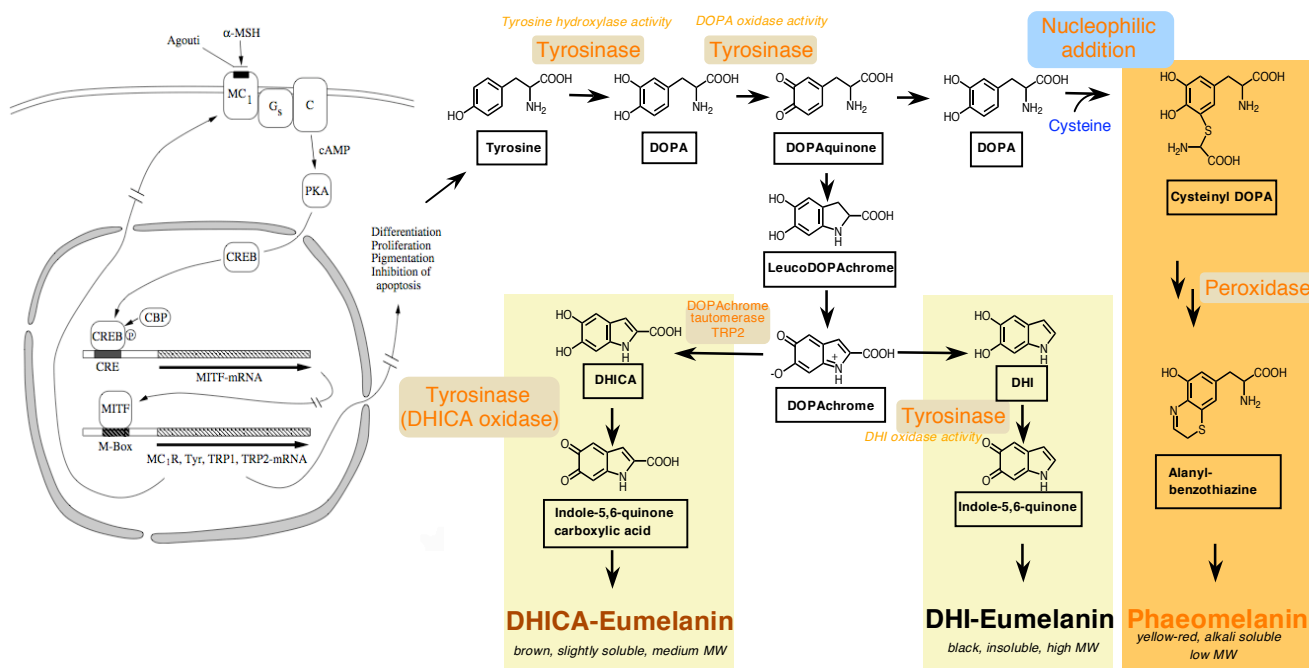
Figure 4: Melanogenesis pathway (modified and completed from Wikberg et al.[325] and from V.J. Hearing[140]).

As shown in **Figure 4**, pigmentation regulation involves several layers of control: UV irradiation of the dermis increases production of melanocortic peptides. These first bind to the MC1 receptor, thus stimulating adenylyl cyclase (C) and hence the production of cAMP. Protein kinase A (PKA) is then activated by this cAMP, leading to the phosphorylation of CREB (cAMP-responsive element-binding protein) and *cis*-activation of the microphthalmia-associated transcription factor (MITF) promoter. MITF therefore regulates the transcription of the tyrosinase gene. MITF belongs to the basic-helix-loop-helix-zipper family and is known to interact with a specific DNA sequence termed M-Box with the sequence GTCATGTGGCT present in the promoter region of the tyrosinase gene[35]. The intracellular second messenger cAMP increases tyrosinase gene expression by enhancing the interaction between MITF and the M-Box. MITF finally induces expression of tyrosinase, TRP1 and TRP2 (tyrosinase-related proteins 1 and 2), and likely other genes as well. These proteins in turn influence differentiation, proliferation, formation of pigment and inhibit apoptosis. The system is positively coupled: activation of cAMP leads to increased formation of MC1 receptors, which in turn allow to form even more cAMP. Therefore, the increased MC1 receptors production causes an increased sensitivity to melanocortic peptides[325]. The actual biochemical synthesis really starts after expression by MITF-mRNA of the several genes mentioned earlier. Negative regulation is achieved by agouti protein, which acts as an inverse agonist on MC1R[4]. Agouti leads to the preferential formation of pheomelanins (details see below).

The brown-black eumelanin and the yellow-reddish pheomelanin mainly differ in their biochemical structure and ultrastructural appearance within melanosomes[268]. Both are derived from the naturally occurring amino acid tyrosine, and the whole melanin biosynthesis pathway itself is mainly regulated by the enzyme tyrosinase, which catalyses multiple steps in the biosynthesis of melanin through tyrosine hydroxylase, DOPA oxidase and dihydroxyindole oxidase activities.

The early steps on the melanogenic pathway, i.e. the *O*-hydroxylation of L-Tyr to L-3,4-dihydroxyphenylalanine (DOPA) in presence of elementary oxygen (O_2), as well as the oxidation of L-DOPA to L-dopaquinone, are catalyzed by the enzyme tyrosinase[184,199]. Tyrosinase is an important key enzyme of 65 kDa (75 kDa when glycosylated), is the rate-limiting enzyme in the melanin biosynthesis and requires copper on two binding sites. All tyrosinases have in common a binuclear type III copper centre within their active site, where two copper atoms are each coordinated with three histidine residues. The two copper atoms within the active site of tyrosinase enzymes interact with dioxygen to form a highly reactive chemical intermediate that then oxidizes the substrate[292]. The activity of tyrosinase is similar to catechol oxidase, a related class of copper oxidase. Tyrosinases and catechol oxidases are collectively termed polyphenol oxidases. The uniqueness of tyrosinase lies in the fact that it requires DOPA as cofactor for the tyrosine hydroxylase reaction[142]. The product is therefore the cofactor for the synthesis of the product. Rates of tyrosine hydroxylation in the absence of the cofactor are negligible, raising the question of where the cofactor comes from, since DOPA is not a normal amino acid available within the cell. This interesting question is to date still unsolved. The kinetics of reduction and oxidation of the active site iron in tyrosine hydroxylase may have an influence on the regulation of the reaction[107].

Tyrosinase can be divided into three domains: an inner domain that resides inside the melanosome, a transmembrane domain and a cytoplasmatic domain. The larger part of the enzyme resides inside the melanosome and only 10% or 30 amino acids belong to the cytoplasmatic domain[280]. The activity of tyrosinase is enhanced by DOPA and is stabilized by tyrosinase-related protein 1 (TRP1) in human and mouse. The regulation of the activity of tyrosinase is managed by phosphorylation of the enzyme by protein kinase C-β[230].

DOPA can spontaneously autooxidize to dopaquinone in the absence of tyrosinase, but at slower rates than in presence of the enzyme. Dopaquinone is an extremely reactive compound that undergoes an irreversible intramolecular cyclization, the nitrogen of the side chain attaching itself to the 6-position of the benzene nucleus, leading to the formation of leucodopachrome and then dopachrome in the absence of thiols (e.g. from cystein) in the vicinity. Dopachrome is able to decarboxylate spontaneously to dihydroxyindole (DHI). In the presence of divalent cations and the enzyme DOPAchrome tautomerase (also called tyrosinase-related protein 2, TRP2) though, the intermediate 5,6-dihydroxyindole-2-carboxylic acid (DHICA) is formed. DHI is then oxidized to indole-5,6-quinone and DHICA is oxidized to indole-5,6-quinone-carboxylic acid. It was speculated that the oxidation of DHICA was catalyzed by an enzyme called DHICA oxidase. There was also a speculation that TRP1 mRNA expression would be correlated with DHICA oxidase activity, which has been confirmed for the murine model but not for the human[43]. TRP1, at

least in mice[167], is able to promote the oxidation of DHICA but in humans, this catalytic function of TRP1 seems to be lost. Human tyrosinase seems capable to accelerate DHICA consumption.

Further investigations have shown that human tyrosinase actually functions as DHICA oxidase, as opposed to the mouse enzyme. Therefore, human tyrosinase displays a less specific substrate specificity than its murine counterpart, and thus might be responsible, at least partially, for incorporation of DHICA units into human eumelanins[224]. This leads to a much slower further oxidation and polymerization than for DHI-eumelanin, resulting in a more soluble, lower molecular weight and lighter colored melanin known as DHICA-eumelanin. On the other side, DHI is rapidly cyclized, decarboxylated, oxidized and polymerized to form a very black, insoluble and high molecular weight pigment, the previously mentioned DHI-eumelanin. Both types of melanin bear an indole non-repeating scaffold and their exact structure remains unknown. The quinones are thought to be responsible for this oxidative polymerization. Whether this polymerization step lies under enzymatic control is not yet clear. It is thought that peroxidase or the melanocyte-specific protein Pmel-17 play a role in this step of melanin synthesis.

Table 1: Characteristics of melanogenic enzymes

	Tyrosinase	**TRP1**	**TRP2**
Synonym	Monophenol monooxygenase	DHICA oxidase Catalase B Glycoprotein-75 Melanoma antigen gp75	Dopachrome tautomerase Dopachrome deltaisomerase
Specificity	Melanocyte	Melanocyte	Melanocyte
Catalytic Activity	Tyrosine → DOPA DOPA → Dopaquinone DHI → Indolquinone	DHICA → Indolquinone carboxylic acid	Dopachrome → DHICA
Miscellaneous	Heat-stable Protease-stable Chelator-sensitive Glycosylated Membrane-bound DOPA cofactor-dependant	Glycosylated Membrane-bound	Heat-sensitive Protease-sensitive Chelator-insensitive Glycosylated Membrane-bound DOPA cofactor independent

The various steps of the synthesis are also likely to be regulated specifically, due to the variety of factors involved. One more regulation mechanism possibly involving the P gene is under investigation. The P protein (encoded by the P gene), a transmembrane protein in the melanosomes, is most likely involved in the transport of tyrosine as initial precursor of the synthesis. The observation that melanosomes isolated from melanocytes with mutations in both copies of the P gene will produce more pigment when incubated in concentrated solutions of tyrosine could be a possible proof[117]. Another hypothesis is that the P protein is involved in maintaining a low pH within the melanosomes, as a low pH is required for normal tyrosinase activity[241,243]. Stimulations from outside the cell via MC1R increase the production of eumelanin at the expense of pheomelanin. Competitive inhibitors of tyrosinase activity include hydroquinone and L-phenylalanine.

The biosynthesis of pheomelanin is different from that of eumelanin in various aspects:

1. It is less dependent on tyrosinase activity than eumelanin synthesis, as pheomelanin is even produced when the levels of tyrosinase activity are virtually undetectable[50].

2. Pheomelanins follow another main route of biosynthesis from the dopaquinone key step. In the presence of thiol donors like cysteine, dopaquinone is converted to cysteinyl-DOPA by nucleophilic addition. Following the same kind of sequence as for eumelanin biosynthesis, cysteinyl-DOPA undergoes oxidation by peroxidase, cyclization to form alanyl-hydroxyl-benzothiazine, and finally a polymerization step leading to the formation of pheomelanin. Pheomelanins have a yellow-reddish color, are soluble in alkali and have a rather low molecular weight.

These various types of melanin are responsible for hair color variations in mammals (humans included). In humans, yellow to bright red hair results from the production of pheomelanin, whereas brownish, black, grey and blond hair have their origin in eumelanin production[156,226]. It is not clear how the switch from eumelanin production to pheomelanin production, or vice-versa, is controlled. Mutations in genes coding for certain proteins may produce phenotypic modifications leading to variations in coat color in the mouse and to different hues in the hair and skin of humans[27,28]. Additionally, it is known that in mice the interactions of MSH and agouti protein play a major role in this regulation. In contrast to the human, mouse coat color genetic analyses provided explanations for red hair other than through MC1R allelic variation. The key player is the agouti protein, a paracrine signaling molecule inhibiting the effects of melanocortin signaling. Agouti protein is the only known native competitive antagonist of the MC1R. It inhibits the binding of melanocortins and therefore their ability to activate the MC1R. The modulation of the signaling by altering the levels of antagonist against a constant background level of melanocortin ligand avoids the necessity for a mechanism adjusting α-MSH levels independently of other POMC-derived products, such as ACTH and β-endorphin. The existence of MC1R gene sequence variations was also reported in humans. For example, variations were found in over 80% of individuals with red hair and/or fair skin, but in less than 20% of individuals with brown or black hair, and in less than 4% of those showing a good tanning response. These findings suggested that MC1R in humans (as in other mammals) is a switch regulating the pigmentation cascade. Additionally, variations in this protein may lead to a poor tanning response[315].

Keratinocytes also play an important role in the regulation of melanocyte growth and differentiation. They produce a whole variety of factors acting on melanocytes. Under normal conditions, melanocytes do not produce their own growth factors and their proliferation is regulated by keratinocytes through the production of the autocrine basic fibroblast growth factor (bFGF). Other melanocyte growth factors include mast cell growth factor (MGF) and hepatocyte growth factor (HGF), but their effects are not specific to melanocytes. Cytokines and other inflammatory mediators are locally produced factors regulating melanocytes. It has been suspected that some of these substances may mediate the effects of UV-radiation and post-inflammatory pigmentary responses. The cytokines interleukin-1 (IL-1), interleukin-6 (IL-6) and tumor necrosis factor-α (TNF-α) have been reported to inhibit both melanogenesis and melanocyte proliferation.

These, together with tumor necrosis factor-β (TNF-β), interleukin-7 (IL-7) and interferon-γ (INF-γ) also induce the expression of intercellular adhesion molecule-1 (ICAM-1).

Endothelins also play a role in melanocyte development, growth, melanogenesis, motility and dendricity. Studies show that endothelin-1 (ET-1) affects melanocyte dendricity[136], proliferation[329] and melanogenesis[155], while endothelin-3 (ET-3) plays an important part in regulation of progenitor number and differentiation in melanocyte development[245].

Beside their ability to distribute melanin to surrounding keratinocytes, melanocytes are also able to produce a wide range of signal molecules, such as cytokines, melanocortin peptides, catecholamines, serotonin, eicosanoids, and nitric oxide (NO). Upon UV radiation (UVR) and other stimuli they secrete for example NO as a signaling molecule. Human melanocytes produce NO that can be effected by α-MSH, in response to UV radiation and bacterial lipopolysaccharides (LPS)[310]. Why the melanocytes and melanoma cells produce NO is not quite clear. It was shown that NO stimulates melanin production and, as it is released by keratinocytes in response to UV radiation, it could serve as a paracrine factor in UVR-induced melanogenesis[257]. But melanocytes are capable of producing higher amounts of NO than keratinocytes, indicating the possibility that NO acts as an autocrine factor to regulate melanogenesis. However, the main importance of NO in melanocytes appears not to be its function as an autocrine mediator, but as a signaling molecule linking the melanocyte with other systems in the skin. NO could be related to a phagocytotic property of melanocytes as they produce a number of cytokines. α-MSH also plays a role in the modulation of the immune system. There is evidence that it has potent anti-inflammatory and immunomodulatory properties through its ability of being a competitor for proinflammatory cytokines[310,311]. These examples make it quite clear that melanocytes have various functions beside their ability of producing and distributing melanin.

1.3 α-Melanocyte-stimulating hormone (α-MSH)

The "melanophore stimulants" have a long history. They were discovered about ninety years ago, when it was shown that α-MSH induces skin darkening in amphibians, from whence its name derived. Surgical ablation experiments showed that the pituitary gland is involved in the control of skin color, and was one of the first observations of its decisive role in endocrine function.

1.3.1 The pituitary gland or hypophysis

The pituitary gland, commonly called hypophysis, is an endocrine gland located in a small bony cavity (*sella turcica*) covered by a dural (from the *dura mater*) fold at the base of the brain. The pituitary fossa, in

which the pituitary gland sits, is situated in the sphenoid bone in the middle cranial fossa at the base of the brain. The pituitary gland secretes hormones regulating homeostasis, including trophic hormones that stimulate other endocrine glands. It is functionally connected to the hypothalamus by the median eminence. The pituitary is functionally linked to the hypothalamus. In the adult human, it is composed of two main lobes, the adenohypophysis and neurohypophysis, whereas in most other vertebrates, an intermediate lobe is present as well.
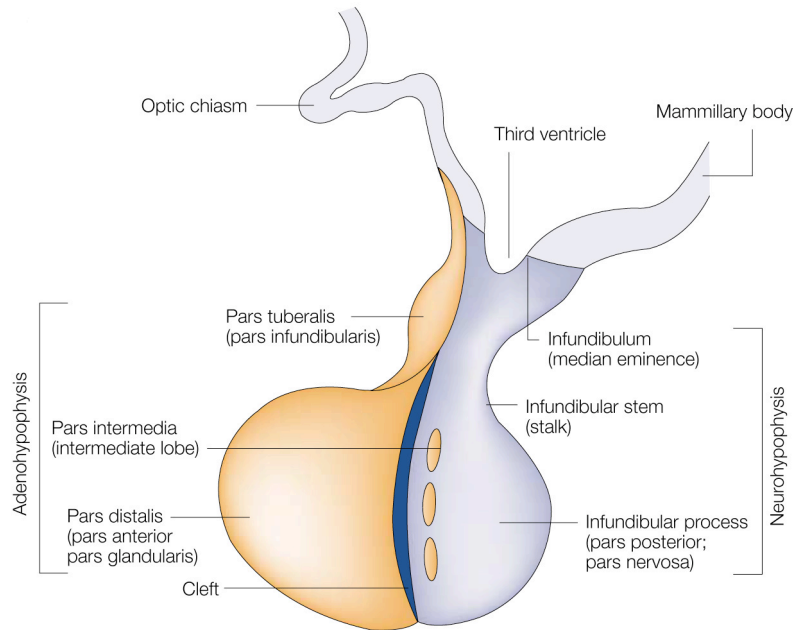
Figure 5: Pituitary anatomy (from S.L. Asa and S. Ezzat)[17].

The normal pituitary is a bean-shaped gland that has two components. The neurohypophysis, also known as the posterior lobe, is an extension of the hypothalamus that descends into the sella turcica. It is composed of neuronal processes that secrete hormones that are produced in the cell bodies of hypothalamic ganglion cells of the infundibulum; these cell processes are supported by glial cells known as pituicytes. The adenohypophysis is composed of hormone-secreting epithelial cells, known as adenohypophysial cells, which are derived from the oral ectoderm and ascend as Rathke's pouch during development. They lose contact with the oral ectoderm where the bone of the sella forms. The bulk of this tissue is the anterior lobe or pars distalis of the gland. The intermediate lobe, or pars intermedia, is composed of epithelial cells from the posterior limb of Rathke's pouch. This structure is composed mainly of corticotrophs and is well developed in most mammals, but is only rudimentary in humans. The pars tuberalis is a small rim of the adenohypophysis that is wrapped around the pituitary stalk; it is composed mainly of gonadotrophs.

The adenohypophysis, also referred to as the anterior pituitary, is divided into anatomical regions known as the *pars tuberalis* and *pars distalis*. The adenohypophysis synthesizes and secretes important endocrine hormones, such as ACTH, TSH, prolactin, growth hormone, endorphins, FSH, and LH. These hormones are released from the anterior pituitary under the influence of hypothalamic hormones. The hypothalamic hormones travel to the anterior lobe by way of a special capillary system, called the hypothalamic-hypophyseal portal system. The neurohypophysis is also referred to as the posterior pituitary. It is functionally linked to the hypothalamus by the pituitary stalk, whereby hypothalamic releasing factors are released and in turn stimulate the release of posterior pituitary hormones. Hormones are made in nerve cell

bodies positioned in the hypothalamus, and these hormones are then transported down the nerve cell's axons to the posterior pituitary. The hormones secreted by the posterior pituitary are:

- Oxytocin, which is released from the paraventricular nucleus in the hypothalamus.
- Antidiuretic hormone (ADH, also known as vasopressin and AVP, arginine vasopressin), is released from the supraoptic nucleus in the hypothalamus.
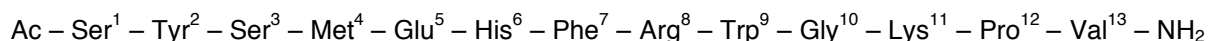
As mentioned, there is also an intermediate lobe in many animals. For instance, in fish, it is believed to control physiological color change. In adult humans it is just a thin layer of cells between the anterior and posterior pituitary. The intermediate lobe produces MSH, although this function is often (imprecisely) attributed to the anterior pituitary.

1.3.2 Melanocortins and α-MSH

In the 1930s and 1940s, various bioassays were developed, allowing the quantitative isolation of the "melanophore stimulants". However, these could only be characterized in the 1950s with the development of an isolated frog skin bioassay and better purification and sequencing methods. These allowed molecular characterization and sequence determination of α-MSH and other MSHs from pig. Isolations from bovine, equine, ovine, as well as macaque, camel, dogfish and salmon pituitary glands followed. Later, a functional relationship between the so-called melanocortins and adrenocorticotropin, lipotropin and endorphin could be proven. Shortly after the isolation of MSH peptides, peptide chemistry adopted new concepts enabling the synthesis of these peptides, as well as the synthesis of numerous peptide hormone analogues. In the last 40 years, the mode of action of melanotropins could be partly elucidated thanks to the pharmacological structure-activity studies developed since then. And these contributions and discoveries, associated with the functional relationship shown earlier, culminated in the isolation and sequence analysis of the common precursor to all melanotropins, proopiomelanocortin (POMC), in 1979. The first melanocortins to be purified and sequenced were α-MSH, β-MSH and ACTH. The α- and β-MSH were initially known as basic and acidic melanocyte-stimulating principles due to the difference in their isoelectric points. Once the sequences were established, α-MSH was found to share the sequence of $ACTH_{1-13}$, but carrying a N-terminal acetyl group and bearing an amidation at the C-terminus. The sequence of β-MSH was different, but also shared a common partial sequence with ACTH and α-MSH.

α-MSH consists of a 13-amino acid residue and, as mentioned, carries either a free or acetylated N-terminal serine and the C-terminal valine contains in most cases a carboxamide group:

$$\text{Ac} - \text{Ser}^1 - \text{Tyr}^2 - \text{Ser}^3 - \text{Met}^4 - \text{Glu}^5 - \text{His}^6 - \text{Phe}^7 - \text{Arg}^8 - \text{Trp}^9 - \text{Gly}^{10} - \text{Lys}^{11} - \text{Pro}^{12} - \text{Val}^{13} - \text{NH}_2$$

These C- and N-terminal modifications give α-MSH more stability, as they inhibit degradation by exopeptidases. In addition, they increase the potency of the peptide in many bioassays[87]. The C-terminus of mammalian α-MSH is amidated. The N^{α}-amino group of Ser[1] is either free or blocked with an acetyl group, depending on the tissue. In some cases, α-MSH occurs in its diacetylated form, the second acetylation being found on the side-chain hydroxyl group of the N-terminal serine, forming the [N,O-bisacetyl-Ser[1]]-α-MSH. Acetylation of α-MSH and β-endorphin is an important process in the regulation of the biological activity of these peptides[77]. Acetylation in melanotrophs (cells of the intermediate lobe of the hypophysis producing melanocyte-stimulating hormone) of the *pars intermedia* takes place in secretory granules by opiomelanotropin *N*-acetyltransferase (NAT)[56]. This enzyme uses acetyl coenzyme A as acetyl donor and differs from the soluble acetyltransferase. The preferential acetylation reaction is that of $ACTH_{1\text{-}14}$ or $ACTH_{1\text{-}13}$, and to a lesser degree that of β-endorphin. The double acetylation of N-terminal Ser[1] may result from an *O*-acetylation, followed by a spontaneous O→N-shift of the acetyl group. This process is often observed during coupling reactions in peptide synthesis. A possible evidence for the increased potency of diacetylated α-MSH was shown by recruitment of lactotrope cells secreting prolactin in a primary culture of rat anterior pituitary cells by α-MSH, diacetyl-α-MSH, or N-acetylated β-endorphin. The secretion of prolactin was significantly increased by the latter two peptides[316].
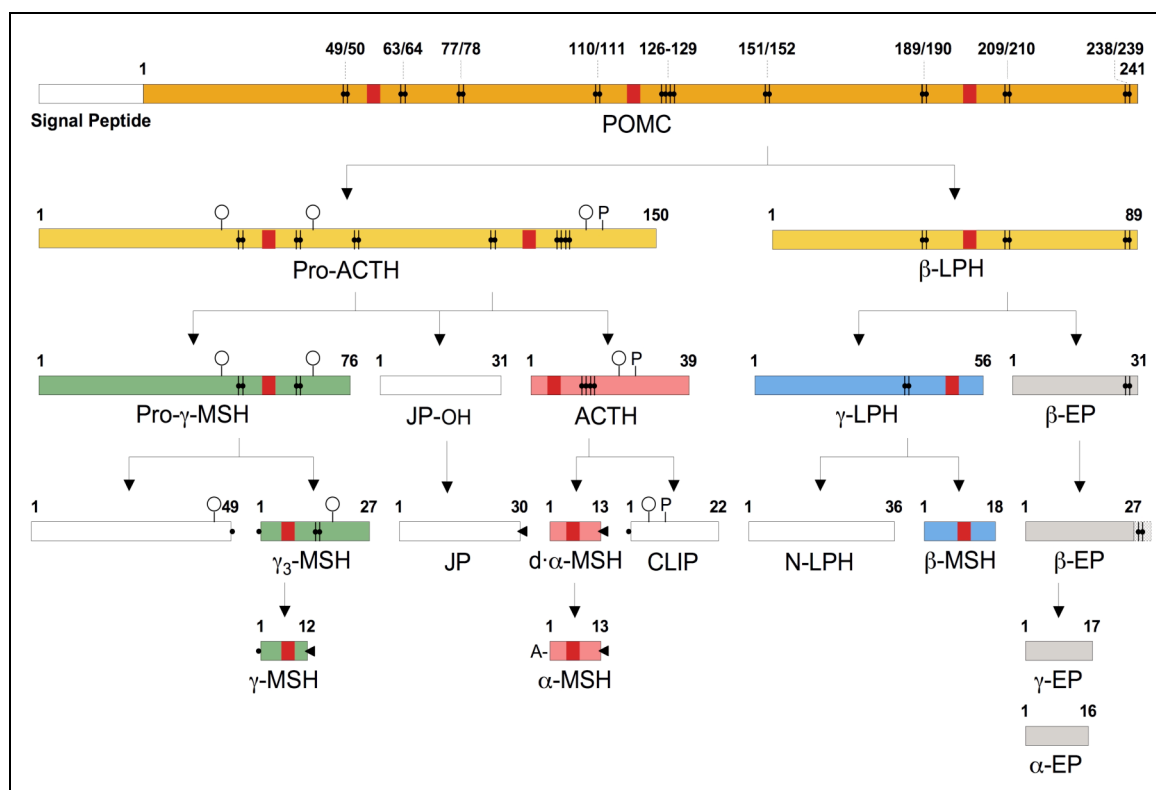
Figure 6: Sites of cleavage in POMC of human. Pattern of processing of POMC in melanotrophs of the pars intermedia[87].

The mammalian α-MSH is a basic peptide with a pI of 10.5-11.0 and has a molecular weight of 1664.93 Da (acetylated N-terminus, C-terminal amide group, without counterions). It is more or less heat stable (can be heated up to 80°C under physiological conditions for a short period) but very prone to oxidation of the Met[4] residue. Oxidation dramatically decreases the biological activity of α-MSH. It is thought that α-MSH

occurred in an early phase of evolution because its sequence is preserved in many different species with only slight differences. For example Xenopus α-MSH differs from mammalian peptide only by a single mutation at the N-terminus, where Ser^1 is replaced by Ala [88].

As mentioned earlier, all melanocortin peptides are derived from a large (31-36kDa) precursor called proopiomelanocortin (POMC). POMC is mainly synthesized in the *pars intermedia* and *pars distalis* of the pituitary gland, but also in other regions of the brain and in several peripheral tissues (e.g. skin, testes, ovaries, placenta, adrenal medulla, gastrointestinal tract, cells of the immune system and tumor cells), where the precursor is also processed. Induction of corticotropin releasing hormone (CRH) in the hypothalamus-pituitary-axis activates CRH-receptors and induces production and secretion of POMC. Proteolytical cleavage of the large precursor converts the prohormone into its bioactive form. All the melanocortins (α-, β-, γ-MSH and ACTH) share a common MSH core sequence bearing the amino acids His–Phe–Arg–Trp. Interestingly, investigations about the relative levels of the different POMC-derived peptides and thus the processing level of POMC showed predominant presence of the unprocessed hormone in the blood, indicating that POMC is inefficiently processed in the pituitary[125]. Similarly, POMC processing seems to be incomplete in the skin as well. It has been shown that cultured human keratinocytes and melanocytes secrete high levels of unprocessed POMC[260]. These observations lead to the conclusion that an excess of POMC is synthesized in the hypophysis and the skin. This may happen to ensure sufficient stocks of ligands for the melanocortin receptors that can be secreted instantly in response to physiological demand. Clearly, only a small proportion of POMC is proteolytically converted to ACTH and MSH peptides, the excess being secreted. Therefore, the levels of POMC processing may be the limiting factor in the signaling pathway.

The biosynthesis of POMC seems to be controlled by MSH release-inhibiting factors, such as dopamine, neuropeptide Y (NPY), or γ-aminobutyric acid (GABA). They lower the cAMP levels of melanotrophic cells, which results in a reduced capacity of the cell to synthesize POMC mRNA. In contrast, POMC transcription is enhanced by MSH releasing factors such as adrenalin by elevating the cAMP levels in the cell. Adrenalin is released in stress situations.

α-MSH has various physiological functions and acts as a pleiotropic peptide affecting many different kinds of cells in the nervous system and many peripheral organs. As mentioned earlier, it interacts with several subtypes of melanocortin receptors. In lower vertebrates such as Xenopus or Rana, it is responsible for the adaptation of skin color to the light intensity and the pattern of the environment. In the mammal, α-MSH was found to be present in the skin, where it is localized in keratinocytes, melanocytes, and Langerhans cells[318]. In the skin it normally acts together with ACTH, which shows an even greater occurrence than α-MSH. In human melanomas, the extent of its production and release could be correlated with the expression of MC1 receptors. α-MSH apparently decreases expression levels of tumor necrosis factor (TNF-α), which normally stimulates synthesis of the intercellular adhesion molecule-1 (ICAM-1)[213], supposedly mainly responsible for tumor aggressiveness and metastatic potential. As a further function,

α-MSH is thought to regulate inflammation and hyperproliferative skin diseases. The following scheme (**Figure 7**) describes the pleiotropic actions of α-MSH in various human skin cell types.
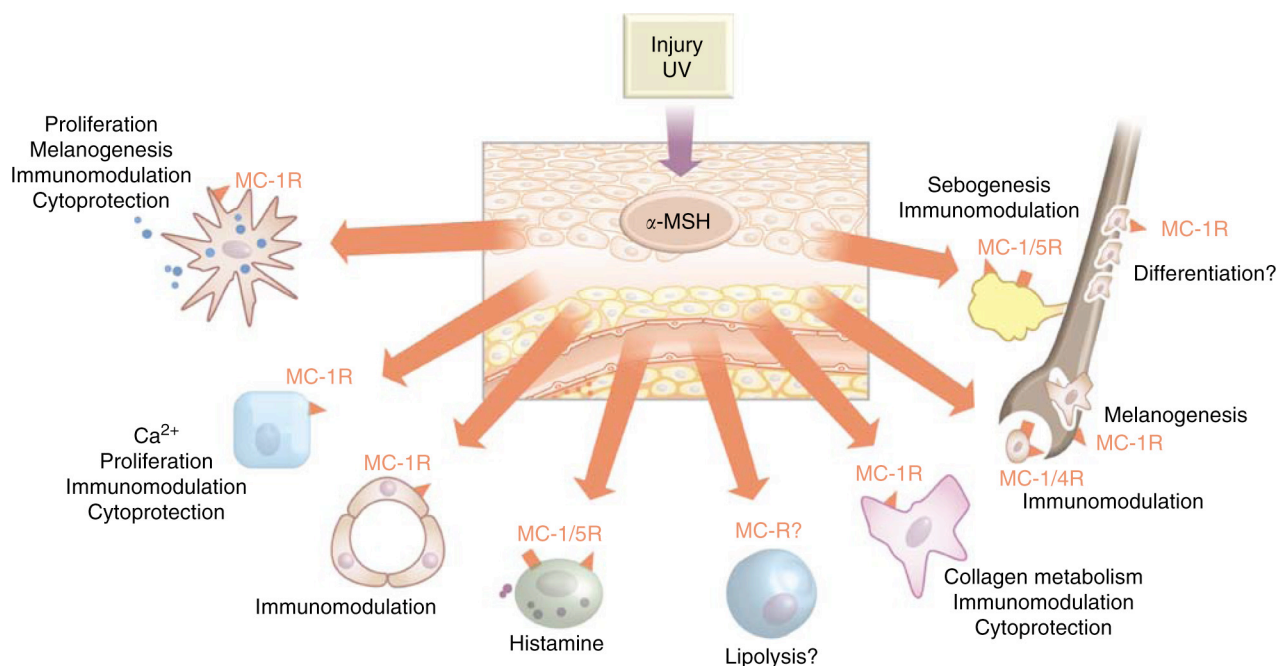
Figure 7: Pleiotropic actions of α-MSH in human skin cells[42]**.**

Depicted are the various skin cell types (from left to right: epidermal melanocytes and keratinocytes, endothelial cells, mast cells, adipocytes, fibroblasts, and cells of the pilosebaceous unit, that is, follicular melanocytes and keratinocytes, dermal papilla cells, and sebocytes), which were shown to express MCRs and to react with α-MSH. Note that generation of α-MSH is not limited to the epidermis but can be induced in many other cutaneous cell types upon exposure to prototypical stressors. In addition, MC peptides can be delivered to the skin via the classical endocrine pathway.

In the brain, α-MSH exhibits a trophic effect on the outgrowth of neuritis from PNS and CNS, and exerts a positive effect on short-term memory, activates sexual behavior, stimulates aggression and social behavior, grooming, stretching and yawning. Most of these effects are mediated over the MC3 or MC4 receptors. MC4R and α-MSH also exert a tonic inhibition on food intake (anorexigenic effect) that plays an important role in diseases like obesity, insulin resistance and type II diabetes. Many other effects of α-MSH are known, such as stimulation of the activity of sebaceous glands, increase of prolactin release in lactotrophs, modulation of the neuroactivity of the retina, increase in permeability of the blood-aqueous barrier of the eye, and stimulation of the release of progesterone from prepubertal ovaries in females.

1.4 The melanocortin-1 receptor (MC1R)

Communication of living cells with their environment is really critical. It is so critical that some entire protein families are totally and exclusively dedicated to the reception of external stimuli, such as chemical messengers or physical stimuli. They are then capable of giving an adaptive response to these triggers.

1.4.1 GPCRs and the MC1R as superfamily member

The G protein-coupled receptor (GPCR) superfamily is the largest with over 1000 members. GPCRs mediate responses to a whole variety of stimuli, including light, odorants, taste molecules, ions, neurotransmitters and hormones. Consequently, they involve a whole collection of responses implying a wide range of physiological functions, including stress and immune response, sexual behavior, cardiovascular regulation, energy homeostasis and of course skin pigmentation through regulation of the activity of metabolic enzymes and pathways, ion channels and membrane transporters. This variety of functions may be the reason why they are the most investigated group of target proteins for drug development[187].

Ligand-binding studies by Donatien et al.[81], Ghanem et al.[122] and Siegrist et al.[284] demonstrated that MC1R is a GPCR expressed in melanocytes and melanoma cells. MC1R is a major regulator of pigmentation of the skin (type and amount of pigment) and thus one of the determinants of the skin's phototype and sensitivity. As mentioned in the previous chapter, POMC-derived small peptide hormones (the melanocortins) act as physiological agonists. MC1R belongs to a five-member subfamily of GPCRs, the melanocortin receptors (MCRs), which mediate the physiologic actions of melanocortins by a G_s-protein-dependent activation of the cAMP signaling pathway. MC1R was cloned and mapped to a locus known to influence pigmentation in the mouse[276]. Since then, genetic analysis, phenotypic association and structure-function studies opened new perspectives for the assignment of its function as a key regulator of skin biological events.

This receptor is a member of the large superfamily of seven transmembrane-domains receptors[64,121,214,291], and it has 39-61% homology with a family of GPCRs that all bind melanocortin peptides. This family also includes MC2-, MC3-, MC4- and MC5-receptors. mRNA expression of the five receptors allowed for their localization in various tissues, summarized in **Table 2**. Eberle described the whole variety of their related effects, ranging from food intake regulation and energy homeostasis to cortisol secretion, sexual behavior, exocrine gland secretion and of course pigment production and regulation[87].

Table 2: Melanocortin receptors and their tissue localizations

Receptor	Tissues or cell types
MC1-R	Melanocytes, melanoma, macrophage, brain
MC2-R	Adrenal cortex, adipose tissue
MC3-R	Brain, placenta, duodenum, pancreas, stomach
MC4-R	Brain, spinal cord
MC5-R	Skin, adrenal cortex, adipose tissue, skeletal muscle

MC1R is expressed with the highest density on melanocytes[191]. As GPCR, it activates G proteins that bind GTP and GDP as intermediary messengers. G proteins are usually named after their α-subunits. Four distinct types of α-subunits are known:

- G_s proteins, which stimulate adenylyl cyclase;
- G_i proteins, which inhibit adenylyl cyclase and activate G protein-coupled inwardly rectifying potassium (GIRK) channels as well;
- G_q proteins, which activate phospholipase Cβ;
- G_{12} proteins, which activate Rho guanine-nucleotide exchange factors (GEFs).

The MCRs signal primarily by activation of the heterotrimeric G_s protein and stimulation of adenylyl cyclase. The resulting increase in intracellular cAMP is responsible for most, if not all, melanogenic actions of α-MSH[52]. The pathway following adenylyl cyclase stimulation has been described earlier in chapter **1.2.3** and in **Figure 4**. Agonistic activation of the receptors induces conformational changes, which seem to involve rearrangements of the transmembrane domains III and VI. This "activated receptor" can interact with the heterotrimeric G protein, and serves as guanine-nucleotide exchange factor to promote GDP dissociation, and GTP binding and activation. The activated heterotrimer then dissociates into an α-subunit and a βγ-dimer. Both these subunits have an independent capacity to trigger cell response through separate effectors. After hydrolysis of GTP to GDP, the heterotrimer is reassociated and the activation cycle is terminated[235]. The whole physical dissociation process of α from βγ is though contested and remains an issue[165]. As already mentioned, G_sα with bound GTP is able to activate adenylyl cyclase, leading to an increased production of cAMP. This increase in cAMP levels result in the activation of tyrosinase via PKA. Evidence suggests that the expression, *de novo* synthesis and activation of tyrosinase are increased by the binding of a ligand. It has been shown in B16 mouse melanoma cells that inhibition of phosphatidylinositol-3-kinase (PI3-kinase) and its target, the serine/threonine kinase p70[S6], increases the melanin content of these cells[51], as well as their dendrite outgrowth (PI3-kinase only). Therefore, the PI3-kinase pathway may be involved in regulating melanogenesis as well. In contrast, the melanocyte-specific activation of the MAP-kinase pathway by cAMP may in some cases downregulate melanogenesis: MAP kinase ERK2 phosphorylates MITF, thereby targeting the transcription factor to proteasomes for degradation[52].

1.4.2 Agouti protein, agouti signaling protein and agouti-related protein

Agouti is a paracrine signaling molecule whose expression in rodents is normally limited to skin and whose biological function in that tissue is to act at the hair follicle melanocyte to modulate eumelanin synthesis[211]. It blocks the actions of α-MSH on melanocytes of the hair follicle. This antagonism forces the melanocyte to switch from eumelanin to pheomelanin biosynthesis. Control over time of agouti expression leads to the typical banding observed on the coat of several animals[189]. Although no similar phenotypic property can be observed in the human hair color, a human counterpart of agouti protein has been cloned and

characterized: the agouti signaling protein (ASIP)[326]. As observed for most melanocortin peptides, ASIP mRNA was also detected in a wide range of tissues, such as heart, ovaries and testis or adipose tissue. The physiological functions of ASIP in these tissues remains mostly unclear. It is widely accepted that ASIP antagonizes the effect of melanocortins by directly binding to target MCRs and may thus play a role in the regulation of human pigmentation by inhibiting melanogenesis[300]. Its role appears to be comparable to that of agouti in the murine model. Agouti-related protein (AGRP) is a more recently discovered neuropeptide of the central nervous system. Various evidences suggest a major role in the regulation of mammalian feeding behavior[225,282]. AGRP was identified because of its sequence similarity to the agouti protein[332].

Ubiquitous expression of agouti in mice generates several pleiotropic effects, such as yellow coat, obesity, insulin resistance, increased body length and premature infertility[182]. Obesity and diabetes caused by ectopic *agouti* expression are explained by its ability to mimic AGRP, since ubiquitous expression of AGRP in transgenic mice causes an increased weight gain and body length phenotype identical to that produced by ubiquitous expression of *agouti*. Structurally, however, the similarity between agouti and AGRP is confined almost entirely to their 40-residue carboxyl termini where a total of 20 residues, including 10 cysteine residues, are identical. Both agouti and AGRP have been shown to antagonize the action of melanocortic peptides such as α-MSH and ACTH at specific melanocortin receptor subtypes[332]. Whether it was competitive antagonism, inverse agonism or activation of an effector other than adenylyl cyclase, was not easy to assess. Studies in several laboratories proved that these molecules bind to MCRs in a competitive mechanism and function as inverse agonists[332].

1.4.3 Structure of the MC1R and ligand binding

Structure

MCRs are not closely related to any other G protein-coupled receptor, even though they can be classified as class A GPCRs (whose prototype is rhodopsin) after analysis of the sequence similarity. GPCRs cannot readily be crystallized, and the only templates available delivering information about their secondary and tertiary structures are a low-resolution electron microscopy structure of bacteriorhodopsin[296] and the famous crystal structure of rhodopsin by Palczewski et al. in 2000[229]. MCR was computer-modeled according to this structure[149,240], from which it was concluded that MCR shares homologies with GPCRs such as the extracellular N-terminus, the seven-transmembrane helical core domain joined by three intracellular and three extracellular loops, and the intracellular C-terminal extension. Human MC1R is composed of 317 amino acids and murine MC1R of 315. The human *MC1R* gene coding for the receptor was first cloned independently by Chhajlani and Wikberg[64] and by Mountjoy et al.[214], both in 1992. Many particularities of the different parts of MC1R are or have been discussed[120]. Some of them are though of higher interest for ligand binding.
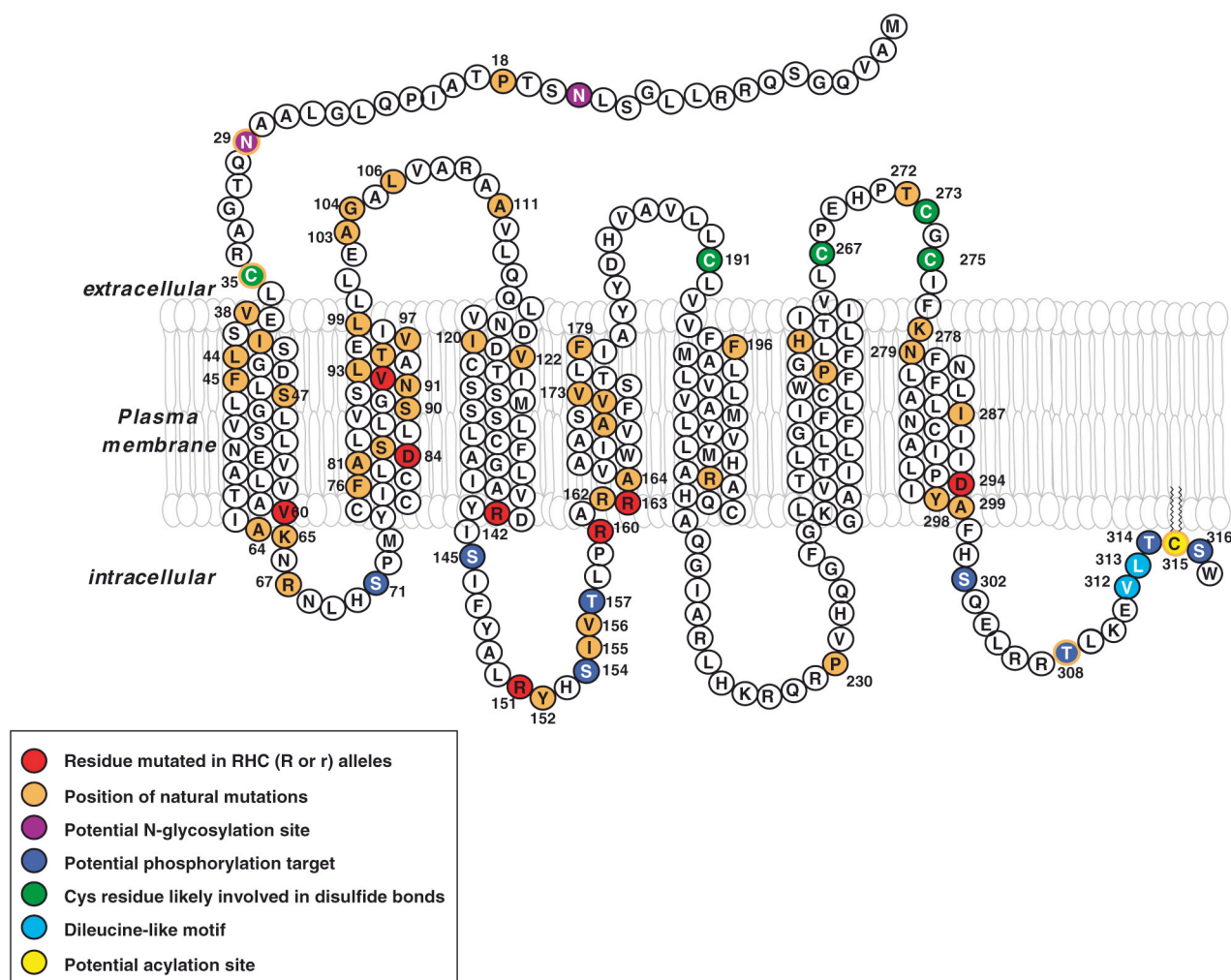
Figure 8: Structure of the human melanocortin-1 receptor[120].

The positions for TM helices are drawn according to the two-dimensional model of Ringholm et al.[253]. The amino acid sequence corresponds to the wild type consensus (GenBank accession number AF326275). Positions for natural non-synonymous mutations are shown in red (for RHC alleles) or orange. Potential post-translational modification sites are also highlighted.

The extracellular loops

For instance, binding affinity of agonists has been shown to be weaker in the case of a mutation of Glu[269] and Thr[272] for Ala in the third extracellular loop[65], but whether these residues provide contact and are really implicated in the binding affinity, is discussed. Indeed, transmembrane domain 6 (TM6) is connected to the extracellular loop 3, and the binding of agonists is mostly accounted for by a network of charged and aromatic residues located in several transmembrane domains, including TM6. Glu[269] and Thr[272] might just induce a change in the position of TM6 and alter the configuration of the binding pouch. As mentioned by García-Borrón et al., Cys[267] and Cys[275] might form an essential intramolecular disulfide bond between TM6 and TM7, as mutations of both of them to Gly or Ala leads to loss of function[106,120]. Also, all three Cys residues of the extracellular loop 3 are conserved in all MCRs, indicating a probable crucial functional role for one intraloop and one interloop disulfide bonds.

The intracellular loops

The intracellular loops of GPCRs usually contain all phosphorylation targets that are important for internalization, cycling and thus the regulation of signaling. They mostly provide the binding interfaces for the heterotrimeric G proteins[120]. The second intracellular loop also contains conserved phosphorylation sites of protein kinase A (PKA), as well as a target for protein kinase C (PKC). The third intracellular loop is poorly conserved in MCRs.

The transmembrane domains

The transmembrane domains are positioned almost perpendicularly to the plane of the membrane. Several transmembrane domains contribute to form the ligand-binding pocket located, for class A GPCRs, below the interface formed by the plasma membrane and the extracellular medium. The Arg residue in the core sequence His-Phe-Arg-Trp (HFRW) shared by natural melanocortins presumably interacts with a highly charged region containing Glu^{94} (TM2), Asp^{117} and Asp^{121} (TM3), according to three-dimensional models of ligand-receptor complexes by Haskell-Luevano et al.[138]. The positive charge of the arginine is supposed to change the arrangement of TM2 and TM3. The induced movement, especially on TM3, is thought to induce a conformational change of the second intracellular loop. This region, containing the conserved DRY tripeptide (characteristic of class A receptors) at the interface between TM3 and the second intracellular loop, is known to be important for functional coupling. Its rearrangement is supposed to allow for interaction with the G_s protein[190]. Also, TM4, 5 and 6 contain aromatic residues and may form interactions with the aromatic residues of potential ligands, thus contributing to the binding affinity[331].

Quaternary structure

The quaternary structure of MC1R probably plays a role in the various properties displayed by the receptor. The ligand binding and the coupling efficiency can be dramatically influenced by dimerization or oligomerization. A BRET assay (bioluminescence resonance energy transfer) by Mandrika et al.[196] suggested a constitutive dimerization process in cells overexpressing the receptor. This dimerization appears early in the biosynthesis of MC1R and seems to be constitutive, but MC1R was not found to show cooperativity in agonist binding[120].

1.4.4 Selectivity

The MCRs share some common properties, including recognition of the HFRW pharmacophore pattern, giving the MCRs the ability to bind several melanocortins, but with different affinities[288]. Most of these results were obtained by transfection of human *MC1R* into cultured cells. MC1R shows high affinity for α-MSH and slightly lower affinity for the other melanocortins. MC1R binds several ligands, both natural and synthetic. The order of potency is: Nle^4-D-Phe^7-α-MSH (synthetic) > α-MSH > ACTH > β-MSH > γ-MSH. MC2R displays a strong selectivity for ACTH only. MC3R is the least selective receptor and binds all natural melanocortins, but has a slightly higher affinity for γ-MSH. MC4R has a very slight preference for β-

MSH over α-MSH, but a very low affinity to γ-MSH. MC1R and MC4R are not able to distinguish well between ACTH and α-MSH. MC5R binds melanocortins in the same potency sequence as MC1R (α-MSH > ACTH > β-MSH > γ-MSH), though with much lower affinities[271].

Table 3: Specificity of melanocortin receptor subtypes.

Receptor subtype (human)	Ligand Specificity
MC1R	α-MSH > ACTH > β-MSH > γ-MSH
MC2R	ACTH only
MC3R	α-MSH = β-MSH = γ-MSH = ACTH
MC4R	α-MSH = ACTH = β-MSH >> γ-MSH
MC5R	α-MSH > ACTH > β-MSH > γ-MSH

ACTH was reported to bind to MC1R with a potency between that of α-MSH and of β-MSH, but Schiöth et al. pointed out that this may be due to degradation of ACTH to α-MSH[139,270]. Nevertheless, conclusions (especially those regarding cutaneous pigmentation) drawn from transfection of human *MC1R* into cultured cells are limited. Several factors can limit the credibility of the results[139]:

- α-MSH may stimulate pigmentation via the protein kinase C pathway in addition to the adenylyl cyclase pathway.
- POMC breakdown products are produced in different ratios in melanocytes and keratinocytes for example, and thus the concentrations used for *in vitro* studies may differ from the ones used *in vivo* for ligand binding and receptor activation.
- There are potential phosphorylation sites on PKA and PKC of MC1R, but the effect of phosphorylation and whether ligand binding is influenced is not known.

These findings show that absolute receptor subtype selectivity is not to be expected from the melanocortins, and thus that a strategy aiming at targeting one or the other receptor subtype may not be successful or result in severe side or adverse effects. Nevertheless, in the case of MC1R, it was proven that the receptor is overexpressed at the surface of human melanocytes (though only 700-1000 receptors per cell[81] are found), and even more at the surface of human melanoma cells (a few thousands per cell[284]), but these amounts remain quite low compared to MC1R on mouse melanocytes (approximately 10,000 per cell[285]). MC1R is also expressed in numerous other cell types such as keratinocytes, fibroblasts, endothelial cells, sebocytes, Langerhans cells, monocytes, dendritic cells, neutrophils, granulocytes, natural killer cells, osteoclasts and others[255]. However, quantitative comparisons have shown that MC1R mRNA is much lower in non-melanocytic cells. Roberts et al. showed that levels of MC1R mRNA in various cultured human skin cells were at least 11-fold lower than that within melanocytes[254]. Additionally, only the higher amounts found in these studies resulted in clearly detectable protein. Thus, the conclusion can be drawn that MC1R protein in cell types other than melanocytes is not expressed at physiologically relevant levels. This shows that even though MC1R is expressed throughout the body, relevant expression is only found in melanocytes or melanoma cells. In concert with the high and quite specific affinity of MC1R for α-MSH, it is reasonable to think that a targeting strategy mimicking α-MSH would be successful and might be exempt of severe adverse effects.

1.5 Melanoma

1.5.1 Overview of cancer

1.5.1.1 Historical considerations

Cancer

Cancer has plagued all multicellular organisms since the beginning of time. In fact, paleopathologists have found melanotic masses of tissues and diffuse metastases in pre-Colombian Inca mummies being more than 2,400 years old[313]. Indeed, cancer has always proven to be an elusive adversary in the field of medicine. The Greek physician Galen (128-200 A.D.), among others, noted similarities between crabs and some tumors with swollen veins, and called tumors *"karkinos"*, Greek word meaning either crab, tumor or the zodiac constellation. Later, the Roman physician Celsus (28 B.C.-50 A.D.) translated the word *"karkinos"* into *"cancer"*, Latin word with the same meanings.

Oncology

Oncology (from the Greek words *onkos* (mass or tumor), and *logos* (study) is the study of neoplastic diseases. Early authors suggested that certain families, races, and working classes were predisposed to neoplastic transformations. In 1862, Edwin Smith, an American Egyptologist, discovered the apparently earliest recordings of the surgical treatment of cancer. Written in Egypt circa 1600 B.C., this treatise was based on teachings possibly dating back to 3000 B.C. The Egyptian author advised surgeons to contend with tumors that might be cured by surgery but no to treat those lesions that might be fatal.

Hippocrates (460-375 B.C.) was the first to describe the clinical symptoms associated with cancer. He advised against treating terminal patients, who would enjoy a better quality of life without surgical intervention[145]. He also coined the terms carcinoma (crab legs tumor) and sarcoma (fleshy mass). In the second century A.D., Galen published his classification of tumors, describing cancer as a systemic disease caused by an excess of black bile[14]. Galen cautioned that as a systemic disease, cancer was not amenable to cure by surgery, which was often promptly followed by patient death. This strong admonition against surgery persisted for more than 1500 years until in the eighteenth century pathologists discovered that cancer often grew locally before spreading to other anatomic sites[148].

Various other discoveries helped physicians understand underlying cancer mechanisms as well as develop appropriate surgical techniques and anesthesia, but surgical oncology was still associated with high patient mortality rates. The main issue was that cancer was rarely diagnosed early enough. However, several important developments in this era (such as the microscope, gentle tissue handling, meticulous surgical

technique) led to rapid advancements in surgical oncology. Ongoing innovations continue to advance effective surgical primary tumor control linked to improved surgical outcomes and better quality of life. Enhanced biomedical monitoring and the emergence of critical care medicine have made it possible to safely undertake increasingly complicated surgical procedures. A more sophisticated awareness of the patterns of tumor progression have made possible less-invasive surgical approaches (sentinel node biopsy instead of formal lymphadenectomy in early stage breast carcinoma, radiofrequency ablation with ultrasonography guidance, etc.)[148].

1.5.1.2 General pathophysiology of cancer

Cancer is the common term for neoplasms, or tumors, that are malignant. Nearly all cancers are caused by abnormalities in the genetic material of the transformed cells. Tumors arise from a large number of sequential mutations within a cell's genome that are often prompted by cellular or environmental stress (carcinogens like tobacco smoke, radiations, chemicals or infectious agents) on the cells. Complex interactions between carcinogens and the host genome may explain why only some develop cancer after exposure to a known carcinogen. New aspects of the genetics of cancer pathogenesis, such as DNA methylation and microRNAs are increasingly being recognized as important. Simple mutations are common and regular within the genome of any living organism. Several mechanisms are in place to detect and to correct all these mistakes happening during the DNA replication and transcription processes, but once these mechanisms are overcome, the cells may lose their ability to regulate cellular growth and proliferation. In addition, cancer cells, unlike normal cells, lack contact inhibition usually limiting their ability to control growth via intra-cell communication.

A number of key cancer-promoting oncogenes and tumor suppressor genes are present in all cells. These regulate key mechanisms for the cells' survival, such as senescence, cell cycle, or for the programmed cell death. Inherently, these genes serve as gatekeepers to disease progression. If a mutation occurs on an oncogene and for instance permanently activates it, cells may acquire new properties, such as hyperactive growth and division, protection against programmed cell death, loss of respect for normal tissue boundaries, and the ability to become established in diverse tissue environments. If a tumor suppressor gene is inactivated, cells may lose their normal functions, such as accurate DNA replication, control over the cell cycle, orientation and adhesion within tissues, and interaction with protective cells of the immune system. In both cases, cells lose their innate ability to communicate, to autoregulate or to autodestruct, which leads to the formation of tumors.

Cancer is actually more a group of diseases, in which cells are aggressive (grow and divide without respect to normal limits), invasive (invade and destroy adjacent tissues), and/or metastatic (spread to other locations in the body). These three malignant properties of cancers differentiate them from the benign tumors, which are self-limited in their growth and do not invade or metastasize (although some benign tumor types are capable of becoming malignant). Unlike benign tumors, malignant tumors consist of

undifferentiated cells that show an atypical cell structure and do not function like the normal cells of the organ they originate from[148].

Basically, there are more than 100 different types of cancer. The main categories include[216]:

- *Carcinoma*: cancer that begins in the skin or in tissues that line or cover internal organs.
- *Sarcoma*: cancer that begins in bone, cartilage, fat, muscle, blood vessels, or other connective or supportive tissue.
- *Leukemia*: cancer that starts in blood-forming tissue such as the bone marrow and causes large numbers of abnormal blood cells to be produced and enter the blood. Circulating tumor cells.
- *Lymphoma and myeloma*: cancers that begin in the cells of the immune system. Solid tumor state.
- *Central nervous system cancers*: cancers that begin in the tissues of the brain and spinal cord.

Usually the various cancer types are classified according to the tissue from which the cancerous cells originate (location), as well as the normal cell type they most resemble (histology). Histological examination of a tissue biopsy is required to establish a definitive diagnosis, even though initial suspicion of malignancy can come from symptoms or radiographic imaging abnormalities[3].

Once detected, cancer is usually treated with a combination of surgery, chemotherapy and radiotherapy. Some can be cured depending on the type, location and stage. Treatments are also becoming more specific for some types of cancer with the development of targeted therapies acting specifically on molecular defects in certain tumors, thus sparing healthy cells and therefore involving less side effects or toxicity-related limitations.

1.5.1.3 Challenges

The advances in medicine of the last 50 years have had a dramatic impact on most common diseases. However, although those advances have drastically helped increase patients' life span, cancer death rates have remained more or less unchanged, as shown in **Figure 9** below[3]. Three major shortcomings in the field of oncology may be responsible for this issue:

- insufficient detection methods;
- a lack of preventive treatment options;
- relapse of the disease.

There is currently no accurate early screening method for cancer, leaving detection up to the patient in the form of obvious signs of disease, often meaning it is already too late. Improved detection methods would

be very profitable for both early and late stage cancers, as they would allow an earlier treatment start, thereby improving the general prognosis of the patient.
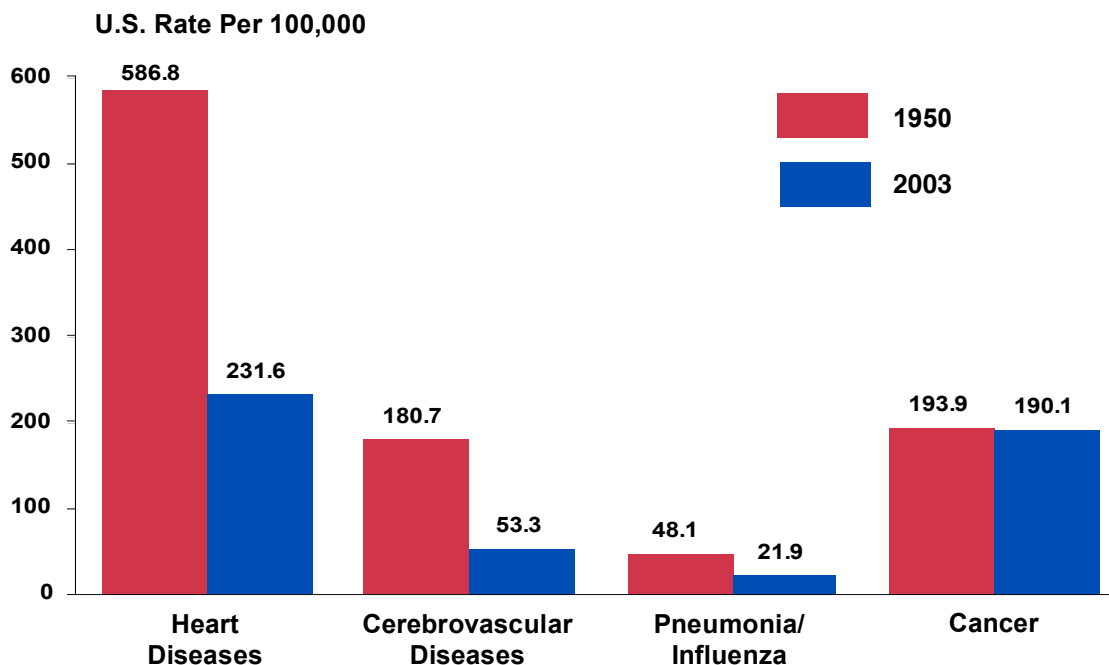
U.S. Rate Per 100,000

Figure 9: U.S. death rates of various diseases per 100'000 inhabitants from 1950 to 2003[3].

Then, there is a lack of preventive treatment options to cut or slow the disease progression from the beginning[294]. Various studies have been conducted concerning natural products and dietary phytochemicals containing anti-oxidative molecules and free radicals scavengers such as plant oils, flavonoids, glutathione, vitamins C and E and various enzymes such as peroxidases. Low levels of antioxidants, or inhibition of the antioxidative enzymes causes oxidative stress and may damage cellular components such as DNA, proteins or lipids[289,317], which may lead to mutagenesis. Although there is no real chemopreventive treatment (such as e.g. atorvastatin against cardiovascular diseases, a drug generating $12 billion per year)[294], some relatively simple preventive habits have though been proven to dramatically lower the incidence of cancer. More than 250 population-based studies, including case-control and cohort studies, show that people eating about five servings of fruits and vegetables a day have approximately half of the risk of developing cancer (particularly cancers of the digestive and respiratory tracts) compared to those eating less than two servings a day. Substances as lycopenes (tomato), catechins (green tea) gingerol (ginger), curcumin (turmeric) and many more are known chemopreventive phytochemicals[299]. The change probably has to happen in the population's dietary habits, as this type of chemoprevention can now be considered to be an inexpensive, readily applicable, acceptable and accessible approach to cancer prevention. Additionally, with healthcare costs being a key issue today,

promotion of the awareness and of the consumption of fruits and vegetables (and thus of phytochemicals) would be a simple and cost-effective measure to deploy[299].

Another major problem to overcome is relapse. Recurrence of disease following primary treatments remains capital for physicians and patients. This recurrence results from disseminated or metastatic cells that have broken off of the primary tumor site and relocated at a distant site. Relapse often occurs after successful treatment of the primary disease, however, cancer finally remains the cause of death.

These are only a few of the numerous obstacles still to be overcome in order to improve the final prognosis for the patient. This work attempts to provide an improved method, based on earlier research in the field of melanoma, for the detection and eventual treatment of malignant melanoma and early metastases, with the hope of eventually meeting some of the challenges set forth by cancer today, specifically that of early detection and detection of potential relapse of disease.

1.5.2 Melanoma

1.5.2.1 Overview and epidemiology

Cutaneous malignant melanoma (CMM) is a tumor derived from transformed genetically altered epidermal melanocytes in the skin, as a result of complex interactions between genetics and environmental factors. It is the most serious type of skin cancer. It is one of the rarer types of skin cancer (4% of skin cancer cases, according to the *American Cancer Society*) but causes the majority of skin cancer-related deaths[232]. It also tends to occur at a younger age than most cancers with half of all melanomas found in people under the age of 57. It is actually the most common malignancy among young adults as well. Its incidence has substantially increased among all Caucasian populations in the last few decades[80]. The number of melanoma cases worldwide is increasing faster than any other cancer. Its incidence rate showed a general increase of 3-7% per year for fair-skinned Caucasian populations, with estimated doubling incidence rates every 10-20 years[119]. Australia is probably the most affected country, with very high incidence rates. In Australia, CMM has become the fourth most common cancer among males and the third most common among females[75]. As shown in **Figure 10**, the lifetime risk of developing malignant melanoma in the U.S.A. has also dramatically increased during the last 70 years[183], probably due to new socio-cultural behaviors such as tanning and the excessive use of solarium booths in order to meet the new beauty standards. The widening gap in the earth's ozone layer might play a big role as well, especially in Australia. It will be interesting to observe if newer findings that the ozone layer gap is slowly stabilizing, and that it may probably recover by 2050[327], will involve a diminution of UV-exposition-related skin cancers.
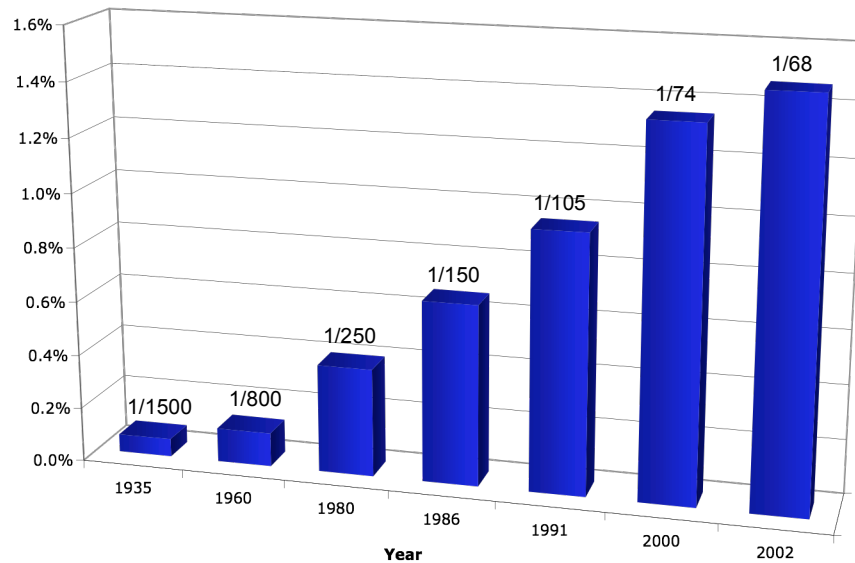
Figure 10: Evolution of the lifetime risk of developing malignant melanoma in the U.S.A. since 1935[183].

Malignant melanoma is the most dangerous type of human skin cancer, as it may be very difficult to detect. Indeed, the lesions are usually very small at the beginning, and approximately 10% of melanomas are *amelanotic*, meaning that they do not produce (or overproduce) melanin and are thus almost invisible. Additionally, their metastasizing potential is really high and they are extremely resistant to current systemic therapies.

1.5.2.2 Etiology

Although the etiology of melanoma is unknown, case-control studies have identified a number of characteristics present in populations presenting the highest risk for melanoma development[83,194]. These studies have shown that melanoma is largely a disease of individuals with fair complexions. Individuals with red or blond hair and fair skin, who usually do not tan well and burn easily even after short exposures, or have a history of severe sunburn, are at substantially higher risk of developing melanoma than more darkly pigmented, age-matched controls. Individuals bearing more nevi or having a tendency to develop freckles are also at increased risk for developing melanoma[194].

A review from Longstreth[188] suggests that ultraviolet light may be a critical factor for the development of cutaneous melanoma. There is an increasing incidence of melanoma in fair-skinned populations and a correlation with increasing distance from the poles. Also, adults migrating to sunny climates are at lower risk of developing melanoma than similar individuals born there, emphasizing the importance of the

duration of exposure to UV radiation. Freckles and nevi are induced by solar exposition and are risk factors for the development of melanoma. Solar radiation induces acute and chronic reactions in both human and animal skin. Chronic and repeated exposures to UV radiation are the major cause of malignant skin tumors, partially including malignant melanoma (not only after cumulative exposure, see below), via gene mutations and immunosuppresion. UVB radiation (290-320 nm), especially, has been reported to be much more mutagenic and carcinogenic in animal experiments than UVA radiation (320-400 nm). DNA damage is mainly caused by UV radiation through mutations in *p53* and *ras*. UVB is also known to upregulate gene expression through intracellular signal transduction pathways contributing to the development of skin cancer at the tumor promotion stage. Furthermore, it is proven that UVB suppresses immune reactions, leading to antigen tolerance. Additionally, indirect stress through DNA repair mechanisms and reactive oxygen species (ROS) such as peroxides and superoxides, mostly formed through UVA exposure, has been discussed and proven[154]. These free radicals can cause damage to cellular proteins, lipids and saccharides.

Observations suggest that sun exposure may not be the only risk factor in the development of melanoma. Indeed, melanoma can occur in relatively unexposed areas of skin, such as the palms and soles. Another observation is that melanoma is not directly related to cumulative sun exposure, as are squamous and basal cell carcinoma. Individuals having an outdoor occupation are less at risk than white-collar workers, confirming findings in animal experiments that the risk of developing melanoma is not only related to the cumulative level of sun exposure, but also to acute, intense and intermittent exposure associated with blistering sunburn[83]. Changes in socio-cultural behaviors of the western populations are also to blame. Indeed, changes in clothing styles and materials, as well as in the recreational habits and in beauty criteria (tanning) have without a doubt contributed to increase melanoma incidence: incidence has dramatically increased on the legs in females and the trunk in males. Additionally, it appears that some forms of malignant melanoma are genetically inheritable. Members of certain families are more susceptible to the development of the genetic abnormalities associated with melanoma. As a result, these family members have an exceedingly high risk of developing melanoma, with around 8 to 12% of all cutaneous melanomas occurring in individuals with familial predisposition. Familial human melanoma is characterized by an increased risk of developing primary melanoma, a higher incidence of multiple primary lesions and an earlier age at onset[193]. Finally, two major types of precursor lesions may increase incidence of melanoma, but they will not be extensively discussed here.

- Dysplastic nevus syndrome (DNS) is a familial form of malignant melanoma distinguished by multiple, large (>5 mm diameter) macular moles with irregular borders and often variable shades of brown, black and red. Melanoma may arise from dysplastic nevi or from apparently normal skin remote from nevi in patients with DNS.
- Congenital nevi are present at birth and usually classified as small or giant congenital nevi, bearing a grossly irregular surface, increased pigmentation in varying shades of brown, and hypertrichosis. Although melanoma may arise *de novo*, it arises in association with congenital nevi at increased frequency, and all congenital nevi should be viewed with suspicion[252].

1.5.2.3 Melanoma classification

Various forms of melanoma can be observed, depending of their different clinical and biological characteristics, and are described by the American Joint Committee on Cancer (AJCC)[6]. There are five distinct kinds:

- Superficial spreading melanoma (SSM): it is the most common form of melanoma, accounting for approximately 70% of all melanomas. SSM generally arises in a preexisting lesion, and usually appears flat with irregular borders. The lesions are generally multicolored with shades of tan, brown, black, red and white. An irregular surface may appear as the lesion grows. SSM usually appears on the head, neck and trunk in males and on the extremities in females throughout adulthood with a peak in the fifth decade of life.

- Lentigo maligna melanoma (LMM): it represents about 10% of all melanomas. It arises from lentigo maligna (melanotic freckle of Hutchinson or precancerous melanosis of Dubreuilh). LMM is most commonly found on sun-exposed skin in elderly patients (median age is 70 years). Lesions are large (3-4 cm in diameter) and flat with irregular borders, in variable shades of tan to dark brown. The invasive melanoma stage generally has a long history of 5-15 years of the precursor lesion (lentigo maligna).

- Nodular malignant melanoma (NM): with 10-15 % of all melanomas, it accounts for the second most common pattern. It is mostly found on the trunk of men, but may arise on any body surface. Biologically, it is thought to be more aggressive than SSM. Dark lesions uniform in color are its major clinical pattern. One particularity is that melanocytic abnormalities in the vicinal epidermis are totally absent, and additionally, around 5% of NM are amelanotic. NM does not go through the radial growth phase, its very rapid evolution leading quickly to vertical growth and invasion of the dermis. For this reason, nodular melanomas tend to be thicker, higher-risk lesions.

- Acral-lentiginous melanoma (ALM): only 3-5% of melanomas are from the ALM type. It usually occurs on the palms, soles and subungual regions, representing a higher proportion of all melanomas in dark-skinned individuals such as African Americans, Asians and Hispanics. Lesions are large (3 cm in diameter) with irregular borders, and generally occurs in older individuals (median age is 59 years). The great toe or thumb are the most concerned by subungual melanoma. ALM often appears as a tan to dark brown macule with an irregular border, but may be ulcerating in more advanced lesions. Its clinical pattern being quite similar to LMM, ALM is though a biologically much more aggressive lesion, with a relatively short evolution to the vertical growth phase.

- Mucosal lentiginous melanoma (MLM): it is similar in appearance to ALM, but occurs on the various mucosae of the body, such as the oral cavity, oesophagus, anus, vagina and conjunctiva.

1.5.2.4 *Melanoma development, progression and staging*

Clinical and histological studies have resulted in defining relatively distinct steps of melanoma development and progression.

- Step 0: normal melanocytes.
- Step 1: common acquired and congenital nevi with structurally normal melanocytes.
- Step 2: dysplastic nevi with structural and architectural atypia.
- Step 3: melanoma in situ and radial growth phase, nontumorigenic primary melanomas without metastatic competence.
- Step 4: vertical growth phase, tumorigenic primary melanomas with competence for metastasis.
- Step 5: metastatic melanoma.

As in any neoplastic system, melanomas can skip steps in their development, appearing without identifiable intermediate lesion. The progression from each stage to the next is strongly associated with specific biological changes, and this staging is based on experimental models and clinical and histopathological observations. The transition from mature melanocytes to the formation of a nevus can be characterized by an interruption of the cross-talk between melanocytes and keratinocytes that leads to loss of control of the keratinocytes on the melanocytes. Thus, cells from a nevus show limited proliferation and cells in common acquired nevi do not have any apparent chromosomal aberration. Nevi can develop not only through stimulatory factors, but through this loss of control as well. Cells then presenting cytological atypia may then separate from the basal membrane without undergoing apoptosis, generating architectural disorders in the lesion and hence transformation of normal melanocytes or common acquired nevi into dysplastic nevi or melanoma with radial growth phase. These radial growth phase melanoma cells have biological properties that are sort of "hybrid" between benign and malignant. Vertical growth phase melanoma cells, therefore, are highly aneuploidic and relatively plastic, some of them being able to acquire metastatic competence. A high level of genetic instability and phenotypic plasticity are the major characteristics of metastatic cells. They are highly motile, independent of growth factors, and capable of invasion of other tissues or organs.

The following illustration (**Figure 11**) depicts and describes melanoma progression:
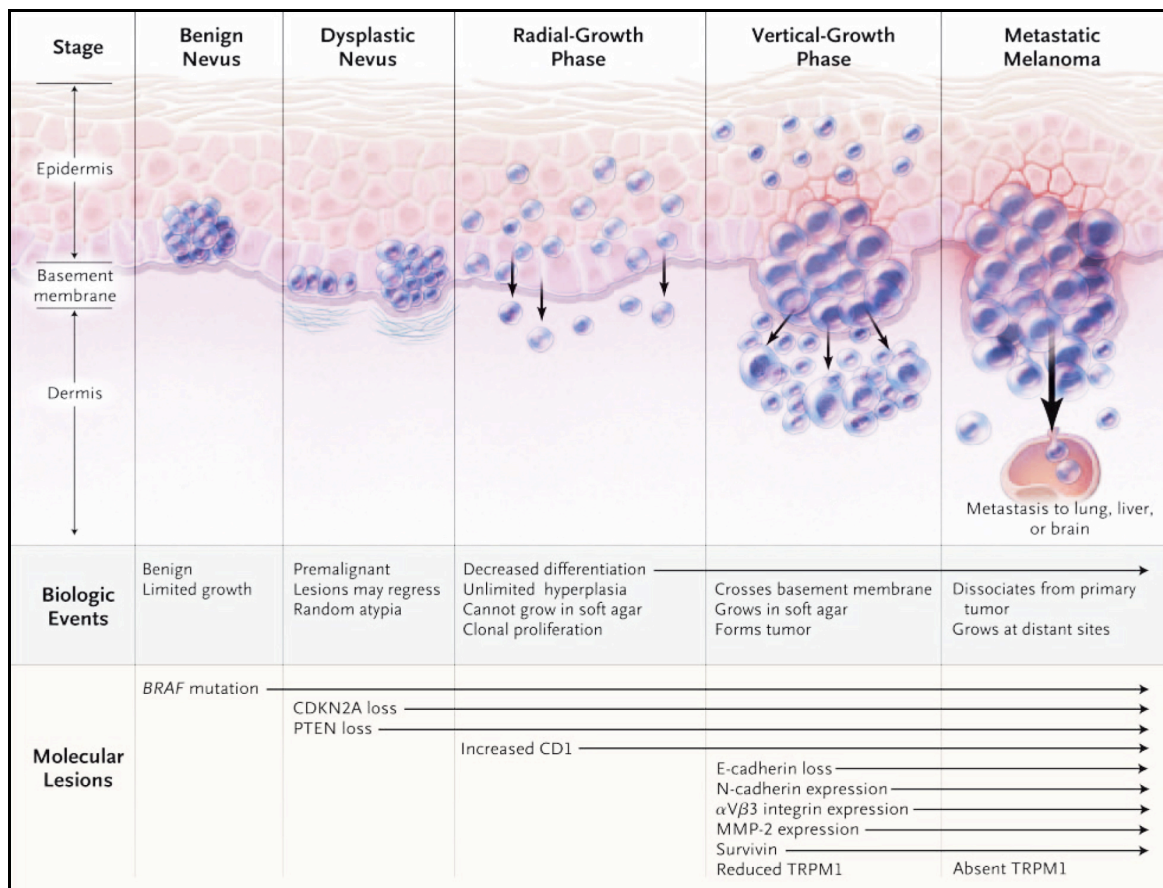
Figure 11: Biologic events and molecular changes in the progression of melanoma[210].

Malignant melanoma usually arises, as previously mentioned, from precursor lesions such as dysplastic nevi, congenital nevi, or simply from cutaneous melanocytes. Melanocytes are usually arranged individually at the epidermal junction or in small organized clusters of benign nevi. Some atypical ones may then proliferate to form atypical nevi. Further proliferation leads to the stage of early melanoma in radial growth phase, which, if it keeps on proliferating, may reach the lower layers of the skin (dermis) and become an invasive melanoma in vertical growth phase. The depth of invasion is usually the major determinant of the prognosis. As it reaches the dermis and thus comes closer to the circulatory system, it may then start to metastasize throughout the body.

A more precise melanoma staging than the one mentioned above has been described by Clark et al.[68] as early as 1969, and although other techniques of melanoma staging are in use (such as "Breslow's microstaging method"[47], measuring the vertical thickness of the primary tumor and being simpler and more reproducible than Clark's method), it gives a precise description of the various stages.

- *Level I*   Tumor cells are located above the basal membrane (*in situ* melanoma, quite rare).
- *Level II*   Neoplastic cells have broken through the basal membrane and spread into the papillary dermis but not into the reticular dermis. An individual cell or a small cell cluster may reach the reticular dermis, but the tumor will stay a level II lesion.
- *Level III*   When cells tend to accumulate at the interface between both papillary and reticular dermal regions, the tumor is classified as level III.
- *Level IV*   Neoplastic cells start to appear between the collagen bundles, which are typical of the reticular dermis.
- *Level V*   Invasion of the tumors cells into the subcutaneous tissues and fat.

Clark mentions in his paper that his definition of level III melanoma is the only level which is different from the ones used by the Australian group from the Queensland Melanoma Project[242]. He writes that a number of melanomas have been observed where the base of the tumor seemed to form almost a straight line and impinge upon the upper part of the reticular dermis without showing any significant invasion of the reticular dermis[68]. Currently, depth of invasion of a vertically growing melanoma is usually determined by both Clark's level and Breslow's thickness, and these both criteria allow to set a prognosis.

The TNM Staging System

The TNM Staging System[6] is another way of staging cancer in general, and counts for one of the most (if not the most) commonly used staging systems. It is also used for melanoma staging. This system was developed and is maintained by the American Joint Committee on Cancer (AJCC) and the International Union Against Cancer (UICC). The TNM classification system was developed as a tool for physicians to allow the staging of different types of cancer based on certain standard criteria. The TNM Staging System is based on the extent of the tumor (T), the extent of spread to the lymph nodes (N), and the presence of metastasis (M).

The T category describes the primary tumor.

TX	Primary tumor cannot be evaluated
T0	No evidence of primary tumor
Tis	Carcinoma in situ (early cancer that has not spread to neighboring tissue)
T1-4	Size and/or extent of the primary tumor

The N category describes whether or not the cancer has reached nearby lymph nodes.

NX	Regional lymph node cannot be evaluated
N0	No regional lymph node involvement (no cancer found in the lymph nodes)
N1-N3	Involvement of regional lymph nodes (number and/or extent of spread)

The M category tells whether there are distant metastases.

MX	Distant metastasis cannot be evaluated
M0	No distant metastasis
M1	Distant metastasis

Each cancer type has its own classification system, letters and numbers not always meaning the same thing for every kind of cancer. Once the T, N, and M are determined, they are combined, and an overall "Stage" of I, II, III, IV is assigned. Sometimes these stages are subdivided as well, using letters such as IIIA and IIIB[6].

1.5.3 Metastases

Metastases are the major reason for relapses in cancer patients and the cause of 90% of cancer-related deaths. Microscopic or clinically evident metastases are present in 60% of cancer patients at the time of primary tumor treatment[54]. They usually are considered as the most advanced form of cancer (end-stage). Although their exact mechanism of formation remains under debate, it is commonly accepted that finding a method able to stop the spread of metastasis would have a dramatic and revolutionary impact on cancer survival rates. The first step involves of course detection of secondary lesions, which remains one of the major issues in this quest. This subchapter describes the general pathways leading to the formation of metastases.

1.5.3.1 Transformation

A whole cascade of sequential events involving multiple host-tumor interactions leading to dissemination is responsible for the metastasizing process[126]. The unregulated growth and eventual loss of mutual adherence of cells presenting multiple abnormalities results in the dissemination of free carcinomic cells. Migration of these cells through the tumor membrane and extra-cellular matrix is favored, as well as their travel to new sites via the lymphatic and/or circulatory systems[126]. By entering the lymphatic systems, they acquire the ability to migrate to the lymph nodes before rejoining the blood stream. Further progression allows for a new focus to undergo neovascularization. However, Chambers[55] affirms that a majority of tumor cells leaving the primary tumor fail to develop metastases. It results in a large number of single disseminated cancer cells in the circulatory system. Chambers noted as well that most of these metastatic cells are not destroyed by the immune system, probably due to a lack of recognition signals and pathways between tumor cells and antibodies.

1.5.3.2 Intravasation and extravasation

Tumor cells have first to lose their mutual adherence capability to initiate the metastasizing process, or they have to break bonds or lose the functionality between cadherins and integrins of the extracellular matrix[54]. Cadherins are transmembrane glycoproteins that mediate calcium-dependent cell-cell adhesion in normal tissue[305]. Integrins are a family of heterodimers (VLA-1 to VLA-6) that serve as receptors for extracellular matrix components including recognition of vascular cell adhesion molecules and cellular communication[153]. Following detachment from the extracellular matrix, neoplastic cells must penetrate the basement membrane and invade the interstitial stroma by active proteolysis. Subsequently, intravasation requires tumor cell invasion of the subendothelial basement membrane. In a similar manner, only reversed,

tumor cell extravasation occurs, allowing the metastatic disease to exit the blood or lymph streams and establish a distant metastatic site.
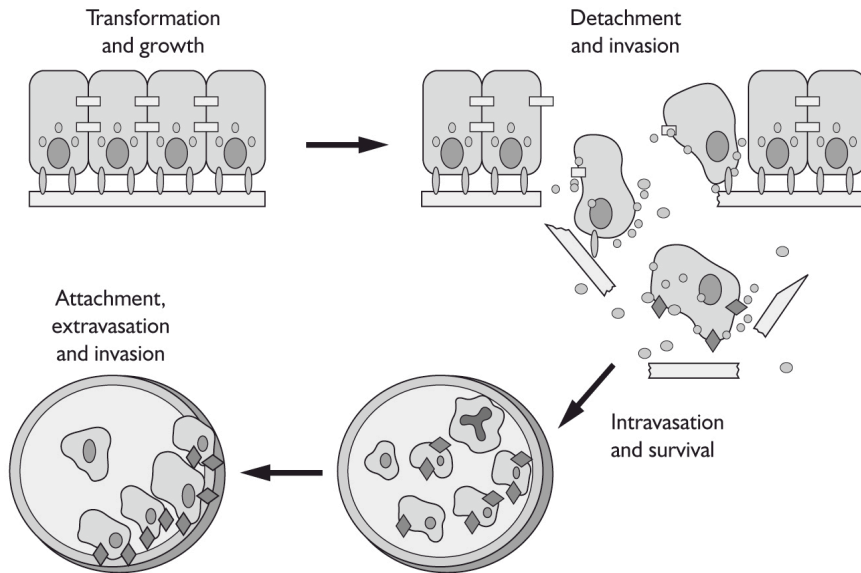

Figure 12: Metastatic process[54].

To initiate the metastatic cascade, neoplastic cells must first penetrate the basement membrane and then invade the interstitial stroma by active proteolysis. Subsequently, intravasation requires tumor cell invasion of the subendothelial basement membrane. To successfully establish a metastatic colony, circulating neoplastic cells must survive immunological surveillance, arrest at a distant vascular step, and extravasate. Finally, cells must invade and proliferate in the secondary organ.

1.5.3.3 Secondary tumor formation

Tumor-induced angiogenesis is associated with the development of a distant secondary tumor site. The angiogenesis process not only allows tumor growth, but also facilitates access to the vascular compartment, thus favoring metastatic spread. Angiogenesis is the process leading to formation of new blood vessels around a solid tumor. Although most human cancers may persist *in situ* for months in a prevascular phase, growth beyond 2-3 mm^3 requires new blood vessel formation[105]. Neovascularization prompts tumor growth by increasing perfusion and supplying nutrients and oxygen. In addition to these events prompting tumor growth, tumor cells are also stimulated in a paracrine fashion by several growth factors produced by capillary endothelial cells. The success rate of the metastasizing process seems to increase with the size of the primary tumor, so that angiogenesis may play an important role in determining cancer spread. Indeed, the degree of angiogenesis has proved to be predictive for metastatic disease in some neoplasms, whereas areas with the highest density of microvessels contains cells that are most likely to metastasize[322]. The process of angiogenesis can be divided, paralleling the tumor cell invasion process:

- Proliferation of endothelial cells;
- Breakdown of the extracellular matrix;
- Migration of endothelial cells.

The induction of this process is mediated by angiogenic factors released by both tumor and host cells and depends on the net balance of positive and negative regulators. The major pro-angiogenic factor is of course the vascular endothelial growth factor (VEGF). It is a regulator of both physiological and pathological neovascularization[54]. These factors and regulators will not be covered in this work.

1.6 Melanoma treatment

As mentioned earlier, the prognosis of malignant melanoma is strongly dependent on the time point, and thus at which stage it was detected. Patients with tumors that were diagnosed early and surgically excised have a high probability of total remission[118,163]. However, although many therapeutical efforts have been achieved, the 5-year survival rate of patients whose disease has spread to the sentinel lymph node is only 54%[163], only 6% for patients with disseminated melanoma, and a median survival of 7.5 months[24]. The biological and clinical aspects of melanoma progression are relatively well defined. Its molecular mechanism, however, is not yet well characterized. Neither are the genetic markers associated to the metastatic process.

High-throughput technologies helped a lot to shed light on previously unknown candidate genes (*WNT5A*, *BRAF*), oncogenes or tumor suppressors (e.g. PTEN, RAS, MYC) that may be involved in melanoma pathogenesis. Although most of them have not been attributed to precise melanoma subtypes or validated as prognostic markers, some correlations have been observed between molecular biology and clinical survival data. For example, the oncogene Akt is a serine/threonine kinase leading to cell cycle progression and proliferation. Inhibition of apoptosis is correlated to this oncogene as well. Interestingly, Akt expression increases with melanoma progression and invasion. Patient survival, implicitly, is inversely correlated with Akt expression, and consequently could serve as independent prognostic marker[72]. However, little consensus currently exists regarding a "standard" therapy, which most likely reflects the low level of activity of all available agents. Agents such as dacarbazine and temozolomide are widely used as monotherapies or combined therapies. A small randomized trial has demonstrated similar response rates for dacarbazine and temozolomide (10-20%)[217].

1.6.1 Excision

Surgery provides the most effective and longest-lasting therapy for melanoma. The type of surgery that is chosen depends on the stage of the melanoma. Primary melanoma (melanoma *in situ* or stage I or II) is treated with surgical excision of the lesion. If the depth of invasion is low and if the surrounding healthy tissue is not invaded, complete removal of the lesion usually leads to complete remission. Stage III primary melanoma with lymph node involvement is treated with surgery to remove the primary melanoma and

lymph nodes in the region of the primary melanoma. This procedure may cure or extend the survival rates. The goal of treatment for metastatic melanoma (stage IV) is to relieve symptoms and prolong life. It does not usually cure the cancer. Therefore, excision is not applicable to stage IV melanoma.

1.6.2 Systemic therapies

There is no standard therapy for the treatment of disseminated melanoma. Patients are treated very differently in various clinical trials or cancer centers. Several therapy strategies have been tried out, such as mono-chemotherapy, poly-chemotherapy, combined therapies with cytokines, or even complex schemes with up to five different drugs. However, real improvement of the patients' survival could not be achieved, and most therapies yielded only temporary clinical responses.

Dacarbazine
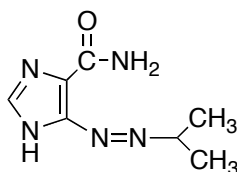
Dacarbazine is one of the drugs that has been tested as monotherapy in several randomized clinical trials and served as reference in most of them. Dacarbazine (also known as DIC or imidazole carboxamide) is an antineoplastic chemotherapeutic drug used in the treatment of various cancers, such as Hodgkin lymphoma or malignant melanoma. Its cytotoxic effect comes from its antineoplastic activity (interferes with cell growth and prevents formation of new (tumor) tissue). Its exact mechanism is not known, but two main hypotheses have been proposed. First, dacarbazine belongs to the family of alkylating agents, which are drugs attaching an alkyl group to DNA. They stop tumor growth by cross-linking guanine nucleobases in DNA double-helix strands. This makes the strands unable to uncoil and separate. Secondly, dacarbazine inhibits DNA synthesis by acting as a purine analog, impairing DNA replication[261]. Both mechanisms blocked by the drug are necessary for DNA replication, and consequently the cells can no longer divide. This drug acts nonspecifically, but as cancerous cells usually proliferate more than normal cells, they are consequently more sensitive to DNA damage[163]. Dacarbazine remains a standard of care in community practice, and has been used as a standard for comparing the efficacy of new regimens.

Temozolomide
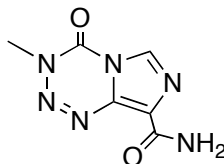
Temozolomide is an imidazotetrazine derivative of dacarbazine and is studied in many trials as first line therapy of melanoma. Temozolomide is a prodrug and is not directly active but undergoes rapid nonenzymatic conversion at physiologic pH to the reactive compound MTIC (3-methyl-(triazen-1-yl)imidazole-4-carboxamide). The cytotoxicity of MTIC is thought to be primarily due to alkylation of DNA. Alkylation (methylation) occurs mainly at the O^6 and N^7 positions of guanine. It is normally indicated in treatment of recurrent glioma, where it demonstrated activity. In a recent randomized trial, concomitant and adjuvant temozolomide chemotherapy with radiation significantly improves progression free survival and overall survival in glioblastoma multiforme patients. Temozolomide is highly genotoxic, teratogenic and foetotoxic[163,261]. The probable mechanism of action of temozolomide is described in **Figure 13**.
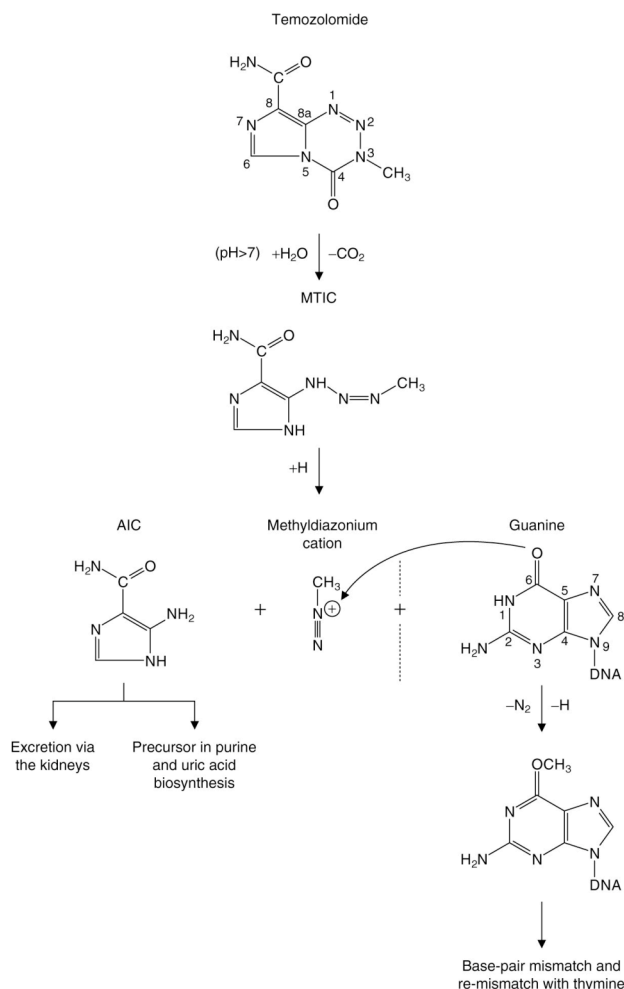

Figure 13: The putative molecular mechanism of action of temozolomide[73].

The first two steps also account for its pH-dependent elimination. Although O^6-guanine methylation accounts for only 5% of the total DNA-adducts formed, this lesion is regarded as the most cytotoxic. **AIC** = 5-aminoimidazole-4-carboxamide; **MTIC** = methyltriazen-1-ylimidazole-4-carboxamide.

Interleukin-2

Interleukin-2 (IL-2) was approved by the Food and Drug Administration (FDA) for treatment of metastatic melanoma in 1998. Physiologically, upon binding to its receptor (IL-2R), IL-2 stimulates the growth, differentiation and survival of antigen-selected cytotoxic T cells via the activation of the expression of specific genes. Synthetic IL-2 can be used in the treatment of melanoma and kidney cancer. Highly dosed intravenous bolus IL-2 treatment resulted in overall objective response rates of about 12-21% in melanoma. IL-2 was able to induce durable complete responses in approximately 6% of patients and partial responses in 10% of patients with metastatic melanoma, albeit with high levels of toxicity[217].

Other systemic therapeutic strategies include chemotherapy, bio-chemotherapy, immune adjuvants, cancer-specific vaccines, cytokines, monoclonal antibodies and immunostimulants. Drugs such as carmustine (antineoplastic alkylating agent), paclitaxel (mitotic inhibitor; works by interfering with normal microtubule growth during cell division by hyperstabilizing the structures of these microtubules) and cisplatin (mitotic inhibitor; works by cross-linking with DNA in different ways, thus interfering with cell division and triggering DNA repair mechanisms, including apoptosis) have shown single-agent activity in metastatic disease[161]. High-dosed IFN-α and high-dosed IL-2 administered together or in addition to temozolomide constitute possible therapy strategies. Curiously, and although only few patients really profit from this strategy (less than 20% in average) in terms of long-term survival, it is the only immunological approach approved by the FDA. Additionally, both drugs show a very toxic profile and are pricy.

These elements really emphasize the need for innovative treatment alternatives. Some of the most promising and viable options investigated at the moment are: antiangiogenic and immunomodulatory drugs, Bcl-2 antisense therapy, B-RAF inhibitors, heat shock protein modulators and anti-cytotoxic T lymphocyte-associated protein 4 (CTLA-4) monoclonal antibody. This list of strategies is of course not comprehensive. It consists of a selection of some of the techniques investigated, and there are other strategies under ongoing investigation.

1.6.2.1 *Antiangiogenic and immunomodulatory drugs*

The antiangiogenic properties of thalidomide were discovered by inadvertence in the 1960s, when severe teratogenicity was reported after children were born with crippled extremities. Indeed, it was found that the drug inhibited blood vessel growth in the foetus. The drug, at that time, had been introduced to treat sleeping disorders (hypnotic effect) and morning sickness in pregnant women (antiemetic effect). Thalidomide is a racemic mixture: it contains both left- and right-handed isomers in equal amounts. In fact, only its (*R*) enantiomer bears these positive effects, its (*S*) enantiomer being teratogenic. At the time it was introduced, this property had not been discovered, as rodent models did not display any drug toxicity (it was not even possible to determine a LD_{50}). However, both enantiomers have the ability to convert into each other *in vivo*, thus not reducing the risk of teratogenicity by administrating only one isoform.
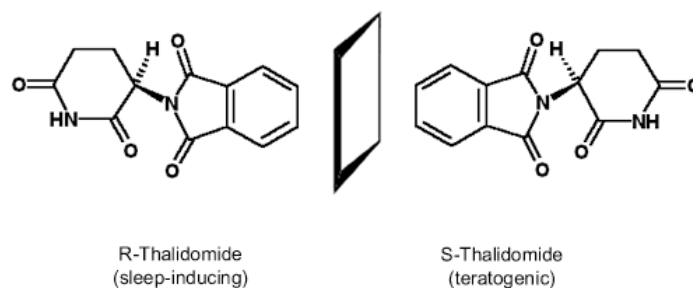
Figure 14: Both enantiomers of thalidomide.

Thalidomide found its renaissance in the 1990s when it was found to inhibit the basic fibroblast growth factor (bFGF) as well as the vascular endothelial growth factor (VEGF)[71]. Additional effects were observed on NF-κB (inhibition), alterations of CD8^{+} and CD4^{+} T cell function, stimulation of cytokine production of IL-2 and IFN-γ[163]. Thalidomide happened to be efficient in multiple myeloma, but less active in solid tumors. Nevertheless, promising results were observed in Kaposi's sarcoma and malignant melanoma. Particularly its combination with the previously mentioned temozolomide proved its efficacy in metastatic melanoma in several clinical studies[163]. New derivatives of thalidomide were recently synthesized and displayed less severe side-effects. Preliminary results show a relatively good efficacy and a diminution of side-effects with lenalidomide (CC-5013), and other results are awaited.

Figure 15: Tumor angiogenesis and its inhibition. From Becker et al.[29].

Angiogenesis depends on the expression of specific mediators such as VEGF, FGF (fibroblast growth factor), interleukin-8, and angiopoietins. Newly formed tumor-related blood vessels sprout into the extracellular matrix (ECM), a process dependent on the ability of proliferating endothelial cells to interact with diverse glycoprotein components of this ECM. This inter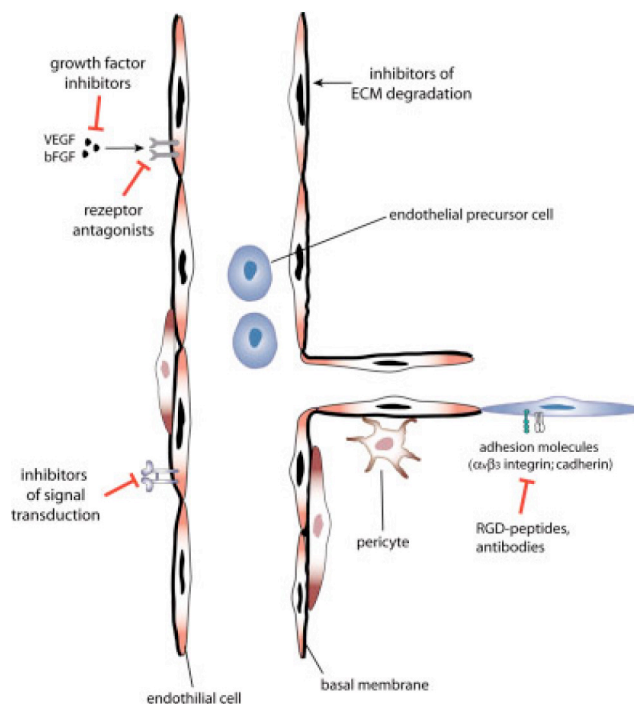action is mediated by endothelial transmembrane receptors or integrins $\alpha_v\beta_3$ and $\alpha_v\beta_5$. Bevacizumab is a humanized antibody against VEGF, and is another drug candidate in the class of antiangiogenic drugs. Several studies are going on at the moment and there are no results available yet. Most investigations are combined therapies with dacarbazine, paclitaxel or INF-α[163].

1.6.2.2 Bcl-2 antisense therapy

The tumor of over 80% of patients with several cancer types (including melanoma) overexpresses the *Bcl-2* gene. It was among the first genes identified in the apoptosis pathway[169]. Oblimersen (G3139, Genasense®, Genta Inc.) is a Bcl-2 antisense compound targeting Bcl-2 mRNA and causing a decrease in Bcl-2 protein translation and production. Down-regulation of Bcl-2 protein and induction of apoptosis could be demonstrated in several preclinical studies[163]. Positive preclinical data gave way to phase I, II and then III studies with dacarbazine and oblimersen, which showed an increase (almost doubling) in the response rate in patients that received concomitant injection of oblimersen versus dacarbazine alone. However, even if the progression-free survival time was longer, overall survival was not affected[163].
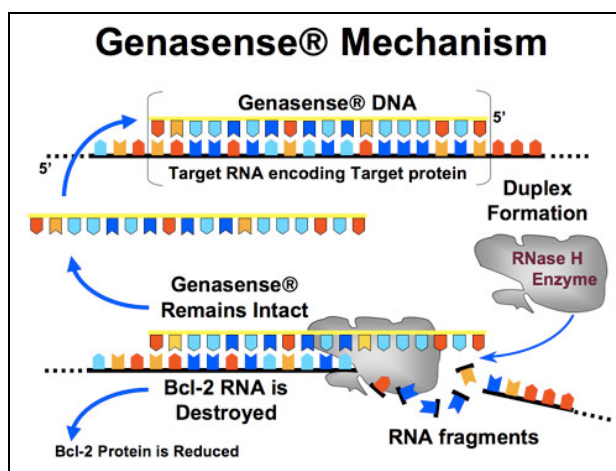

Figure 16: Mechanism of oblimersen (Genasense®). Image from www.genta.com.

1.6.2.3 B-RAF targeting

RAF proteins are a family of serine/threonine-specific protein kinases that form part of a signaling pathway regulating cell proliferation, differentiation and survival. The *ras* gene encodes these kinases. Mutations of the *ras* gene can lead to continuous cell proliferation and inhibition of apoptosis. There are three isoforms (A-RAF, B-RAF and C-RAF), of which B-RAF is mutated in a high proportion (50-70%) of melanomas. A review by Gray-Schopfer et al.[130] describes its role in melanoma very well. B-RAF is apparently an important oncogene in most melanomas, and it plays a major role in the regulation of cellular responses (proliferation, survival and metastasizing). Therefore, B-RAF might be an interesting therapeutic target for melanoma therapy[162,163].
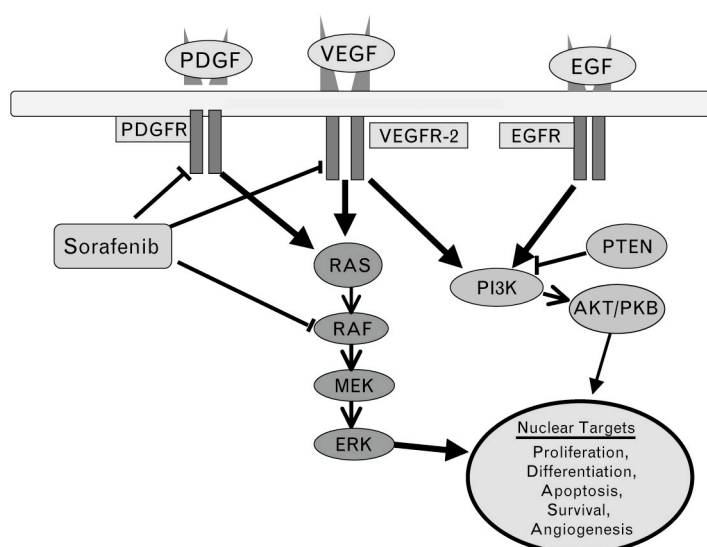
Figure 17: Ras/Raf kinase pathway and inhibition of kinase signaling by sorafenib[134].

Sorafenib (BAY 43-9006, Nexavar®) is a C-RAF and VEGFR inhibitor that also shows activity against oncogenic B-RAF and that was found to induce apoptosis. Several studies showed that sorafenib was active, but only for part of the patients. And most of the responses were only partial. Still, sorafenib helped stabilize the disease without heavy side effects (it only showed skin toxicity and diarrhea). Therefore, new studies (in various phases) with sorafenib in combination with other targeted agents (such as paclitaxel, carboplatin and CCI-779, an mTOR inhibitor) have just started[163]. B-RAF inhibitors may develop into an important therapeutic tool in melanoma, but further effort is needed in order to find more potent and more selective agents[163].

1.6.2.4 Heat shock protein modulators

Heat shock proteins are usually produced in response to physical, chemical or immunological stress, and they are multifunctional. Their abilities range from mediation of apoptosis and regulation of proteasomal destruction to binding to other proteins and various immunological properties. HspPC-96 is a protein peptide complex consisting of a 96 kDa heat shock protein (HSP), gp96, and an array of gp96-associated cellular peptides. Immunization with HspPC-96 induces T-cell specific immunity against these peptides; gp96 is not immunogenic per se. It has demonstrated positive preclinical melanoma-specific T cell-mediated reactions. It shows low toxicity and is therefore relatively well tolerated. Several studies using a combination of HspPC-96 with other agents such as granulocyte macrophage colony-stimulating factor (GM-CSF) and INF-α have shown interesting rates of stabilized diseases (18-29%). Results from a study with patients being treated with HspPC-96 versus "physicians' choice" including IL-2 and/or chemotherapy are awaited[163].

1.6.2.5 Cytotoxic T lymphocyte-associated protein 4 (CTLA-4) inhibition

The immune system is able to recognize and react to various targets and antigens, but has also developed tolerances with the time regarding autoimmunity. Indeed, it usually does not respond to self-antigens. But unfortunately, many tumor cells express self-antigens, preventing them of being correctly and effectively eliminated by the immune system[161,163].

CTLA-4 is one of the proteins that induces tolerance and down regulation of immune responses to tumor antigens. It is produced by suppressor cells called T regulatory cells. CTLA-4 inhibits T cell responses in an ongoing immune response. Blockade of CTLA-4 by antibody was shown to enhance T cell response and to help reject established tumors in mouse models. Additionally, a combined therapy with a tumor vaccine has been shown to enhance antitumor responses, though with a concomitant induction of autoimmunity. Therefore, various antibodies have been developed and are or have been tested in clinical trials in humans[161]. The results from some of the completed studies showed that various monoclonal antibodies against CTLA-4 were able to induce an immune response, in various extents though. Again, as with other therapy strategies mentioned earlier, combination therapies were more efficient, or at least led to higher response rates. However, some severe autoimmune responses have also been observed, which could be a limiting factor in the therapy. Among around 10 ongoing clinical trials, several are large phase III studies aimed at studying efficacy, drug safety and toxicity. Further developments in drugs leading to CTLA-4 blockade are awaited and will focus on clinical efficacy and on the reduction of the side effects[161,163].

1.6.2.6 Targeting of the vasculogenic mimicry

Tumors are able to call up a strategy different from the VEGF pathway to ensure their blood supply. They engage in a sort of vasculogenic mimicry requiring the synergistic effects of laminin 5 (Ln-5) γ2 chain and matrix metalloproteinases (MMPs) MMP-2 and membrane type 1 (MT1)-MMP. Highly aggressive melanoma cells have the ability to use this strategy to induce vasculogenic mimicry in poorly aggressive tumor cells, thus affecting the whole tumor microenvironment. Moreover, generation of Ln-5 γ2 chain promigratory fragments by MMP-2 and MT1-MMP proteolysis is necessary for an aggressive tumor cell-preconditioned matrix to induce this vasculogenic mimicry. These persisting modifications (even after removal or destruction of the tumor) of the tumor microenvironment are not taken into account by most treatment strategies, usually targeting aggressive tumor cells only, and may lead to a recurrence of the tumor. Therapeutic strategies that target endothelial cells have no effect on tumor cells that engage in vasculogenic mimicry (VM). Indeed, anginex (betapep-25), TNP-470 and endostatin were effective angiogenesis inhibitors against endothelial cells but not against aggressive melanoma tumor cells with VM. VM-targeting strategies include suppressing tyrosine kinase activity and using a knockout EphA2 gene, downregulating VE-cadherin, using antibodies against human MMPs and the laminin 5 γ2-chain, and using anti-PI3K therapy[335]. Some researchers focus on the extracellular matrix, which is involved in VM formation. It has been demonstrated that a purified anti-laminin antibody is able to inhibit channel formation by tumor cells[266].

Another interesting strategy involves tetracycline derivatives. Tetracyclines are a group of broad-spectrum antibiotics inhibiting cell growth by inhibiting translation. They bind to the 16S part of the 30S ribosomal subunit and prevent the amino-acyl tRNA from binding to the A site of the ribosome. Their general usefulness has been reduced with the onset of bacterial resistance. Despite this, they remain the treatment of choice for some specific indications. Seftor et al. showed that the addition of a chemically modified tetracycline (CMT-3; COL-3) to a three-dimensional culture of aggressive metastatic melanoma cells inhibited MMP activity, and thus the vasculogenic mimicry as well as the vasculogenic mimicry-associated genes in these cells. Additionally, it also inhibited the induction of vasculogenic mimicry in poorly aggressive cells seeded onto an aggressive cell-preconditioned matrix[277]. Another study in a murine B16 melanoma model by Sun et al. showed as well lower vasculogenic mimicry and a diminution of the expression levels of MMP-2 and MMP-9 after treatment with doxycyclin. A partial suppression of the tumor growth was also observed[297].

1.6.2.7 Adoptive T-cell therapy

Adoptive T-cell therapy is an immune-based therapeutic strategy significantly boosting tumor-specific T-cell immunity above that observed by vaccination alone[57]. It involves the *ex vivo* selection and expansion of

antigen-specific T-cell clones, and is a way of augmenting the antigen-specific immunity without the *in vivo* constraints linked to vaccine-based strategies. The identification of T-cell-defined tumor antigens in melanoma has led to clinical trials targeting cancer cells. The immunogenic potential of antigens in the vaccination strategy has been used to induce T-cell responses. Adoptive cellular therapy, in which antigen-specific T-cells are isolated and expanded *ex vivo* and then infused to increase the number of effector cells *in vivo*, has also been used to trigger an immune response. Unfortunately, most responses were low or undetectable, and clinical responses were consequently low as well. Thanks to the adoptive T-cell therapy, a higher load of T-cells in circulation was reached than with normal immunization treatments[333].

The major advantages of using CD8^{+} T-cells for adoptive therapy are their ability to specifically target tumor cells through the recognition of specific tumor proteins on the cell surface, and their long clonal life span. Moreover, T-cells are well suited for genetic manipulations, which have enabled the evaluation of genetically enhanced or retargeted T-cells in pilot clinical trials for cancer as well as other diseases[160].
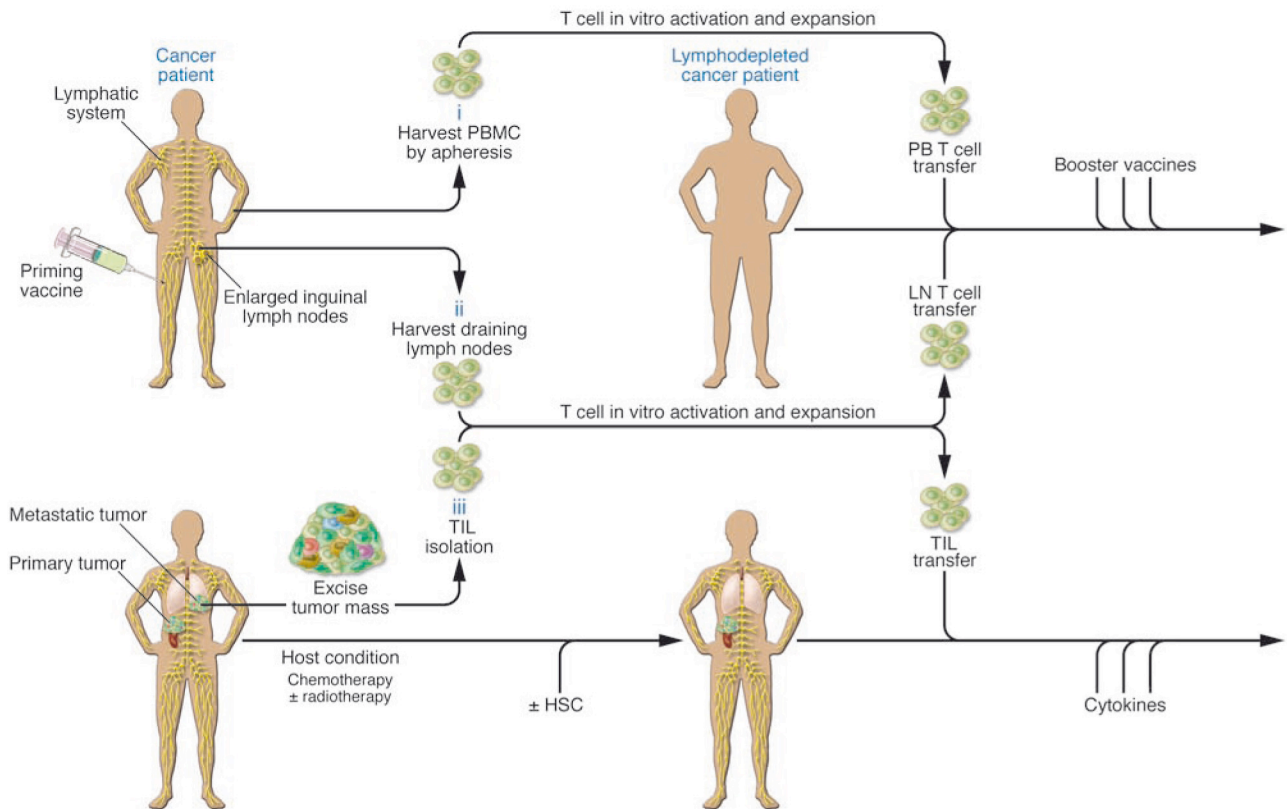
Figure 18: Schemes for adoptive transfer of autologous, vaccine-primed, *in vitro* expanded T cells[160].

Patients are primed with tumor vaccine followed by lymphocyte harvest. Autologous T cells are harvested from peripheral blood (i) or draining lymph nodes (ii), undergo polyclonal *in vitro* activation and expansion, and are reinfused after lymphodepleting chemotherapy. Antigen-specific immune function is measured after the administration of booster vaccines. (iii) TILs can be isolated from resected surgical specimens and expanded *in vitro* for adoptive transfer after lymphodepleting chemotherapy. Most adoptive transfer therapy approaches using TILs have involved the use of IL-2 infusion following T cell transfer in order to select tumor-specific T cells.

T cells engineered to express suicide molecules

Severe graft-versus-host diseases (GVHD) represent a frequent complication of allogeneic immunotherapy and donor lymphocyte infusion (DLI). The interest to develop T cells with an inducible suicide phenotype was raised by promising results obtained with DLI. This approach was proven viable by engineered T cells expressing herpes simplex virus thymidine kinase (HSV-TK). It was shown that the transduced cells could be ablated by administration of aciclovir or ganciclovir[143]. This strategy has been used in clinical trials and its efficiency is now proven, even inducing total remissions in a significant number of patients. Severe GVHD could also be avoided thanks to administration of ganciclovir. These advances even allowed the planning of a phase III clinical trial. An excellent review by C.H. June describes these strategies in more detail[160].

Unfortunately, HSV-TK has been shown to generate potent HSV-TK-specific immune responses, leading to the elimination of the adoptively transferred T cells despite administration of ganciclovir. HSV-TK might confer immunogenicity to the transfused cells, their survival being strongly affected and excluding any retreatment eventuality in case of cancer relapse. New approaches using suicide switches expected to be nonimmunogenic, because of their endogenous base, are under investigation[160].

T cells engineered to express tumor antigen–specific receptors

The poor antigenicity of tumors leads to a major limitation of adoptive T-cell therapy. Two strategies are under investigation and even tested in the clinic to try to circumvent the problem. The first provides T cells with novel receptors by introduction of "T bodies", chimeric receptors that have antibody-based external receptor structures and cytosolic domains that encode signal transduction modules of the T-cell receptor[160]. However, most studies showed that even though the approach was safe for the patient, its major issue was the poor persistence of the T cells in the body. A technical challenge is now proposed to reduce the host immune response causing the elimination of the adoptively transferred T cells.

T cells engineered for enhanced survival

The low short-term persistence of the CTLs in the host without Th cells (helper cells) and/or cytokine infusion is a limitation in adoptive T-cell therapy. One group has transduced human CTLs with chimeric granulocyte colony stimulating factor (GM-CSF)-IL-2 receptors delivering an IL-2 signal upon binding GM-CSF. This modification has the potential to extend the circulating half-life of CTLs, as their stimulation with antigens caused GM-CSF secretion and resulted in an autocrine growth loop allowing CTL clones to grow even in the absence of cytokines[97,160].

The future of the adoptive therapy with engineered T cells is promising. Indeed, new cell culture and gene transfer techniques provide new tools for further developments. For instance, retroviral vectors lead to high-level expression of transgenes, but the upcoming challenge will be the silencing of their expression (for their usability in long-term therapies). The efficiency of human T-cell engineering was dramatically increased by the evolution of lentiviral vectors, and various preclinical test show that they are less prone to insertional mutagenesis, thus minimizing safety concerns with this type of vectors. Nevertheless, long-term

observational studies with larger data sets about patient safety are required to assess real safety issues. Finally, as mentioned by June is his review[160], "a primary issue that could limit the ultimate safety of the approach is the immunogenicity of the proteins that the T cells are engineered to express; this is likely to be a larger problem in humans than in mice because activated human T cells, unlike mouse T cells, express MHC class II molecules and have been shown to function as effective antigen-presenting cells."

1.7 Targeting methods under development

Selective localization of chemotherapeutic compounds at tumor sites is crucial in cancer research, given the usually high cytotoxicity of drugs used in cancer treatment. The concept of tumor targeting is fundamental in order to reduce or exclude severe side-effects. Indeed, large quantities of drugs are usually required to kill a sufficient number of tumor cells, and thus to reach and preserve complete remission. These drugs are generally targeted at rapidly proliferating tumor cells, but physiologically proliferating non-malignant cells can obviously be affected. Therefore, modern anti-cancer research aims at developing more selective chemotherapeutics. However, the development of a drug bearing both cytotoxicity and tumor selectivity properties in a single molecule is very difficult to reach.

A whole variety of new entities called vehicles has therefore been developed, such as antibodies, peptides, globular proteins, small organic molecules or even polymers. The tumor physiology allows different targeting strategies through properties shared by all cancerous cells, or by properties shared within the specific types of cancers. The approach is modular, as typically two molecules with different functions are linked together, allowing different combinations in the case of a very specific "carrier"-molecule for instance. Moreover, these agents can be deployed both for diagnosis and for therapy. Some of these techniques are described below.

1.7.1 Paclitaxel encapsulated in cationic liposomes

Paclitaxel was discovered in a National Cancer Institute program at the Research Triangle Institute in 1967 when Monroe E. Wall and Mansukh C. Wani isolated it from the bark of the pacific yew tree, *Taxus brevifolia,* and named it "taxol". Paclitaxel (Taxol®; commercialized under this name by Bristol-Myers Squibb), as mentioned earlier, interferes with the normal function of microtubule growth. It stops their function by hyperstabilizing their structure. The cell loses then the flexibility of its cytoskeleton. Paclitaxel binds to the β-subunit of tubulin, and the resulting microtubule/paclitaxel complex does not disassemble. Cell function is then impaired because the dynamic instability necessary for the transport of other cellular components (such as chromosome positioning during mitosis) is not available anymore[172]. Additionally, paclitaxel seems to induce apoptosis in cancer cells by binding to Bcl-2 (B-cell leukemia 2), a proto-

oncogene known to prolong cellular viability and to antagonize apoptosis[279]. The highly lipophilic properties of paclitaxel create a real galenical problem. Commercially available injection formulations of the drug in Cremophor EL® (a non-ionic solubilizer and emulsifier used in aqueous preparations of hydrophobic substances) and dehydrated alcohol lead to severe side-effects, as well as difficult handling (Cremophor EL® interacts with PVC containers)[1].

This issue was addressed by encapsulating paclitaxel in liposomes, thus providing a carrier until the site of action. However, a generally rapid clearance of the liposomes by cells of the reticuloendothelial system (primarily monocytes and macrophages that accumulate in the lymph nodes and the spleen)[164,238] is a major drawback.
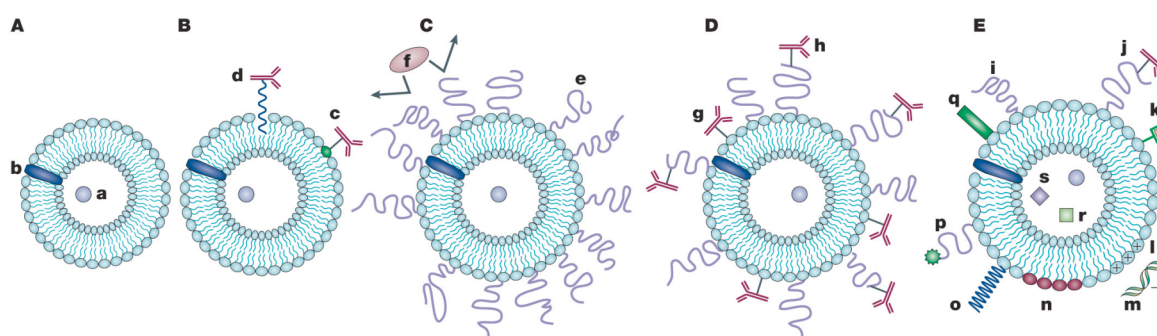

Figure 19: Evolution of liposomes[309].

AI Early traditional phospholipids 'plain' liposomes with water soluble drug (**a**) entrapped into the aqueous liposome interior, and water-insoluble drug (**b**) incorporated into the liposomal membrane (these designations are not repeated on other figures). **B**I Antibody-targeted immunoliposome with antibody covalently coupled (**c**) to the reactive phospholipids in the membrane, or hydrophobically anchored (**d**) into the liposomal membrane after preliminary modification with a hydrophobic moiety. **C**I Long-circulating liposome grafted with a protective polymer (**e**) such as PEG, which shields the liposome surface from the interaction with opsonizing (*making cells more susceptible to the action of phagocytes*) proteins (**f**). **D**I Long-circulating immunoliposome simultaneously bearing both protective polymer and antibody, which can be attached to the liposome surface (**g**) or, preferably, to the distal end of the grafted polymeric chain (**h**). **E**I New-generation liposome, the surface of which can be modified (separately or simultaneously) by different ways. Among these modifications are: the attachment of protective polymer (**i**) or protective polymer and targeting ligand, such as antibody (**j**); the attachment/incorporation of the diagnostic label (**k**); the incorporation of positively charged lipids (**l**) allowing for the complexation with DNA (**m**); the incorporation of stimuli-sensitive lipids (**n**); the attachment of stimuli-sensitive polymer (**o**); the attachment of cell-penetrating peptide (**p**); the incorporation of viral components (**q**). In addition to a drug, liposome can be loaded with magnetic particles (**r**) for magnetic targeting and/or with colloidal gold or silver particles (**s**) for electron microscopy.

Cationic liposomes are able to escape this degradation and are enriched within vessel walls. Additionally, angiogenic endothelial cells show an improved uptake of cationic liposomes compared to normal endothelial cells. A study by Kunstfeld et al.[174] showed that paclitaxel encapsulated in cationic liposomes prevents tumor angiogenesis and melanoma growth, whereas paclitaxel in Cremophor EL® does not, although their *in vivo* antiproliferative effect was comparable. Further studies by Schmitt-Sody et al.[272] showed an interesting retardation in tumor growth with paclitaxel encapsulated in cationic liposomes, compared to placebo, Taxol® (paclitaxel solubilized in Cremophor EL®) or unloaded liposomes. Moreover, the appearance of regional lymph node metastases was significantly delayed by the treatment.

A further development of the liposomal vehicle was achieved with paclitaxel-loaded PEGylated immunoliposomes. Immunoliposomes are liposomes designed to actively target solid tumors by virtue of the monoclonal or polyclonal antibodies attached to their surface. The ability of immunoliposomes to target tumor cells overcomes many limitations of conventional liposomal formulations and provides a novel strategy for tumor-targeted drug delivery. PEGylated immunoliposomes are stabilized with PEG, and thus show an increased circulation time. Therefore, the drug itself is able to circulate a longer time in the blood, increasing its potential efficacy. In addition, the selectivity provided by the antibody can increase the therapeutic index of an encapsulated drug by promoting selective delivery to cells overexpressing a receptor. An excellent review by Torchilin[309] describes new technologies and strategies used for liposomal vectors.

1.7.2 RGD-liganded carriers

The metastasizing ability of a tumor is due to a cascade of events in the cells themselves, but on a more macroscopic level as well. Indeed, other cascades are involved in the spreading of the cancer cells throughout the body. As mentioned in **1.5.3**, this suite of events includes detachment and intravasation of tumor cells from primary tumors (or from existent metastases), adhesion to and invasion of the endothelium and subendothelial regions of the target organ, and neoplastic growth at the new location. It was found out that opportune interferences in these cascades could be favorable to fight the metastasizing process. Selectins and integrins, as adhesion molecules, play a central role in the adhesion process and in the invasion process through basement membranes or the extracellular matrix. Additionally, a major component of the extracellular matrix, fibronectin, is known to contribute to adhesion and invasion as ligand for several integrins[175].

Pierschbacher and Ruoslathi discovered the arginine-glycine-aspartic acid (RGD) cell attachment site in fibronectin in 1984[236], but at that time probably did not expect such a short sequence to be a crucial recognition pattern for cells and proteins. RGD-recognition sites were reported in other extracellular matrix proteins as well. Moreover, RGD pattern-recognition is also used by viruses and bacteria to gain entry into host cells, and RGD-motifs have been found in snake venoms, enabling interference with blood coagulation[306]. Therefore, angiogenesis-associated integrin $\alpha_v\beta_3$, for instance, represents an attractive target for therapeutic intervention because it becomes highly upregulated on angiogenic endothelium and plays an important role in the survival of endothelial cells. These discoveries helped to figure out a possible exploitation of this RGD/integrin system to target cells and contribute to internalization of drug carriers. Synthetic molecules, including peptides based on the RGD sequence may inhibit adhesion and invasion of tumor cells and hinder the metastasizing process. However, as many peptide derivatives, they undergo rapid hydrolysis *in vivo* and, as a result, their circulation time is quite short due to rapid renal and hepatic metabolization. Various strategies have been tried out to circumvent the problem, including cyclization of the peptides (conferring rigidity and stability to the structure), insertion of non-natural amino-acids (D-amino

acids in particular, or peptidomimetics), macromolecules such as polymers, or therapeutic proteins equipped with RGD-motifs, and these modifications yielded increased specificity and affinity[306]. Finally, some specific systems have been developed, such as liposomes, nanoparticles or non-viral gene vectors, and even adenoviral vectors, and have been equipped with RGD mostly via extended PEG tethers, to prevent unwanted interactions with non-target cells.

RGD-liganded liposomes

One of the most interesting techniques is the RGD-liganded liposome. They have been shown to impair metastasizing on B16BL6 murine melanoma cells. Liposomes can carry thousands of RGD or RGD-related peptides on one macroscopic particle, and they are more resistant in the blood stream. Oku et al. synthesized such derivatives by grafting hydrophobic molecules onto RGD-related peptides and incorporating the resulting RGD analogs into liposomal membranes. They were successful in suppressing lung colonization of B16BL6 melanoma cells in both experimental and spontaneous tumor metastases[223].

It is suspected that RGD-related peptides incorporated into liposomal membranes bind strongly to metastatic cells by cooperative binding mediated by RGD molecules exposed on the surface of liposomes. There is no effect on primary melanoma, indicating that the suppression of metastases is not due to direct toxicity against tumor cells[175].

Phage display technology

Phage display allows the presentation of large peptide and protein libraries on the surface of filamentous phage, which leads to the selection of peptides and proteins, including antibodies, with high affinity and specificity to almost any target. The technology involves the introduction of exogenous peptide sequences into a location in the genome of the phage capsid proteins. The encoded peptides are expressed or "displayed" on the phage surface as a fusion product with one of the phage coat proteins. In this way, instead of having to genetically engineer different proteins or peptides one at a time and then express, purify, and analyze each variant, phage display libraries containing up to 10^{10} variants can be constructed simultaneously[15].

An application of this technique has shown good potency of its "expressed" ligand. A cyclic structure containing two disulfide bonds (ACDCRGDCFCG), called RGD4C and binding avidly to $\alpha_V\beta_1$ integrin, was much more potent than commonly used peptides at inhibiting cell attachment to fibronectin. RGD4C has then been exploited as targeting ligand for the delivery of cytostatic drugs. Several other RGD peptidomimetics have been reported with further improved binding to α_v integrins, but only few have been exploited for targeting or diagnostics. This is partly due to the fact that they lack groups suitable for the coupling of drug or drug carriers. Likely, peptidomimetics will be applied more often as targeting moiety, thanks to their excellent binding properties and their stability.

Figure 20: Phage structure[15].

Phage structure. PIII, pVI, pVII, pVIII and pXIX represent phage proteins. Exogenous peptides are expressed or "displayed" usually on pIII or pVIII.

RGD-liganded monoclonal antibodies

Another interesting α_v-integrins targeting approach is the coupling of RGD-related peptides to monoclonal antibodies. Their major advantage is also a prolonged circulation time *in vivo*. This effect could be observed for humanized monoclonal antibodies (HuMAb) coupled to cyclic RGD peptides (e.g. cRGDfK). HuMAb enables the coupling of multiple RGD-related peptides, and consequently increases their affinity to α_v-integrins compared to free peptides. As well, the size of such a macromolecular construct allows the coupling of other molecules along the peptide backbone, such as therapeutic agents. This conjugation may reduce the toxicity some drugs exhibit in free form. Immunohistochemistry, though, showed localization of the peptide not only in the endothelial cells, but also in the liver and the spleen, which could possibly lead to side effects in a long-term therapy. Nevertheless, the construct is apparently internalized and degraded via a lysosomal pathway, although this internalization was only shown in primary human umbilical vein endothelial cells (HUVEC) and not in tumor cells.

Only some of the major developments of RGD-derived carriers have been described here. Nevertheless, they show that carrier systems like liposomes, nanoparticles, proteins and other polymers bearing multiple RGD-peptides are more likely to be internalized via receptor-mediated endocytosis than single peptide constructs. Several other common advantages are attributable to RGD-equipped macromolecular carriers even though they represent a diverse group.

These kinds of carriers have some major interesting advantages over single peptide constructs. First, there is an inhibition of the renal filtration because of the high molecular size of the carrier, thus preventing glomerular filtration. This may lead to longer circulation times and extended presentation of the ligand to the target receptor (but also to a higher toxicity due to the delay in excretion). Secondly, the drugs are mostly protected by their carrier against the "destructive" action of enzymes present in the blood stream or in some tissues. Finally, the high molecular weight of most carriers leads to passive retention in a tumor, via the so-called enhanced permeability and retention (EPR) phenomenon. For example, RGD4C-equipped polymers accumulated in the course of 3 days, while radioactivity in other organs decreased, resulting in a 50:1 tumor:blood ratio at day 3. The control polymer without RGD-targeting motif accumulated in the tumor to a lesser extent, demonstrating the contribution of RGD-mediated targeting to the EPR effect[306].

1.7.3 DNA vaccines against VEGF receptor 2 (also called FLK-1)

Angiogenesis plays a central role in various processes of solid tumor progression, including invasion, growth and metastasizing. Angiogenesis can even be seen as a rate-limiting step in tumor growth. Indeed, tumor growth is generally limited to 1-2 mm^3 in the case of a missing vasculature or neovasculature. The inhibition of tumor growth by attacking the tumor's vascular supply provides obviously a primary target for anti-angiogenic intervention, and offers several advantages. Firstly, the inhibition of tumor neoangiogenesis is a physiological mechanism inherent to the host, and thus should not trigger the development of resistance. Then, hundreds of tumor cells are supplied by each capillary, and targeting the vascular system of the tumor potentiates the antitumor effect. Thirdly, efficiency of the therapeutic agents is increased by the direct contact of the vasculature with the blood stream[218].

The vascular endothelial growth factor receptor 2 (VEGFR2 or FLK-1) is a receptor binding five isomers of murine VEGF. Its expression on endothelial cells is restricted but it is upregulated in case these cells proliferate during angiogenesis in the tumor vasculature. It is necessary for tumor angiogenesis, and therefore plays a determinant role in tumor growth (as mentioned earlier), invasion and metastasis, making it a very interesting therapeutic target[192,218,336].

1.7.4 Salmonella delivery system

As mentioned earlier for VEGF, live attenuated *Salmonella* strains constitute an interesting delivery system for heterologous antigens implicated in the construction of DNA vaccines, and allow stable and regulated expression of the foreign antigen in the host cell. Indeed, upon penetration of the bacteria in the cell, plasmid-encoding antigens under eukaryotic promoters may be transferred to the host cell, resulting in expression of the foreign antigen by the host cell[228]. The preference of *Salmonella* for macrophages and

dendritic cells allowed live bacteria to be used to target immunomodulatory molecules to antigen-presenting cells, thus providing an effective way to modulate immune responses[259].

More recently, *Salmonella* strains have been used as vectors for the delivery of cytokine-encoding plasmids, and their immunomodulatory effects were studied in experimental models. For instance, they are able to influence the immune response against the Frag C antigen (fragment C of tetanus toxin) or the specific immune response elicited during a parasitic infection (*Echinococcus granulosus*). The cytokines used in these studies were interleukin-4 (IL-4) and IL-18[259]. Both of them being known to have antitumoral activities, they have been used in experiments aiming at evaluating their efficacy as oral gene therapy for cancer in a melanoma mouse model. Cytokine-encoding plasmids were introduced into *Salmonella enterica* serovar Typhi (*S.* Typhi) or serovar Typhimurium (*S.* Typhimurium), and the recombinant strains were administered to mice by mucosal or systemic route. The results showed that delivery of DNA-encoding cytokines to the immune system was successful, and that the cytokines markedly influenced the host's immune response[259]. Recent work from the same group showed extended survival time of mice carrying subcutaneous melanoma, as well as higher levels of IFN-γ, in experiments with orally administered single doses of *Salmonella* carrying various cytokine-encoding plasmids[5].

1.7.5 Peptides and peptidomimetics, and their radioactive derivatives

As mentioned earlier, surgery is the major treatment modality for primary tumors and large metastases. Chemotherapy, which is used for disseminated tumors and has curative effects in cases of lymphomas, testicular tumors and tumors in pediatrics, yields poor results in the treatment of melanoma. There is currently no curative treatment against other large groups of tumors, such as breast, prostate, colorectal, lung and ovarian tumors, and many more. Only a palliative effect can be achieved with chemotherapy in these fields. Therefore, it is necessary that new treatment modalities are developed to complete surgical and chemotherapeutical treatments. Radionuclide therapy is one of them, but for radionuclide therapy to be an interesting complement or alternative, it is necessary that disseminated tumor cells and small metastases are targeted and eradicated. Peptides and peptidomimetics are excellent candidates for the targeting of specific cell types. Indeed, most of their properties have revealed interesting applications in the drug discovery field[91].

- They usually are or mimic native ligands that target the cells in a mostly receptor-mediated way, thus allowing to apply whole or partial sequences found out by the nature and therefore to simplify the process.
- They offer the availability of infinite combinations of amino acids, thus providing a great amount of possible variations in their sequence. This property is especially interesting, as it relies on simple synthesis (thanks to the solid-phase synthesis approach) and the use of

amino acid sequence variations in high-throughput screening (HTS) systems, now widely established in pharmaceutical companies.

- They offer the possibility to replace only one amino acid, leading to interesting and systematic structure-activity relationship studies.

- One or more amino acids can be replaced by non-natural amino acids providing peptidase resistance, rigidity and general *in vivo* stability, or even derivation possibilities by displaying functional groups on side chains.

- These derivations can offer a direct linking opportunity for toxic components, or a coupling position for further carriers (e.g. metal chelator complexes such as DOTA, allowing the labeling of the molecule with radiometals).

- Peptides usually have excellent tumor penetration, a low bone marrow accumulation and quite fast blood clearance.

- The chemistry used to produce peptides is generally mild, as most reactions proceed at room temperature in relatively common solvents and reagents that are not extremely toxic.

- By contrast to monoclonal antibodies used in similar applications, production of peptides with a molecular weight <1500 Da is cheaper.

Further modifications of these peptides enable the complexation of radioactive metals to build diagnostic tools for the imaging technology, or even therapeutic tools. Oncology is a particularly demanding domain for such tools, as tumors and above all metastases are difficult to detect sometimes. Most cancers tend to overexpress surface receptors, and this property offers new perspectives to the now old concept of "magic bullet". It raises the possibility to target the therapeutic agent specifically to the site of action, and gives an opportunity to expose the cancer cells to *in situ* generated radiation, ionizing radiation being one of the major strategies to kill tumor cells in patients. The elegance of the method comes naturally from its selectivity, as a whole-body exposition to radiations leads to severe side-effects and complications, thus lowering patient condition and treatment compliance. Additionally, some short-lived isotopes are of great interest, as the total exposition remains limited in time.

The general principle of tumor targeting was well described in a review by Eberle et al.[91]. The illustration (**Figure 21**), modified from that review, gives an overview of the basic strategy of receptor-mediated tumor targeting using radiopeptides. "The radiopharmaceutical is applied systemically, in most cases intravenously, leading to accumulation in the target organ, and also in nontarget tissues, mainly the kidneys, spleen, and liver. Binding of the radiopeptide to its receptor induces receptor down-regulation and internalization of the receptor-ligand complex. The internalized receptor-ligand complexes are first found in endosomes, and later part of the radioactivity may be seen in the nucleus and also in the mitochondria (…). The selection of the radioisotopes depends on the purpose of the targeting: for diagnostic applications, isotopes emitting γ-radiation are necessary, such as ^{99m}Tc, ^{111}In, or positron-emitters (e.g. ^{68}Ga), which also lead to γ-radiation. For therapeutic application, short-range α-emitters (rare) or β-emitters (more frequent) are selected or, alternatively, isotopes that emit Auger electrons." (cited from Eberle et al.[91]).
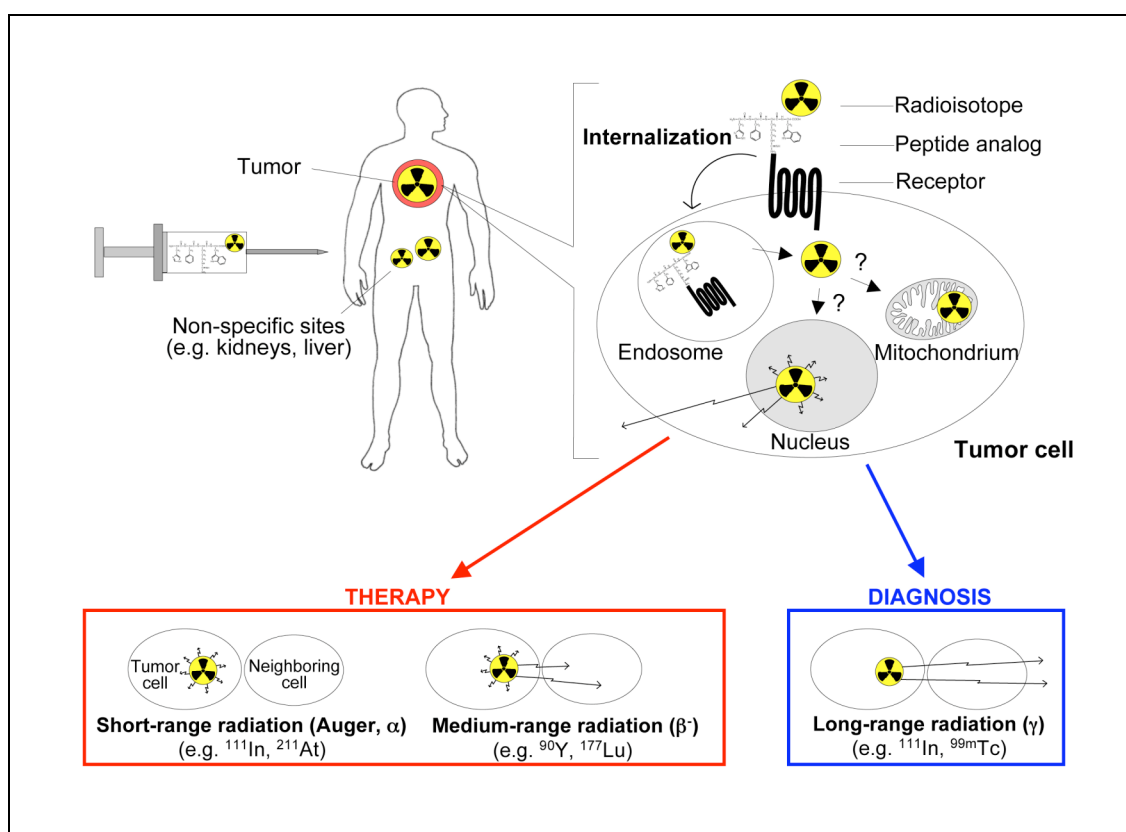
Figure 21: General principles of receptor-mediated targeting of tumor cells by radiopeptides labeled with diagnostic and therapeutic radioisotopes (modified from A.N. Eberle et al.[91]).

The interest in radiopeptides was growing only after radiopeptides became available that offered structural stability and high biological activity. These new analogues were also able to carry chemical groups intended for the incorporation of various radioisotopes. Although most *in vitro* assays worked quite well, the first peptides tested *in vivo* suffered from two major drawbacks. The advances in the structural stability of the peptides did not meet the requirements of *in vivo* transport and resistance to peptidases, and the first radiopeptides to be tested were labeled with tritium, whose radiotoxicity was much lower than required. Nevertheless, uptake and accumulation of the peptides in the tumor cells could be observed.

Great advances in the field of radiopeptides were achieved with somatostatin derivatives. Indeed, its receptor subtypes can be found on various types of tumors, and this contributed to the interest for this research field. Somatostatin research even led to the first radiopharmaceutical to be registered, octreotide (OctreoScan®), which was labeled with ^{111}In, for tumor scintigraphy; further development even led to the first therapeutic radiopharmaceutical, OctreoTher®, which was labeled with ^{90}Y.

As mentioned earlier (see **1.4.4**), MC1R usually are expressed at the surface of melanocytes, and even overexpressed at the surface of melanoma cells[285,286]. Therefore, the perspective of developing a diagnostic, staging or even a therapeutic tool against malignant melanoma by targeting the MC1R became very promising. First, radiolabeled monoclonal antibodies and antibody fragments against specific

melanoma cell epitopes have been investigated[197,265]. Unfortunately, it was discovered that individual tumor variants occurred, and their clinical application was thus limited. Additionally, monoclonal antibodies have quite poor tissue penetration abilities, they tend to accumulate in the bone marrow, and their cost of production is high. A new class of peptidic derivatives was then developed, based on the sequence of α-MSH, MC1R's native ligand. Their shorter sequence provides stability in the serum, especially against carboxypeptidases and other serum proteases. Their main advantage over antibodies or antibody fragments resides in their low immunogenic potential, faster blood clearance and better tumor penetration, and it has been proven with the development of the commercially available OctreoScan® that they are suitable tools for diagnostic purposes[22]. Indeed, the coupling of a chelating complex to the selective peptides enables the incorporation of radioactive metal isotopes such as ^{111}In, ^{67}Ga, ^{99m}Tc for diagnostic purposes, or [67]Cu, [188]Re and ^{90}Y for therapy[91]. Nevertheless, the major drawback of these new chelated targeting peptides is their *in vivo* pharmacokinetical behavior. While the tumor uptake of these new peptides has increased, their kidney uptake has dramatically increased as well, making the new α-MSH analogs relatively unsuitable for diagnostic or therapeutic applications.

Again, after solving existing issues, new difficulties appeared that had to be overcome. The main strategies and sensitive parameters able to influence the pharmacokinetical profile of α-MSH analogs will be detailed in the next main chapter (chapter **2**). For this thesis, three major concepts were adopted in order to improve the ratio between the tumor uptake and the kidney uptake of radiolabeled α-MSH analogs. These new strategies are described in the following chapter.

1.8 Aims of the thesis

Improving the tumor uptake of ^{111}In-labeled α-MSH analogs instead of reducing their kidney uptake may be an efficient strategy to obtain improved tumor-to-kidney ratios. As dimeric ACTH or derivatives of α-MSH had been shown to display markedly increased receptor affinity compared to monomeric analogs, it was tempting to analyze this approach more closely. A synergistic effect was suspected to lead to a higher tumor uptake of the dimeric radiopeptides. Indeed, dimers present two core sequences available for binding in the vicinity of the receptor, thus providing two binding motifs on one ligand. To this end, three dimeric derivatives of α-MSH were synthesized and tested *in vitro* and *in vivo*, in order to assess their binding affinities as well as their pharmacokinetical profiles, with the aim of improving their general tumor-to-non-target-tissue ratio by increasing their tumor uptake when used as radiopharmaceuticals.

Glycosylation represents a very efficient way to influence the pharmacokinetical profile of a whole range of drugs. Changes in the hydrophilicity, either local or molecule-wide, modification of the specific interactions with the targeted receptors, improved penetration of membranes (particularly the blood-brain barrier[93]) and interaction with uptake, re-uptake or non-specific receptors of non-target tissues throughout the body represent some of the main goals through which glycosylation can display significant effects in affinity and biodistribution profiles. Previous studies with glycopeptides have shown switches from the hepato-biliary towards the renal excretion way after carbohydration as well. In order to improve the pharmacokinetical profile of radioactive α-MSH analogs through reduction of the kidney uptake, six glycopeptidic derivatives of α-MSH were synthesized and tested both *in vitro* and *in vivo*. The aim of this strategy was to determine the influence of glycation on the receptor binding affinity and on the pharmacokinetical profile of radioactive α-MSH analogs. The peptides were glycated at various positions along the peptide sequence and with different carbohydrate moieties, in order to help to draw conclusions about structure-activity relationships in this class of glycopeptides.

It has been shown that amount and repartition of charges on peptides or other molecules had an impact on their pharmacokinetical profile. As the surface of the cells building the proximal tubules is negatively charged, molecules carrying negative charges as well may undergo a lower reuptake in the kidney through electrostatic repulsion. The urinary excretion of these molecules would thus presumably be increased, and therefore their therapeutic index improved. Localization of the negative charge seems to be a fundamental parameter to take into account. To investigate this approach, a new radiolabeled α-MSH derivative with an overall negative charge was synthesized and tested.

2 Radioactive α-MSH analogs for melanoma targeting: State of the art

Having to face new setbacks with optimized derivatives required investigations about the underlying mechanism of kidney retention. These findings allowed to improve non-specific uptake issues, and led to ameliorations at different levels, including a better understanding of structure-activity relationships.

2.1 Proposed mechanism of radiopeptide retention in the kidney

The kidney is a major site of catabolism of low-molecular-weight proteins. Proteins and peptides are first filtrated by the glomerulus in a molecular-weight-dependent manner, then reabsorbed by tubular cells along the nephron, and finally degraded in the lysosomes. In addition to the size-exclusion filtration, the basement membrane of the glomerulus is negatively charged, thus helping cationic peptides and proteins to attach and to pass into the primary urine. Anionic peptides and proteins appear to be less efficiently filtrated, due to repulsing electrostatic forces[33]. In the case of radiopeptides, the mechanism of reabsorption is quite similar to the one just described. The peptides are then delivered to lysosomes where they are hydrolyzed to a final radioactive metabolite that cannot leave the lysosomes, leading to long-term sequestration of the radioisotope in the proximal tubular cells. Indeed, whereas the resulting catabolic products of

Figure 22: Schematic representation of the physiology of protein reabsorption and metabolism in the renal proximal tubule cells (from Behr et al, Eur J Nucl Med 25 (1998), 201-212).

radioiodinated proteins and peptides are rapidly excreted, radiometal chelates remain partially trapped within lysosomes. The effect of injection of pharmacological amounts of cationic amino acids and their derivatives can be a tubular proteinuria by neutralization of negative charges on the luminal cell surface of tubular cells, which are thought to be essential for the binding of proteins and peptides to their respective receptors[33].
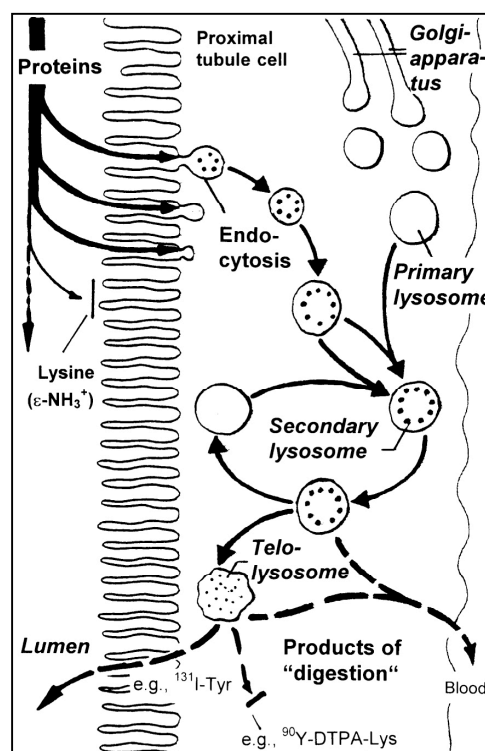
2.2 Choice of radionuclides

Several types of radionuclides are adapted to tumor diagnosis or therapy. Depending on the desired application, various types of radiations are desirable in a tracer, and thus often different radionuclides. For instance, to allow detection by external scanners, long-range radiation is needed. This type of radiation travels through almost all kinds of tissues until it reaches detectors processing the signal and building an image of the targeted area. Medium- and short-range radiations are more therapy-oriented, as they allow, if an adequate radionuclide emitting sufficient energy is chosen, to destroy the targeted cells, or the targeted cells and additionally their surrounding cells. The range of emission is not the only criteria. The type of emission is also fundamental for the choice of an adequate radionuclide. There are 4 major types of radiation emission[157]:

- In γ-decay, a nucleus changes from a higher energy state (obtained, e.g., by preceding β^--decay of a higher-order nuclide) to a lower energy state through the emission of electromagnetic radiation (photons). The number of protons (and neutrons) in the nucleus does not change in this process, so the parent and daughter atoms are the same chemical element.
- In β^--decay, the weak interaction converts a neutron (n^0) into a proton (p^+) while emitting an electron (e^-) and an antineutrino (ν_e). In β^+-decay, energy is used to convert a proton into a neutron, a positron (e^+) and a neutrino (ν_e).
- α-decay is a type of radioactive decay in which an atomic nucleus emits an alpha particle (two protons and two neutrons bound together into a particle identical to a helium nucleus) and decays into an atom with a mass number 4 less and atomic number 2 less. α-decay is a form of nuclear fission where the parent atom splits into two daughter products.
- The Auger effect is a phenomenon in which the emission of an electron from an atom causes the emission of a second electron. When an electron is removed from a core level of an atom, leaving a vacancy, an electron from a higher energy level may fall into the vacancy, resulting in a release of energy. Although sometimes this energy is released in the form of an emitted photon, the energy can also be transferred to another electron, which is ejected from the atom. This second ejected electron is called an Auger electron.

2.2.1 Tumor diagnosis

Diagnosis requires a radiation type that is mostly detectable from outside the body or tissue. Thus, long-range radiation is needed, such as γ-radiation or β^+-radiation, required for scintigraphic applications. γ-radiation can be detected by γ-counters, for example, to measure the amount of radioactivity emitted by organs collected after dissection of laboratory animals in biodistribution experiments, or to allow patient imaging by a γ-camera or a single photon emission computed tomography, also called SPECT (similar

principle as a γ-camera, but allowing 3D-imaging by views taken from various angles and computer processing). The detection process for β^+-radiation, on the other hand, is not a direct detection of the emitted particles. As the isotope undergoes positron emission decay, it emits a positron, which is the antimatter counterpart of an electron. This positron travels up to a few millimeters to encounter and annihilate with an electron, producing a pair of annihilation γ-photons, moving in opposite directions. These are detected by a scintillating material in the PET-scanner, which creates an emission of light detected by photomultipliers, then able to rebuild an image.

The first α-MSH analogs were labeled with ^{14}C, but its specific radioactivity definitely remained too low for biological studies[146]. α-MSH analogs were then labeled with tritium (^{3}H, 2 to 12 tritium atoms), and the obtained compounds were suitable for tissue distribution and stability studies *in vivo*. They showed a good uptake in melanoma cells *in vitro* and in melanoma tumors *in vivo*, but because of its too low-energy β^- emission, tritium did not affect tumor growth, and thus was abandoned[87,90]. Then ^{125}I, a γ-emitter, became available and increased the specific activity by a factor 10. It allowed determination of the number of functional receptors expressed by various melanoma cell lines, the development of competitive binding assays as well as determination of ligand and receptor distribution *in vitro* and *in vivo*. Unfortunately, although the derivatives remained biologically active and had an interesting specific activity, a dehalogenation reaction was observed *in vivo* with radioiodinated α-MSH analogs, which reduced their potential as therapeutic tools[90].

New analogs bearing chelating complexes such as DTPA or DOTA (described in the next chapter) were then synthesized. The chelates allowed the complexation of charged radiometals, such as ^{99m}Tc, $^{67/68}$Ga, ^{64}Cu, ^{86}Y or ^{111}In. The major advantage of such radionuclides is their high specific activity, thus dramatically reducing the amount of peptide to inject, and by reducing the peptide load a lower non-specific accumulation can be reached[91,249]. This high specific activity, coupled to the γ-radiation emitted, allows a low detection threshold and represents one of the main interests of ^{111}In for biodistribution experiments in animals. The γ-radiation emitted also allows local or whole-body imaging without being harmful to patients or animals at adequate doses. Additionally, ^{111}In does not emit any β-radiation, which makes it safer to handle in experiments preceding therapeutic experiments involving much stronger radionuclides such as e.g. ^{90}Y. Finally, its half-life of 67.9 h is very suitable for observations and measurements over several days. Unfortunately, its major drawbacks are its price and availability, as ^{111}In can only be produced in a cyclotron. From another point of view, the relatively short half-life of ^{68}Ga (68 min) is overcome by its availability. Indeed, it is generator-produced by decay of the parent ^{68}Ge, displaying a half-life of 280 days, thus giving the generator a long half-life and allows PET imaging at institutions without an on-site cyclotron.

Table 4: Radioisotopes used for tumor diagnosis[91].

Type	Isotope	$T_{1/2}$ (h)	Decay Mode[a] (%)	E [keV] (%)
γ-emitter[b]	^{99m}Tc	6.02	γ Auger	141 (98.3) 143 (1.7)
	^{111}In	67.9	EC (100) Auger γ (3 energies)	19 (16); 3 (100) 171 (90) 245 (94)
	^{67}Ga	77.8	EC (100) Auger γ (10 energies)	93 (69) 185 (23) 300 (19)
	^{123}I	13.2	EC (100) Auger γ (14 energies)	159 (99)
β$^+$-emitter[c]	^{18}F	1.83	β$^+$ (97) EC (3)	635
	^{124}I	99.6	β$^+$ (23) EC (77) γ (mult. energies)	2,146 (13) 1,500 (12) 603 (61)
	^{64}Cu	12.9	β$^+$ (19) EC (43) β$^-$ (38) γ (weak)	654 (19) 573 (40) 1,346 (weak)
	^{68}Ga	1.13	β$^+$ (89) EC (10) γ (8 energies)	836 (88) 352 (1) 1,077 (3)
	^{86}Y	14.7	β$^+$ (33) EC (66) γ (mult. energies)	1,250 (11) 1,077 (83)

[a]Decay mode and ensuing γ-radiation (last line in the box), usually with multiple energies of which the most important are listed in column 5.
[b]X-ray emission accompanying electron capture (EC) decay (approx. 25 keV) is not shown.
[c]The 512 keV annihilation γ-radiation always present in β$^+$ decay is not shown.

^{99m}Tc is the most important radionuclide for diagnostic nuclear applications used in the clinic. Radiopharmaceuticals labeled with ^{99m}Tc represent about 80% of all radioisotopes used clinically. It is a very convenient isotope, as it is easy to handle, it can be produced at a quite low cost, has an almost exclusively γ-radiation (no β and no α) of 141 keV and excellent imaging properties. The supply problem is overcome by obtaining the parent ^{99}Mo, which has a longer half-life (67 h) and continually produces ^{99m}Tc. The parent is delivered in a radionuclide generator allowing the easy separation of the daughter. The only disadvantage of ^{99m}Tc is a relatively short half-life of 6 h, making longer or delayed observations impossible[91]. Three methods are available for the labeling with ^{99m}Tc:

- Direct labeling, which is a direct chelation of the metal by available sulfide groups in the peptide. A reducing agent converts cystein disulfide bridges into free thiols that bind with ^{99m}Tc. Of course, one limitation is the availability of cysteines along the peptide sequence. Additionally, the obtained complexes usually have a poor *in vivo* stability. Chen et al.[58] used this technique to label early cyclic α-MSH analogs.

- Labeling can be performed with a preformed chelate approach. The radionuclide binds to a bifunctional chelating agent in a step preceding the attachment to a peptide. Its drawback is the multiple step approach, inapplicable to routine applications.

- The best method is probably the indirect method, consisting of the attachment of a bifunctional chelating agent to the peptide during its synthesis, and of its subsequent labeling with ^{99m}Tc. This procedure is usually the standard procedure for the complexation of radiometals other than ^{99m}Tc to peptides[91] as well. It is routinely used by several groups for labeling applications e.g. in the fields of somatostatin[60] and α-MSH[110].

^{99m}Tc is used in more than 20 million diagnostic nuclear medical procedures worldwide every year. Depending on the transporter (drug, vector) it labels, it allows imaging of a lot of pathologies. For example, when exametazime is labeled with ^{99m}Tc, it is possible to image the cerebral perfusion, as exametazime is able to cross the blood brain barrier[95,173]. [^{99m}Tc]-sestamibi (methoxyisobutylisonitrile) can be used for myocardial perfusion imaging[275] or parathyroid imaging[312]. Assessment of renal function performance and its imaging uses [^{99m}Tc]-mercapto acetyl triglycine, also known as a MAG3 scan[8].

γ-Emitting radionuclides are used for γ-camera or SPECT imaging. Practical applications are readily available, particularly with ^{99m}Tc and ^{111}In. In the field of somatostatin, the synthesis and clinical application of OctreoScan® brought new perspectives for the imaging of neuroendocrine tumors expressing somatostatin receptors[37,49]. It is now routinely used for the diagnosis of such tumors. It is also used for diagnostic purposes in clinical studies investigating new treatments, e.g. recruitment and follow-up diagnostic imaging of a treatment of the ileal carcinoid with ^{90}Y-DOTATOC (somatostatin derivative) were realized with OctreoScan®(**Figure 23**)[37].
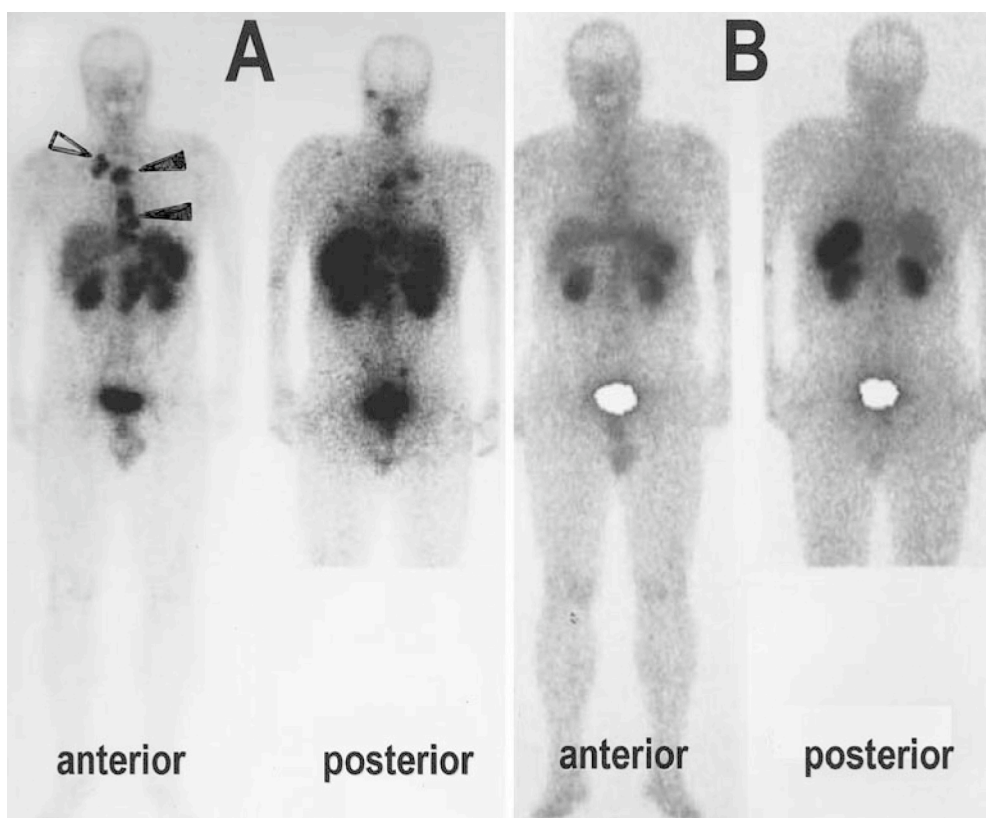
Figure 23: Bone and lymph node metastases from ileal carcinoid before and after ^{90}Y-DOTATOC therapy[37]**.**

A OctreoScan at recruitment. Black arrows indicate bony lesions. The open arrow indicates lymph nodes. **B** OctreoScan 9 months after the second cycle: there is no more evidence of pathological uptake.

As mentioned above, β^+-emitting radionuclides are needed for PET imaging. [64]Cu, ^{68}Ga and [86]Y are suitable for PET imaging, thanks to the appropriate specific activities displayed. [68]Ga exhibits a very short half-life of 1.13 h. The technical timely difficulty can though be overcome, as it was shown in an experiment on mice bearing a subcutaneous malignant melanoma[114]. Nevertheless, peptides labeled with ^{68}Ga do not allow longer-term observations in patients, due to the short-lived nature of the radionuclide. The other radionuclides display more interesting half-lives with 12.9 h for ^{64}Cu and 14.7 h for [86]Y. [64]Cu, though, has suboptimal properties for PET-imaging, as only 19% of its decay mode consists of β^+ radiation. [86]Y has very similar properties to ^{68}Ga, and its much longer half-life makes its preparation and application easier. A further diagnostic radioisotope to shortly mention is [18]F. [18]F is a β^+-emitter mostly used in fluorodeoxyglucose (FDG), which is an analog of glucose commonly used in PET imaging. FDG is taken up by high-glucose-using cells such as brain, heart, kidney, and cancer cells, where phosphorylation prevents glucose from being released intact. The oxygen attached to C-2 in glucose is needed in further steps of the glycolysis, so that (as for 2-deoxy-D-glucose) FDG, whose hydroxyl group at position 2 is substituted by ^{18}F, cannot be further metabolized in cells, and therefore the FDG-6-phosphate formed does not undergo glycolysis before radioactive decay. As a result, the distribution of ^{18}F-FDG is a good reflection of the distribution of glucose uptake and phosphorylation by cells in the body. After FDG decays radioactively, ^{18}F is converted into [18]O and after catching a proton from the environment, FDG becomes glucose-6-

phosphate labeled with a "heavy" oxygen at position 2, and thus will be normally metabolized during glycolysis[246].

Table 5: Characteristics of different radionuclides used for radiolabeling of peptides[222].

Advantages	Limitations
Technetium-99m	
• Easy availability and low cost	• Not suitable for delayed imaging studies
• Easy to handle	
• Reasonable half life of 6 h	
• 140 keV γ-emission	
• Excellent imaging characteristics	
• Absence of α and β radiations	
• Favorable dosimetry	
Iodine-123	
• 159 keV γ-emission	• High cost
• 13 h half-life	• Limited availability
• Good imaging characteristics	• Cyclotron-produced radionuclide
Indium-111	
• 171 and 245 keV γ-emissions	• High cost
• Half life of 2.8 days	• Limited availability
• Useful for acquiring delayed images	• Cyclotron-produced radionuclide
	• Relatively high radiation burden to patients
	• Suboptimal nuclear characteristics
Copper-64	
• Emissions of β⁻(573 keV) and β⁺(655 keV)	• Limited availability
• Suitable for both imaging and radiotherapy	• Costly production and shipment
• Half life of 12.7 days	• Suboptimal characteristics for PET imaging due to low abundance of β⁺ (19%)
• Can be produced using a generator system or biomedical cyclotron	
Gallium-66/67/68	
• Suitable for γ-scintigraphy and PET imaging	• High cost
• Half-lives of ⁶⁶Ga (9.5 h), ⁶⁷Ga (78.3 h), and ⁶⁸Ga (68 min)	• Limited availability
• Useful physical characteristics	• Cyclotron-produced radionuclides (⁶⁶Ga, ⁶⁷Ga)
Fluorine-18	
• Can be produced in high quantity (i.e., Ci)	• High cost
• Low positron energy of 0.635 MeV	• Limited availability
• High resolution and sensitivity	• Cyclotron-produced radionuclide
• Low radiation dose to patients	
• The half-life of 110 min permits both radiopharmaceutical preparation and imaging studies	

2.2.2 Tumor therapy

Whilst γ-emission is needed for diagnostic purposes, radionuclide therapy requires other types of radiation in order to cause cell death. β$^-$-particles are generally preferred, thanks to their longer range (higher energy), to α-radiation or Auger electrons. The latter two usually require cell internalization (for Auger electrons even intranuclear localization) for the delivery of lethal doses. Achieving a high level of selectivity (targeting) is crucial for therapeutical applications, as normal tissues could otherwise be strongly affected or destroyed by the radiation of such radionuclides. It can be an advantage if the chosen radionuclide also emits γ-radiation for simultaneous imaging or for dosimetry.

β$^-$-Emitters

Thanks to the high-energy β$^-$-particles (2.3 MeV) emitted by ^{90}Y, it has been very popular for the labeling of antibodies and peptides. Its longer-range radiation (1.1x10^{-2} m), though, is not ideal for the treatment of small cell clusters. Additionally, it does not emit any γ-radiation, making imaging and dosimetry impossible. Its favorable half-life (2.5 days) and high-energy are very suitable for the treatment of large tumor cell clusters, as is ^{188}Re (2.12 MeV, 80%), which also emits sufficient γ-radiation for dosimetry and imaging[293]. Nevertheless, ^{90}Y remains an interesting radionuclide for some applications. In studies involving the previously mentioned diagnostic OctreoScan, which is labeled with ^{111}In, therapeutic experiments were carried out with high doses and showed tumor regression in some patients. The Auger electrons may have had this therapeutic effect, but their energy and range are very limited (2.6 keV, 3.7x10^7 m). Therefore, new experiments were realized by replacing ^{111}In with ^{90}Y for the high energy and greater range of its radiation, and showed promising results (see **Figure 23** above). ^{186}Re (1.07 MeV, 73%), displaying a medium-energy β$^-$-radiation, is more suitable for intermediate-sized cell clusters. ^{177}Lu (0.498 MeV, 90%), has received attention, since its energy (and thus the range of its β$^-$-particles) is considerably lower than e.g. ^{90}Y, thus allowing to spare the neighboring, potentially healthy tissue. Additionally, ^{177}Lu is a γ-emitter. Its half-life (6.7 days) may be too long, depending on the type of peptide used. ^{67}Cu and ^{131}I fall in the same class of radionuclides, with emissions comparable to those of ^{177}Lu[91,293,319].

Radioiodinated peptides are routinely used in *in vitro* studies (^{125}I). Single photon imaging studies have been realized with ^{123}I (the γ-radiation emitted by ^{125}I has a too low energy), and ^{131}I is a potentially therapeutic radionuclide. ^{131}I can be produced in a nuclear reactor by fission at a relatively low cost. Labeling with iodine is usually a direct labeling, involving *in situ* generation of electrophilic species of radioiodine (with oxidants such as chloramine-T or Iodogen®), which react with tyrosine residues. It is difficult to obtain mono-iodinated products, as Tyr bears 2 sites for insertion of radioidide. Additionally, dehalogenation of Tyr occurs *in vivo* that makes iodine unsuitable for *in vivo* diagnosis and limits its application for therapy[23].

α-Emitters

The short range in tissue (< 0.1mm) and the high linear energy transfer associated with α-particle emitters results in a more concentrated deposition of energy at the site of radionuclide decay. Literally, a single atom emitting an α-particle can kill a target cell. Thus, if α-radiolabeled antibodies or peptides can be bound to malignant cells specifically, a high differential cell killing can be achieved between malignant and normal cells[151]. Their short-ranged radiation and high relative biological efficiency (5-20-fold that of β⁻-particles) are highly advantageous for the treatment of small tumors and micrometastases[219]. They are even suitable for the destruction of individual cells as for example for the treatment of leukemias[334]. α-Emitting radionuclides have been applied mostly to immunoconjugates for radioimmunotherapy. Miao et al.[205] studied the effect of a cyclic α-MSH analog labeled with ^{212}Pb on melanoma-bearing mice and reported a longer survival time and even total remissions. Unfortunately, as observed earlier for the same derivatives labeled with ^{111}In, kidney uptake remained a major issue. ^{211}At and ^{213}Bi have also been tested, but because of their usually short half-lives (7 h and 47 min, respectively) and the time required to achieve a useful tumor-to-normal tissue ratio after administration, α-emitters may be of limited value in the treatment of tumor masses when conjugated to intact antibodies[319].

Table 6: Beta- and alpha-emitting radioisotopes used for tumor therapy[91].

Type	Isotope	$T_{1/2}$ (h)	Decay Mode[a] (%)	E [keV] (%)
β⁻-emitter	^{67}Cu	61.9	β⁻ (100)	570
			γ (6 energies)	93 (31)
				185 (48)
	^{90}Y	64.1	β⁻ (100)	2280
			γ (weak)	1,761 (weak)
	^{131}I	193	β⁻	807
			γ (mult. energies)	80 (6)
				284 (6)
				364 (83)
				637 (7)
	^{177}Lu	161	β⁻	497
			γ (6 energies)	113 (21)
	^{186}Re	90.5	β⁻ (93.5)	1,070
				930
			EC (6.5)	
			γ (7 energies)	137 (21)
	^{188}Re	16.98	β⁻	2,116
			γ (mult. energies)	155 (15)
α-emitter	^{211}At	7.2	α	5,867 (42)
			EC	(58)
			γ (6 energies)	1,067 (strong)
	^{213}Bi	0.76	α (2.2)	5,870
			β⁻ (97.8)	1,420
			γ (6 energies)	440 (21)
	^{225}Ac	240	α (100)	5,830
			γ (mult. energies)	116 (15)

[a]Decay mode and ensuing γ-radiation (last line in the box), usually with multiple energies of which the most important are listed in column 5.

Auger electron cascade

The very short range of radiation of Auger electrons makes them a suitable alternative for therapy. As most radionuclides used in diagnostic applications emit Auger electrons (like ^{111}In, discussed above), these may also be used as therapeutic tools if sufficient doses are able to reach tumor cells and, above all, if strategies are found that allow Auger emitters to reach the nucleus. Very high doses of the therapeutic agent have to be injected for these means, which usually results in a relative decrease in its uptake by the tumor. The uptake by non-target organs, on the other side, is normally not proportionally reduced, or may even increase. Therefore, the tumor-to-non-target tissue ratios may find themselves reduced, resulting in limited therapeutic indexes. Another limitation of very short-ranged emitters is their short tissue penetration (0.02-10 μm), which is unsuitable if not all cells constituting the tumor express the target receptor[91].

2.3 Chelates for peptide labeling

As mentioned for ^{99m}Tc in the previous chapter, one of the best labeling techniques is to use chelating complexes. These metal-chelating agents allow control over the behavior and localization of metal ions. Several types of chelating agents are available: simple chelators like ethylenediaminetetraacetic acid (EDTA), as well as bifunctional chelating agents bearing a chelating group on one end, and a chemically reactive functional group on the other, allowing further coupling to targeting molecules[201]. The first chelate to be introduced was the hexadendate EDTA. It was coupled to bleomycin to complex [57]Co for diagnostic tumor targeting[186]. It was then tried as chelate for magnetic resonance imaging with Gd(III), but a higher toxicity was reported *in vivo* than with diethylenetriamine-pentaacetic acid (DTPA) as chelate. In experiments with a bleomycin analog carrying EDTA and labeled with ^{111}In, background radioactivity in various tissues made detection difficult[129]. Further studies involving ^{111}In-labeling of proteins such as albumin and fibrinogen coupled to an EDTA-derivative revealed interesting properties but also a higher non-specific uptake[298]. Unfortunately, an EDTA-type complex of an In(III) ion is less stable than other In(III)-complexes formed in the blood stream. This instability is probably due to the very low concentration of the synthetic complex and the relatively high concentration of transferrin in the serum. However, some EDTA-derivatives were designed to have a slower rate of dissociation, and In(III) remained complexed *in vivo* for a longer time[201].
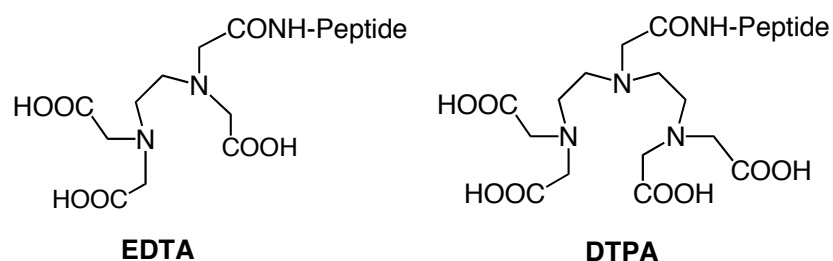

Figure 24: Structures of EDTA and DTPA coupled to peptides[91].

DTPA, an octadendate chelate, is an efficient chelate. It consists of a diethylenetriamine backbone modified with five carboxymethyl groups. The molecule can be viewed as an elongated version of EDTA. At first, it has been used to form stable complexes with Gd(III) for magnetic resonance imaging, and a further derivative was later approved for clinical applications[91]. Since then, DTPA and its derivatives have been important chelators in many domains, including somatostatin derivatives[112,178,179,320] and α-MSH analogs[19,20]. OctreoScan®, which was already mentioned above, is a commercially available somatostatin analog (octreotide) bearing the DTPA chelate for the complexation of ^{111}In for the diagnosis of neuroendocrine tumors. Nevertheless, attempts to label antibodies or small molecules with ^{90}Y for radiotherapeutic applications using DTPA or DTPA derivatives as chelates were hampered by myelotoxicity, due to the *in vivo* instability of the ^{90}Y-DTPA complex and the subsequent radioactivity uptake by the bone[109]. Additionally, DTPA-α-MSH analogues were also shown to nonspecifically accumulate in sites of distant melanoma metastases such as the liver. This side-effect prevented further developments of this class of α-MSH derivatives, as nonspecific accumulation in non-target tissues might have damaged the distant organ, or have prevented detection of metastases located in the same region[20]. The major problem of EDTA and DTPA seems to be the *in vivo* instability of the complex they form with metals. The anionic complexes of EDTA or DTPA with e.g. copper, indium and yttrium are either readily protonated or attract other competing metal ions (Ca^{2+}, Mg^{2+} and Zn^{2+} are present in great amounts in human blood) to form mixed complexes with a reduced kinetic stability. Additionally, the following dissociation of the metal ion *in vivo* is essentially irreversible, as serum proteins such as transferrin or albumin will rapidly sequester the metal ion while the chelate will simultaneously be occupied by serum cations. Their relative instability at low pH (for example in the liver) also is a cause for the dissociation of the complex and thus involved metabolic issues[231].

The interest then switched to macrocyclic complexes which tend to undergo slower acid dissociation and cation exchange reactions. Peptides and antibodies carrying the macrocyclic DOTA (1,4,7,10-tetraazacyclododecane-1,4,7,10-tetraacetic acid) metal chelator, for example, were synthesized and tested. This chelator complex is able to incorporate a broader range of 2^+ or 3^+-charged radiometals than DTPA. Indeed, DOTA is almost a universal chelator, capable of strongly complexing metals such as ^{111}In and ^{67}Ga for single photon emission tomography, ^{68}Ga, [86]Y and ^{64}Cu for PET, as well as ^{90}Y for therapy[144] and even lanthanides. Their stability was tested and, for example, less than 0.5% of Y dissociated from a DOTA-type ligand over 18 days in serum (pH 7.4, 37°C). In a similar manner, the ^{90}Y-DOTA complex displayed no change during 72 h at pH 5.5, even in presence of a 500-fold excess of DTPA[158]. The complexes exhibit remarkable rigidity and are nonlabile, properties mostly not displayed by acyclic analogs such as EDTA and DTPA. The tetraaza macrocycle of DOTA acts as a frame to constrain its eight donor atoms (four tertiary nitrogen atoms and four carboxylic groups) into a nearly spherical arrangement. DOTA is usually attached to peptides or proteins through one of the carboxymethyl groups or a derivative thereof, thus leaving three free carboxylate groups for the complexation, in addition to the four nitrogen atoms[158]. Tumor-targeting studies have shown that DOTA-peptides have favorable properties in both animal models and humans, particularly regarding receptor binding, tumor uptake and tumor-to-non-target-tissue ratios, in both the

somatostatin and the melanocortin fields[74]. The development of various DOTA-peptides delivered molecules with better pharmacokinetic properties and thus a better therapeutic interest.
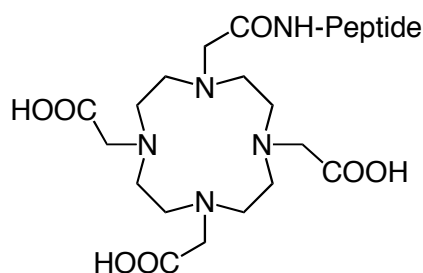

Figure 25: Structure of DOTA coupled to a peptide.

Rigidified DOTA analogs with methylated arms have been synthesized as well. They are supposed to increase the stability of the complex, but have not been tested *in vivo* yet[244]. Other new bifunctional DOTA derivatives have been developed, bearing modifications on the macrocycle. 2-(*p*-nitrobenzyl)-DOTA, for example, was synthesized partly as precursor to other DOTA-derivatives. It was shown to bind a variety of metals better than other chelators, probably thanks to an additional free carboxylate, as in this case the chelate is bound to the peptide or protein through the *p*-nitrobenzyl extension or a derivative thereof, as it was shown by the same group for EDTA-derivatives. The additional carboxylate adds stability and strength to the complex, and it was shown to hold yttrium, for example, remarkably well under physiological conditions in human serum[201,247].
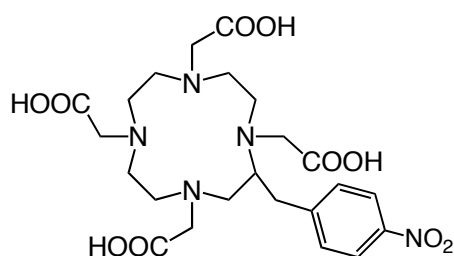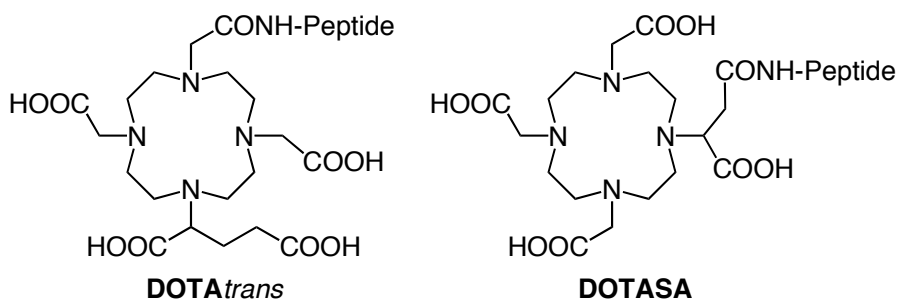

2-(*p*-nitrobenzyl)-DOTA

DOTA*trans*

DOTASA

Figure 26: Structures of 2-(*p*-nitrobenzyl)-DOTA, DOTA*trans* **and DOTASA.**

Other derivatives of the same kind, such as DOTASA and DOTA*trans*, have been synthesized and tested as well, but unfortunately, it appears that the *in vitro* and *in vivo* data of octreotide labeled with such chelates hardly revealed an advantage compared to standard DOTA. Adding methylene groups to increase the size of the macrocycle (one methylene group yielding TRITA or two TETA) and thus providing a more rapid complexation with the radiometal did not solve issues, as the stability constant for many metal ions[91] was reduced.

An additional potential problem of DOTA or DOTA-like compounds is their relative slow complexation rate. It may interfere with the quite short half-life of some of the complexed radionuclides. In order to accelerate this reaction, heating at 80-100°C during 20-30min is required, depending on the metal, to incorporate the metal ion[46]. This may bring up stability issues with thermolabile proteins or peptides, as the reaction remains incomplete at lower temperatures. Additionally, as radiolabeled DTPA-peptides tended to accumulate in the liver and other organs, the first DOTA-peptides unfortunately tended to accumulate in the kidney almost as well as in the primary tumor. Some derivatives even accumulate much better in the kidney than in the tumor. Their therapeutic efficacy is thus strongly reduced, nephrotoxicity being the dose-limiting factor[70,177]. Additionally, the strong uptake of these derivatives by the kidney implies the same detection issue as the nonspecific uptake of the DTPA-peptides: indeed, any other tumor or distant metastasis located in the kidneys or the renal surroundings would be masked by the radioactive tracer taken up by the kidneys. This issue is not specific to somatostatin or melanocortin analogs, as it was observed with other peptides or antibody fragments as well[32].

Further developments yielded a whole variety of chelates. 1,4,7-triazacyclononane-1,4,7-triacetic acid (NOTA), for example, is a macrocycle with a smaller ring structure, bearing only three nitrogen atoms and three carboxylates. One derivative, NOTAGA, has one of its "arms" branched with a spacer bearing one more carboxylate group for peptide or protein binding. It was coupled to octreotide for experimentation, and yielded very stable complexes. It produced interesting results in cell binding assays as well as in *in vivo* assays with a high uptake in target tissues and a fast excretion, particularly at short times after injection. The authors suggest that the spacer separating the chelate from the pharmacophore is mainly responsible for the improved biological behavior[94].
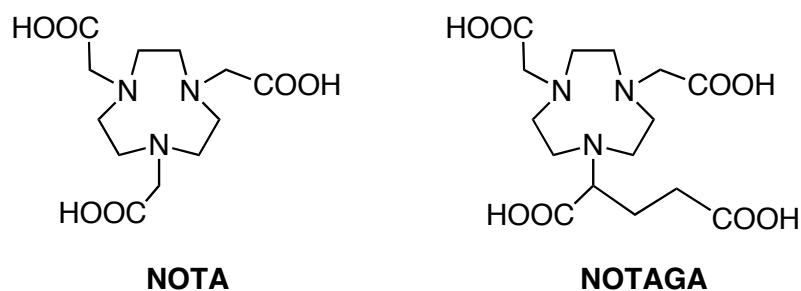

Figure 27: Structures of NOTA and NOTAGA.

This chelate could be an interesting alternative to DOTA and may have a positive effect on the biological properties of α-MSH analogs as well, although no apparent dramatic kidney uptake reduction was observed.

For copper labeling, peptides, proteins or mAb have to be coupled to another type of chelate: 4-(1,4,8,11-tetraazacyclotetradec-1-yl)-methyl benzoic acid tetrahydrochloride (CPTA) has already been extensively used, and appears to deliver an interesting kinetic stability[290]. It was also reported that mAb bearing CPTA and labeled with [67]Cu displayed improved pharmacokinetical properties, thanks to the cellular retention of the [67]Cu-CTPA complex leading to an increased accumulation of radioactivity in the target cells, compared to its radioiodinated equivalent[220].
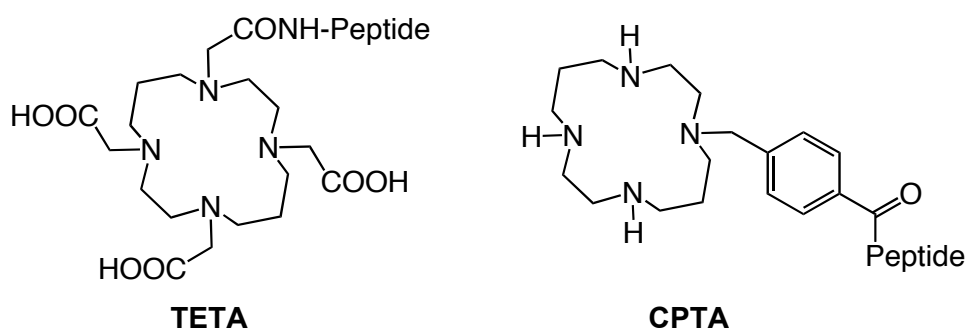

Figure 28: Structures of TETA and CPTA.

[64]Cu-labeled octreotide analogs, with either CPTA or TETA as chelate, have been synthesized and compared. Both derivatives have shown higher affinity for the somatostatin receptor in mouse cell membranes, and displayed a specific uptake in target tissues as great or greater than their ^{111}In-DTPA-labeled counterpart. Their biological clearances, though, were different. The TETA-derivative exhibited a renal clearance similar to the ^{111}In-DTPA reference peptide, while the CPTA-derivative, being more lipophilic, had a hepato-biliary clearance way. The TETA-derivative was shown to be pharmacokinetically superior to the CPTA-derivative[13]. In another group, an antineuroblastoma antibody was labeled with [67]Cu using either CPTA or 1-(p-aminobenzyl)-1,4,7,10-tetraazacyclodecane-4,7,10-triacetate (DO3A), and investigated in biodistribution assays. It was shown that the use of DO3A improved the biodistribution of the mAb with an increase in tumor uptake and a reduction of kidney uptake at 48 h[220]. Nevertheless, CPTA definitively remains an interesting chelate for copper labeling. It exhibits a particularly high stability towards acid-promoted dissociation of copper in environments such as lysosomes or the liver. Another advantage of this chelate is the low temperature needed for the complexation of copper (room temperature), compared to other chelates such as TETA and DO3A (75°C), which can very destructive with thermolabile proteins or mAb[221]. CPTA is currently still successfully used in many investigations for the labeling of peptides or, mostly, mAb[131,166].

In conclusion, the DOTA chelate remains the method of choice for the labeling of α-MSH analogs, thanks to the positive effect it brings to the pharmacokinetic properties of the peptides it is coupled to. The stability

of the complex it forms with radionuclides and its ability to complex various 2^+ and 3^+-charged radiometals are certain advantages over other chelates. Additionally, most α-MSH analogs are relatively heat-resistant, and the heating needed for the labeling reaction certainly does not constitute a drawback to their use. These are the reasons why DOTA was chosen as chelate for the design of the α-MSH analogs developed in this work.

2.4 Peptide design

Naturally occurring peptides are great tools for receptor targeting. They are small enough to show adequate *in vivo* distribution profiles, and usually big enough to stand modifications such as attachment of carriers or chelates without these affecting their biological properties. Their limited stability in the circulation, though, represents their major drawback, as they can be rapidly degraded by proteases. The stability issue can be overcome with an adequate peptide design, the challenge remaining the synthesis of a protease-resistant peptide conserving its biological properties (binding affinity, pharmacokinetical profile, etc.). Some important aspects have to be kept in mind:

- The affinity for the receptor should be high.
- The molecular weight should be kept below 1,500 gmol^{-1}.
- The ratio hydrophilicity/hydrophobicity should be balanced.
- The stability in the serum should be sufficient.
- Plasma and kidney clearances should be adequate.
- The selectivity should be kept high.
- The labeling conditions should match the peptide stability.

Peptides can be stabilized in different ways. The introduction of D-amino acids is certainly an efficient method, as proteases are not able to cleave the peptide anymore and the side chain of the amino acid remains the same. β-peptides may also be of interest, as their stability is dramatically increased *in vivo*. 50% of a radiolabeled β-peptide were found intact in blood seven days after injection. This result is promising, but such a long presence in the body could also be problematic as it may lead to side-effects, particularly with radioactive tracers[91]. Other methods involve *N*-methylation, substitution of peptide bonds, N-terminal acetylation and C-terminal amidation, introduction of unnatural amino acids, cyclization, etc. *N*-methylation of the backbone amine brings resistance to proteolysis[234] at the expense of a somewhat more difficult coupling step in the synthesis of the peptide. N-terminal acetylation and C-terminal amidation have many advantages: enhanced cell permeability, stability toward aminopeptidases, peptide ends are blocked against synthetase activity and the amidation often enhances the activity of peptide hormones. The enhanced rigidity brought by cyclization limits its conformational possibilities, and allows to find key pharmacophore elements in three-dimensional space. It also avoids degradation and digestion by stabilizing the peptide structure[26]. All these methods are commonly used in syntheses of peptidic

derivatives. Several modifications can be adopted simultaneously, with regard to the needs and constraints of peptide synthesis, bioavailability, pharmacological behavior, metabolism and excretion.

A further advantage of peptides as drugs is the possibility to modify their side chains almost at will, in order to influence their pharmacological or pharmacokinetical properties. For example, introduction of positive or negative charges by modifying amino acid side chains or by replacing amino acids with others may have a dramatic influence on their binding affinity and on their pharmacokinetical profile. Functional groups, carbohydrates or any other chemical entity can be grafted to peptides at various positions, provided the free functional groups of the peptide allow it, and lead to the same kind of steering of their physicochemical properties and desired effects[26].

The list of modifications mentioned above is not comprehensive, and various other chemical alterations can be applied, but these will not be covered in this work. Indeed, the focus of this thesis will remain on modifications of α-MSH analogs, part of which will be reviewed in the following chapter. Some of the possibilities mentioned earlier were used in this work and by others, and have proven their usefulness by influencing various biological parameters to various extents.

2.5 Improvement of the tumor-to-kidney ratio of α-MSH analogs: various strategies

In order to obtain suitable derivatives for tumor diagnosis and treatment, the effort has concentrated on reducing the uptake of DOTA-radiopeptides by the kidney. Various methods have been developed to address this issue:

- *Co-injection of basic amino acids or basic amino acids cocktails.* Thanks to this method, the kidney uptake of Fab' fragments could be reduced 5 to 6-fold in a dose-dependent manner[30], and the kidney uptake of octreotide (labeled with either ^{111}In or ^{90}Y) could be reduced by more than 50% for DTPA-octreotide derivatives, and by 65% for a DOTA-octreotide derivative (^{90}Y-DOTATOC)[34]. The kidney uptake of α-MSH analogs (e.g. ^{67}Ga-DOTA-NAPamide) could also be dramatically reduced by co-injection of high-dosed L-Lysine[58,114]. On a molecular basis, the effect seems to rely essentially on the presence of a positively charged amino group[33]. L- and D-lysine were equally effective, whether given i.p. or orally. D-Glucosamine also showed efficiency, but its *N*-acetylated derivative, lacking the positive charge, did not. Basic polypeptides (e.g. poly-L-lysine) were also effective, their potency increasing together with their molecular weight (and thus the number of positive charges).

- *Use of different metal isotopes.* In the case of α-MSH analogs, the best peptide (DOTA-NAPamide) labeled with ^{67}Ga even showed a lower kidney uptake and a simultaneously higher tumor uptake

than ^{111}In-DOTA-NAPamide[114]. The extent of this reduction does not improve the tumor-to-kidney ratio sufficiently, and further ameliorations with the use of other radiometals are improbable.

Although these methods significantly improved the tumor-to-kidney ratios of the peptides, the results did not yet match the requirements for internal radiotherapy. Thus, new approaches had to be envisaged that would lower the kidney uptake of the α-MSH derivatives.

Indeed, the key to the kidney uptake issue may reside more in the basic structure of the derivatives than in the type of isotope used (although ameliorations were observed with some) or the co-injection strategy. Therefore, existing analogs were modified in order to influence their bioavailability, their pharmacokinetical properties, or their possible direct interaction with surface receptors located in the kidney. Efforts are focusing on the elucidation of the mechanism leading to kidney retention of the radiopeptides.

The two main goals to achieve to improve the tumor-to-kidney ratio of the α-MSH analogs are either an enhancement of the tumor uptake or a diminution of the kidney uptake.

2.5.1 The superpotent [Nle^4, D-Phe^7]-α-MSH (NDP-MSH)

Ac-Ser-Tyr-Ser-Nle-Glu-His-D-Phe-Arg-Trp-Gly-Lys-Pro-Val-NH2

By searching a way to prolong the biological activity of α-MSH, Sawyer et al. found (in 1980) that a synthetic analog carrying a norleucine at position 4 (replacing native Met) and a D-phenylalanine at position 7 (replacing native L-Phe) exhibited a better resistance to enzymatic degradation in the serum than native α-MSH. Indeed, following a statement by Lande and Lerner (as early as 1967) saying that "it is important that α-MSH be made with D-amino acids in one or two places. If the site of racemization can be pinpointed, it may be possible to produce well-characterized peptides more active than the natural hormone"[180], Sawyer et al. introduced the two unnatural amino acids mentioned above and were successful at prolonging the biological activity of α-MSH. Additionally, the peptide exhibited a dramatically increased biological activity (26-fold that of α-MSH) in adenylate cyclase assays. The racemization process happened under heat-alkali treatment[267].

These amino acid substitutions constitute the most striking effect achieved by modifying α-MSH.

Unfortunately, *in vivo* dehalogenation reactions were observed with peptides labeled with iodine isotopes. These peptides are therefore less suitable for in vivo imaging and therapy. In tissues, iodine isotopes are most likely released from the Tyr they are attached to and the free radioiodide is cleared via the kidneys. Indeed, despite considerable biliary excretion, nearly all excreted radioactivity was found in the urine, and only a very small amount in the feces[23].

Radioiodinated NDP-MSH is still routinely used in *in vitro* assays as a competitive antagonist of other α-MSH analogs.

2.5.2 Shorter sequence: [DOTA-β-Ala³,Nle⁴,Asp⁵,D-Phe⁷,Lys¹⁰]-α-MSH₃₋₁₀ (DOTA-MSH$_{oct}$)

> **DOTA-β-Ala-Nle-Asp-His-D-Phe-Arg-Trp-Lys-NH2**

In order to favor blood clearance of the radiopeptide, Froidevaux et al.[110] synthesized a shorter α-MSH analog carrying a DOTA chelator complex at its N-terminal end. It was then labeled with ^{111}In and compared to the previously mentioned NDP-MSH, to which DOTA was also attached. The shorter sequence displayed favorable properties regarding tumor-to-non-target-tissue ratios and blood clearance, indicating possible future applications for tumor diagnosis and therapy. Like for most radiopeptides, the quite high kidney uptake remained its main issue, but the strategy of using a shorter peptide appeared to be promising. Additionally, autoradiographies of various organs (including distant metastases) were realized and revealed several interesting points[110]:

- **Melanotic** melanoma metastases could be detected precisely on organs (liver and lungs).
- **Amelanotic** melanoma metastases could be detected as well (lung).
- Radioactivity in the kidneys appeared to be localized only in the cortical region, suggesting that ^{111}In-DOTA-MSH$_{oct}$ is retained in the proximal tubules, probably after tubular reuptake.

A new approach was being suggested with these findings, and further developments favored the use of shorter peptides.

2.5.3 Position of DOTA: [Nle⁴, Asp⁵, D-Phe⁷, Lys¹¹(DOTA)]-α-MSH₄₋₁₁ (DOTA-NAPamide)

> **Ac-Nle-Asp-His-D-Phe-Arg-Trp-Gly-Lys-NH2**
> **|**
> **DOTA**

The basic structure of DOTA-NAPamide is quite similar to DOTA-MSH$_{oct}$, but it still displays some critical differences:

- The position of DOTA in the peptide is different: in DOTA-NAPamide, the DOTA moiety is coupled to the side chain of Lys¹¹ (ε-amino group), on the C-terminal end of the peptide. Thereby, it neutralizes the positive charge of the Lys¹¹ side-chain. In DOTA-MSH$_{oct}$ it was coupled to the N-terminal end of the peptide.

- Gly[10] was restored in the sequence of the peptide in DOTA-NAPamide, as it was shown to play a role in MC1R affinity[263].
- The net charge of the peptide was changed: +1 for DOTA-NAPamide vs. +2 for DOTA-MSH$_{oct}$.

Upon synthesizing this peptide, Froidevaux et al. expected it to have a more favorable biodistribution profile than DOTA-MSH$_{oct}$. Indeed, with Gly reinforcing the core structure of the peptide sequence and thus increasing the affinity for the receptor, and with a reduction of the net charge of the peptide (known to be associated with a reduction in both glomerular filtration and tubular reabsorption; as mentioned previously, Lawrence et al.[181] showed that luminal cells carry negative charges on their surfaces), a better tumor-to-kidney ratio could reasonably be expected. Additionally, Akisawa et al. had shown that renal uptake of [111]In-[DTPA-D-Phe[1]]-octreotide was enhanced upon replacement of D-Phe[1] by Lys, but reduced when D-Phe[1] was substituted with Asp. This statement demonstrates the influence of charge on kidney retention of chelator-peptide conjugates[7,114].

The potency of DOTA-NAPamide in competitive binding assays was much higher compared to DOTA-MSH$_{oct}$. Apparently, allocation of the ε-amino group of Lys[11] to DOTA does not affect the binding affinity. This result is in agreement with the biodistribution data: ^{111}In-DOTA-NAPamide displayed a higher tumor uptake and a lower kidney accumulation than DOTA-MSH$_{oct}$, and the observed kidney uptake was the lowest observed until then. The tumor-to-kidney ratio could even be increased by incorporating, as mentioned in **1.7.5**, ^{67}Ga instead of ^{111}In, probably due to a different coordination geometry of the metal isotope in the chelator complex[113]. As mentioned earlier as well, further reduction of the renal accumulation could be obtained by co-administration of L-lysine, however to a larger extent than with other radiopeptides (64% vs. 40-52%)[114]. Further experiments confirmed the suitability of gallium-labeled DOTA-NAPamide for imaging of metastases, e.g. with ^{67}Ga in autoradiographies of both distant melanotic and amelanotic melanoma lesions, and with ^{68}Ga for PET-imaging[114].

2.5.4 Structure-activity relationships study of NAPamide derivatives

DOTA-Nle-Asp-His-ᴅ-Phe-Arg-Trp-Gly-Lys-NH2
|
NH$_2$

DOTA-Nle-Asp-His-ᴅ-Phe-Arg-Trp-Gly-Lys-NH2
|
Ac

DOTA-Nle-Asp-His-ᴅ-Phe-Arg-Trp-Gly-Lys-COOH
|
Succ

DOTA-Nle-Asp-His-ᴅ-Phe-Arg-Trp-Gly-Lys-NH2
|
Succ

After the good results shown by DOTA-NAPamide, further attempts were made to try to increase the tumor-to-kidney ratio. Moving the DOTA moiety back to the N-terminus of the peptide dramatically increased the kidney uptake (3x). But by acetylating the free ε-amino group of Lys[11] (and thus leaving its side chain neutral instead of carrying a positive charge), the kidney uptake was reduced to "normal", supporting the statement that kidney uptake was relying more on charge than on the position of DOTA.

Following these findings, new experiments were made with DOTA-NAPamide derivatives carrying negative charges on Lys[11]. It was envisaged that negative charges, found on both the proximal tubular cells and on the peptide, could have a repulsive effect on each other, and thus favor renal excretion of the peptide instead of reabsorption. To this end, DOTA-NAPamide was succinylated on the side chain of Lys[11], and thus the whole peptide charge was neutral. On a second derivative, to accentuate the potential effect of negative charges, Lys[11] was succinylated and the C-terminal amide was removed to make way for a carboxylate group, and thus the peptide carried a net charge of -1. Unfortunately, these modifications did not alter kidney accumulation. The peptide carrying the negative net charge showed only a very slight reduction in kidney uptake[115]. About this reduction, it was hypothesized that charge location within the peptide would have an influence rather than its net charge.

It was also observed that the structure of the peptide does apparently not have a large influence on the release of radioactivity from tumors and the kidneys. Generally, it was observed that the release from the melanomas was much faster than from the kidneys. A proposed hypothesis mentions the documented upregulation of lysosomal enzymes in melanomas[170], leading to a higher rate of radiopeptide hydrolysis and thus to a faster production of small radioactive metabolites with higher release potential[115].
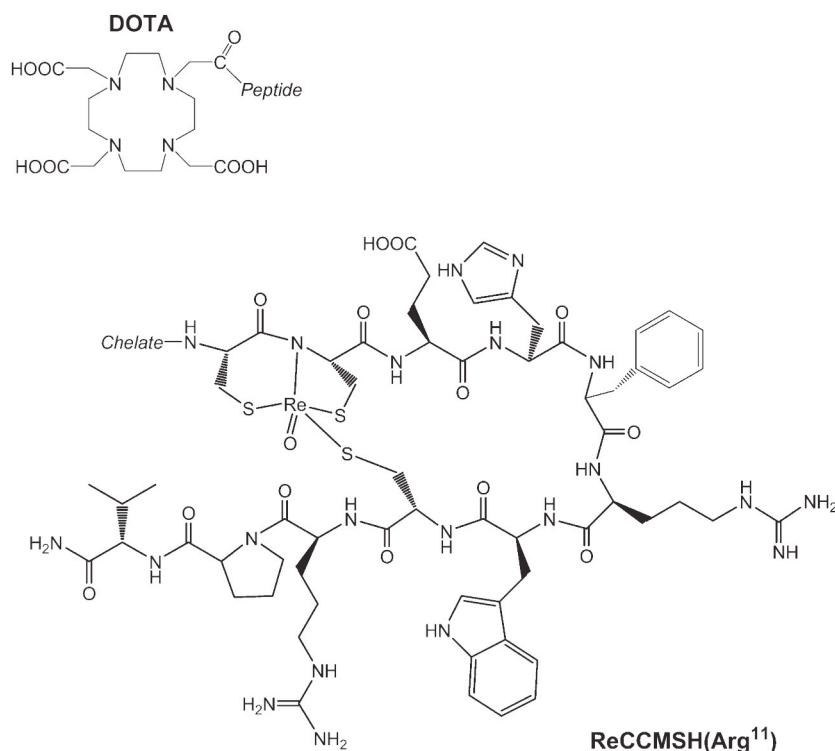
2.5.5 Cyclic peptides: CCMSH and derivatives

Figure 29: The cyclic peptide ReCCMSH(Arg[11]), cyclized via rhenium-complexation[321].

As it had been reported that α-MSH peptides cyclized either via a disulfide bond between two cysteines ([Cys(4, 10), D-Phe[7]]α-MSH)[69] or via a lactam bond between the aspartate and the lysine ([Nle[4],Asp[5],D-Phe[7],Lys[10]]α-MSH)[9] displayed increased receptor binding affinities and resistance to proteolysis, a research team around T.P. Quinn and S.S. Jurisson studied this class of derivatives for use as radiopeptides. They reported a whole series of cyclic derivatives that had not been cyclized via the two methods mentioned above, but via metal coordination, using three Cys[3,4,10] sulfhydryls and one Cys[4] amide nitrogen positioned in the sequence of the peptide[124] for metal coordination. The peptides were mostly cyclized by complexing ^{99m}Tc or [188]Re and displayed good tumor-targeting properties, but the kidney uptake issue was still present. Further derivatives were then synthesized with non-radioactive cores using ReO and TcO and coupled to a chelate (mostly DOTA) complexing various metal isotopes ([86]Y, ^{64}Cu, ^{111}In). ReO and TcO are commonly used as cores because of their ability to form stable complexes with amide nitrogens and thiolate sulfurs, both found in peptides.

Most of the peptides did not show any amelioration of the tumor-to-kidney ratio compared to DOTA-NAPamide (our reference)[59,203,209], but some of them showed very good *in vivo* biodistribution, keeping up with DOTA-NAPamide. Indeed, particularly ^{111}In-DOTA-Re(Arg[11])CCMSH achieved a tumor-to-kidney ratio at 4h of 2.36 (^{111}In-DOTA-NAPamide: 1.63[115], ^{67}Ga-DOTA-NAPamide: 2.37[114]), which is quite interesting

for an indium-labeled peptide[60]. It would be interesting to compare their tumor-to-kidney ratio of the AUC (4-48h), but unfortunately most of the published results consider data in the time interval from 4 h to 24 h.

2.5.6 Summary of the major modifications of α-MSH analogs

As mentioned above, a number of derivatives of α-MSH have been synthesized, some of them delivering some major breakthroughs. Not all existing modifications that had been examined could be described here and the following table only lists some of the main strategies developed to improve the pharmacokinetic properties of α-MSH analogs for melanoma targeting and the observed effects. Nevertheless, it attempts to deliver an overview of the main existing strategies.

Table 7: Summary of the major modifications of α-MSH analogs, and observed effects on pharmacokinetics thereof.

Peptide	Config- uration	Radio- nuclide	4h tumor- to-kidney ratio	Reference
DOTA-CCMSH	L	^{111}In	0.12	Chen et al. (2001)[59]
DOTA-ReCCMSH	C	^{111}In	1.02	Chen et al. (2001)[59]
DOTA-NDP-MSH	L	^{111}In	0.78	Froidevaux et al. (2002)[110]
DOTA-MSH$_{oct}$	L	^{111}In	0.32	Froidevaux et al. (2002)[110]
DOTA-Re(Arg^{11})CCMSH	C	^{111}In	2.36	Cheng et al. (2002)[60]
^{188}Re-CCMSH	C	^{188}Re	0.17	Miao et al. (2003)
^{188}Re-(Arg^{11})CCMSH	C	^{188}Re	0.32	Miao et al. (2003)
DOTA-NAPamide	L	^{67}Ga	2.37	Froidevaux et al. (2004)[114]
DOTA-NAPamide	L	^{111}In	1.63	Froidevaux et al. (2005)[115]
[DOTA-Nle^4,Asp^5,D-Phe^7,Ac-Lys^{11}-NH$_2$]-α-MSH$_{4-11}$	L	^{111}In	1.06	Froidevaux et al. (2005)[115]
[DOTA-Nle^4,Asp^5,D-Phe^7,Suc-Lys^{11}-NH$_2$]-α-MSH$_{4-11}$	L	^{111}In	0.58	Froidevaux et al. (2005)[115]
DOTA-Re(Arg^{11})CCMSH	C	^{90}Y	0.57	Miao et al. (2006)[207]
DOTA-Re(Glu^2,Arg^{11})CCMSH	C	^{90}Y	1.30	Miao et al. (2006)[207]
DOTA-Re(Glu^2,Arg^{11})CCMSH	C	^{177}Lu	1.57	Miao et al. (2006)[207]
DOTA-Cyc-MSH (lactam cyclized)	C	^{111}In	0.35	Miao et al. (2008)[209]
DOTA-GlyGlu-Cyc-MSH (lactam cyclized)	C	^{111}In	0.61	Miao et al. (2008)[209]

(L stands for linear, C for cyclic)

Table 7 indicates that most modifications adopted did not improve the tumor-to-kidney ratio of α-MSH analogs. For example, different cyclized peptides appear to have similar or inferior properties than the latest linear peptides. One cyclic peptide (DOTA-Re(Arg^{11})CCMSH) labeled with ^{111}In seems to have excellent properties *in vivo*, but the same peptide labeled with ^{90}Y exhibits much inferior properties.

On the other side, not all modifications of linear peptides were successful at improving the tumor-to-kidney ratio, but investigations led to a very promising peptide, DOTA-NAPamide, that has since its development also been used by other groups[62,63]. Indeed, investigations showed that the properties of DOTA-NAPamide observed when labeled with ^{111}In were even improved when labeled with ^{67}Ga. Isotopes of Ga have many advantages. ^{68}Ga can be produced from an on-site generator, and its half-life is quite short (68 min). ^{67}Ga is suited for tumor diagnosis and potentially for internal radiotherapy (Auger electrons). Therefore, Ga-

labeled analogs would provide polyvalent tools for the clinical management of melanoma, including PET-diagnosis or -staging[114].

Linear peptides certainly remain a very promising tool, as they are easier to synthesize than cyclic peptides and their potential has apparently not been fully exploited yet. Some critical parameters improving their pharmacokinetical profile, though, still have to be discovered or improved. It appears that the choice of ^{111}In as labeling radionuclide is adequate, as it constitutes an excellent "precursor" to studies with gallium isotopes. DOTA as chelate represents the method of choice as well, for its ability to bind various radiometals and for the stability of its complexes, as already mentioned in chapter **2.3**.

To improve the pharmacokinetical properties of α-MSH analogs, several of these modifications and ameliorations were considered and combined to new features in this work. As mentioned in the "aims of the thesis" (see chapter **1.8**), new types of derivatives were synthesized. First, peptide dimers, then glycopeptides, and finally negatively-charged peptides. The results obtained will be described and analyzed in the next three chapters (chapters **3**,**4** and **5**), that represent or contain manuscripts of three papers which already appeared (chapter **3**) or will be submitted for publication (chapters **4** and **5**).

3 Dimeric peptides

3.1 Published manuscript

Dimeric DOTA-α-Melanocyte-Stimulating Hormone Analogs: Synthesis and *In Vivo* Characteristics of Radiopeptides with High *In Vitro* Activity[*]

Jean-Philippe Bapst, Sylvie Froidevaux[†], Martine Calame, Heidi Tanner and Alex N. Eberle

Laboratory of Endocrinology, Department of Research, University Hospital and University Children's Hospital, Basel, Switzerland

Address correspondence to Prof. Dr. Alex N. Eberle, Department of Research, University Hospital Basel, Klingelbergstrasse 23, CH-4031 Basel, Switzerland. Fax: +41-61-265-2706; E.mail: Alex-N.Eberle@unibas.ch

Running title: Dimeric DOTA-α-MSH analogs for melanoma targeting

Key words: Melanoma, MC1R, α-MSH, DOTA, dimeric peptide, tumor targeting

Abbreviations: α-MSH, α-melanocyte stimulating hormone; AUC, area under the curve; DOTA, 1,4,7,10-tetraazacyclododecane-1,4,7,10-tetraacetic acid; DTPA, diethylenetriaminepentaacetic acid; ID/g, injected dose per gram; MC1R, melanocortin-1 receptor.

[*]This paper is dedicated to Professor Dr. Günther Jung, University of Tübingen, Germany, on the occasion of his 70th birthday.

[†]Present address: Actelion Pharmaceuticals Ltd., CH-4123 Allschwil, Switzerland.

ABSTRACT

Dimeric analogs of α-melanocyte stimulating hormone (α-MSH) labeled with radiometals are potential candidates for diagnosis and therapy of melanoma by receptor-mediated tumor targeting. Both melanotic and amelanotic melanoma (over-)express the melanocortin-1 receptor (MC1-R), the target for α-MSH. In the past, dimerized MSH analogs have been shown to display increased receptor affinity as compared to monomeric MSH, offering the possibility of improving the ratio between specific uptake of radiolabeled α-MSH by melanoma and non-specific uptake by the kidneys. We have designed three linear dimeric analogs containing a slightly modified MSH hexapeptide core sequence (Nle-Asp-His- D-Phe-Arg-Trp) in parallel or antiparallel orientation, a short spacer and the DOTA chelator for incorporation of the radiometal. *In vitro*, all three peptides were more potent ligands of the mouse B16-F1 melanoma cell melanocortin-1 receptor (MC1-R) than DOTA-NAPamide which served as standard. The binding activity of DOTA-diHexa(NC-NC)-amide was 1.75-fold higher, that of diHexa(NC-NC)-Gly-Lys(DOTA)-amide 3.37-fold higher, and that of DOTA-diHexa(CN-NC)-amide 2.34-fold higher. Using human HBL melanoma cells, the binding activity of diHexa(NC-NC)-Gly-Lys(DOTA)-amide was 6-fold higher than that of DOTA-NAPamide. Uptake by cultured B16-F1 cells was rapid and almost quantitative. *In vivo*, however, the data were less promising: tumor-to-kidney ratios 4 h post-injection were 0.11 for [111In]DOTA-diHexa(NC-NC)-amide, 0.26 for diHexa(NC-NC)-Gly-Lys([111In]DOTA)-amide, and 0.36 for [111In]DOTA-diHexa(CN-NC)-amide, as compared to 1.67 for [111In]DOTA-NAPamide. It appears that despite the higher affinity to the MC1-R of the peptide dimers and their excellent internalization *in vitro,* the uptake by melanoma tumors *in vivo* was lower, possibly because of reduced tissue penetration. More striking however was the marked increase of kidney uptake of the dimers, explaining the unfavorable ratios. In conclusion, although radiolabeled α-MSH dimer peptides display excellent receptor affinity and internalization, they are no alternative to the monomeric DOTA-NAPamide for *in vivo* application.

INTRODUCTION

A variety of human tumors express or overexpress receptors for one or more of the many known regulatory neuropeptides or peptide hormones, thereby offering attractive targeting systems for tumor diagnosis and imaging[248]. Radiolabeled antibodies and peptides are the tools of choice for this kind of cancer management[91,137]. Because of their much lower molecular weight, and hence their very low immunogenicity and excellent tumor penetration, radiopeptides have attracted steadily increasing interest in receptor-mediated tumor targeting during the past fifteen years. The list of the different regulatory peptides for tumor targeting in preclinical development has now exceeded the number of thirty[48,91,198], but routine application as diagnostics in the clinic is confined to a much smaller number[250], and internal radiotherapy is currently carried out with only a few selected radiopeptides[251]. The best example illustrating the rational of the strategy of receptor-mediated tumor targeting are radiolabeled analogs of somatostatin which are routinely used to image tumors expressing somatostatin receptors, thus demonstrating promise for internal radiotherapy in patients[112]. Yet, retention of considerable amounts of the injected dose by the kidneys limits the therapeutic efficacy of radiopeptides, as renal toxicity is the dose-limiting factor[70,177,227]. For the same reason diagnosis of tumors localized in the kidney region is strongly compromised. Renal accumulation of radiopeptides is however not specific to somatostatin analogs containing metal chelators such as macrocyclic DOTA (1,4,7,10-tetraazacyclododecane-1,4,7,10-tetraacetic acid) or linear DTPA (diethylenetriaminepentaacetic acid)[109]; it is also observed with other peptides or antibody fragments[31]. Methods have therefore been developed to reduce uptake by the kidneys, such as infusion of basic amino acid cocktails[31,34]. Although much experience with the dosing of ^{90}Y- or ^{177}Lu-labeled somatostatin analogs has been acquired in the meantime[38,92,96,176], the success of the therapeutic strategy with any other radiopeptide will rely on the possibility to lower their renal uptake[39]. Efforts are therefore focusing on the elucidation of the mechanism of retention of radiopeptides in the kidneys: It is now relatively well established that radiopeptides are reabsorbed by proximal tubules via luminal endocytosis after glomerular filtration. The peptides are then delivered to lysosomes where they are hydrolyzed to a final radioactive metabolite that cannot leave the lysosomes, leading to long-term sequestration of the radioisotope in the proximal tubular cells[33,39]. Radiopeptides exhibiting lower renal uptake *per se* would clearly represent a major step forward. However, as this is difficult to achieve, an alternative strategy is the development of radiopeptides with markedly enhanced tumor uptake so that the dose of injected radiopeptide can be reduced, leading to lower kidney uptake.

The tridecapeptide hormone α-melanocyte stimulating hormone (α-MSH, MSH) has been studied extensively in the context of its melanogenic activity in melanocytes and melanoma cells (reviewed in [87-89,98]). MSH and its target, the type-1 melanocortin receptor (MC1-R), have turned out to be important regulators of pigment formation in mammalian skin[87], including man[2], and it was even proposed that MSH may be a useful pharmacological regulator of human skin tanning in the absence of or synergistically with sun light[82,132]. Whereas human melanocytes generally express low numbers of MC1-R[76] and none of the other four MC receptor subtypes (i.e. MC2-R to MC5-R), melanoma cells frequently overexpress MC1-R which is therefore regarded as useful malignant melanoma marker[21,122,159,264,284,287]. This was the basis for

our original studies on the *in vivo* targeting of melanoma with ^{111}In-labeled α-MSH containing DTPA as chelator for insertion of a radiometal[19,20]. In the past few years, we have developed short linear α-MSH analogs containing the macrocyclic DOTA chelator, e.g. DOTA-[βAla[3], Nle[4], Asp[5], D-Phe[7], Lys[10]]-α-MSH$_{3-10}$, (DOTA-MSH$_{oct}$)[110] or [Nle[4], Asp[5], D-Phe[7], Lys[11](DOTA)]-α-MSH$_{4-11}$ (DOTA-NAPamide)[114], in which DOTA was conjugated to the N-terminal or, respectively, the C-terminal end of the peptide. After labeling with ^{111}In or ^{67}Ga/^{68}Ga, high and specific melanoma uptake and relatively moderate or low kidney uptake was observed in mice. The amount of radioactivity accumulation in the kidneys observed with [^{67}Ga]DOTA-NAPamide was the lowest reported to date compared with other synthetic DOTA-α-MSH analogs[59-61,90,202,204,207]. For example, [^{111}In]DOTA-MSH$_{oct}$, which shares 6/8 amino acids with DOTA-NAPamide, exhibited a kidney uptake of 13.5% ID/g 4 h post-injection[110] whereas renal uptake of [^{111}In]DOTA-NAPamide was only 3.98% ID/g[114], making this analog a promising radiopeptide for diagnosis and bringing internal radiotherapy of metastatic melanoma further within reach. Therefore, DOTA-NAPamide has in the meantime been employed as melanoma-targeting agent also by other researchers[62,63]. Nevertheless, reducing the kidney uptake further is of great importance, and as introduction of negative charges into the DOTA-NAPamide molecule did not alter kidney uptake[115], we thought to investigate possibilities of increasing the MC1-R receptor-affinity of the radiolabeled α-MSH ligand, thereby achieving the goal of higher tumor-to-kidney ratios by lowering the doses of the radiopharmaceutical for *in vivo* application, while maintaining excellent tumor uptake.

Various strategies have been employed to increase the potency of the α-MSH molecule (reviewed in [87]). The most striking effect was the introduction of a D-Phe residue in the place of Phe[7] of α-MSH, either in combination with simultaneous replacement of Met[4] by Nle[(267)] or maintaining the original Met at position 4[(87)]. This led to an elevation of receptor binding and activation by an average factor of 10 (depending on the biological system studied) and also to an increased duration of the response (owing to high resistance against proteolysis). Reduction of the α-MSH sequence with simultaneous modification of certain residues[10,87,215] or cyclization of the peptide sequences[123,124,133,267] also positively affected the stability, potency and selectivity to MC receptor subtypes, but all these structural changes were much less striking than the insertion of the D-Phe residue at position 7. Another striking effect on the potency of α-MSH peptides has already been reported in 1977, when several MSH molecules were covalently attached to albumin or thyroglobulin[84,85], or to the tobacco mosaic virus (TMV)[171], leading to a marked increase of potency of the complexes as compared to the free ligand. This synergistic effect was particularly evident with the TMV complex which contained approximately 300 α-MSH molecules per virus particle and displayed a 1,500-fold higher potency than α-MSH[171]. During these studies we noticed[86,87] that also dimerized α-MSH, which was prepared by introducing a maleimido group in the N-terminus of the molecule, followed by crosslinking two molecules with dithioethane, displayed a 2.2- to 4.5-fold higher activity than α-MSH in the Cloudman S91 tyrosinase assay and the *Rana pipiens* pigment migration assay, respectively. Vaudry and colleagues[100] investigated dimerized ACTH(1-24), ACTH(7-24) and ACTH(11-24) on frog adrenal gland slices (expressing MC2-R) and found that dimeric ACTH(1-24) had reduced steroidogenic activity as compared to monomeric ACTH(1-24) but dimerized ACTH(7-24) and (11-24) displayed marked antagonist activity which was more prominent than that of the monomer compounds. Finally, Hruby and

colleagues[314] later prepared a series of short MSH tetra- and hexapeptide dimers, linked with different types of spacer; the general findings were that dimerization led to enhanced potency for several of these peptides[314]. A dimerized MSH analog for tumor imaging had already been reported by Bagutti *et al.*[21] who attached two MSH moieties to one DTPA chelator molecule; this compound displayed high *in vitro* activity. The current study followed a different approach: three homodimer hexapeptide MSH fragments with different orientation and containing only one chelator molecule at different positions were designed (**Figure 30**) synthesized and studied *in vitro* and *in vivo*. We demonstrate that high *in vitro* potency at the melanoma MC1-R will not necessarily lead to elevated melanoma-to-kidney ratios *in vivo*.
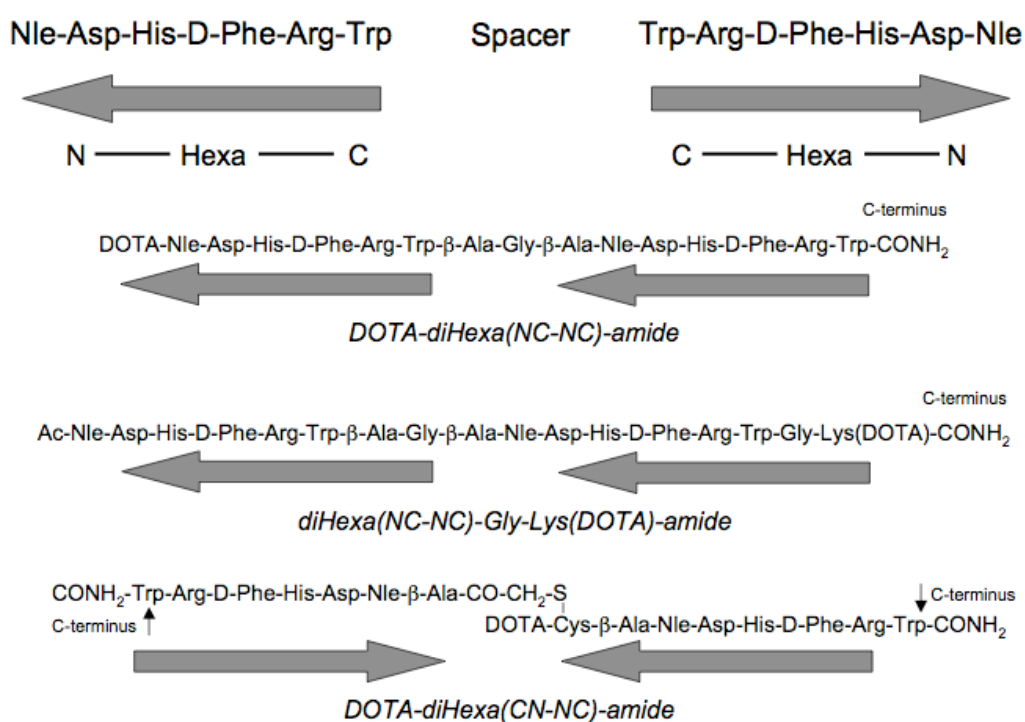

Figure 30: General orientation of the hexapeptide Nle-Asp-His-D-Phe-Arg-Trp sequence in the dimer peptides: DOTA-diHexa(NC-NC)-amide and diHexa(NC-NC)-Gly-Lys(DOTA)-amide contained the two hexapeptides in linear parallel and consecutive N-to-C–spacer–N-to-C orientation; the spacer was β-Ala-Gly-β-Ala. In DOTA-diHexa(NC-NC)-amide, the DOTA moiety was attached at the N-terminus. In diHexa(NC-NC)-Gly-Lys(DOTA)-amide, the sequence was extended at the C-terminus by a –Gly-Lys-amide containing the DOTA in the e-amino position of Lys. The DOTA-diHexa(CN-NC)-amide contained the two hexapeptides in antiparallel C-to-N–linker–N-to-C orientation. The linker consisted of a Cys-β-Ala attached to the N-terminus of one hexapeptide and, respectively, a β-Ala (containing a iodoacetyl group at its amino group) attached to the N-terminus of the other hexapeptide. The hexapeptide dimer was obtained by reacting the SH group of Cys with iodoacetyl of β-Ala, leaving the amino group of Cys free for attachment of DOTA.

MATERIALS AND METHODS

Reagents

α-MSH was a gift from Novartis (Basel, Switzerland). [Nle[4], D-Phe[7]]-α-MSH (NDP-MSH) was purchased from Bachem (Bubendorf, Switzerland). 9-Fluorenylmethoxycarbonyl-(Fmoc-)amino acids were from Novabiochem (Läufelfingen, Switzerland), Fmoc-PAL-PEG-PS polystyrene resin from Applied Biosystems (Rotkreuz, Switzerland), and 1,4,7,10-tetraazacyclododecane-1,4,7-tris-*tert*-butyl acetate-10-acetic acid (DOTA-tris(*t*-butyl ester)) from Macrocyclics (Dallas TX, USA). *N*-Succinimidyl iodoacetate and Iodogen tubes were obtained from Pierce Biotechnology Inc. (Rockford IL, USA), Na[125]I (3.7 GBq/mL) from Amersham Bioscience (Otelfingen, Switzerland), [111]InCl$_3$ (370 MBq/mL) from Mallinckrodt (Petten, The Netherlands). 1,10-Phenanthroline was bought from Merck (Darmstadt, Germany) and all other organic reagents were obtained from Fluka or Sigma (Buchs, Switzerland) and were of highest purity available. Cell culture media were from Biochrom AG (Berlin, Germany) and Sigma (Buchs, Switzerland). Penicillin, streptomycin, vitamins and nonessential amino acids were all from Gibco/Invitrogen (Carlsbad CA, USA).

Instrumentation

Peptide synthesis was carried out on a Pioneer peptide synthesizer from PerSeptive Biosystems Inc. (Framingham MA, USA). Analytical reversed-phase-(RP)-HPLC was performed on a PU-980 system from Jasco Inc. (Easton MD, USA) with either Vydac 218TP54 C18 analytical columns (5 μm, 4.6×250 mm) or Waters Symmetry C18 analytical columns (5 μm, 3.9×150 mm). Preparative RP-HPLC of peptides used the same system but either with Vydac 218TP510 C18 semi-preparative columns (5 μm, 10×250 mm) or Waters SymmetryPrep C18 preparative columns (7 μm, 19×150 mm). Peptides were chromatographed with a gradient between solvent A (0.1% TFA in H$_2$O) and solvent B (0.1% TFA in 70:30 acetonitrile/H$_2$O). The 32-min gradient cycle consisted of the following parts: 95-10% A (0-27 min), 10-95% A (27-30 min), 95% A (30-32 min); the flow rate was 1 mL/min for the analytical columns, 3 mL/min for the semi-preparative column and 5 mL/min for the preparative column. UV absorption was recorded at 280 nm using a Jasco UV-1570 detector. Mass spectra were recorded on a Finnigan LCQ Deca electrospray ion trap MS system.

Purity of radioligands was assessed by RP-HPLC using a dedicated Jasco PU-980 chromatography system connected to a Radiomatic 500TR LB506C1 γ-detector (Packard, Meriden CT, USA) and equipped with a Spherisorb ODS2/5-μm column. Solvent A was 0.1% TFA in water; solvent B was 0.1% TFA in acetonitrile; the gradient cycle consisted of 96% A (0-2 min), 96-45% A (2-22 min), 45-25% A (22-30 min), 25% A (30-32 min), 25-96% A (32-34 min); the flow rate was 1.0 mL/min.

Cell-bound radioactivity from binding assays was collected on filters using a cell harvester (Packard) and measured on a TopCount microplate scintillation counter (Packard). Radioactivity in internalization and

biodistribution assays was measured on a Cobra II Auto-Gamma γ-counter (Packard). Melanin content in cell culture media was quantified at 310 nm with a Spectra Max 190 microplate reader (Molecular Devices, Menlo Park CA, USA).

Peptide synthesis

General

The peptides were synthesized in our laboratory on an automated Pioneer instrument using standard continuous-flow technology and Fmoc strategy[18]. As solid-phase support, flow-compatible Fmoc-PAL-PEG-PS polystyrene resin containing the acid-labile amide linker PAL (5-[(4-Fmoc-aminomethyl-3, 5-dimethoxyphenoxy]-pentanoic acid-polyethyleneglycol/polystyrene; substitution 0.21 mmol/g) was employed. Each synthesis cycle consisted of an Fmoc deprotection step (20% piperidine in DMF; 5 min), a coupling step (4 eq of Fmoc-amino acid; DIPEA and TBTU/HOBt in DMF; 60 min), and two washing steps after deprotection and coupling, respectively, using DMF (3 min). The following protecting groups were used for *o*-protection: Trt for Cys, Boc for Lys and Trp, *t*Bu for Asp, Pbf for Arg, and Trt for His. Manual Fmoc deprotection was also carried out with 20% piperidine in DMF (20 min), followed by a short wash with 20% piperidine/DMF and 5 washes of DMF; the deprotection was controlled by Kaiser test. Cleavage of the peptides from the resin was performed by addition of a solution containing 90% trifluoroacetic acid (TFA), 5% thioanisole, 4.5% H_2O and 0.5% 1,2-ethanedithiol. After 2 h the solution was filtrated and the peptide precipitated.

Conjugation of DOTA-tris(*t*-butyl ester) to the peptide derivatives was performed by addition of a solution containing the deprotected peptide (1 eq) and DIPEA (N,N'-diisopropylethylamine; 1.5 eq) in DMF (0.5 ml) to a solution containing DOTA-tris(*t*-butyl ester) (1 eq) which had been preincubated for 10 min with HATU (0-[7-azabenzotriazole-1-yl]-1,1,3,3-tetramethyluronium hexafluorophosphate; 1.2 eq) in DMF (0.5 ml). After 1 h of incubation at room temperature, another portion of preactivated DOTA-tris(*t*-butyl ester) was added in two portions. After a total reaction time of 2 h and subsequent precipitation of the peptides in ice-cold *t*-butylmethyl ether, deprotection of DOTA was performed by the addition of a solution of 90% TFA, 5% thioanisole, 4.5% H_2O and 0.5% 1,2-ethanedithiol (4 ml/5 mg of peptide). The mixture was stirred for 4 h, deprotected DOTA-peptide precipitated with ice-cold *t*-butylmethyl ether, resuspended in 10% acetic acid and purified by RP-HPLC. The major peaks were collected and analyzed by electrospray ionization ion trap mass spectrometry. All reactions and manipulations with DOTA were done in acid-treated (1 M HCl, >1 h) glassware.

DOTA-NAPamide

NAPamide was synthesized according to the general methods described above. The peptide was N-terminally acetylated before cleavage from the resin: *p*-nitrophenyl acetate (2 eq) pre-activated with HOBt (1 eq) in DMF for 10 min was added to resin-bound NAPamide (1 eq) and incubated for 24 h, keeping the

volume of DMF as low as possible. The resin was filtrated and washed 5× with DMF and 4× with isopropanol. Cleavage from the resin and purification was done according to standard methods. The DOTA moiety was coupled to the ε-amino group of C-terminal Lys and the peptide conjugate deprotected and purified as described above. RP-HPLC on a Waters Symmetry analytical column: t_R = 9.53 min. Calculated monoisotopic mass: 1485.64 gmol^{-1}; found: 1485.65 gmol^{-1}.

DOTA-diHexa(NC-NC)-amide

DiHexa(NC-NC)-amide (**Figure 31**) was synthesized according to the general methods and DOTA was coupled to the N-terminus of the peptide when still attached to the resin. The conjugate was cleaved, precipitated, purified by HPLC and lyophilized. Calculated monoisotopic mass: 2312.55 gmol^{-1}; found: 2313.2 gmol^{-1}.
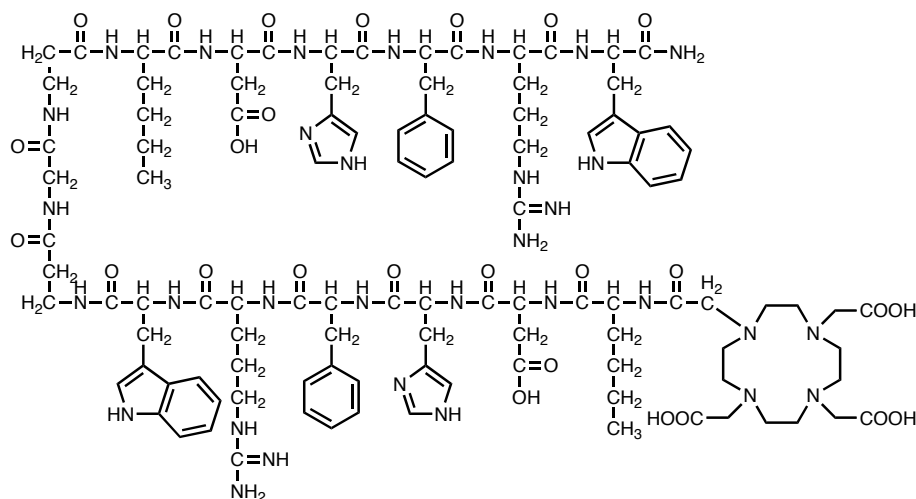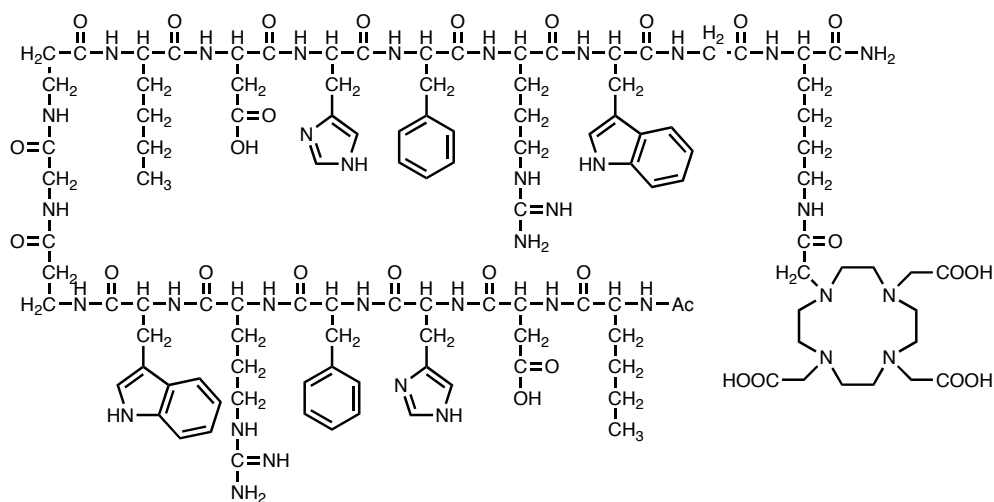

DOTA-diHexa(NC-NC)-amide

Figure 31: Chemical structure of DOTA-diHexa(NC-NC)-amide.

DiHexa(NC-NC)-Gly-Lys(DOTA)-amide

DiHexa(NC-NC)-Gly-Lys-amide (Figure 32) was synthesized according to the general methods. A small amount of resin-bound tetradecapeptide was cleaved using the standard cleavage mixture, precipitated, purified by RP-HPLC and analyzed by mass spectrometry. RP-HPLC on a Waters Symmetry analytical column: t_R = 10.85 min. Calculated monoisotopic mass: 2110.08 gmol-1; found: 2110.21 gmol-1.

N-terminal acetylation of resin-bound diHexa-(NC-NC)-Gly-Lys was carried out as described above for NAPamide. After cleavage from the resin and precipitation, the purification by RP-HPLC on a Waters Symmetry analytical column yielded a product peak at t_R = 12.8 min. Calculated monoisotopic mass: 2153.41 gmol^{-1}; found: 2153.2 gmol^{-1}.

diHexa(NC-NC)-Gly-Lys(DOTA)-amide

Figure 32: Chemical structure of diHexa(NC-NC)-Gly-Lys(DOTA)-amide.

DOTA-tris(t-butyl ester) was coupled to the ε-amino group of C-terminal Lys using standard procedures. After removal of the DMF, the product was dried in high vacuum for several hours. DOTA was deprotected in standard 90% TFA-mixture for 4 h, the peptide conjugate precipitated with t-butylmethyl ether, dried, purified by RP-HPLC, and lyophilized. RP-HPLC on a Waters Symmetry analytical column: t_R = 13.12 min. Calculated monoisotopic mass: 2539.81 gmol-1; found: 2539.80 gmol-1.

DOTA-diHexa(CN-NC)-amide

DiHexa(CN-NC)-amide (**Figure 33**) was assembled by first synthesizing the two fragments A and B separately on the automated synthesizer, followed by fragment coupling. Fragment A, H-βAla-Nle-His-D-Phe-Arg-Trp-amide, was prepared, purified and analyzed by mass spectrometry according to the general methods. Calculated monoisotopic mass: 943.08 gmol[-1]; found: 943.5 gmol[-1]. Fragment B, H-Cys-βAla-Nle-His-D-Phe-Arg-Trp-amide, was synthesized in the same way. Calculated monoisotopic mass: 1046.225 gmol[-1]; found: 1046.5 gmol[-1].
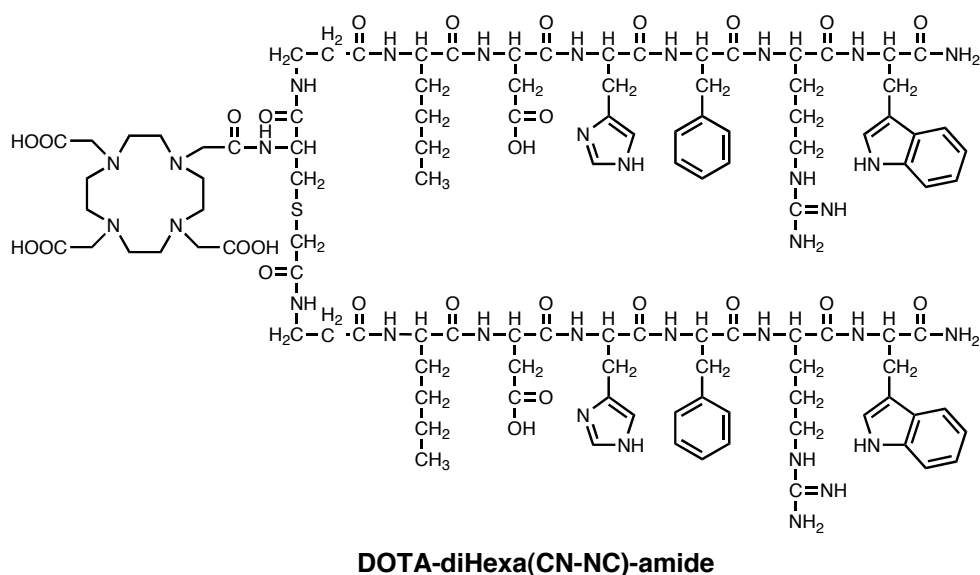
DOTA-diHexa(CN-NC)-amide

Figure 33: Chemical structure of DOTA-diHexa(CN-NC)-amide.

The two fragments were coupled by first dissolving fragment A (1 eq) in DMF, adding *N*-succinimidyl iodoacetate (1.7 eq) dissolved in DMF, and then adding 2.5 volumes of a borate/EDTA buffer (0.16 M Na-borate, 50 mM EDTA, pH 8). The mixture was incubated under argon at room temperature for 30 min. Fragment B (1 eq) was dissolved in DMF, added to iodoacetylated fragment A and incubated under argon at room temperature for 60 min. The conjugate was purified by RP-HPLC and lyophilized. The DOTA moiety was then coupled to the peptide using the usual procedures. After deprotection of DOTA in standard 90% TFA-mixture for 4 h and precipitation, DOTA-diHexa(CN-NC)-amide was purified by RP-HPLC and lyophilized. Calculated monoisotopic mass: 2415.69 gmol^{-1}; found: 2415.7 gmol^{-1}.

Radiolabeling of peptides

Labeling with ^{111}In

Incorporation of ^{111}In into dimer DOTA-peptides was performed by the addition of 55.5 MBq of ^{111}InCl$_3$ to the DOTA-peptides (10 nmol) dissolved in 54 μl acetate buffer (0.4 M, pH 5) containing 2 mg of gentisic acid. After 10 min of incubation at 95°C, the radiolabeled DOTA-peptides were purified on a small reversed-phase cartridge (Sep-Pak C18, Waters) by first washing the column with 0.4 M sodium acetate buffer (pH 7) and then eluting it with ethanol. The purity of the radioligands was assessed by RP-HPLC/γ-detection (see above). The specific activity of the radioligand was always >7.4 GBq/μmol.

Radioiodination

Radioiodination of NDP-MSH was performed with the Iodogen® (Pierce) method. To this end, NDP-MSH (12.14 nmol) was mixed with Na^{125}I (37 MBq; Amersham) in 60 μl phosphate buffer (0.3 M, pH 7.4) in a Iodogen®-precoated tubes. After a 15-min incubation at room temperature under shaking, the iodination

mixture was loaded onto a small reversed-phase cartridge (Sep-Pak C18, Waters) which was washed consecutively with water and acetic acid (0.5 M), and finally the peptide was eluted with methanol and collected. The fractions containing [^{125}I]NDP-MSH were supplemented with dithiothreitol (1.5 mg/mL) and stored at –20°C. Preceding each binding experiment, an additional purification was performed by RP-HPLC, and the radiotracer was lyophilized from lactose/bovine serum albumin (BSA) (20 mg of each per ml H_2O).

Cell culture

The mouse B16-F1 melanoma cell line[101] was cultured in modified Eagle's medium (MEM) supplemented with 10% heat-inactivated fetal calf serum, 2 mmol/L L-glutamine, 1% nonessential amino acids, 1% vitamin solution, 50 IU/mL penicillin and 50 μg/mL streptomycin, in an atmosphere of 95% air/5% CO_2 and at a temperature of 37°C. For cell expansion or experiments with isolated cells, the B16-F1 cells were detached with 0.02% EDTA in PBS (phosphate-buffered saline; 150 mM, pH 7.2-7.4). The human HBL melanoma cell line was cultured in modified RPMI medium supplemented with 10% heat-inactivated fetal calf serum, 2 mM L-glutamine, 50 IU/mL penicillin and 50 μg/mL streptomycin in the same conditions as for B16-F1 cells.

In vitro *binding assay*

Competition binding experiments were performed in 96-well U-bottom microplates (Falcon 3077), each well containing 100 μL of B16-F1 or HBL cell suspensions adjusted to 4×10^6 cells/mL. The binding medium consisted of MEM with Earle's salts, 0.2% BSA and 0.3 mM 1,10-phenanthroline. Triplicates of competitor peptide solution (50 μL), yielding a final concentration ranging from 1×10^{-6} to 1×10^{-12} M, were added, followed by the addition of 50,000 cpm [^{125}I]NDP-MSH in 50 μL to each well[111]. The incubation conditions were 15°C for 3 h for B16-F1 cells and 37°C for 2 h for HBL cells. The reaction was stopped by placing the plates on ice for 10 min. The cell-bound radioactivity was collected on filters (Packard Unifilter-96 GF/B) by use of a cell harvester, and the radioactivity was counted on a TopCount scintillation counter (Packard). The IC_{50} values were calculated with Prism software (GraphPad Software Inc., San Diego CA, USA).

In vitro *melanin assay*

The biological activity of the α-MSH derivatives was assessed with an *in situ* melanin assay[283]. Briefly, B16-F1 cells (2,500 cells per well in 100 μl) were distributed into 96-well flat-bottom cell culture plates, using MEM without phenol red and supplemented with 10% heat-inactivated fetal calf serum, 2 mM L-glutamine, 1% nonessential amino acids, 1% vitamin solution, 50 IU/mL penicillin and 50 μg/mL streptomycin. After incubation for approximately 16 h (overnight) at normal cell-culture conditions, serial concentrations of α-MSH derivatives ranging from 1×10^{-8} to 1×0^{-12} in 100-μL volumes were added and the incubation was continued for an additional 72 h. Melanin production was quantified by determining the absorbance at 310 nm in a microplate reader.

In vitro *internalization assay*

B16-F1 cells were seeded in 6-well plates and incubated overnight in MEM at 37°C. For the internalization experiments, the MEM was replaced by 1 mL mouse binding medium (MBM) internalization buffer, consisting of MEM with Earle's salts, 0.2% BSA and 0.3 mM 1,10-phenanthroline. After a 1-h incubation at 37°C, 74 kBq of radioligand were added and the plates incubated for different times. Nonspecific internalization was determined by addition of 50 μL of a 1 μM α-MSH solution to the incubation mixture. At the various time points indicated, the cells were extensively washed with MBM kept at 37°C to remove excess radioligand. The cells were then incubated in 2 ml ice-cold acid buffer (acetate-buffered Hank's balanced salt solution, pH 5) for 10 min to allow dissociation of surface-bound ligand. After collection of the acid buffer fraction, the cells were rinsed once with cold MBM and the washings were pooled with the acid buffer fraction. The cells were then washed once more with MBM kept at 37°C, lysed in 1% Triton X-100 and finally transferred to tubes for quantification. The radioactivity of all collected fractions was measured in a γ-counter. Results are expressed as percent of the added dose per million cells.

Biodistribution and stability of radioligands in B16-F1 tumor-bearing

All animal experiments were performed in compliance with the Swiss regulations for animal welfare. Female B6D2F1 mice (C57BL/6×DBA/2F1 hybrids; breeding pairs obtained from IFFA-CREDO, France) were implanted subcutaneously with 500,000 B16-F1 cells in phosphate buffered saline (PBS), pH 7.4, to generate a primary skin melanoma. One week later, 185 kBq of [^{111}In]DOTA-peptide in 200 μL PBS containing 0.1% BSA were injected i.v. into the lateral tail vein of each mouse. To allow determination of non-specific uptake of radioligand, 50 μg α-MSH were coinjected with the radioligand in control animals. The animals were killed at the indicated time points; organs and tissues of interest were dissected and rinsed of their excess blood, weighed, and their radioactivity was measured in a γ-counter. The percentage of the injected dose per gram tissue (%ID/g) was calculated for each tissue. The total counts injected per animal were calculated by extrapolation from counts of a standard taken from the injected solution for each animal.

As part of the biodistribution experiments, samples of urine were collected from melanoma-bearing mice at 10, 15, 20 min and 4 h after injection of 185 kBq [^{111}In]DOTA-peptide and kept frozen at -80°C until use. Urine (1 vol) was mixed with methanol (2 vol) to precipitate the proteins and the supernatant was analyzed by RP-HPLC/γ-detection, as described above.

Analysis of data

Unless otherwise stated, results are expressed as means ± SEM. Statistical evaluation of the binding assays was performed using the Student's *t* test. For analysis of biodistribution experiments, each mean value obtained for each organ was compared individually using the Student's *t* test and the results were corrected using the Bonferroni correction. A P value of <0.05 was considered statistically significant. The

area under the curve (AUC) was calculated for a particular time period (4-48 h) using the Prism software; mean tissue uptake values at each time point were taken for this calculation.

RESULTS

Design, synthesis and labeling of dimer DOTA-MSH hexapeptide analogs

Three dimer MSH peptides were designed which contained a slightly modified hexapeptide core sequence of the α-MSH molecule, Nle-Asp-His-D-Phe-Arg-Trp, in either parallel N-to-C–spacer–N-to-C orientation or in antiparallel C-to-N–linker–N-to-C orientation. DOTA-diHexa(NC-NC)-amide and diHexa(NC-NC)-Gly-Lys(DOTA)-amide contained the two hexapeptides in the former orientation; the two hexapeptides and the tripeptide spacer βAla-Gly-βAla as well as the dipeptide –Gly-Lys extension at the C-terminus of the second peptide were assembled as linear 15-residue and, respectively, 17-residue peptides (Fig. 1). In DOTA-diHexa(NC-NC)-amide, the DOTA moiety was attached at the N-terminus, in analogy to DOTA-MSH$_{oct}$[110]. In diHexa(NC-NC)-Gly-Lys(DOTA)-amide, the DOTA was incorporated in the sequence extension at the C-terminus (–Gly-Lys(DOTA)-amide) to allow for easier fragmentation and excretion in the kidneys, similar to DOTA-NAPamide[114]. The third dimer peptide, DOTA-diHexa(CN-NC)-amide, contained the two hexapeptides in antiparallel C-to-N–linker–N-to-C orientation. The dimer was obtained by first extending one of the hexapeptides by a βAla at its N-terminus, followed by coupling iodoacetyl to its free terminal amino group. The other hexapeptide was extended at its N-terminus by a Cys-βAla moiety. The resulting hepta- and octapeptides were then linked through a thioether bond by reaction of the SH group of Cys with the iodoacetyl of βAla, leaving the amino group of Cys free for attachment of DOTA.

The synthesis, cleavage from the resin and purification of the linear hepta-, octa-, pentadeca- and heptadecapeptides were as straightforward as for NAPamide. Small amounts of the unprotected peptides were kept for biological assays. The larger part was used for attachment of DOTA (for the diHexa(CN-NC)-amide preceded by thioether bond formation), yielding highly pure final products after RP-HPLC purification (for analytical details see Materials and Methods). It is important to note that during purification we noticed a marked stickiness to surfaces of all dimer DOTA-peptides.

The radiolabeling of the dimer DOTA-peptides with ^{111}In was much less straightforward and the first experiments yielded low incorporation of the radiometal. It appeared that prolonged heating during the labeling reaction was detrimental for these peptides. Therefore, the labeling reaction was minimized to a 10-min incubation at 95°C and in addition, the labeling vial was precoated with 2% BSA to reduce non-specific adsorption of the dimer peptides. Although good incorporation could now be obtained, the stickiness of the dimer [^{111}In]DOTA-peptides was markedly higher than for monomeric DOTA-NAPamide.

Receptor binding and melanogenic activity

The newly designed dimeric MSH analogs were first tested in a competition binding assay using B16-F1 cells and [^{125}I]NDP-MSH as radioligand. **Figure 34** shows an exemplary experiment comparing diHexa(NC-NC)-Gly-Lys(DOTA)-amide with α-MSH as reference compound. The dimer peptide was about 4-fold more potent than the standard. The binding activity of diHexa(NC-NC)-Gly-Lys-amide without DOTA was about 3-fold higher than that of the DOTA-containing analog, i.e. the dimeric diHexa(NC-NC)-Gly-Lys-amide peptide was about 12-fold more potent than α-MSH and hence the most potent of the three different dimers (**Table 8**) to DOTA-NAPamide, diHexa(NC-NC)-Gly-Lys(DOTA)-amide displayed a 3.4-fold higher affinity in mouse B16-F1 cells, a 2.5-fold higher biological activity in the melanin assay, and a 6-fold higher affinity in human HBL cells, making it a promising candidate for *in vivo* targeting.
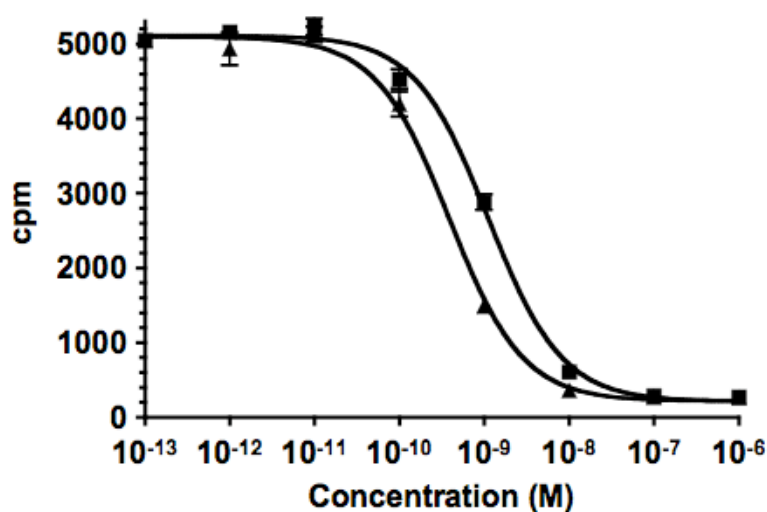

Figure 34: Exemplary competition binding experiment with diHexa(NC-NC)-Gly-Lys(DOTA)-amide (triangles) and α-MSH (squares) using B16-F1 mouse melanoma cells and [125I]-NPD-MSH as radioligand. Each value represents the mean ± SEM (n = 9: triplicate values of three

In the B16-F1 binding assay, DOTA-diHexa(NC-NC)-amide, which contained the DOTA at the N-terminus, was almost 2-fold less potent than diHexa(NC-NC)-Gly-Lys(DOTA)-amide. The difference between the two peptides was less prominent when the corresponding analogs without DOTA were compared (**Table 8**). The binding activity of DOTA-diHexa(CN-NC)-amide lay between the two other dimeric DOTA-peptides, differing from each by about a factor of 1.4. Interestingly, diHexa(CN-NC)-amide without DOTA was 1.5-fold less potent than the DOTA-containing analog. Summarizing these findings, the dimeric MSH peptides displayed enhanced biological activity in B16-F1 cells (and partly verified with HBL cells); the values were ranging between a 3- to 5-fold higher activity than that observed for the corresponding monomeric derivatives.

Table 8: MC1-R affinity and biological activity of α-MSH analogs with mouse B16-F1 and human HBL melanoma cells.

Peptide	B16-F1 Binding IC_{50} (nmol/L)[*]	HBL Binding IC_{50} (nmol/L)	Melanogenesis rEC_{50} (α-MSH = 1)[†]
α-MSH	1.74 ± 0.12	1.91 ± 0.26[‡]	1
DOTA-NAPamide	1.38 ± 0.35	3.09 ± 1.11	0.66 ± 0.35
diHexa(NC-NC)-amide	0.22 ± 0.01[‡]	ND	ND
DOTA-diHexa(NC-NC)-amide	0.79 ± 0.15	ND	ND
diHexa(NC-NC)-Gly-Lys-amide	0.14 ± 0.02[‡]	ND	ND
diHexa(NC-NC)-Gly-Lys(DOTA)-amide	0.41 ± 0.03	0.51 ± 0.04[‡]	0.27 ± 0.05
diHexa(CN-NC)-amide	0.87 ± 0.15	ND	ND
DOTA-diHexa(CN-NC)-amide	0.59 ± 0.02	ND	ND

[*]MC1R affinity of α-MSH analogs was assessed by competition binding experiments with B16F1 cells and ^{125}I-NDP-MSH as radioligand (n=3-26)

[†]Biological activity of α-MSH analogs was determined in melanin assay with B16-F1 cells, and the results are expressed as relative concentration (α-MSH = 1) inducing half-maximal response (rEC_{50}; n = 3-10).

[‡]$P < 0.05$ vs. DOTA-NAPamide

Internalization of diHexa(NC-NC)-Gly-Lys([^{111}In]DOTA)-amide

Internalization experiments were confined to one of the three dimer MSH radioligands. **Figure 35** shows data on the rate of internalization of the diHexa(NC-NC)-Gly-Lys([^{111}In]DOTA)-amide tracer into B16-F1 cells: after 30 min, 71% of total cell-bound radioligand was internalized, after 2 h internalization was 84%, and after 3.5 h 92%. This demonstrates that down-regulation/internalization of MC1-R in mouse melanoma cells was not retarded by dimer MSH radioligands.
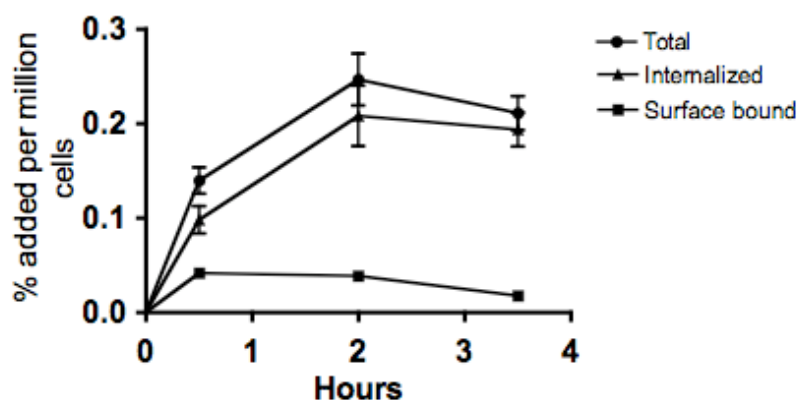

Figure 35: Determination of internalization of diHexa(NC-NC)-Gly-Lys([111In]DOTA)-amide by cultured B16-F1 cells exposed to the peptide at 37°C for 0.5 h, 2 h and 3.5 h. Surface bound radioligand was released by an acid buffer wash and internalized radioligand was determined by lysing cells with detergent. Results are expressed in percent of the added dose per million cells.

Biodistribution in melanoma-bearing mice

Table 9 presents the *in vivo* biodistribution of ^{111}In-labeled DOTA-containing dimer α-MSH analogs and NAPamide in B16-F1 melanoma-bearing mice 4 h, 24 h and 48 h post-injection, when tissues including melanoma tumors were collected. The three dimeric DOTA-MSH analogs accumulated in melanoma to different degrees. After 4 h, [^{111}In]DOTA-diHexa(CN-NC)-amide displayed a 1.17-fold higher accumulation in the tumor than [^{111}In]DOTA-NAPamide. By contrast, with [^{111}In]DOTA-diHexa(NC-NC)-amide only about 50% of the radioactivity and with diHexa(NC-NC)-Gly-Lys([^{111}In]DOTA)-amide about 65% were found in the tumor as compared to that of [^{111}In]DOTA-NAPamide (set as 100%). The radioactivity in the tumor delivered by dimer peptides also appeared to be lost at a slightly higher rate than after delivery with DOTA-NAPamide.

Table 9: Tissue distribution, including melanoma tumor, of 111In-labeled DOTA-containing dimer a-MSH analogs and NAPamide 4, 24 and 48h after injection.

Tissue distribution, including melanoma tumor, of ^{111}In-labeled DOTA-containing dimer α-MSH analogs and NAPamide 4, 24 and 48 h after injection.

Peptide	Time (h)	Blood	Tumor	Stomach	Kidney	Liver	Spleen	Lung	Small Intestine	Pancreas	Heart	Bone	Muscle	Skin
									%ID/g of Tissue†					
DOTA-NAPamide*	4	0.09 ± 0.02	7.77 ± 0.35	0.09 ± 0.01	4.77 ± 0.26	0.34 ± 0.05	0.14 ± 0.01	0.08 ± 0.01	0.07 ± 0.01	0.04 ± 0.00	0.05 ± 0.01	0.11 ± 0.02	0.05 ± 0.01	-
	24	0.02 ± 0.00	2.32 ± 0.15	0.12 ± 0.02	2.41 ± 0.20	0.31 ± 0.02	0.11 ± 0.01	0.05 ± 0.01	0.08 ± 0.01	0.03 ± 0.00	0.03 ± 0.00	0.14 ± 0.02	0.02 ± 0.00	-
	48	0.00 ± 0.00	1.41 ± 0.12	0.11 ± 0.05	1.55 ± 0.07	0.27 ± 0.02	0.10 ± 0.01	0.03 ± 0.00	0.05 ± 0.01	0.02 ± 0.00	0.01 ± 0.00	0.05 ± 0.01	0.01 ± 0.00	-
DOTA-diHexa(NC-NC)-amide	4	0.09 ± 0.00	3.81 ± 0.11‡	0.07 ± 0.02	34.78 ± 1.23‡	1.13 ± 0.06‡	0.33 ± 0.02‡	0.22 ± 0.02‡	0.10 ± 0.01	0.07 ± 0.00‡	0.08 ± 0.01	0.16 ± 0.01	0.06 ± 0.01	0.17 ± 0.03
	24	0.02 ± 0.00	1.21 ± 0.03‡	0.18 ± 0.04	20.30 ± 0.97‡	0.71 ± 0.02‡	0.31 ± 0.01‡	0.18 ± 0.04‡	0.08 ± 0.01	0.05 ± 0.00‡	0.06 ± 0.00‡	0.17 ± 0.01	0.04 ± 0.00‡	0.13 ± 0.01‡
	48	-	-	-	-	-	-	-	-	-	-	-	-	-
diHexa(NC-NC)-Gly-Lys(DOTA)-amide	4	0.05 ± 0.01	5.07 ± 0.98‡	0.29 ± 0.11‡	24.6 ± 5.84‡	1.89 ± 0.42‡	0.40 ± 0.10‡	0.09 ± 0.02	0.09 ± 0.03	0.16 ± 0.11	0.05 ± 0.01	0.08 ± 0.01	0.03 ± 0.01	0.17 ± 0.05
	24	0.02 ± 0.00	1.74 ± 0.12	0.12 ± 0.03	16.20 ± 0.99‡	1.79 ± 0.07‡	0.41 ± 0.02‡	0.10 ± 0.04	0.14 ± 0.07	0.09 ± 0.05	0.06 ± 0.01‡	0.11 ± 0.01	0.03 ± 0.00	0.07 ± 0.02
	48	0.01 ± 0.00‡	0.75 ± 0.05‡	0.06 ± 0.00	11.82 ± 1.01‡	1.41 ± 0.08‡	0.30 ± 0.04‡	0.13 ± 0.04	0.06 ± 0.01	0.04 ± 0.00‡	0.05 ± 0.00‡	0.09 ± 0.00‡	0.03 ± 0.00‡	0.07 ± 0.02
DOTA-diHexa(CN-NC)-amide	4	0.05 ± 0.01	9.08 ± 0.20	0.15 ± 0.03	25.12 ± 1.81‡	1.96 ± 0.12‡	0.33 ± 0.01‡	0.16 ± 0.02‡	0.16 ± 0.01‡	0.09 ± 0.00‡	0.12 ± 0.01‡	0.21 ± 0.01‡	0.06 ± 0.00	0.19 ± 0.01
	24	0.02 ± 0.00	2.19 ± 0.15	0.12 ± 0.01	15.65 ± 2.68‡	1.22 ± 0.11‡	0.24 ± 0.03‡	0.09 ± 0.01‡	0.13 ± 0.02	0.07 ± 0.01‡	0.09 ± 0.01‡	0.18 ± 0.02	0.05 ± 0.01‡	0.13 ± 0.02
	48	-	-	-	-	-	-	-	-	-	-	-	-	-

*Data for DOTA-NAPamide from Froidevaux et al. (J Nucl Med (2005) **46**, 887-895).
†Tissue radioactivity is expressed as mean ± SEM (n = 3-12).
‡P < 0.05 vs. DOTA-NAPamide.

Whereas incorporation of the radioactivity into the tumor was only marginally affected by dimerization of the MSH core sequence, the non-specific uptake by other tissues, most notably by the kidneys but also by the stomach, liver, spleen, and pancreas, were elevated by a factor of 3-10 (**Table 9**). Of the three dimeric analogs, the highest kidney values were observed with [^{111}In]DOTA-diHexa(NC-NC)-amide, the lowest with diHexa(NC-NC)-Gly-Lys([^{111}In]DOTA)-amide, and it was also noted that the clearance of ^{111}In from the kidneys was much retarded when compared with [^{111}In]DOTA-NAPamide. Whether uptake by the kidneys could have been modulated, e.g. by infusion of basic amino acids (see above) was not studied. When the biodistribution pattern of diHexa(NC-NC)-Gly-Lys([^{111}In]DOTA)-amide was compared with [^{111}In]DOTA-NAPamide (**Figure 36**), it was obvious that the dimeric MSH radioligands were much inferior as compared to DOTA-NAPamide. Hence, the *in vitro* data were not predictive for the *in vivo* biodistribution characteristics.
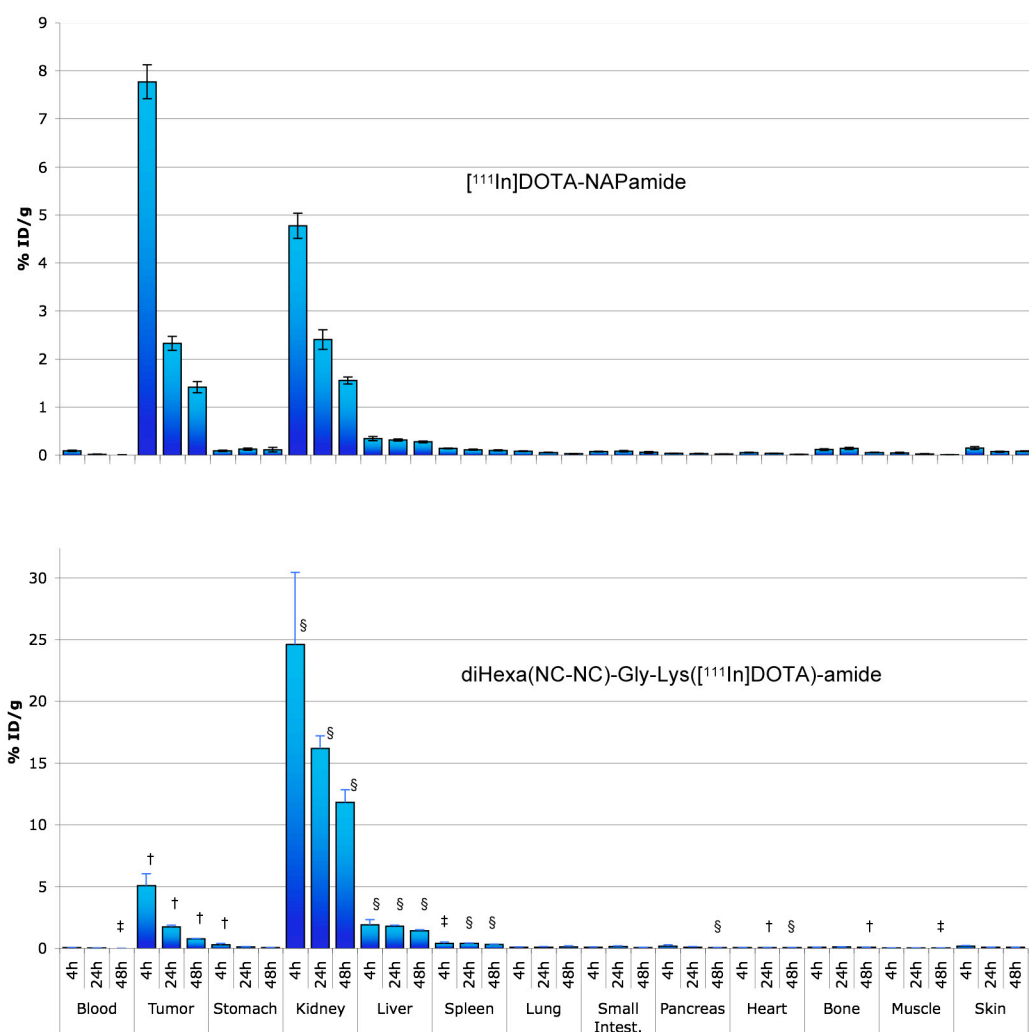
Figure 36: Comparison of organ distribution of diHexa(NC-NC)-Gly-Lys([^{111}In]DOTA)-amide with [^{111}In]DOTA-NAPamide at 4 h, 24 h and 48 h post-injection. The radiopeptides were injected into B16-F1 melanoma-bearing mice, and tissues were collected at the time points indicated. Results are expressed % of injected dose per g of tissue (%ID/g; mean ± SEM, n = 4-12). †$P < 0.05$ vs. ^{111}In-DOTA-NAPamide. ‡$P < 0.001$ vs. ^{111}In-DOTA-NAPamide. §$P < 0.0001$ vs. ^{111}In-DOTA-NAPamide.

Effect of the position of DOTA on kidney uptake

As demonstrated, kidney uptake of all three dimer MSH radioligands was much increased. The highest accumulation was observed for [^{111}In]DOTA-diHexa(NC-NC)-amide which may indicate that N-terminal incorporation of DOTA is the least favorable. C-terminal DOTA in diHexa(NC-NC)-Gly-Lys([^{111}In]DOTA)-amide and insertion of DOTA into Cys of [^{111}In]DOTA-diHexa(CN-NC)-amide both displayed a 1.4-fold lower kidney uptake. Comparison of tumor-to-kidney ratios at 4 h showed that the latter two peptides yielded values of 0.26 and 0.36, respectively, whereas the former peptide gave a value of only 0.11 (**Figure 37**). These low values are in sharp contrast to the corresponding value for [^{111}In]DOTA-NAPamide which was 1.67. It should be noted in this context that in the DOTA-NAPamide molecule, the position of DOTA in the peptide chain did not affect kidney uptake apart from a charge neutralization effect of the Lys side-chain[115]. As there was no extra charge in the dimer MSH peptides which could have affected kidney uptake, it may therefore be concluded that an N-terminal position of DOTA in this type of dimer MSH conjugates should be avoided.
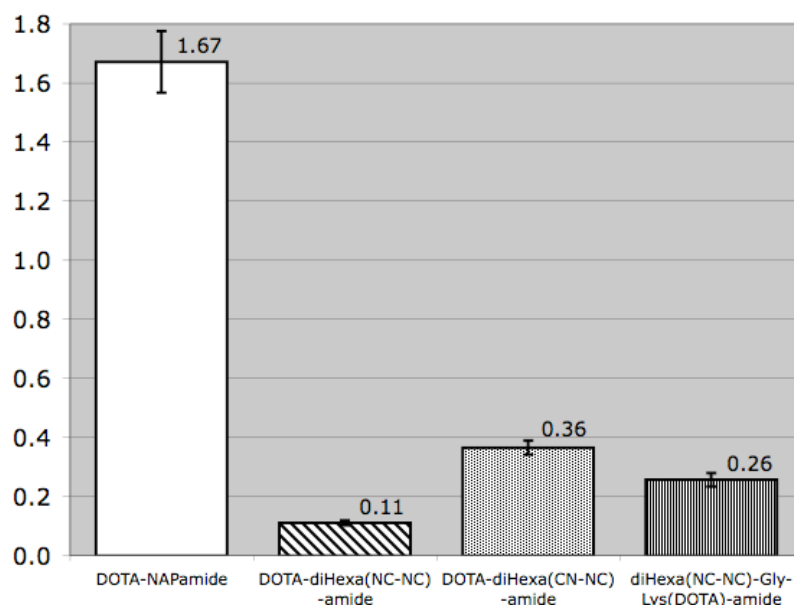

Figure 37: Tumor versus kidney uptake of [^{111}In]DOTA-NAPamide, [^{111}In]DOTA-diHexa(NC-NC)-amide, diHexa(NC-NC)-Gly-Lys([^{111}In]DOTA)-amide, and [^{111}In]DOTA-diHexa(CN-NC)-amide. The radiopeptides were injected into B16-F1 melanoma-bearing mice and the radioactivity that accumulated in tumor and kidney was measured 4 h post-injection. Results are expressed as tumor-to-kidney ratios of the means.

DISCUSSION

In previous reports, we presented promising data on receptor-mediated tumor targeting using short linear DOTA-α-MSH analogs, DOTA-MSH$_{oct}$[110] and DOTA-NAPamide[114], as melanoma vectors. In tumor-bearing mouse models, [111]In- and [67/68]Ga-labeled DOTA-NAPamide exhibited high melanoma and low kidney uptake, leading to tumor-to-kidney ratios of the 4-h to 48-h AUC of 1.11 and 1.82, respectively[114].

However, DOTA-MSH$_{oct}$ demonstrated much inferior biological performance with a tumor-to-kidney ratio of AUC calculated for the same time period as low as 0.24, suggesting that a small alteration in the chemical structure within the DOTA-NAPamide molecule was responsible for its superior melanoma targeting ability. As a high value for the tumor-to-kidney ratio is important for diagnostic application and imperative for therapeutic purpose (to reduce nephrotoxicity which is currently the dose-limiting factor), we thought to investigate MSH analogs that displayed increased receptor affinity so that lower doses could eventually be applied, concomitantly reducing kidney uptake. The previous finding in our[84-87,171] and other laboratories[100,314] that dimer and multimer α-MSH conjugates displayed markedly enhanced receptor activity prompted us to investigate dimerized DOTA-MSH analogs *in vitro* and *in vivo*.

In this report, we described the design, synthesis and biological characteristics of three dimer MSH peptides containing a modified hexapeptide core sequence of α-MSH, Nle-Asp-His-D-Phe-Arg-Trp, in either parallel or antiparallel orientation, separated by a short spacer or linker. The spacer length was kept short as there was no intention to hit simultaneously two receptors with one and the same dimer conjugate. Instead, the concentration of binding species in the vicinity of the receptor should be elevated by the dimerization so that with one ligand molecule two binding motifs are offered to the receptor, hence increasing the apparent affinity of the ligand. Introduction of any unnecessary positive charge should be avoided because the investigations by Froidevaux *et al.*[115] on the effect of different charges on the DOTA-NAPamide molecule with respect to non-specific kidney uptake revealed that a positive charge on, e.g., a C-terminal Lys side-chain increased kidney retention considerably. Therefore, positive charges on the dimer peptides should be confined to the two core sequences where they are important for receptor binding[87,88]. In all three dimer peptides, the terminal charges were blocked by introducing a C-terminal amide group and an N-terminal acetyl group (or DOTA), respectively.

The first type of peptide, diHexa(NC-NC)-amide, contained the two hexapeptides in the same orientation, separated by a tripeptide spacer; it had two negative charges and four positive charges originating from the side-chains of Asp, His, and Arg. The chelating analog, DOTA-diHexa(NC-NC)-amide, displayed additional charges on the DOTA moiety. The solubility of this pentadecapeptide was good but its stickiness to surfaces may have resided in either a possible tendency to form aggregates or in the hydrophobic central part around the spacer sequence. The second type of dimer peptide, the heptadecapeptide diHexa(NC-NC)-Gly-Lys(DOTA)-amide, was almost identical with the first, except for its –Gly-Lys-NH$_2$ extension at the C-terminus for attachment of DOTA, and the chemical characterstics were also very similar. The reason for the introduction of the –Gly-Lys(DOTA)-NH$_2$ as C-terminal extension was the expectation, based on previous observations, that the Lys(DOTA)-NH$_2$ would be readily cleaved from the molecule and excreted by the kidneys. The third peptide, DOTA-diHexa(CN-NC)-amide, was the least stable, possibly because of potential *S*-oxidation of the thio-ether group at elevated temperature (e.g. during the ^{111}In-labeling reaction).

In vitro, the biological characteristics of the three dimeric DOTA-MSH conjugates were excellent as they retained higher MC1-R receptor affinity than any other DOTA-MSH analog reported to date, in both mouse B16-F1 and human HBL melanoma cells (the latter was only studied with diHexa(NC-NC)-Gly-Lys(DOTA)-

amide); hence the three dimer peptides exceeded the remarkable activity profile of DOTA-NAPamide. The diHexa(NC-NC)-Gly-Lys([111In]DOTA)-amide also showed rapid internalization into cultured B16-F1 melanoma cells. However, the decreased tumor uptake *in vivo* and the disappointingly high kidney uptake precluded their further use as radiopharmaceuticals for direct receptor targeting. The difference between tumor uptake of dimer peptides and DOTA-NAPamide may reside in a lower tissue penetration of the dimers, owing to their stickiness to surfaces. Interestingly, there was no difference between diHexa(NC-NC)-Gly-Lys([111In]DOTA)-amide and [111In]DOTA-NAPamide with respect to release of radioactivity from melanoma and kidneys following biodistribution. Both types of DOTA-α-MSH analogs were found to be much more rapidly released from melanoma than kidney leading to a decreasing tumor-to-kidney ratio over time. The reason for this differential excretion rate is not clear since DOTA-α-MSH analogs are assumed to undergo a similar process in kidney and melanoma after cellular uptake[115]. Indeed, [111In]DOTA-α-MSH analogs were shown to accumulate in the endosomal/lysosomal compartment of B16F1 cells after in vitro exposure (Froidevaux et al., unpublished observation). It appears that for both monomeric and dimeric DOTA-α-MSH radioligands, the rate of peptide hydrolysis was equally elevated in melanoma lysosomes (compared to kidneys), resulting in faster production of small radioactive metabolites. The significant difference in kidney retention between monomeric and dimeric DOTA-peptides is not well understood at present as both peptides contain the DOTA moiety in the e-amino group of C-terminal Lys-NH$_2$. Our assumption of an efficient cleavage of –Gly-Lys(DOTA)-NH$_2$ or –Lys(DOTA)-NH$_2$ from diHexa(NC-NC)-Gly-Lys(DOTA)-amide by the kidneys did not come true. Interestingly, dimer peptide uptake by the liver – although elevated – was far lower than that of the first DTPA-dimer α-MSH conjugate reported by Bagutti et al.[20]. Taken together, a first conclusion about the biological data is that no correlation can be made between the receptor affinity determined in the *in vitro* binding assay and the pharmacokinetic characteristics observed *in vivo* and that kidney retention of radiopeptides is unpredictable. Indeed, it appears that high receptor affinity *in vitro* of a radiopeptide does not implicitly result in high *in vivo* tumor accumulation.

MC1 receptor-mediated melanoma targeting with different types of α-MSH-based [67]/[68]Ga-, [111]In-, [64]Cu-, [90]Y-, or ^{177}Lu-labeled peptide radiopharmaceuticals studied in different laboratories[19,20,59-63,90,110,114,115,200,202,204,321] has brought together a wealth of information and ideas for melanoma diagnosis and therapy in the past 13 years. More recently, [90]mTc-labeled MSH has been added to the list[208], and therapy experiments using an animal model and b-radiation ([188]Re) or a-radiation have been carried out[205,206]. Although the experimental data obtained with the α-MSH/MC1-R system are of comparable quality to those using somatostatin receptor targeting, clinical studies have been scarce so far because melanoma can nowadays be diagnosed well with ^{18}F-fluorodesoxyglucsose/positron emission tomography (FDG-PET). By contrast, receptor-mediated targeting for therapy of melanoma metastases, which is the main goal of the studies with MSH/MC1-R, requires novel strategies to further increase the tumor-to-kidney ratio in order to minimize nephrotoxicity of these radiopharmaceuticals. The dimer peptide approach is obviously not the solution for therapy but dimeric or multimeric peptide conjugates could nevertheless become important if the strategy will not be based on direct labeling of the dimeric compounds. Instead such dimers or multimers may serve as one of the components of a pretargeting system in which the

labeled component is pharmacokinetically less problematic and of smaller size. This may be the strength of peptide multimers or dendrimers which are currently receiving much attention[135,262,304,330].

In conclusion, the biological evaluation of three dimeric MSH peptides containing the DOTA chelator for incorporation of radiometals has demonstrated that these compounds have very high *in vitro* affinity to the MC1-R which however was not mirrored by their *in vivo* melanoma tumor uptake. In addition, the uptake by the kidneys of all three dimeric peptides was about 5 times higher than that of monomeric DOTA-NAPamide, precluding their direct use as radiopharmaceuticals. The high receptor affinity of dimeric or multimeric α-MSH conjugates may perhaps be of use in a pretargeting strategy, whereby receptor-bound dimer or multimer containing a specific affinity group may serve to fish a radioactive counterpart.

ACKNOWLEDGMENTS

4 Glycopeptides

4.1 Background

At first, glycopeptides were introduced to improve drug delivery to target tissues, either by taking advantage of specific uptake mechanisms or by enhancing the peptide bioavailability. Peptides were shown to exhibit prolonged effects (glycosylated enkephalin peptides[93]) due to better delivery to the target tissue, enhanced renal peptide uptake from blood (glycosylated Arg^8-vasopressin), an improved stability toward enzymatic degradation *in vivo*, or a better intestinal absorption, thus enhancing the bioavailability of the peptides[324].

Other effects of glycation on peptide properties emerged, including (depending on the attached sugar) higher or lower accumulation in the proximal tubules of the renal cortex. Suzuki et al. made systematic investigations in the field of modified Arg-vasopressin (AVP) by linking it to a variety of sugars[281,302]. They listed structural requirements to exploit or to avoid targeting of the kidney[301], and they synthesized derivatives based on their "alkylglycoside", a novel targeting vector for the kidney. SAR studies revealed the influence of the sugar type on the affinity for the kidney membrane cells. Various positions of the hydroxyl groups of the carbohydrates were found to be essential (in this case, equatorial OH at position 4 is mandatory, OH at position 2 could either be oriented or absent, etc.) for the targeting of the kidney.
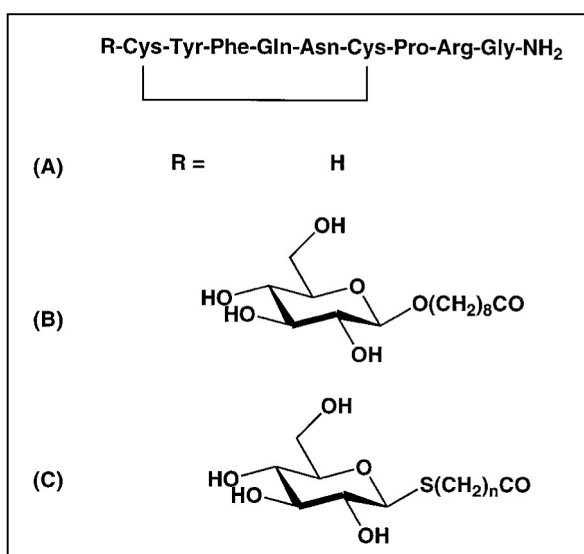

Figure 38: Structure of some compounds used by Suzuki et al. as "alkylglycosides".[302]

A, AVP; B, Glc-O-C8-AVP; C, Glc-S-Cn-AVP (n = 5, Glc-S-C5-AVP; n = 8, Glc-S-C8-AVP; n = 11, Glc-S-C11-AVP).

Keeping in mind that these findings are specific to the alkylglycoside derivatives, it is clear nevertheless that carbohydrated derivatives can have a major influence on the pharmacokinetics of peptides, either positively or negatively.

Wester et al. also mention in their review[324] that after carbohydration of somatostatin derivatives, a switch in the way of excretion could be observed. It appeared that the glycopeptides tended to exhibit a lower hepatic clearance as well as a lower hepatic and intestinal uptake, exhibiting a switch towards renal

excretion. The uptake of some octreotide derivatives in SST-expressing tissue remained mostly unchanged, except for [^{125}I]Gluc-TOC, exhibiting a tumor uptake of 160% of the reference.
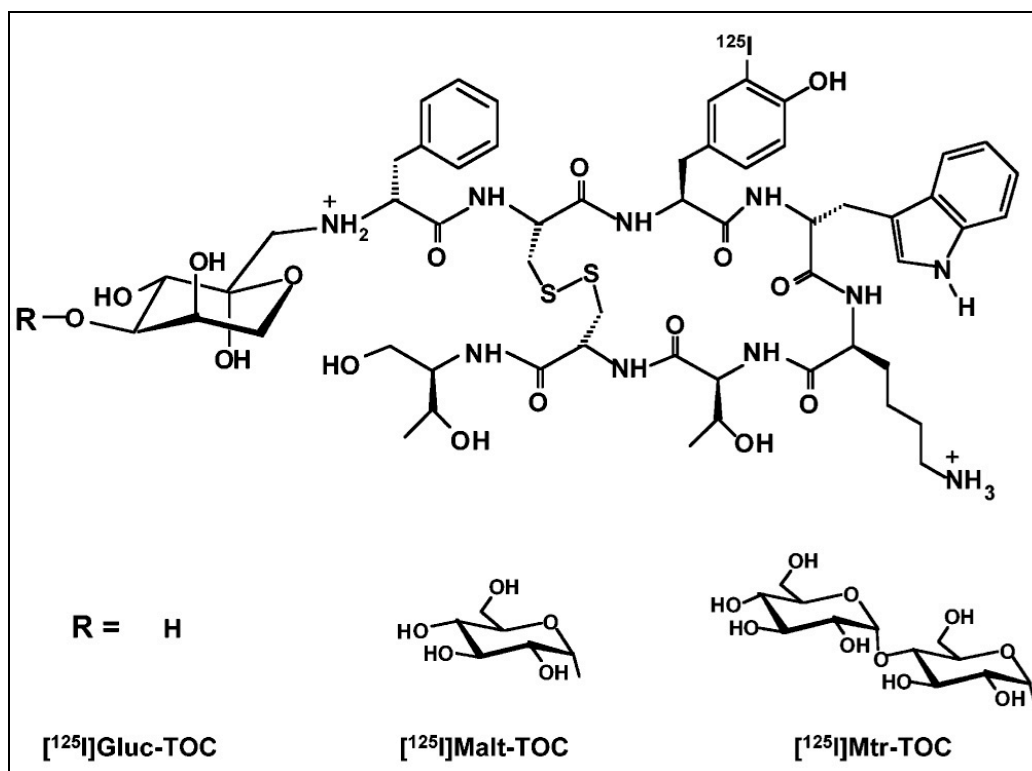

Figure 39: Some of the derivatives synthesized by Schottelius et al.. Structures of [^{125}I]Gluc-TOC, [^{125}I]Malt-TOC and [^{125}I]Mtr-TOC[273]**.**

Various other carbohydrated derivatives were investigated by the same group, and in the different approaches adopted, it appeared that glycopeptides could dramatically influence the pharmacokinetic behavior of somatostatin derivatives (blood and whole body clearance, clearance pathways, reduction of liver uptake, reduction of renal uptake, enhancement of urinary excretion, or even increased tumor uptake)[273,274,323,324].

These promising findings led to the development of carbohydrated α-MSH derivatives in our group. Indeed, as seen earlier in this thesis, the main issue of most radiolabeled α-MSH tracers remains their relatively high kidney uptake. Therefore, given the potential reduction of the kidney uptake or the increase of tumor uptake observed with other peptide derivatives, a similar approach with α-MSH analogs was tempting, and is described in the next subchapter.

4.2 Carbohydrated α-MSH analogs

Carbohydration of peptides represent an interesting approach to improve the general pharmacokinetic properties of diagnostic and therapeutic peptides. A systematic approach was adopted regarding the screening of potential glycopeptidic derivatives of radiolabeled α-MSH analogs. Indeed, various carbohydrate moieties were attached at various positions along a chosen peptide backbone, in an attempt to optimize its pharmacokinetical profile. It was logical to use the most successful peptide of our laboratory as basis for the synthesis of glycated derivatives.

Ac-Nle-Asp-His-D-Phe-Arg-Trp-Gly-Lys-NH2
I
DOTA

DOTA-NAPamide
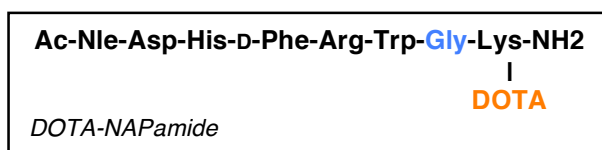
Simple and commonly found sugars were used to determine the influence of glycation on the *in vitro* and *in vivo* profiles of the chosen radiopeptide. Carbohydrate moieties such as glucose (Gluc), galactose (Gal) and maltotriose (Mtr) were coupled to the NAPamide sequence using different synthetical approaches, ranging from synthesis with building blocks to the use of the naturally occurring Maillard reaction (see chapter **4.3.2**). As mentioned, their affinity profiles were then assessed by use of competitive binding assays on murine (B16F1) or human (HBL) cell lines, their internalization profiles on the same murine cells using the radiolabeled (^{111}In) peptide, as well as their biological activity (melanin production assay) with the unlabeled peptide. Finally, their pharmacokinetical profiles were determined in *in vivo* biodistribution assays on B6D2F1 melanoma-bearing mice.

4.3 Syntheses of the carbohydrated derivatives

4.3.1 The "building blocks" strategy

First, it was planned to adopt a "building blocks" strategy in order to facilitate the synthesis of derivatives in a "high-throughput screening" combinatorial chemistry way for potential further developments. To this end, a carbohydrate derivative based on galactose and bearing a carboxylic group at its anomeric center was synthesized. This synthesis was originally described by Arya et al., and the supporting material of the publication mentions the synthesis of various carboxylic derivatives [16]. The carbohydrate was incorporated as α-linked C-glycoside.
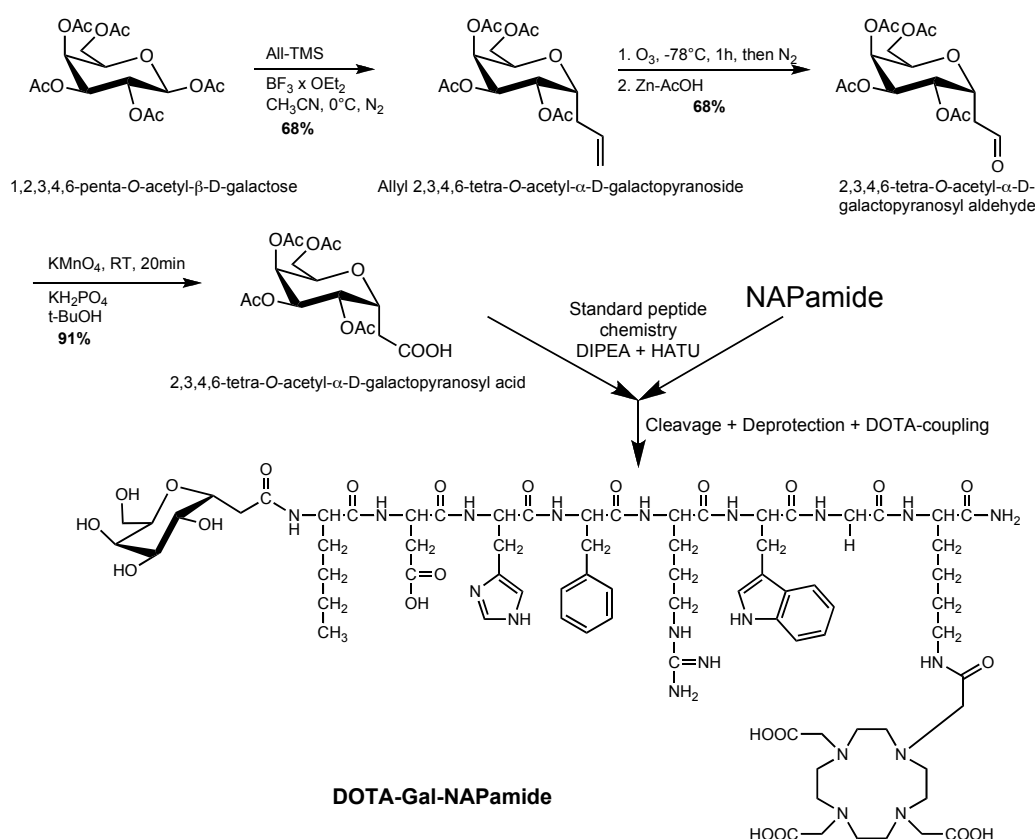
Figure 40: Synthesis strategy of DOTA-Gal-NAPamide.

Commercially available penta-*O*-acetyl-protected β-D-galactose was allylated at position 1 to form the α-allylated D-galactopyranoside. It was then oxidized through ozonolysis to form the aldehyde derivative. Finally, the aldehyde was oxidized by potassium permanganate to form the ethanoic acid. The compound was then coupled to the free N-terminus of NAPamide on solid phase through HATU-mediated coupling, and the peptide was cleaved from the resin (simultaneously, its side-chains were deprotected) using TFA. This step yielded 25% product. The 4 *O*-acetyl protecting groups from the carbohydrate were cleaved using hydrazine hydrate. The DOTA chelator complex was coupled, and its protecting groups were cleaved, yielding final DOTA-Gal-NAPamide.

The HATU (*O*-(7-azabenzotriazol-1-yl)-N,N,N',N'-tetramethyluronium hexafluorophosphate) approach was chosen for its improved properties compared to other HOBt-based or even to some HOAt-based phosphonium and uronium salts. In the presence of base, HATU cleanly converts carboxylic acids to the corresponding OAt esters. These esters are far more reactive than the corresponding OBt esters towards aminolysis, due to OAt being a better leaving group than OBt and the active participation of the pyridine nitrogen in the amide bond forming reaction. This greater reactivity leads to higher coupling yields with less enantiomerization[53,185,212].
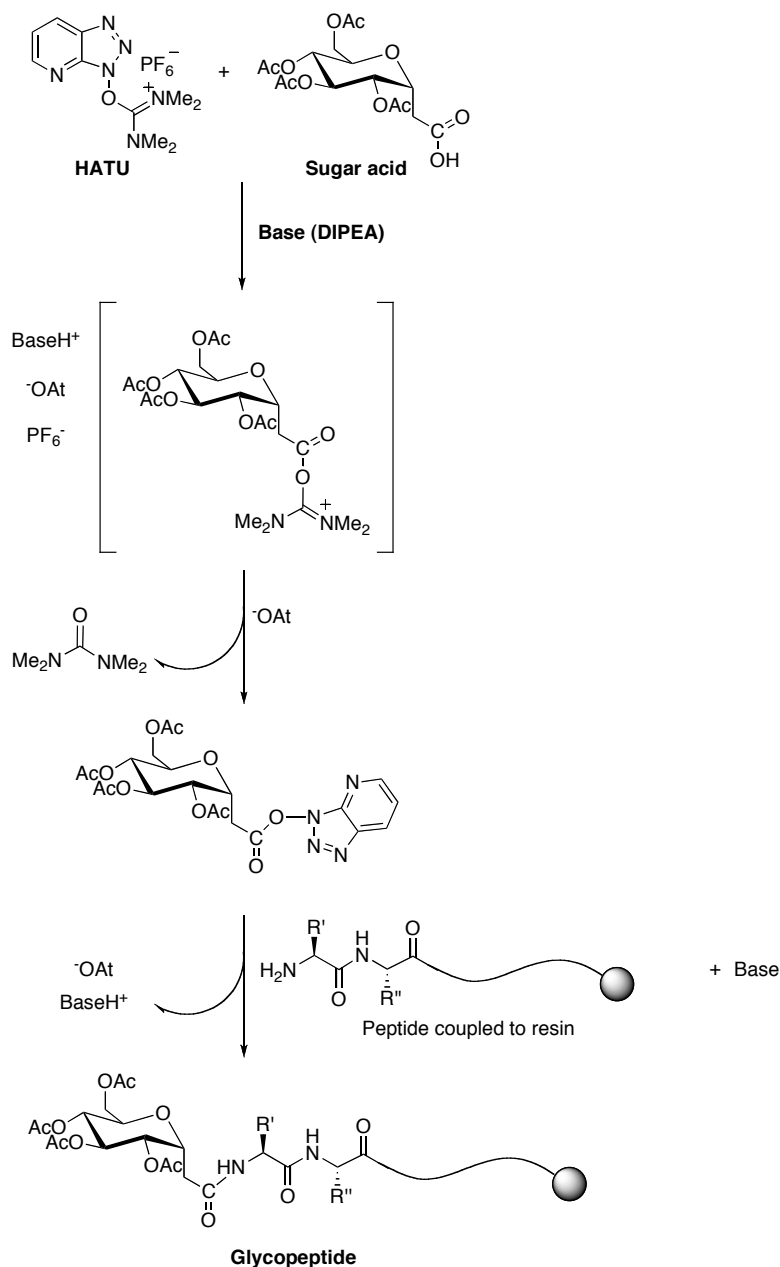
Figure 41: The proposed mechanism of the HATU-mediated glycation reaction in detail.

In our case, the total reaction could be achieved, but it also involved unusual laboratory equipment (especially for the ozonolysis step) during the preparation of the carbohydrate moiety, i.e. equipment that was not always at our disposal. The purification of the allylic derivative was very difficult, as several by-products present after the synthesis could not be well separated from the desired product. Then, the obtained yields for the glycation step were acceptable (25%), but the sugar moiety had later to undergo 2 deprotection steps, as the first turned out to be incomplete. This caused additional product losses. Finally, due to the poor yields commonly obtained in the DOTA-coupling step, total yields were quite low (~7.4%). Therefore, and although two final glycopeptides (DOTA-Gal-NAPamide and DOTA-NAPamide-Gal) could be synthesized using this strategy, it was decided to adopt another, simpler and more quantitative strategy. DOTA-NAPamide-Gal was synthesized later than several of the derivatives produced with the Maillard

reaction, but due to the requirements of a C-terminal coupling strategy, the HATU-mediated glycation way was the method of choice. 1-Amino-1-deoxy-β-D-galactose was the commercially available carbohydrate moiety used for this synthesis. Again, quite poor yields were obtained (7.7% for the sole glycation step).

4.3.2 The Maillard reaction

The Maillard reaction is a very common chemical reaction (usually associated with heat) in the food industry, as it is responsible for a whole range of colors and flavors. It was investigated in the 1910s by Louis-Camille Maillard[195]. It is implicated in the roasting of coffee and the browning of bread or other bakery products. It is present in malted barley as in malt whiskey or beer and in roasted or seared meat, etc. In all these areas, it is responsible for the characteristic brown color and some very specific aromas and flavors. Less than 0.1 ng/l of some end products are needed to reach the human odor threshold. It is a form of non-enzymatic browning (as is caramelization, though in a totally different way, caramelization involving simple pyrolysis of certain sugars) promoted by heating. The Maillard reaction is a reaction between an amino acid and a reducing sugar. The reactive carbonyl group of the sugar reacts with the nucleophilic amino group of the amino acid, and forms a variety of interesting but poorly characterized molecules responsible for a range of odors and flavors. The process is accelerated in an alkaline environment, as the amino groups are deprotonated and hence have an increased nucleophilicity. Hundreds of different flavor and color compounds may be formed by this reaction. The product pattern is subject to large variations, depending on parameters such as the reaction time, the temperature, the concentration of the reactants, the pH of the reaction, and of course the amino acids and sugars involved. This reaction is the basis of the flavoring industry, since the type of amino acid determines the resulting flavor.

This reaction was already used by other groups for the glycation of various peptidic derivatives. Albert et al. used it successfully as one of the first in peptide synthesis[11]. More particularly, Schottelius et al. synthesized several somatostatin analogues derivatives using this technique[273,274,323,324].

Reaction

Three main stages may be considered in the Maillard reaction. The early stage is the formation of a Schiff base which, through rearrangements, produces an "Amadori product" (ketoamine), if the reducing sugar is an aldose. This Amadori product is then degraded to a variety of carbonyl compounds. It is an important intermediate in the Maillard chemistry. The Amadori products are mainly degraded through dehydration of the sugar moiety, forming deoxyglucosones. A later stage leads these highly reactive carbonyl compounds to the formation of a group of substances known as advanced glycation end products, or AGEs. AGEs are often colored and prone to produce crosslinks in proteins, and this may be the cause of their potential implication in complications of various diseases (e.g. diabetes, ageing)[150].

Steps:

- Formation of a Schiff base: for example the aldehyde group of a glucose molecule will combine with the amino group of a lysine molecule (in a protein) to form an imine or Schiff base, which is a double bond between the carbon atom of the glucose and the nitrogen atom of the lysine.

- Formation of an Amadori product: the Amadori product is a re-arrangement from the Schiff base wherein the hydrogen atom from the hydroxyl group adjacent to the carbon-nitrogen double bond moves to bond to the nitrogen, leaving a ketone.

- Formation of an advanced glycation end product (AGE): the Amadori product is oxidized, most often by transition metal catalysis.

The first two steps in this reaction are both reversible, but the last step is irreversible. The reaction mechanism is described in the following figure (**Figure 42**):
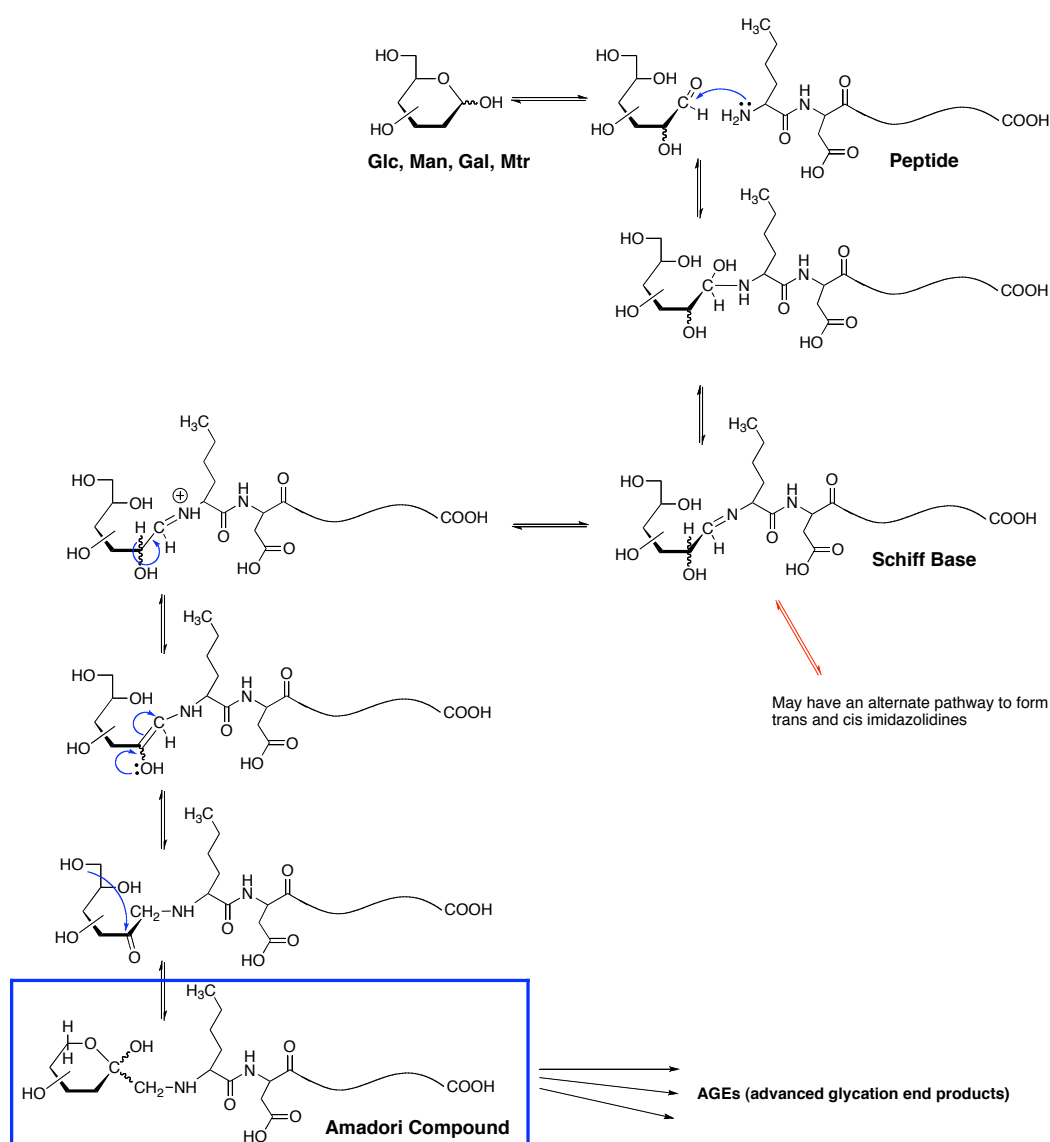

Figure 42: Detailed mechanism of the Maillard reaction until the Amadori compound (adapted from Horvat et al.[150,258]).

This reaction happened to work quite well for all the peptides that were synthesized with this simpler approach, compared to the HATU-mediated coupling of a sugar acid. Yields between 16% and 31% were obtained for the Maillard reaction for "normal" N-terminal coupling, but a lysine ε-amino-group-coupling yielded as little as 1.5% product. It is noteworthy that the DOTA chelator complex was already present on the peptide when the carbohydrate was coupled, which probably had an influence on glycation because of sterical hindrance, leading to such a low yield.

The main interest of the Maillard reaction resides in the fact that carbohydrates as simple as β-D-glucose, β-D-galactose, or maltotriose, can be inserted into peptides bearing a free N-terminal end. The reaction (under slight heating, 60°C under reflux) is spontaneous, although quite a long reaction time is needed (72 h), but it does not require any specific reagent or any preparation of starting products. It is carried out in an acidic mixture of MeOH/AcOH (95/5). The simplicity of the reaction definitely represents its main advantage over other methods, which is the reason why it was the strategy chosen for the synthesis of peptide derivatives that allowed it. Peptides synthesized this way were DOTA-Glc-NAPamide, DOTA-Mtr-NAPamide and N^{α}-DOTA-[Lys(Gluc)^8]-NAPamide.

4.4 Manuscript to be submitted

Glycosylated Analogs of DOTA-α-Melanocyte-Stimulating Hormone for Melanoma Targeting: The Site of Carbohydration Modulates In Vivo Biodistribution

Jean-Philippe Bapst; Martine Calame-Christe, PhD; Heidi Tanner; and Alex N. Eberle, PhD

Laboratory of Endocrinology, Department of Biomedicine, University Hospital and University Children's Hospital, Basel, Switzerland

ABSTRACT

α-Melanocyte-stimulating hormone (α-MSH) is known to bind to the melanocortin receptor 1 (MC1R), which is overexpressed at the surface of both melanotic and amelanotic melanoma cells. α-MSH analogs are potential candidates for specific targeting of metastatic melanoma. Several peptides were already designed and tested in the past, and showed high affinity for the MC1R *in vitro*, as well as a good incorporation in tumor xenografts *in vivo*. However, considerable kidney reabsorption of radiolabeled MSH analogs could not be avoided. In this study, we synthesized several carbohydrated derivatives with the aim to increase the tumor-to-kidney ratio. **Methods:** Six glycosylated derivatives of NAPamide, an α-MSH octapeptide analog with high tumor selectivity, were synthesized and coupled to the chelator DOTA (1,4,7,10-tetraazacyclododecane-1,4,7,10-tetraacetic acid). The peptides were evaluated *in vitro* for MC1-R binding and agonist bioactivity and, after labeling with ^{111}In, for *in vitro* cellular uptake and *in vivo* tissue distribution in the B16F1 melanoma mouse model. **Results:** The glycopeptides showed excellent binding affinities in the low nanomolar or sub-nanomolar range with both murine and human melanoma cell lines. However, five glycopeptides displayed lower selectivity *in vivo* than the parent DOTA-NAPamide, because of either a lower tumor uptake or a higher kidney uptake. In particular C-terminal extension of the amide group by a galactosyl moiety increased the kidney retention dramatically. By contrast, the N-terminally positioned galactose residue in DOTA-Gal-NAPamide improved the tumor-to-kidney ratio (4-48 h AUC of 1.34) by a factor of about 1.2 as compared to the parent DOTA-NAPamide (4-48 h AUC of 1.11). **Conclusion:** A new carbohydrated α-MSH analog, DOTA-Gal-NAPamide, displays promising pharmacokinetic properties with higher tumor-to-kidney ratio than previously investigated peptides.

Key words: melanoma targeting; α-melanocyte-stimulating hormone; DOTA; glycopeptide; melanocortin-1 receptor; internal radiotherapy

INTRODUCTION

Overexpression of melanocortin type-1 receptors (MC1R) on the surface of melanoma cells is known as a potential target for the diagnosis or therapy of malignant melanoma[21,122,284]. Radiolabeled α-melanocyte-stimulating hormone (α-MSH), the natural ligand of MC1R, and numerous types of synthetic analogs have been studied as potential candidates for diagnosis or therapy of melanoma metastases[59,60,110,114,115,203,207]. Radiopeptide targeting of primary tumors and metastases has been proven to be a highly sensitive and selective approach now routinely used in the clinic mainly for the diagnosis and therapy of tumors expressing somatostatin receptors[113].

Some α-MSH analogs show excellent binding properties to both murine and human tumor cells *in vitro*. However, major side effects of an unspecific retention in the kidneys *in vivo* refrain from a possible use in human clinical applications. As shown for radiolabeled somatostatin analogs, the general renal toxicity of radiopeptides remains their main dose-limiting factor[70]. Various approaches of modification of the chelator-peptide structures have been applied to improve in vitro and in vivo characteristics of peptide hormone analogs, e.g. structural modifications of the peptide itself or its overall peptide length[110], structural variation of the chelator for the radiometal[22,108,328], the use of different radiometals such as $^{67/68}$Ga, ^{111}In, ^{90}Y, ^{177}Lu, ^{99m}Tc, ^{188}Re[114], the adjustment of the net charge of chelator-peptide complex[7,115], the position of the chelator on the peptide[115], cyclization of the peptides via a rhenium core[60,207], and the synthesis of dimerized α-MSH analogs[25]. Another approach to reduce non-specific uptake by the kidneys is the co-injection of cationic amino acids[33], All these strategies, though, did not sufficiently lower the kidney uptake so that radiotherapy can ever become an option.

Thus, alternative approaches need to be studied for the identification of new leads that may yield α-MSH compounds with improved pharmacokinetic properties, in particular high receptor affinity, low non-target tissue retention and almost exclusively urinary excretion route. The kidney reabsorption and retention, though, should be further reduced to minimize nephrotoxicity. Coupling of carbohydrate moieties to peptides can strongly influence the pharmacokinetics of peptides, owing to the more hydrophilic character which they provide to the molecule. Their excretion in the primary urine may be favored and re-uptake by the tubular system of the kidneys reduced, as shown for glycosylated peptides and proteins[281,303]. It has been shown that carbohydrates, if properly positioned, preserve structure-activity relationships (SAR) of the peptides with their target receptors. For example, glycosylated enkephalin derivatives have been shown to keep their binding properties and to exhibit prolonged bioavailability[102,237]. The *in vivo* stability of renin inhibitors could also be improved[103], and it has been shown that carbohydration of somatostatin analogs improved their pharmacokinetical profile by reducing their liver uptake and biliary excretion[273,323,324], switching their excretion route from hepato-biliary to renal. Suzuki et al. investigated numerous modifications of Arg-vasopressin by coupling of a whole variety of different sugar moieties in order to target the kidney. Their investigations revealed how the affinity of the peptides for kidney membrane cells could be influenced, depending on the type of sugar used[281,301,303].

In this study, we synthesized and evaluated, both *in vitro* with mouse and human melanoma cells and *in vivo* with biodistribution experiments using tumor-bearing mice, several radiolabeled carbohydrated α-MSH analogues based, on the structure of the very efficient derivative [^{111}In]DOTA-NAPamide previously synthesized in our laboratory[114]. The peptides varied in the nature and position of the carbohydrate moieties which were inserted into the C-terminal, N-terminal as well side-chains of the NAPamide peptide. The novel MSH peptides studied included DOTA-NAPamide-Gal, N^α-DOTA-[Lys(Gluc)^8]-NAPamide, DOTA-[Asp(Gal)^2]-NAPamide, DOTA-Mtr-NAPamide, DOTA-Gluc-NAPamide, DOTA-Gal-NAPamide (**Figure 43**).

MATERIALS AND METHODS

Peptides and Analytical Procedures

α-MSH was a gift from Novartis and (Nle^4, D-Phe^7)-α-MSH (NDP-MSH) was purchased from Bachem (Bubendorf, Switzerland). The reference compound DOTA-NAPamide[114] and all other peptides were synthesized in our laboratory using a Pioneer peptide synthesizer (PerSeptive Biosystems Inc., Framingham, MA, USA) and the continuous-flow strategy with Fmoc (9-fluorenylmethoxycarbonyl) protection of N^α-amino groups (for details see Bapst et al.[25]). Fmoc-amino acids were purchased from Novabiochem (Läufelfingen, Switzerland). Fmoc-PAL-PEG-PS polystyrene resin was from Applied Biosystems (Rotkreuz, Switzerland) and TentaGel S TRT-Lys(Boc)-Fmoc acid-labile resin from Fluka (Buchs, Switzerland). Fmoc-Asp(1,2:3,4-diisopropylidene-6-amino-α-D-galactosyl)-OH was a gift from SynphaBase AG (Muttenz, Switzerland). Other carbohydrates and organic reagents were purchased from Fluka or Sigma (Buchs, Switzerland).

NMR spectra were recorded on a Bruker Avance DMX-500 (500 MHz) spectrometer. Assignment of ^{1}H and ^{13}C spectra was achieved using 2D methods (COSY, HSQC). Chemical shifts are expressed in ppm using residual CDCl$_3$ and CHD$_2$OD as references. Mass spectra (MS) were recorded on a Finnigan LCQ Deca electrospray ion trap small molecules and proteomics MS system. Analytical reversed-phase high-performance liquid chromatography (RP-HPLC) of all peptides was performed on a Jasco PU-980 system (Jasco Inc., Easton, MD, USA) with usually a Waters Symmetry C18 analytical column (5 μm, 3.9 × 150 mm), or (mentioned if used) a Vydac 218TP54 C18 analytical column (5 μm, 4.6 × 250 mm). Preparative RP-HPLC of peptides was performed on the same system but either with a Vydac 218TP510 C18 semi-preparative column (5 μm, 10 × 250 mm) or a Waters SymmetryPrep C18 preparative column (7 μm, 19 × 150 mm). Peptides were eluted by applying a gradient of 5-95% solvent B (solvent A: 0.1% trifluoroacetic acid (TFA) in H$_2$O, solvent B: 0.1% TFA in 70:30 acetonitrile/H$_2$O; gradient cycle: 0-27 min, 95%-10% A; 27-30min, 10%-95% A; 30-32 min, 95% A) in 32 min at constant flows of 1 mL/min for the analytical columns, 3 mL/min for the semi-preparative column and 5 mL/min for the preparative column. UV-detection was performed at 280 nm on a Jasco UV-1570 UV-VIS detector.

Preparation of glycopeptides

DOTA-Gal-NAPamide

The peptide with an N-terminal Gal and DOTA on the Lys side-chain was synthesized by first preparing and attaching a Gal-octanoic acid residue to the N-terminus of partially protected NAPamide:

Allyl-2,3,4,6-tetra-O-acetyl-α-D-galactopyranoside: 1,2,3,4,6-penta-*O*-acetyl-β-D-galactopyranose (10.24 mmol, 1 eq) was dissolved in anhydrous acetonitrile (40 ml) and cooled down to 0°C. Allyl-trimethylsilane (30.76 mmol, 3 eq) and boron trifluoride diethyl etherate (58.4 mmol, 5.7 eq) were carefully added under an N_2-atmosphere. The mixture was slowly warmed up to room temperature and stirred overnight under N_2. It was then neutralized by pouring the solution into an erlenmeyer containing $NaHCO_3$ (40 ml). Once the bubbling was over, the reaction mixture was transferred to a separation funnel, extracted with dichloromethane (2×40 ml) and dried over Na_2SO_4. The crude product was purified by column chromatography (petrol ether/ethyl acetate 3:1 to 2:1), resulting in a clear syrup. Yield: 6.96 mmol (68%).

^{1}H NMR ($CDCl_3$, 500.1 MHz) δ: 1.97 (s, 3H, CH_3), 1.98 (s, 3H, CH_3), 2.01 (s, 3H, CH_3), 2.06 (s, 3H, CH_3), 2.21 (m, 1H, CH_2CH=CH$_2$), 2.40 (m, 1H, CH_2CH=CH$_2$), 4.00-4.04 (m, 2H, H-5, H-6a), 4.14 (m, $^3J_{5,6b}$ = 9.1 Hz, $^2J_{6a,6b}$ =12.9 Hz, 1H, H-6b), 4.24 (m, 1H, H-1), 5.03-5.08 (m, 2H, CH$_2$CH=CH_2), 5.15 (dd, $^3J_{3,4}$ =3.3 Hz, $^3J_{2,3}$ = 9.3 Hz, 1H, H-3), 5.21 (dd, $^3J_{1,2}$ = 5.0 Hz, $^3J_{2,3}$ = 9.3 Hz, 1H, H-2), 5.35 (m, 1H, H-4), 5.69 (m, 1H, CH$_2$CH=CH$_2$). ^{13}C NMR ($CDCl_3$, 125.8 MHz) δ: 20.67, 20.73, 20.74, 20.79 (4C, 4 CH_3), 30.92 (1C, CH$_2$CH=CH$_2$), 61.45 (C-6), 67.58 (C-4), 67.90 (C-3), 68.24 (2C, C-5, C-2), 71.43 (C-1), 117.67 (1C, CH$_2$CH=CH$_2$), 133.30 (1C, CH$_2$$C$H=CH$_2$), 169.81, 169.94, 170.09, 170.56 (4C=O).

2,3,4,6-Tetra-O-acetyl-α-D-galactopyranosyl aldehyde: A solution of allyl-2,3,4,6-tetra-*O*-acetyl-α-D-galactopyranoside (6.96 mmol) was dissolved in anhydrous CH_2Cl_2 (100 ml) and cooled to –70°C. Ozone (O_3) was bubbled through the solution for approximately 1 h, until the solution turned blue. The mixture was de-ozonized by bubbling N_2 through the solution until it was colorless. Acetic acid (10 ml) and zinc dust (7.5 g) were added to the solution and the suspension was slowly warmed up to room temperature overnight under stirring. The suspension was filtrated through Celite and the filtrate was concentrated to dryness. The crude product was purified by column chromatography (petrol ether/ethyl acetate 1.5:1) and dried under high vacuum. Yield: 4.74 mmol (68%).

^{1}H NMR ($CDCl_3$, 500.1 MHz) δ: 2.05 (s, 6H, 2 CH_3), 2.06 (s, 3H, CH_3), 2.11 (s, 3H, CH_3), 2.65-2.76 (m, 2H, CH_2CHO), 4.05-4.11 (m, 2H, H-5, H-6a), 4.32 (m, 1H, H-6b), 4.86 (m, 1H, H-1), 5.17 (dd, $^3J_{3,4}$ = 3.2 Hz, $^3J_{2,3}$ = 8.5 Hz, 1H, H-3), 5.28 (dd, $^3J_{1,2}$ =4.7 Hz, $^3J_{2,3}$ = 8.4 Hz, 1H, H-2), 5.41 (m, 1H, H-4), 9.72 (m, 1H, CHO). ^{13}C NMR ($CDCl_3$, 125.8 MHz) δ: 20.63, 20.67, 20.70 (4C, 4 CH_3), 41.94 (CH$_2$CHO), 60.82 (C-6), 66.62 (C-1), 66.88 (C-4), 67.72 (C-3), 67.84 (C-2), 69.67 (C-5), 169.61, 169.72, 169.88, 170.63 (4 C=O), 198.31 (CHO).

2,3,4,6-Tetra-O-acetyl-α-D-galactopyranosyl ethanoic acid: A solution of 2,3,4,6-tetra-*O*-acetyl-α-D-Galactopyranosyl aldehyde (4.74 mmol) in tert-butanol (20 ml) and a solution of KH_2PO_4 (1.25 M, 8 ml) were added to a vigorously stirred solution of $KMnO_4$ (1 M, 9 ml). The mixture was stirred for 20 min. A solution of saturated Na_2SO_3 was added dropwise until $KmnO_4$ was neutralized, yielding out a brown precipitate of MnO_2 which was filtrated on Celite and washed with ethanol (2 × 25 ml). Ethanol was then removed from the filtrate under reduced pressure and the remaining solution was acidified to pH=3 using 1n HCl, then extracted with dichloromethane (4 × 30 ml). The combined extracts were concentrated and dried under high vacuum to yield a white foam (4.31 mmol, 91%).

^{1}H NMR (CDCl$_3$, 500.1 MHz) δ: 2.04 (s, 6H, 2 CH$_3$), 2.07 (s, 3H, CH$_3$), 2.12 (s, 3H, CH$_3$), 2.63 (dd, $^3J = 5.6$ Hz, $^2J = 15.7$ Hz, 1H, CH_2CO$_2$H), 2.72 (dd, $^3J = 8.9$ Hz, $^2J = 15.6$ Hz, 1H, CH_2CO$_2$H), 4.10-4.17 (m, 2H, H-5, H-6a), 4.24 (dd, $^3J_{5,6b} = 6.9$ Hz, $^2J_{6a,6b} = 10.7$ Hz, 1H, H-6b), 4.70 (m, 1H, H-1), 5.17 (dd, $^3J_{3,4} = 3.3$ Hz, $^3J_{2,3} = 8.9$ Hz, 1H, H-3), 5.33 (dd, $^3J_{1,2} = 5.0$ Hz, $^3J_{2,3} = 8.9$ Hz, 1H, H-2), 5.43 (m, 1H, H-4). ^{13}C NMR (CDCl$_3$, 125.8 MHz) δ: 20.65, 20.65, 20.70 (4C, 4 CH$_3$), 33.02 (CH$_2$CO$_2$H), 61.04 (C-6), 67.04 (C-4), 67.56 (C-2), 67.77 (C-3), 68.73 (C-1), 69.45 (C-5), 169.57, 169.85, 169.98, 170.65 (4 C=O), 174.90 (CO$_2$H).

DOTA-Gal-NAPamide: 2,3,4,6-Tetra-O-acetyl-α-D-galactopyranosyl ethanoic acid (2 eq) in DMF was preactivated with HATU (2 eq) for 10 min and added to a suspension of solid-phase-bound, partially protected NAPamide (1 eq peptide) containing DIPEA (4 eq). After 40 h at room temperature the resin was washed (DMF, MeOH, DMF) and the coupling cycle repeated. After washing of the resin, the peptide was cleaved using a 90% TFA-mixture[25], precipitated in t-butyl methyl ether and purified by RP-HPLC (t_R = 12.51 min). The DOTA moiety was then coupled to the ε-amino group of Lys[11] and deprotected in acid-treated (2 N HCl, >1 h) glassware using the standard procedure[25]. Deprotection of the acetyl groups of the carbohydrate moiety was carried out in liquid phase using hydrazine hydrate (diluted 1:9 in DMF, 1 mL/20 mg peptide) for 5 h, and purified by RP-HPLC (Vydac semi-preparative column, t_R = 14.80 min). Calculated monoisotopic mass: 1647.79 gmol^{-1}; measured: 1647.5 gmol^{-1}.

DOTA-Gluc-NAPamide

The glucose moiety was coupled to solid-phase bound NAPamide using the Maillard reaction which is a slow non-enzymatic chemical reaction of reducing sugars modifying amino groups of peptides, proteins, lipids and nucleic acids[12], thus leading to the formation of Amadori products[11,116,150]. The resin containing NAPamide (1 eq) was stirred in the presence of β-D-glucose (10 eq) under reflux in a mixture of MeOH/AcOH (95:5) at 60°C for 72 h. After washing with MeOH and isopropanol, completion of the reaction was checked by a Kaiser test. The peptide was then cleaved from the resin, precipitated with *t*-butyl methyl ether and purified by RP-HPLC (t_R = 8.94 min). Coupling and deprotection of DOTA followed standard procedures (see above), followed by purification with RP-HPLC (t_R = 9.10 min). Calculated monoisotopic mass: 1605.6 gmol^{-1}; measured: 1605.5 gmol^{-1}.

DOTA-Mtr-NAPamide

The maltotriose moiety was coupled to solid-phase-bound NAPamide using the Maillard reaction, followed by the addition and deprotection of DOTA, as described above for DOTA-Gluc-NAPamide. RP-HPLC yielded the product peak at t_R = 7.80 min. Calculated monoisotopic mass: 1930.03 gmol^{-1}; measured: 1930.1 gmol^{-1}.

DOTA-[Asp(Gal)^2]-NAPamide

To the solid-phase-bound partial NAPamide sequence His-D-Phe-Arg-Trp-Gly-Lys-resin (with side-chain protection) Fmoc-Asp(1,2:3,4-diisopropylidene-6-amino-α-D-galactosyl)-OH and, subsequently, Fmoc-Nle-OH were coupled manually using the HOBt-DIPC method. After cleavage of Fmoc, the N-terminal acetyl group was introduced to the peptide-resin (1 eq, suspended in a very small amount of DMF) by the addition of p-nitrophenyl acetate (2 eq) activated by HOBt (1 eq). After 24 h the resin was filtrated and washed 5× with DMF and 4× with isopropanol. The peptide was cleaved from the resin using a 90% TFA-mixture, precipitated and purified by RP-HPLC (Vydac analytical column, t_R = 13.71 min). The DOTA moiety was then coupled to the ε-amino group of Lys^{11} and deprotected as described above. RP-HPLC on the Waters Symmetry analytical column yielded the product peak at t_R = 10.68 min. Calculated monoisotopic mass: 1646.8 gmol^{-1}; measured: 1646.8 gmol^{-1}.

N$^\alpha$-DOTA-[Lys(Gluc)^8]-NAPamide

Solid-phase bound NAPamide was first N-terminally extended by DOTA, cleaved from the resin and then Gluc was attached to the ε-amino group of Lys^{11}. Protected tri-t-Bu-DOTA (1.2 eq) was preincubated with HATU (1.4 eq) in DMF (~1ml) for 10 min and added in five portions (in 5-min intervals) to the peptide-resin suspension (1 eq) in DMF containing DIPEA (1.5 eq). After 1 h, 0.6 eq of tri-t-Bu-DOTA and 0.7 eq of HATU were added and the reaction was continued for another hour. The peptide was then cleaved from the resin and the chelator complex was simultaneously deprotected using the standard 90% TFA-mixture. After precipitation, the peptide was purified by RP-HPLC (t_R = 9.50 min) and lyophilized. The carbohydrate moiety was coupled using a slightly modified Maillard reaction: N$^\alpha$-DOTA-NAPamide (1 eq) and β-D-glucose (10 eq) were stirred for only 45 h at 60°C under reflux and an N$_2$-atmosphere using a mixture of MeOH/AcOH (95:5). Completion of the reaction was checked by a Kaiser test. The peptide was then directly purified by RP-HPLC (t_R = 8.59 min) and lyophilized. Calculated monoisotopic mass: 1605.75 gmol^{-1}; measured: 1605.8 gmol^{-1}.

DOTA-NAPamide-Gal

NAP (Nle-Asp-His-D-Phe-Arg-Trp-Gly-Lys) was assembled on TentaGel S TRT-Lys(Boc)-Fmoc resin containing an acid-labile linker producing a free C-terminal acid under very mild acid cleavage conditions, without deprotection of the side-chains. The free N$^\alpha$ group of Nle was acetylated as described above and the peptide cleaved from the resin using dichloromethane DCM/TFE/AcOH 7:2:1 (1 ml/0.1 g of resin; 1 h). The solvent volume was reduced by careful evaporation and the peptide precipitated by the addition of 10 volumes of ice-cold diethyl ether and purified by RP-HPLC (t_R = 21.32 min). Calculated monoisotopic mass: 1851.21 gmol^{-1}; measured: 1850.69 gmol^{-1}. The peptide (1 eq) was dissolved in DMF and the free C-

terminal –COOH group preactivated with HATU (2 eq) for 10 min. 1-Amino-1-deoxy-β-D-galactose (2 eq) and DIPEA (4 eq) were added, the mixture was agitated for 1 h and then left at room temperature overnight. Purification by RP-HPLC (t_R = 20.95 min) and lyophilization. Calculated monoisotopic mass: 1770.05 gmol^{-1}; measured: 1770.10 gmol^{-1}. Side-chain protecting groups were now cleaved using a 94% TFA-mixture (2 h) containing only 1% thioanisole which would keep the formation of side-products minimal. Solvents were removed by careful evaporation with the help of added diethyl ether as solvent carrier. The peptide was dissolved by consecutive addition of 20% AcOH, H_2O and CH_3CN and purified by RP-HPLC (t_R = 9.90 min). Finally, the DOTA moiety was coupled to the ε-amino group of Lys[11] and deprotected using standard procedures as described above. Purification by RP-HPLC (t_R = 10.12 min). Calculated monoisotopic mass: 1647.79 gmol^{-1}; measured: 1648.0 gmol^{-1}.

Radioligands

[111]In-Labeled peptides

Incorporation of ^{111}In into DOTA-peptides was performed by the addition of 55.5 MBq of 111In-Cl3 (Mallinckrodt, Petten, The Netherlands; stock concentration: 370 MBq/ml) to the DOTA-peptides (10 nmol) dissolved in 54 μl of acetate buffer (0.4 mol/L, pH=5) containing 2 mg of gentisic acid. After 10 min of incubation at 95°C, the radiolabeled DOTA-peptides were purified on a small reversed-phase cartridge (Sep-Pak C18, Waters), with first sodium acetate buffer (pH=7), then ethanol, as solvents. The purity of the resulting radioligands was assessed by RP-HPLC on a Jasco PU-980 chromatography system, connected to a Radiomatic 500TR LB506C1 γ-detector (Packard) and a Spherisorb ODS2/5-μm column under the following conditions: eluent A = 0.1% TFA in water; eluent B = 0.1% TFA in acetonitrile; gradient = 0-2 min, 96% A; 2-22 min, 96%-45% A; 22-30 min, 45%-25% A; 30-32 min, 25% A; 32-34 min, 25%-96% A; flow rate, 1.0 mL/min. The specific activity of the radioligand was always >7.4 GBq/μmol.

[125]I-Labeled peptide

NDP-MSH was iodinated using the IODO-GEN® method. NDP-MSH (12.14 nmol) was mixed with 37 MBq Na[125]I (Amersham Bioscience, Otelfingen, Switzerland; stock concentration: 3.7 GBq/mL) in 60 μl phosphate buffer (0.3 M, pH=7.4) in IODO-GEN®-precoated tubes (Pierce, Rockford, IL, USA). After 15 min incubation at room temperature under shaking, the mixture was loaded on a small reversed-phase cartridge (Sep-Pak C18, Waters), washed with water and acetic acid (0.5 M) and finally the peptide was eluted with methanol and collected. The fractions containing ^{125}I-NDP-MSH were supplemented with dithiothreitol (1.5 mg/mL) and stored at –20°C. Before each binding experiment, an additional purification was performed by RP-HPLC/γ-detection.

Cell culture

The mouse B16F1 melanoma cell line[101] was cultured in modified Eagle's medium (MEM; Biochrom AG, Germany) supplemented with 10% heat-inactivated fetal calf serum, 2 mmol/L L-glutamine, 1% nonessential amino acids, 1% vitamin solution, 50 UI/mL penicillin and 50 μg/mL streptomycin (all from Gibco/Invitrogen, Carlsbad, CA, USA) at 37°C in an atmosphere of 95% air/5% CO_2. For expansion or experiments, the cells were detached with 0.02% ethylenediaminetetraacetic acid (EDTA) in PBS (150 mmol/L, pH=7.2-7.4).

The human HBL melanoma cell line was cultured in modified RPMI medium (Biochrom AG) supplemented with 10% heat-inactivated fetal calf serum, 2 mmol/L L-glutamine, 50 UI/mL penicillin and 50 μg/mL streptomycin in the same culture and expansion conditions as B16F1 cells.

In vitro *binding assay with B16F1 or HBL cells*

Competitive binding experiments were performed by incubating MC1R-expressing B16F1 or HBL cells in microplates with the radioligand ^{125}I-NDP-MSH and a series of dilutions of competitor peptides (from 1×10^{-6} to 1×10^{-12} mol/L) as described previously[111]. Triplicates of 100 μL B16F1 or HBL cell suspensions adjusted to 4×10^6/mL were incubated in 96-well U-bottom microplates (Falcon 3077) for 3 h at 15°C (B16F1) or for 2 h at 37°C (HBL) with 50 μL of ^{125}I-NDP-MSH (50,000 cpm). The binding medium consisted of MEM with Earle's salts (Biochrom AG), 0.2% bovine serum albumin and 1,10-phenanthroline (0.3 mmol/L; Merck). The reaction was stopped by incubation on ice for 10 min, and the cell-bound radioactivity was collected on filters by use of a cell harvester (Packard, Meriden, CT, USA). The radioactivity was counted by use of a TopCount microplate scintillation counter (Packard) and the 50% inhibitory concentration (IC_{50}) was calculated with the Prism software (GraphPad Software).

In vitro *melanin assay*

The biological activity of the α-MSH derivatives was assessed with an *in situ* melanin assay. B16F1 cells (2,500 per well, 100 μl) were distributed in cell culture flat bottom 96-well plates in medium consisting of MEM without phenol red and supplemented with 10% heat-inactivated fetal calf serum, 2 mmol/L L-glutamine, 0.31 mmol/L L-tyrosine, 1% nonessential amino acids, 1% vitamin solution, 50 U/mL penicillin and 50 μg/mL streptomycin. After overnight incubation in a cell incubator at 37°C, serial concentrations of α-MSH derivatives, ranging from 1×10^{-8} to 1×10^{-12} in 100 μL volume, were added and incubation was prolonged for an additional 72 h. Melanin production was then monitored through measurement of the absorbance at 310 nm in a microplate reader (Spectra MAX 190, Molecular Devices, Menlo Park, CA).

In vitro *internalization assay*

B16F1 cells were seeded in 6-well plates and incubated overnight at 37°C in B16F1 cell culture medium. For the experiments, B16F1 medium was removed and replaced by 1 mL Mouse Binding Medium (MBM) internalization buffer, consisting of MEM with Earle's salts (Biochrom AG, Germany), 0.2% bovine serum albumin and 1,10-phenanthroline (0.3 mmol/L; Merck). After 1 h incubation at 37°C, 74 kBq of radioligand (^{111}In-labeled peptides) were added and the plates were incubated for different times. Nonspecific internalization was assessed by addition of 50 μL of a 1 μM cold α-MSH solution. Samples were taken from the supernatant after 0.5, 2 and 3.5 h to determine the total dose added, immediately followed by extensive washings of the cells (6x) using pre-warmed (37°C) MBM to remove the excess of radioligand. The cells were then incubated in 2 ml ice-cold acid buffer (acetate-buffered HBSS, pH 5) for 10 min to dissociate surface-bound ligand. After collection of the acidic fraction, cells were rinsed once with MBM and the washing pooled with the acid buffer fraction. The cells were then washed once more with MBM (37°C), lysed in 1% Triton X-100 and finally transferred to tubes for quantification. The radioactivity of all collected fractions was determined in a Cobra II Auto-Gamma γ-counter (Packard). One counting plate was submitted to the same treatment as the plate incubated for the longest time. Cells from this plate were not lysed, but detached (EDTA) and counted. Results of the experiments are expressed as percentile of the added dose per million cells.

Biodistribution in B16F1 tumor-bearing mice and stability of radioligands after kidney excretion

All animal experiments were performed in compliance with Swiss regulations for animal welfare. Female B6D2F1 mice (C57BL/6 × DBA/2 F1 hybrids; breeding pairs obtained from IFFA-CREDO) were implanted subcutaneously with 0.5 million B16F1 cells in Phosphate Buffer Saline (PBS) to generate a primary skin melanoma. One week later, 200 μL containing 185 kBq of radioligand diluted in PBS/BSA (pH 7.4) were injected intravenously in the lateral tail vein of each mouse. To allow determination of non-specific uptake, 50 μg α-MSH were co-injected with the radioligand in some mice. The animals were killed at the indicated time points; organs and tissues of interest were dissected and rinsed of their excess blood, weighed, and their radioactivity was measured in a γ-counter. The percentage of the injected dose per gram tissue (%ID/g) was calculated for each tissue. The total counts injected per animal were calculated by extrapolation from counts of a standard taken from the injected solution for each animal.

As part of the biodistribution experiments, samples of urine were collected from melanoma-bearing mice 10, 15, 20 min and 4 h after injection of 185 kBq ^{111}In-DOTA peptide and kept frozen at -80°C until use. Urine (1 vol) was mixed with methanol (2 vol) to precipitate the proteins and was analyzed by RP-HPLC/γ-detection under the conditions mentioned above.

Analysis of data

Unless otherwise stated, results are expressed as mean ± standard error of the mean (SEM). Statistical evaluation of the binding assays was performed by using Student's *t*-test. For the analysis of data collected during biodistribution experiments, the mean value obtained for each organ was compared individually to each DOTA-NAPamide organ values by using Student's *t*-test, and the results were corrected with the Bonferroni correction. A *P*-value of <0.05 was considered statistically significant. The area under the curve (AUC) was calculated for a particular time period (4-48 h) using the GraphPad Prism software; mean tissue uptake values at each time point were used for this calculation.

RESULTS

Synthetic glycosylated DOTA-NAPamide analogs

The preparation of glycosylated DOTA-NAPamide analogs followed four different strategies: (1) synthesis of a galactopyranosyl-ethanoic acid for straightforward attachment to the N^α-terminal amino group of the peptide, as indicated for DOTA-Gal-NAPamide (**Figure 43** and **Figure 44**), requiring a three-step synthesis of the glyco-derivative (allylation of its anomeric center, followed by ozonolysis and oxidation[16]); (2) Maillard reaction of β-D-glucose or maltotriose with the N^α-terminal or the N^ϵ-side-chain amino group, as exemplified for DOTA-Gluc-NAPamide, DOTA-Mtr-NAPamide, or N^α-DOTA-[Lys(Gluc)[8]]-NAPamide (Fig. 1); (3) use of the Fmoc-Asp(1,2:3,4-diisopropylidene-6-amino-α-D-galactosyl)-OH building block for a direct introduction of the carbohydrate during solid-phase assembly into the side-chain position of residue 2 of DOTA-[Asp(Gal)[2]]-NAPamide; and (4) functionalization of the C-terminal amide as glyco-amide, by attachment of 1-amino-1-deoxy-β-D-galactose to the free carboxy terminus of a side-chain protected peptide., followed by deprotection and attachment of the DOTA group at the N^ϵ-side-chain of Lys 8. The final product, DOTA-NAPamide-Gal was obtained in high purity, however in low yield. The other syntheses also produced peptides of high purity and in higher yields.
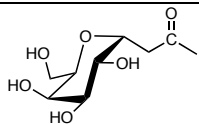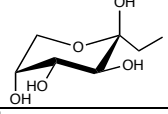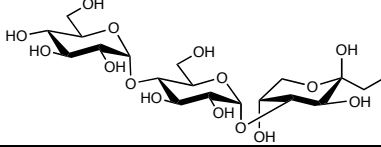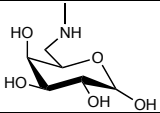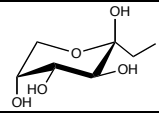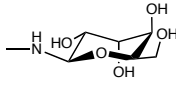
α-MSH:

α-MSH derivatives:

Peptide	W	X	Y	Z
DOTA-NAPamide	Ac	OH	DOTA	NH$_2$
DOTA-Gal-NAPamide		OH	DOTA	NH$_2$
DOTA-Gluc-NAPamide		OH	DOTA	NH$_2$
DOTA-Mtr-NAPamide		OH	DOTA	NH$_2$
DOTA-[Asp(Gal)^2]-NAPamide	Ac		DOTA	NH$_2$
N$^\alpha$-DOTA-[Lys(Gluc)^8]-NAPamide	DOTA	OH		NH$_2$
DOTA-NAPamide-Gal	Ac	OH	DOTA	

Figure 43: Structures of the glycopeptides used in this study. Ac = acetyl group.

Figure 44: Structure of DOTA-Gal-NAPamide.

Receptor binding

MC1R affinity of the glycated NAPamide analogs was assessed by competition binding assays against ^{125}I-NDP-MSH on both murine B16F1 and human HBL melanoma cell lines, using α-MSH and DOTA-NAPamide as reference compounds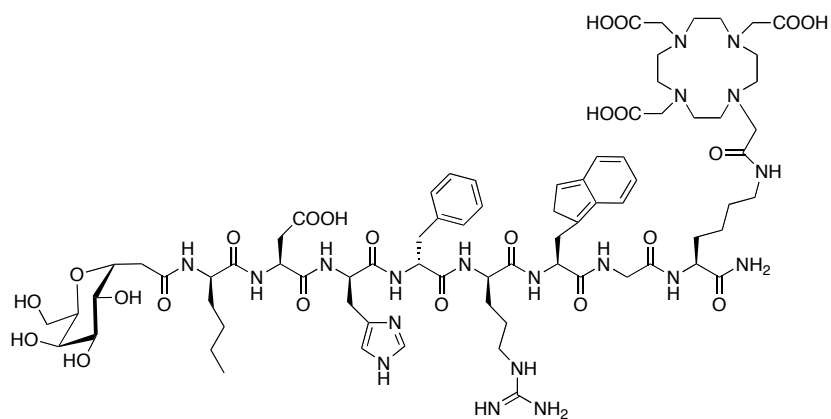. All peptides showed very good binding affinities to mouse and human MC1R with IC_{50}s ranging from 0.45 to 7.61 nmol/L (**Table 10**). DOTA-[Asp(Gal)^2]-NAPamide displayed the highest affinity for the MC1R on both B16F1 and HBL cells and exceeded that of DOTA-NAPamide by a factor of 3 to 3.5. DOTA-NAPamide-Gal was also slightly more active than DOTA-NAPamide. DOTA-Gal-NAPamide and DOTA-Gluc-NAPamide displayed slightly lower IC_{50}s than DOTA-NAPamide, while the affinity of DOTA-Mtr-NAPamide and N$^\alpha$-DOTA-[Lys(Gluc)^8]-NAPamide was about 2- to 3.5-fold lower than that of DOTA-NAPamide. The glycopeptides without the DOTA chelator all showed markedly higher affinity (data not shown).

Table 10: MC1R affinity and biological activity of glycopeptides, compared to α-MSH and DOTA-NAPamide.

MC1R Affinity and Biological Activity of α-MSH Analogs on B16F1 and HBL cells			
α-MSH analogs	B16F1 IC_{50} (nmol/L)[*]	HBL IC_{50} (nmol/L)[*]	rEC$_{50}$ (α-MSH=1)[†]
α-MSH	1.50 ± 0.14	1.91 ± 0.26	1
DOTA-NAPamide	1.38 ± 0.35	3.09 ± 1.11	0.66 ± 0.35
DOTA-Gal-NAPamide	1.62 ± 0.20	5.08 ± 0.25	0.63 ± 0.13
DOTA-Gluc-NAPamide	1.90 ± 0.07	5.57 ± 0.58	0.34 ± 0.03
DOTA-Mtr-NAPamide	2.95 ± 0.17[‡]	7.61 ± 0.66[‡]	0.62 ± 0.37
DOTA-[Asp(Gal)^2]-NAPamide	0.45 ± 0.01[‡]	0.88 ± 0.08	0.26 ± 0.03
N$^\alpha$-DOTA-[Lys(Gluc)^8]-NAPamide	4.58 ± 0.42[‡]	5.61 ± 2.17	1.02 ± 0.21
DOTA-NAPamide-Gal	1.24 ± 0.22	2.00 ± 0.13	0.48 ± 0.17

_____

[*]MC1R affinity of α-MSH analogs was assessed by competition binding experiments with B16F1 or HBL cells and ^{125}I-NDP-MSH as radioligand (n=3-16)

[†]Biological activity of α-MSH analogs was determined in melanin assay with B16F1 cells, and results are expressed as relative concentration inducing half-maximal response (rEC$_{50}$, n=3-10) normalized on α-MSH=1.

[‡]$P < 0.05$ vs. DOTA-NAPamide

Biological activity

In the melanin assay using B16F1 cells, all DOTA-glycopeptides, except for N$^\alpha$-DOTA-[Lys(Gluc)^8]-NAPamide, displayed higher biological (agonist) activity than DOTA-NAPamide, all in the picomolar to range. In order to compare the EC_{50} of different experiments, these were normalized against the EC_{50} of the reference compound α-MSH whose rEC$_{50}$ was defined as 1 (**Table 10**). DOTA-[Asp(Gal)^2]-NAPamide and DOTA-Gluc-NAPamide showed the lowest rEC$_{50}$s with 0.26 and 0.34, respectively. The values of the other glycopeptides were comparable to that of DOTA-NAPamide. The induction of melanin synthesis by B16F1 cells started at doses matching their IC_{50}s and lower. Only DOTA-Mtr-NAPamide showed a slightly worse rEC$_{50}$, but still matching those of α-MSH. Again, DOTA-[Asp(Gal)^2]-NAPamide exhibited the best behavior *in vitro*.

Internalization assay

Internalization assays were carried out to determine if and how fast the glycopeptides were internalized by B16F1 cells. The results were excellent, all glycopeptides being almost totally internalized in 2 h or less. As an example, **Figure 45** shows the internalization kinetic of DOTA-Gal-NAPamide, which reached a plateau after 2 h when internalization of the peptide was almost total. These data show that internalization of the peptide by tumor cells cannot be an issue regarding the *in vivo* tumor uptake.
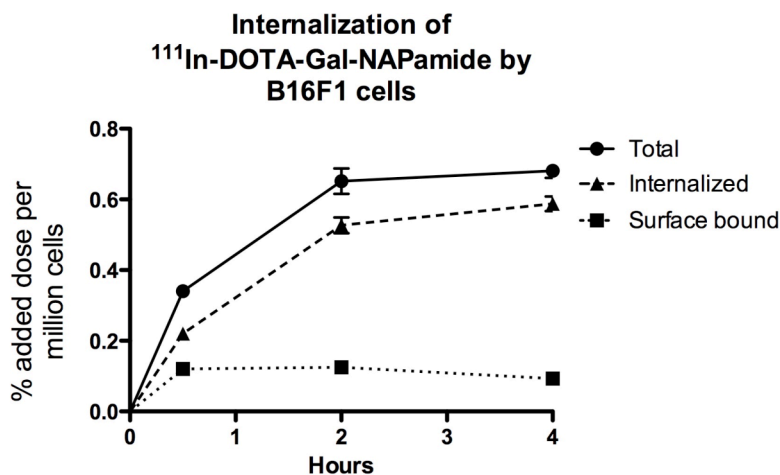
Figure 45: Exemplary internalization experiment with DOTA-Gal-NAPamide.

Biodistribution in melanoma-bearing mice

Table 2 shows the tissue distributions of the different ^{111}In-labeled, glycated DOTA-NAPamide peptides in comparison with [^{111}In]-DOTA-NAPamide at 4, 24 and 48 h after injection of the radioligand. Co-injection of an excess of α-MSH to block MC1R reduced the 4-h tumor uptake of DOTA-Gal-NAPamide by >90%, of DOTA-Mtr-NAPamide by 89%, of N^{α}-DOTA-[Lys(Gluc)[8]]-NAPamide by 86%, of DOTA-Gluc-NAPamide by 80%, of DOTA-NAPamide-Gal by 77%, and of DOTA-[Asp(Gal)[2]]-NAPamide by 75%, indicating that all these derivatives are taken up by melanoma cells through receptor-mediated internalization. DOTA-Gal-NAPamide showed the highest tumor uptake among the glycopeptides, comparable to that of DOTA-NAPamide (**Figure 46**), followed by DOTA-Mtr-NAPamide, DOTA-NAPamide-Gal, DOTA-[Asp(Gal)[2]]-NAPamide, N^{α}-DOTA-[Lys(Gluc)[8]]-NAPamide and DOTA-Gluc-NAPamide. The ranking of melanoma uptake of the different glyco-NAPamide peptides did not correspond with the in vitro MC1R binding affinity.

Table 11: Tissue distribution, including melanoma tumor, of glycated ^{111}In-labeled α-MSH analogs and DOTA-NAPamide 4, 24 and 48h after injection.

Pharmacokinetics of α-MSH analogs 4, 24 and 48 hours after injection (mean ± SEM)[†]

α-MSH analog	Time (h)	%ID/g of tissue[†]												
		Blood	Tumor	Stomach	Kidney	Liver	Spleen	Lung	Small Intestine	Pancreas	Heart	Bone	Muscle	Skin
DOTA-NAPamide[*]	4	0.09 ± 0.02	7.77 ± 0.35	0.09 ± 0.01	4.77 ± 0.26	0.34 ± 0.05	0.14 ± 0.01	0.08 ± 0.01	0.07 ± 0.01	0.04 ± 0.00	0.05 ± 0.01	0.11 ± 0.02	0.05 ± 0.01	-
	24	0.02 ± 0.00	2.32 ± 0.15	0.12 ± 0.02	2.41 ± 0.20	0.31 ± 0.02	0.11 ± 0.01	0.05 ± 0.01	0.08 ± 0.01	0.03 ± 0.00	0.03 ± 0.00	0.14 ± 0.02	0.02 ± 0.00	-
	48	0.00 ± 0.00	1.41 ± 0.12	0.11 ± 0.05	1.55 ± 0.07	0.27 ± 0.02	0.10 ± 0.01	0.03 ± 0.01	0.05 ± 0.01	0.02 ± 0.00	0.01 ± 0.00	0.05 ± 0.01	0.01 ± 0.00	-
DOTA-Gal-NAPamide	4	0.04 ± 0.00	8.30 ± 1.22	0.06 ± 0.01	4.43 ± 0.34	0.26 ± 0.05	0.13 ± 0.01	0.26 ± 0.05[‡]	0.06 ± 0.00	0.04 ± 0.00	0.05 ± 0.00	0.09 ± 0.01	0.03 ± 0.00	0.12 ± 0.01
	24	0.01 ± 0.00	2.00 ± 0.34	0.05 ± 0.00	2.06 ± 0.28	0.17 ± 0.03[‡]	0.11 ± 0.02	0.12 ± 0.04	0.05 ± 0.01	0.03 ± 0.00	0.03 ± 0.00	0.09 ± 0.01	0.02 ± 0.00	0.09 ± 0.01
	48	0.01 ± 0.00[‡]	0.88 ± 0.02[‡]	0.06 ± 0.00	1.15 ± 0.05	0.16 ± 0.01[‡]	0.15 ± 0.01[‡]	0.15 ± 0.03[‡]	0.06 ± 0.01	0.03 ± 0.00[‡]	0.03 ± 0.00[‡]	0.10 ± 0.02[‡]	0.02 ± 0.00[‡]	0.07 ± 0.00
DOTA-Gluc-NAPamide	4	0.09 ± 0.06	4.15 ± 0.18[‡]	0.37 ± 0.13[‡]	4.48 ± 0.39	0.29 ± 0.05	0.30 ± 0.15	0.11 ± 0.04	0.18 ± 0.09	0.22 ± 0.19	0.04 ± 0.01	0.09 ± 0.01	0.03 ± 0.01	0.08 ± 0.02
	24	0.01 ± 0.00	1.40 ± 0.08[‡]	0.11 ± 0.01	2.92 ± 0.37	0.23 ± 0.02	0.15 ± 0.01	0.06 ± 0.01	0.05 ± 0.00	0.03 ± 0.00	0.03 ± 0.00	0.07 ± 0.01	0.02 ± 0.00	0.07 ± 0.01
	48	0.01 ± 0.00	0.62 ± 0.08[‡]	0.05 ± 0.00	1.91 ± 0.19	0.15 ± 0.01[‡]	0.12 ± 0.01	0.05 ± 0.01[‡]	0.05 ± 0.01	0.02 ± 0.00	0.03 ± 0.00[‡]	0.07 ± 0.01	0.02 ± 0.00[‡]	0.06 ± 0.02
DOTA-Mtr-NAPamide	4	0.02 ± 0.00	7.82 ± 0.17	0.16 ± 0.03	5.01 ± 0.40	0.17 ± 0.01	0.10 ± 0.01	0.07 ± 0.01	0.06 ± 0.01	0.03 ± 0.00	0.03 ± 0.00	0.08 ± 0.01	0.02 ± 0.00	0.15 ± 0.02
	24	0.01 ± 0.00	1.02 ± 0.44	0.04 ± 0.02	1.72 ± 0.78	0.08 ± 0.03[‡]	0.05 ± 0.02	0.02 ± 0.01	0.03 ± 0.01	0.02 ± 0.01	0.02 ± 0.01	0.04 ± 0.02	0.01 ± 0.00	0.05 ± 0.02
	48	0.01 ± 0.00	0.64 ± 0.10[‡]	0.09 ± 0.03	1.33 ± 0.17	0.08 ± 0.01[‡]	0.08 ± 0.01	0.03 ± 0.00	0.04 ± 0.00	0.02 ± 0.00	0.03 ± 0.00	0.05 ± 0.00	0.02 ± 0.00[‡]	0.06 ± 0.02
DOTA-[Asp(Gal)²]-NAPamide	4	0.06 ± 0.00	6.04 ± 0.39	0.32 ± 0.12[‡]	5.93 ± 0.64	0.34 ± 0.03	0.31 ± 0.18	0.09 ± 0.01	0.14 ± 0.04	0.40 ± 0.35	0.05 ± 0.00	0.19 ± 0.06	0.04 ± 0.01	0.14 ± 0.02
	24	0.02 ± 0.00	1.67 ± 0.22	0.07 ± 0.00	2.92 ± 0.48	0.27 ± 0.03	0.12 ± 0.01	0.05 ± 0.00	0.06 ± 0.00	0.03 ± 0.00	0.03 ± 0.00	0.09 ± 0.02	0.02 ± 0.00	0.06 ± 0.02
	48	0.01 ± 0.00[‡]	0.91 ± 0.05[‡]	0.06 ± 0.00	1.93 ± 0.10	0.20 ± 0.01	0.11 ± 0.01	0.05 ± 0.01[‡]	0.07 ± 0.01	0.03 ± 0.00	0.03 ± 0.00[‡]	0.09 ± 0.01[‡]	0.02 ± 0.00[‡]	0.07 ± 0.00
Nα-DOTA-[Lys(Gluc)8]-NAPamide	4	0.04 ± 0.00	5.08 ± 0.25[‡]	0.86 ± 0.42[‡]	5.79 ± 0.25	0.21 ± 0.01	0.13 ± 0.00	0.11 ± 0.01	0.08 ± 0.01	0.05 ± 0.01	0.04 ± 0.00	0.11 ± 0.01	0.03 ± 0.00	0.12 ± 0.01
	24	0.01 ± 0.00	1.38 ± 0.15[‡]	0.16 ± 0.05	3.81 ± 0.21	0.16 ± 0.01[‡]	0.12 ± 0.01	0.05 ± 0.01	0.07 ± 0.01	0.04 ± 0.01	0.04 ± 0.00	0.09 ± 0.01	0.02 ± 0.00	0.10 ± 0.03
	48	0.01 ± 0.00[‡]	0.70 ± 0.05[‡]	0.13 ± 0.01	2.04 ± 0.23	0.12 ± 0.02[‡]	0.15 ± 0.05	0.07 ± 0.02[‡]	0.06 ± 0.00	0.03 ± 0.00	0.04 ± 0.00[‡]	0.09 ± 0.01[‡]	0.02 ± 0.00[‡]	0.08 ± 0.02
Ac-NAP-Lys(DOTA)(Gal)	4	0.02 ± 0.00	6.33 ± 1.25	0.13 ± 0.02	5.94 ± 0.63	0.18 ± 0.03	0.10 ± 0.01	0.06 ± 0.01	0.14 ± 0.04	0.04 ± 0.00	0.03 ± 0.00	0.07 ± 0.01	0.03 ± 0.01	0.08 ± 0.02
	24	0.01 ± 0.00	1.74 ± 0.14	0.07 ± 0.02	5.90 ± 1.84	0.17 ± 0.03[‡]	0.08 ± 0.01	0.04 ± 0.01	0.05 ± 0.00	0.03 ± 0.00	0.03 ± 0.00	0.07 ± 0.01	0.03 ± 0.01	0.07 ± 0.01
	48	0.01 ± 0.00	0.95 ± 0.17	0.05 ± 0.01	2.00 ± 0.09	0.11 ± 0.00[‡]	0.09 ± 0.01	0.04 ± 0.00	0.05 ± 0.01	0.03 ± 0.00[‡]	0.03 ± 0.00[‡]	0.08 ± 0.01	0.02 ± 0.00[‡]	0.06 ± 0.00

[*]Data for DOTA-NAPamide from Froidevaux et al., *J Nucl Med* **46** (2005), 887-895.
[†]Tissue radioactivity is expressed as mean ± SEM (*n* = 4-12).
[‡]$P < 0.05$ vs. DOTA-NAPamide.

Clearance of ^{111}In from the kidneys was found to be quite a slow process, as also reported for other peptides. Indeed, 46% of the radioactivity measured in the kidneys 4 h after injection of DOTA-Gal-NAPamide was still present after 24 h, and 26% after 48 h. For DOTA-[Asp(Gal)^2]-NAPamide the values were 49% and 33%, for DOTA-Mtr-NAPamide 34% and 27%, for DOTA-Gluc-NAPamide 65% and 43% and for N$^\alpha$-DOTA-[Lys(Gluc)^8]-NAPamide 66% and 35%. The slowest clearance from the kidneys was observed for DOTA-NAPamide-Gal whose values were 99% and 34% and hence was opposed to the expectation of a marked reduction by glycating the C-terminal amide of Lys^8.
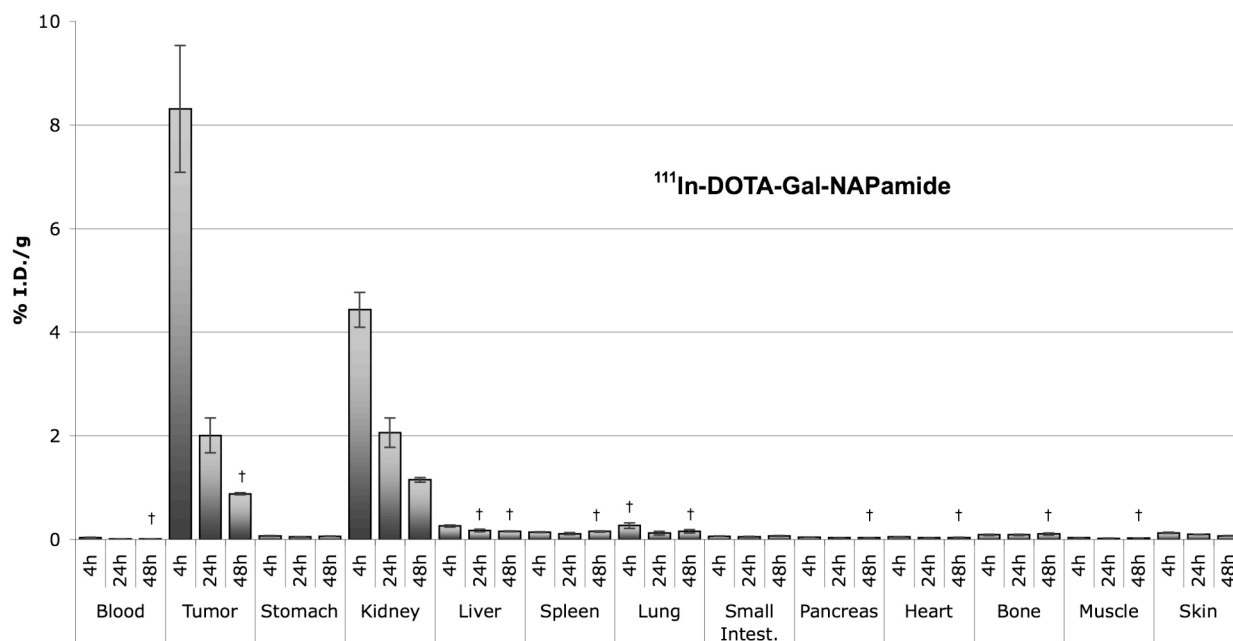
Figure 46: Biodistribution profile of [^{111}In]-DOTA-Gal-NAPamide.

Radioactivity released from the tumor was faster than from the kidneys, with 25% of the radioactivity measured after 4 h still present after 24 h and 11% after 48 h for DOTA-Gal-NAPamide, and slightly higher, but comparable values for DOTA-[Asp(Gal)^2]-NAPamide, DOTA-Gluc-NAPamide, N$^\alpha$-DOTA-[Lys(Gluc)^8]-NAPamide and DOTA-NAPamide-Gal, in part due to their lower overall tumor uptake. Indeed, DOTA-Mtr-NAPamide, which displayed an almost similar tumor uptake as DOTA-Gal-NAPamide after 4 h, exhibited values of 22% and 8% at 24 h and 48 h.

The glycopeptides with the highest in vitro binding affinity displayed a lower in vivo accumulation in melanoma than would have been predicted from their in vitro potency. DOTA-Gal-NAPamide showing an average receptor binding affinity comparable to DOTA-NAPamide, delivered a more favorable biodistribution profile with higher tumor uptake after 4 h (8.30% ± 1.22%ID/g) and higher tumor-to-kidney ratio after 4 h (1.87 ± 0.15) than any other glycopeptide. Indeed, DOTA-Gal-NAPamide exhibited a 4-48 h AUC tumor-to-kidney ratio of 1.34 (**Figure 47**) which exceeds that of DOTA-NAPamide (1.11) by 17%, making it one of the best radiolabeled α-MSH analogs synthesized so far.
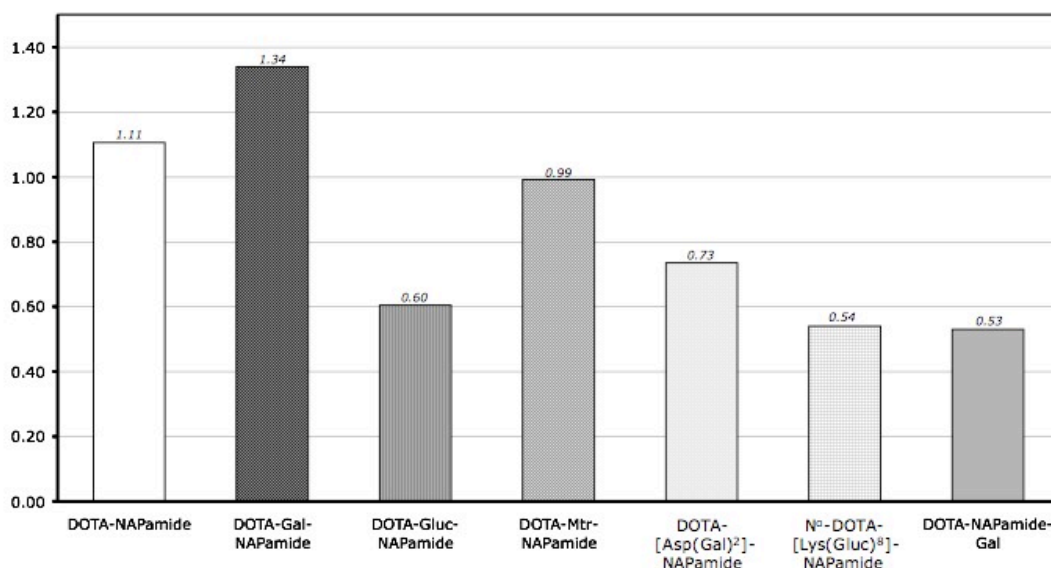
Figure 47: Tumor-to-kidney ratios of the glycopeptides compared to DOTA-NAPamide, calculated from the AUC (4-48h).

DISCUSSION

This study focused on the influence of introducing different types of carbohydrates at N-terminal, C-terminal and side-chain positions of the α-MSH derivative DOTA-NAPamide. In view of the reports that glycosylation of peptides or proteins would reduce re-uptake by the tubular system of the kidneys[281,303], our first attempt was to study a DOTA-NAPamide derivative whose C-terminal amide was glycosylated. Previous observations in our lab (unpublished data) demonstrated that an important metabolite of [^{111}In]DOTA-NAPamide was H-Lys([^{111}In]DOTA)-NH$_2$ which was regularly observed in the urine collected from mice treated with this peptide. However, DOTA-NAPamide-Gal showed a higher and much longer kidney retention than all other glycopeptides which we investigated. Most likely, the C-terminal carbohydration led to increased re-uptake and trapping of the peptide or its metabolites in endosomes in tubular cells of the kidney.

Glycation of the amino acid side-chains of Asp^2 or Lys^8 does not seem to be a good alternative option. DOTA-[Asp(Gal)^2]-NAPamide and N$^\alpha$-DOTA-[Lys(Gluc)^8]-NAPamide both displayed slightly lower tumor uptake and higher kidney uptake than the other glycopeptides. Again, the increased kidney uptake may be the result of higher rate of internalization and marked retention by tubular cells. A precise molecular explanation would require a detailed analysis, particularly in view of the very high in vitro potency of DOTA-[Asp(Gal)^2]-NAPamide which would rule out steric hindrance by the side-chain galactosyl moiety.

Finally, three different glycopeptides bearing a glucose, galactose or maltotriose moiety at their N-terminal end were then examined in order to assess the influence of the type of sugar on the pharmacokinetics. The derivative with a glucose residue displayed poor pharmacokinetic properties, displaying an *in vivo* tumor-to-kidney ratio of its AUC (4-48 h) of only 0.60 (Figure 5), although it exhibited a similarly low kidney uptake after 4h (4.48 %ID/g) as [111In]DOTA-Gal-NAPamide. The analog with N-terminal maltotriose showed much better properties with a tumor-to-kidney ratio (4-48 h AUC) of 0.99. The tumor uptake was similar to that of [111In]DOTA-NAPamide, but the higher kidney uptake led to a lower the ratio as compared to DOTA-NAPamide. The most encouraging data were obtained with [111In]DOTA-Gal-NAPamide which exhibited relatively highest melanoma uptake and lowest kidney uptake *in vivo*, leading to a tumor-to-kidney ratio which exceeded that of [111In]DOTA-NAPamide by a factor of about 1.2. This advance is very valuable, as AUC tumor-to-non-target-tissue ratios are fundamental for future therapeutic applications, nephrotoxicity remaining the main issue of radiolabeled α-MSH analogs.

In conclusion, we demonstrated that introduction of different types of sugars at various positions along the sequence of ^{111}In-labeled NAPamide analogs affected their in vitro binding affinities and their in vivo pharmacokinetic behavior. It is noteworthy that carbohydration generally did not reduce the binding affinity when compared to non-glycosylated reference peptide. Kidney re-uptake and retention, however, was increased with side-chain and C-terminal sugar groups, but decreased with an N-terminal galactosyl group. This compound, DOTA-Gal-NAPamide, exhibited favorable pharmacokinetical data. Its high melanoma uptake and low kidney retention, and above all its improved tumor uptake to kidney uptake ratio calculated from the AUC, opens the doors to a new class of derivatives for melanoma targeting.

5 Negatively charged peptides

5.1 Manuscript to be submitted

To be submitted to Bioconjugate Chemistry.

Improvement of Pharmacokinetics of Radiolabeled α-MSH Analogs for Melanoma Targeting by Introduction and Appropriate Positioning of Negative Charges.

Jean-Philippe Bapst, Heidi Tanner, Martine Calame, and Alex N. Eberle

Laboratory of Endocrinology, Department of Biomedicine, University Hospital and University Children's Hospital, Basel, Switzerland

ABSTRACT

Both melanotic and amelanotic melanomas overexpress receptors (melanocortin type 1 receptors, MC1R) for α-melanocyte stimulating hormone (α-MSH) at their surface. Radiolabeled α-MSH analogs have a great potential as diagnostic or therapeutic tools for the treatment of malignant melanoma. They show high affinity for MC1R *in vitro*, high tumor uptake *in vivo*, but suffer from a high kidney uptake and retention *in vivo*. Several structural modifications were adopted in the past, either to enhance the tumor uptake or to reduce the kidney uptake of the radiolabeled analogs, but were unsuccessful at improving their pharmacokinetical behavior. Various studies showed that the introduction of negative charges into peptides had a strong impact on their general *in vivo* behavior, and particularly on their excretion way. More specifically, it was shown that their kidney uptake could be significantly reduced. For radiolabeled α-MSH analogs, we have shown earlier and confirmed in this study with a derivative carrying two negative charges towards its C-terminal end that the introduction of negative charges at the C-terminus did not deliver any improvement in kidney excretion. Indeed, the derivative used in this study lost its receptor affinity without reducing the kidney uptake. Suspicion that the localization of the negative charge could be a fundamental parameter led to the development of a new derivative carrying an additional negative charge towards the N-terminal end of the peptide. DOTA-phospho-α-MSH$_{2-9}$, bearing a phosphotyrosine in the second position, was evaluated in a comparative study using DOTA-NAPamide, one of the best linear α-MSH analogs, as reference. Although its MC1R affinity was slightly lower than that of DOTA-NAPamide, its biodistribution profile was markedly improved. A significant reduction of the kidney uptake was observed 4 h after injection of the tracer, yielding a 1.6-fold lower accumulation than DOTA-NAPamide. The tumor-to-kidney ratio calculated from the AUC (4-48 h) could consequently be improved, reaching 1.42 for the new derivative (1.11 for DOTA-NAPamide). Therefore, localization of negative charges appears to be crucial for pharmacokinetics, as DOTA-phospho-MSH$_{2-9}$ delivered the best tumor-to-kidney ratio ever reached for linear ^{111}In-labeled α-MSH analogs, and is therefore very promising.

INTRODUCTION

Cutaneous malignant melanoma has become the most common malignancy among young adults[79], and its prognosis is usually poor. As this type of tumor overexpresses melanocortin type-1 receptors (MC1R) at its surface[122,284], it represents a good candidate for targeting using radiolabeled tracers. The hormone α-MSH is the native ligand of MC1R, and peptide analogs with better binding affinities were already synthesized in the past, such as [Nle[4], D-Phe[7]]-α-MSH (NDP-MSH)[267] or DOTA-NAPamide[114]. Such peptides, depending on the isotope used for their labeling, may be used either in diagnostic or therapeutic applications, as it was shown for somatostatin analogs[37]. However, α-MSH analogs suffer from the disadvantage that their benefits of excellent tumor selectivity is diminished by a high kidney uptake[60,114,115]. Several strategies were developed to overcome the kidney uptake, such as the use of different radioisotopes[114], variations in the position of the chelate (DOTA), amidation of the C-terminal end[115], co-injection of basic amino acids[32,34], cyclization[124] and dimerization[25]. Unfortunately, all these methods were unsuccessful in sufficiently improving the tumor-to-kidney ratio of the injected radiopeptides in order to allow their use as diagnostic or therapeutic tools.

Various investigations in the past showed the crucial role of negatively charged peptides (or other molecules) on their pharmacokinetics, more specifically on their excretion way and clearance time. At the level of glomerular filtration, it appears that capillary cells, in addition to their size-exclusion function, seem to play a role in restricting transport of polyanions. As early as in 1980, Deen et al.[78] discussed a "theoretical model for glomerular filtration of charged solutes", which described electrostatic exclusion as the mechanism by which polyanions were less prone to pass through the capillary wall than neutral macromolecules, and the latter less than polycations. Depending on the drug, this could have a negative effect on pharmacokinetics by letting the drug recirculate several times before being finally excreted or metabolized by other organs. Thus, its toxicity might be enhanced.

It has been shown that the surface of tubular cells is negatively charged, and that electrostatic interactions at this level contributed greatly to the reuptake of molecules in the kidney[33]. Christensen et al. revealed the influence of the total molecular charge and the distribution of the local charges on protein binding by the luminal membrane, and thus on their subsequent endocytosis by the proximal tubule[67]. They showed that cationic or neutral molecules or proteins were much more (up to 5 times more) reabsorbed by the proximal tubule than their anionic counterparts. Lawrence et al. also showed that the increased urinary clearance observed with negatively charged bovine albumin derivatives was due to a large reduction in the amount of protein absorbed by the proximal tubular epithelium. They also showed that this reduction in reuptake was able to swamp the effects of the lower glomerular ultrafiltration mentioned above[181]. Kok et al. also confirmed these results by investigating the effect of the presence of positive charges on pharmacokinetics of low molecular weight lysozyme. They compared two modified lysozyme derivatives, one carrying six free primary amino groups, and the other with these six amino groups "blocked" by succinylation. They observed a dramatic increase in excretion for the succinylated derivative, suggesting that reduction of the positive charge has a positive effect on urinary excretion[168].

In the field of somatostatin, Akizawa et al. confirmed the influence of negative charges on the excretion of radiolabeled peptides[7]. Introduction of differently charged amino acids close to the DTPA-chelate involved differences in kidney uptake and retention, and confirmed the findings of the studies mentioned earlier showing the positive impact of negative charges on pharmacokinetics, especially concerning kidney excretion. The derivative carrying L-Asp next to the chelate showed the lowest kidney radioactivity levels of the tested peptides, and conserved its target affinity.

These promising findings led us to consider the introduction of negative charges into α-MSH analogs. Derivatives carrying one or two negative charges through succinimidyl groups at their C-terminal end were synthesized earlier in our group and did not show any amelioration of their pharmacokinetic properties. They carried, though, the DOTA moiety at their N-terminal end. A new derivative bearing two negative charges through introduction of two D-Asp at its C-terminus (DOTA-NAP-D-Asp-D-Asp) was synthesized and tested, with the expectation that the C-terminal Lys(DOTA)-NH$_2$ moiety observed in the urine of treated mice in previous biodistribution experiments (unpublished data) would be more extensively excreted. Additionally, in order to assess the importance of the localization of the negative charges on pharmacokinetics, another novel derivative carrying an additional negative charge (compared to DOTA-NAPamide) through a phosphate functional group positioned towards the N-terminal end of the peptide and delivering a global net charge of -1, was synthesized and tested.

α-MSH:
```
  1                                                              13
Ac—Ser—Tyr—Ser—Met—Glu—His—Phe—Arg—Trp—Gly—Lys—Pro—Val—NH₂
```

DOTA-NAPamide
```
      4                             11
Ac—Nle—Asp—His—D-Phe—Arg—Trp—Gly—Lys—NH₂
                                    |
                                  DOTA
```

DOTA-NAP-D-Asp-D-Asp
```
    4                                  11
Ac—Nle—Asp—His—D-Phe—Arg—Trp—Gly—Lys—D-Asp—D-Asp—NH₂
                                    |
                                  DOTA
```

DOTA-Phospho-MSH$_{2-9}$
```
       2                                9
DOTA—Gly—Tyr—Nle—Asp—His—D-Phe—Arg—Trp—NH₂
          |
       OPO₃H₂
```
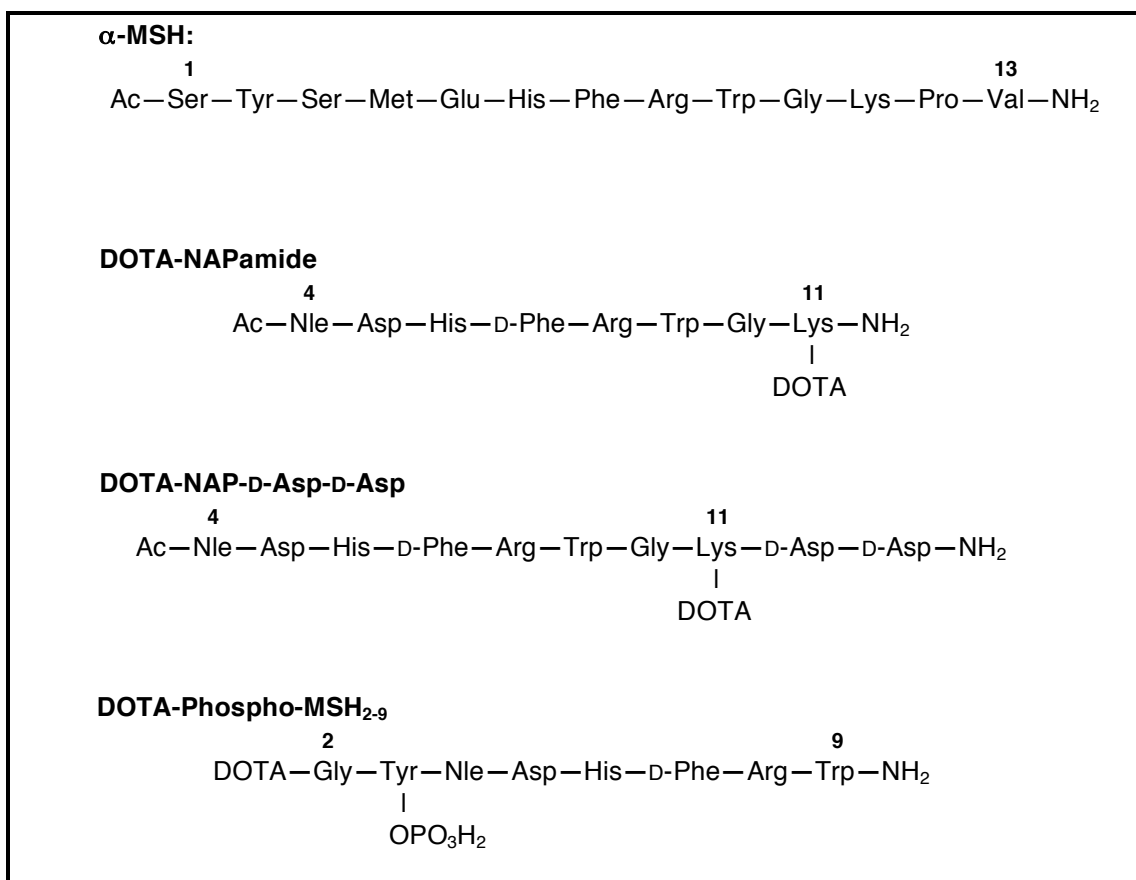
Figure 48: Structures of α-MSH, DOTA-NAPamide, DOTA-NAP-D-Asp-D-Asp and DOTA-Phospho-MSH$_{2-9}$.

Experimental procedures

Reagents

α-MSH was received as gift from Novartis (Basel, Switzerland). [Nle[4], D-Phe[7]]-α-MSH (NDP-MSH) was obtained from Bachem (Bubendorf, Switzerland). Fmoc-PAL-PEG-PS polystyrene resin was purchased from Applied Biosystems (Rotkreuz, Switzerland), TentaGel S AC-D-Asp(tBu)Fmoc resin from Rapp-Polymere (Tübingen, Germany), 9-fluorenylmethoxycarbonyl-(Fmoc-)amino acids from Novabiochem (Läufelfingen, Switzerland), and 1,4,7,10-tetraazacyclododecane-1,4,7-tris-tert-butyl acetate-10-acetic acid (DOTA-tris(t-butyl ester)) from Macrocyclics (Dallas TX, USA). N-Succinimidyl iodoacetate and Iodogen tubes were from Pierce Biotechnology Inc. (Rockford IL, USA), Na^{125}I (3.7 GBq/mL) from Perkin Elmer (Waltham MA, USA), ^{111}InCl$_3$ (370 MBq/mL) from Mallinckrodt (Petten, The Netherlands). 1,10-Phenanthroline was bought from Merck (Darmstadt, Germany) and all other organic reagents were obtained from Fluka or Sigma (Buchs, Switzerland). All reagents were of highest purity available. Cell culture media were from Biochrom AG (Berlin, Germany) and Sigma (Buchs, Switzerland). Penicillin, streptomycin, vitamins and nonessential amino acids were bought from Gibco/Invitrogen (Carlsbad CA, USA) or Sigma (Buchs, Switzerland).

Instrumentation

Continuous flow peptide synthesis was carried out on a Pioneer peptide synthesizer from PerSeptive Biosystems Inc. (Framingham MA, USA). Analytical reversed-phase-(RP)-HPLC was performed on a PU-980 system from Jasco Inc. (Easton MD, USA) with a Vydac 218TP54 C18 (5 μm, 4.6×250 mm) or a Phenomenex Jupiter C18 300 Å (5μm, 4.6×250 mm) analytical columns. DOTA-NAPamide-D-Asp-D-Asp was chromatographed with a gradient between solvent A (0.1% TFA in H2O) and solvent B (0.1% TFA in 70:30 acetonitrile/H2O). The 40-min gradient cycle consisted of the following parts: 95% A (0-2 min), 95-70% A (2-10 min), 70-30% A (10-30 min), 30-5% A (30-34 min), 5% A (34-36 min), 5-95% A (36-38 min), 95% A (38-40 min); the flow rate was 1 mL/min with the Vydac 218TP54 analytical column. UV absorption was recorded at 280 nm using a Jasco UV-1570 detector. DOTA-Phospho-MSH2-9 was chromatographed with the same gradient, but by replacing solvent A with NH4OAc 0.02 M. The analytical column used was the Penomenex Jupiter, and the UV absorption was recorded under the same conditions. Mass spectra were determined on a Finnigan LCQ Deca electrospray ion trap MS system.

Purity of the radioligand was assessed by RP-HPLC using a dedicated Jasco PU-980 chromatography system bearing a Radiomatic 500TR LB506C1 γ-detector (Packard, Meriden CT, USA) and equipped with a Spherisorb ODS2/5-μm column. Solvent A was 0.1% TFA in water; solvent B was 0.1% TFA in acetonitrile; the gradient consisted of 96% A (0-2 min), 96-45% A (2-22 min), 45-25% A (22-30 min), 25% A (30-32 min), 25-96% A (32-34 min); the flow rate was 1.0 mL/min. A cell harvester (Packard) was used to collect cell-bound radioactivity from binding assays on filters. Their radioactivity was measured on a TopCount microplate scintillation counter (Packard). Radioactivity in internalization and biodistribution assays was

measured on a Cobra II Auto-Gamma γ-counter (Packard). In biological activity assays, melanin content in cell culture media of each well was quantified on a Spectra Max 190 microplate reader (Molecular Devices, Menlo Park CA, USA) reading at 310 nm.

Peptide synthesis

General

The peptides were synthesized using standard continuous-flow technology and Fmoc strategy. As solid-phase support, flow-compatible Fmoc-PAL-PEG-PS polystyrene resin containing the acid-labile amide linker PAL (5-[(4-Fmoc-aminomethyl-3, 5-dimethoxyphenoxy]-pentanoic acid-polyethyleneglycol/polystyrene; substitution 0.21 mmol/g) was used. The following protecting groups were used for o-protection: Trt for Cys, Boc for Lys and Trp, tBu for Asp and D-Asp, Pbf for Arg, and Trt for His. Manual Fmoc deprotection was realized with 20% piperidine in DMF (20 min), followed by a short wash with 20% piperidine/DMF and 5 washes with DMF; deprotection completion was assessed by a Kaiser test. Cleavage of the peptide from the resin was performed with a solution of 90% trifluoroacetic acid (TFA), 5% thioanisole, 4.5% H_2O and 0.5% 1,2-ethanedithiol. After 2 h the solution was filtrated and the peptide precipitated with a 10-fold volume of t-Bu-methyl ether or diethylether. All reactions and manipulations with DOTA were carried out in acid-treated (1 M HCl, >1 h) glassware.

DOTA-NAPamide

NAPamide was synthesized according to the general methods described above. The peptide was N-terminally acetylated before cleavage from the resin: for these means, p-nitrophenyl acetate (2 eq) pre-activated with HOBt (1 eq) in DMF for 10 min was added to a suspension of the resin carrying NAPamide (1 peptide eq) and incubated for 24 h. The resin was filtrated and washed 5x with DMF and 4x with isopropanol. Cleavage from the resin and purification was done according to the methods described above. The DOTA moiety was coupled to the ε-amino group of C-terminal Lys and the peptide conjugate deprotected (90% TFA-mixture, 4 h) and purified as described above. RP-HPLC on a Vydac C18 analytical column: t_R = 17.5 min. Calculated monoisotopic mass: 1485.64 gmol^{-1}; found: 1485.65 gmol^{-1}.

DOTA-NAP-D-Asp-D-Asp

Nle-Asp-His-D-Phe-Arg-Trp-Gly-Lys-D-Asp-D-Asp-OH was synthesized on the peptide synthesizer according to the general methods. Its N-terminus was then acetylated by pre-activation of N-hydroxybenzotriazole (HOBt) (1 eq) and p-nitrophenyl acetate (2 eq) for 10 min, reacting with the Fmoc-deprotected on-support peptide (1 eq) for 24 h in as few DMF as possible. The conjugate was then cleaved with the 90%-TFA mixture mentioned above, precipitated in diethylether, purified by HPLC and lyophilized. RP-HPLC: t_R = 16.1 min. Calculated monoisotopic mass: 1330.40 gmol^{-1}; found: 1327.3 gmol^{-1}.

Conjugation of the partially protected DOTA-tris(t-butyl ester) to the peptide derivative was performed by addition of a solution containing the deprotected peptide (1 eq) and DIPEA (N,N'-diisopropylethylamine; 2 eq) in DMF to a solution containing DOTA-tris(t-butyl ester) (1 eq) which had been preincubated for 10 min

with HATU (0-[7-azabenzotriazole-1-yl]-1,1,3,3-tetramethyluronium hexafluorophosphate; 1.2 eq) in DMF. After 1 h at room temperature, half the initial quantity of preactivated DOTA-tris(t-butyl ester) was added to the mixture, and after a total reaction time of 2 h, the peptide was precipitated in ice-cold diethylether. Its DOTA-moiety was then deprotected by addition of 90%-TFA mixture (4 ml/5 mg of peptide). The mixture was stirred for 4 h, and deprotected DOTA-peptide was then precipitated in ice-cold diethylether, resuspended in 10% acetic acid and purified by RP-HPLC.

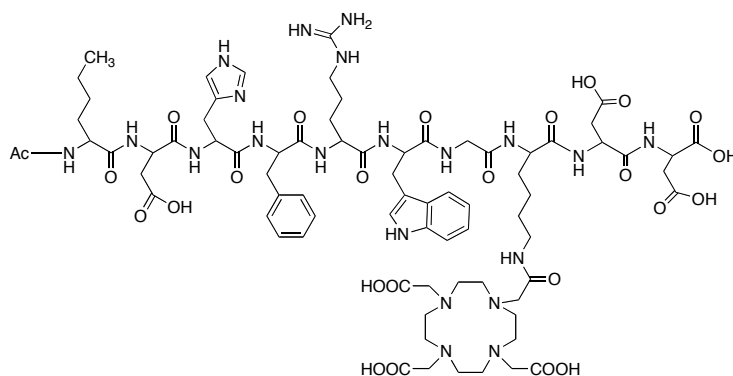RP-HPLC: t_R = 16.7 min. Calculated monoisotopic mass: 1716.80 gmol^{-1}; found: 1716.79 gmol^{-1}.

Figure 49: Structure of DOTA-NAP-D-Asp-D-Asp

DOTA-phospho-MSH$_{2-9}$

The first amino acid was coupled to the Fmoc-PAL-PEG-PS resin by hand. Fmoc-Trp(Boc)-OH (3 eq) was preactivated with HOBt (3 eq + 15%) for 10 min. Then the mixture was added to a suspension of the Fmoc-deprotected resin, and DIPC (3 eq) was added, and let for reaction overnight. It was then washed 5x with DMF, and completion was checked by a Kaiser test. The sequence Nle-Asp-His-D-Phe-Arg-Trp-NH$_2$ was then synthesized on the peptide synthesizer according to the methods mentioned above. After deprotection of the N-terminal Fmoc protecting group, Fmoc-Tyr(PO(OBzl)-OH)-OH (5 eq) was preactivitated with HOBt (1 eq), and then coupled to the peptide (1 eq peptide on resin) by adding TBTU (1 eq) and DIPEA (15 eq). After an overnight incubation, the reaction was repeated in the same conditions. After cleavage from the Fmoc protecting group, Fmoc-Gly-OH was coupled in the same conditions. Finally, after Fmoc deprotection, DOTA was coupled to the on-resin peptide by preactivating DOTA (3 eq) with HATU (3 eq) for 10 min, then by adding DIPEA (9 eq) to the resin suspension (1 eq peptide) for an overnight reaction. The peptide was then simultaneously cleaved from the resin and deprotected, as was the DOTA moiety, by adding the 90% TFA-mixture for 4 h, and precipitated in ice-cold diethylether. The peptide was finally purified by RP-HPLC (t_R = 16.5 min). Calculated monoisotopic mass: 1558.59 gmol^{-1}; found: 1558.30 gmol^{-1}.

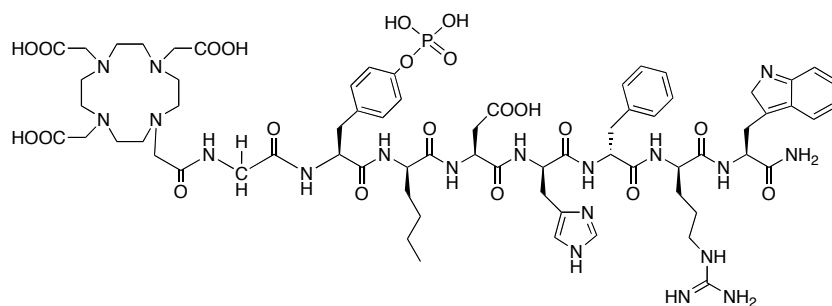**Figure 50: Structure of DOTA-Phospho-MSH$_{2-9}$.**

Radiolabeling of peptides

Labeling with [111]In

Incorporation of ^{111}In into DOTA-peptides was performed by the addition of 55.5 MBq of [111]InCl$_3$ to the DOTA-peptides (10 nmol) that had been dissolved in 54 µl acetate buffer (0.4 M, pH 5) containing 2 mg of gentisic acid. Incubation for 10 min at 95°C allowed completion of the reaction. The radiolabeled DOTA-peptides were then purified on a small reversed-phase cartridge (Sep-Pak C18, Waters) by first washing the column with 0.4 M sodium acetate buffer (pH 7) and then eluting the peptides with ethanol. The purity of the radioligands was assessed by RP-HPLC/γ-detection in the conditions mentioned above. The specific activity of the radioligand was always >7.4 GBq/µmol.

Radioiodination

The Iodogen® (Pierce) method was used for the radioiodination of NDP-MSH. To this end, NDP-MSH (12.14 nmol) was mixed with Na[125]I (37 MBq; Perkin Elmer) in 60 µl phosphate buffer (0.3 M, pH 7.4) in a Iodogen®-precoated tube. After 15 min incubation at room temperature under agitation, the iodination mixture was loaded onto a small reversed-phase cartridge (Sep-Pak C18, Waters), which was washed consecutively with water and acetic acid (0.5 M). Finally, the peptide was eluted with methanol. The collected fractions containing [^{125}I]NDP-MSH were supplemented with dithiothreitol (1.5 mg/mL) and stored at –20°C. Each binding experiment was preceded by an additional purification of the radiotracer by RP-HPLC and subsequent lyophilization from lactose/bovine serum albumin (BSA) (20 mg of each per ml of tracer solution).

Cell culture

The mouse B16-F1 melanoma cell line[101] was cultured in modified Eagle's medium (MEM) containing 10% heat-inactivated fetal calf serum, 2 mmol/L L-glutamine, 1% nonessential amino acids, 1% vitamin solution, 50 IU/mL penicillin and 50 µg/mL streptomycin, in an atmosphere of 95% air/5% CO$_2$ and at a temperature of 37°C. For cell expansion or experiments with isolated cells, the B16-F1 cells were detached with 0.02% EDTA in PBS (phosphate-buffered saline; 150 mM, pH 7.2-7.4). The human HBL melanoma cell line[122] was

cultured in modified RPMI medium supplemented with 10% heat-inactivated fetal calf serum, 2 mM L-glutamine, 50 IU/mL penicillin and 50 μg/mL streptomycin in the same conditions as for B16-F1 cells.

In vitro *binding assay*

Triplicates of 100-μL B16-F1 or HBL cell suspensions adjusted to 4×10^6/mL were incubated in 96-well U-bottom microplates (Falcon 3077). The binding medium consisted of MEM with Earle's salts, 0.2% BSA and 0.3 mM 1,10-phenanthroline. This binding medium was called Mouse Binding Medium (MBM) Triplicates of competitor peptide solution (50 μL), yielding final concentrations ranging from 1×10^{-6} to 1×10^{-12} M, were added. 50,000 cpm [^{125}I]NDP-MSH in 50 μL were finally added to each well. The plates were incubated at 15°C for 3 h for B16-F1 cells and at 37°C for 2 h for HBL cells. The incubation was stopped by covering the plates with ice for 10 min. A cell harvester was used to collect cell-bound radioactivity on filters (Packard Unifilter-96 GF/B). The collected radioactivity was counted on a TopCount scintillation counter (Packard) after addition of 50 μl Microscint-20 scintillation cocktail (Perkin Elmer). The IC$_{50}$ values were calculated with the Prism software (GraphPad Software Inc., San Diego CA, USA).

In vitro *melanin assay*

The biological activity of the α-MSH derivatives was assessed with an *in situ* melanin assay. Briefly, B16-F1 cells (2,500 cells per well in 100 μl) were distributed into 96-well flat-bottom cell culture plates. MEM without phenol red, supplemented with 10% heat-inactivated fetal calf serum, 2 mM L-glutamine, 0.31 mmol/L L-tyrosine, 1% nonessential amino acids, 1% vitamin solution, 50 IU/mL penicillin and 50 μg/mL streptomycin, was used as culture medium. After overnight incubation at cell culture conditions mentioned above, concentrations of α-MSH derivatives ranging from 1×10^{-8} to 1×10^{-12} in 100-μL volumes were added (in 3-fold dilution steps) and the incubation went on for additional 72 h. Melanin production was quantified by determining the absorbance at 310 nm in a microplate reader.

In vitro *internalization assay*

B16-F1 cells were seeded in 6-well plates and incubated overnight in MEM at 37°C. For the internalization experiments, MEM was replaced by 1 mL MBM internalization buffer, consisting of MEM with Earle's salts, 0.2% BSA and 0.3 mM 1,10-phenanthroline. After a 1-h incubation at 37°C, 74 kBq of radioligand (^{111}In-labeled peptides) were added and the plates were incubated for different time periods. Nonspecific internalization was determined by addition of 50 μL of a 1 μM α-MSH solution to the incubation mixture. After the desired incubation times, the cells were extensively washed with MBM kept at 37°C to remove excess radioligand. Incubation in 2 mL ice-cold acid buffer (acetate-buffered Hank's balanced salt solution, pH 5) for 10 min allowed dissociation of surface-bound ligand. After collection of the acid buffer fraction, the cells were rinsed once with cold MBM and the washings were pooled with the acid buffer fraction. The cells were then washed again with MBM kept at 37°C, then lysed in a 1% Triton X-100 solution and finally transferred to tubes for quantification. The radioactivity of all collected fractions was measured in a γ-counter. A counting plate underwent the same treatment as the plate incubated for the longest time, but its cells were detached with 0.02% EDTA in PBS instead of being lysed with the Triton X-100 solution. Cells

from 3 wells were collected, counted, and thus allowed for normalization of the results obtained. Results could be expressed as percent of the added dose per million cells.

Biodistribution and stability of radioligands in B16-F1 tumor-bearing mice

All animal experiments were performed in compliance with Swiss animal welfare regulations. 0.5 million B16-F1 were implanted subcutaneously to female B6D2F1 mice (C57BL/6 × DBA/2F1 hybrids; breeding pairs obtained from IFFA-CREDO, France). 7 days later, 185 kBq of [^{111}In]-labeled ligand in 200 μl PBS/0.1% BSA were injected intravenously into the lateral tail vein of each mouse. Control mice were injected with a mixture of the tracer and 50 μg α-MSH to determine the nonspecific uptake of radioligand. The animals were sacrificed 4, 24 and 48 h *post-injection*. They were dissected and the tissues of interest were collected, rinsed of excess blood and weighed. The radioactivity emitted by each organ was measured in a γ-counter to determine the tissue uptake as percentage of the injected dose per gram of tissue (%ID/g). Total injected counts per animal were determined by extrapolation from counts of a standard collected from the injection solution for each animal. Urine samples were collected at 10, 15, 20 min and 4 h after injection, and kept frozen at -80°C until use. Urine (1 vol) was mixed with methanol (2 vol) to precipitate proteins, and the supernatant was analyzed by RP-HPLC/γ-detection, as described earlier.

Analysis of data

Results are expressed as means ± SEM, unless otherwise stated. Statistical evaluation of the binding assays was performed using the Student's t test. For biodistribution data, each mean value obtained for each organ was compared individually using the Student's t test and the results were corrected by the Bonferroni correction. A P value of <0.05 was considered statistically significant. The area under the curve (AUC) was calculated for the time period of interest (4-48 h) using the Prism software; mean tissue uptake values at each time point were used for this calculation.

RESULTS

Peptide synthesis

The synthesis of DOTA-NAPamide, DOTA-NAP-D-Asp-D-Asp and DOTA-phospho-MSH$_{2-9}$ were performed as described in the Experimental Procedures. DOTA-NAPamide was obtained in >99% purity and in 15% overall yield (after RP-HPLC purification). DOTA-NAP-D-Asp-D-Asp was obtained in >99% purity as well and in 8.3% overall yield. DOTA-phospho-MSH$_{2-9}$ was obtained in >99% purity and in 5.3% overall yield. The expected molecular weights were confirmed by mass spectrometry and are indicated in the Experimental Procedures. The net charges of DOTA-NAP-D-Asp-D-Asp and DOTA-Phospho-MSH$_{2-9}$ at physiological pH are -1, and were calculated on the basis of known pK$_a$ values for amino acid residues and functional groups.

In vitro *receptor binding assay and biologic activity*

The binding affinity of the peptides was assessed by competition binding assays vs. [^{125}I]-NDP-MSH in both the murine B16F1 and the human HBL cell lines. **Table 12** summarizes the IC$_{50}$-values obtained for the tested peptide compared to the values of the native ligand α-MSH and the reference peptide DOTA-NAPamide. DOTA-phospho-MSH$_{2-9}$ displayed affinities in the nanomolar range on both cell lines. Although the IC$_{50}$ obtained for DOTA-phospho-MSH$_{2-9}$ on the B16F1 cell line was slightly lower than that of DOTA-NAPamide, its binding affinity for HBL cells was comparable. DOTA-phospho-MSH$_{2-9}$ displayed a good α-MSH agonist activity (see **Table 12**), as demonstrated by the induction of melanin synthesis by B16F1 cells at a dose matching its IC$_{50}$. On the other side, DOTA-NAP-D-Asp-D-Asp seems to have lost affinity for the receptor through the adopted modifications. Indeed, affinities were between around 10-fold (B16F1) to 100-fold (HBL) lower than those of DOTA-NAPamide. Its biological activity is also around 10-fold lower than the reference peptide.

Table 12: MC1R affinity and biological activity of α-MSH analogs on B16F1 and HBL cells.

α-MSH analogs	B16F1 IC$_{50}$ (nmol/L)[*]	HBL IC$_{50}$ (nmol/L)[*]	rEC$_{50}$ (α-MSH=1)[†]
α-MSH	1.50 ± 0.14	1.91 ± 0.26	1
DOTA-NAPamide	1.38 ± 0.35	3.09 ± 1.11	0.66 ± 0.35
DOTA-NAP-D-Asp-D-Asp	19.7 ± 4.48[‡]	333.9 ± 59.78	7.66 ± 0.33[‡]
DOTA-phospho-MSH$_{2-9}$	2.32 ± 0.80	3.03 ± 0.59	0.85 ± 0.11

---

[*]MC1R affinity of α-MSH analogs was assessed by competition binding experiments with B16F1 or HBL cells and ^{125}I-NDP-MSH as radioligand (*n*=3-16). Data for DOTA-NAPamide are from Bapst et al. (J Recept Signal Transduct Res (2007) **27**, 383-409.

[†]Biological activity of α-MSH analogs was determined in melanin assay with B16F1 cells, and results are expressed as relative concentration inducing half-maximal response (rEC$_{50}$, *n*=3-10) normalized on α-MSH=1.

[‡]*P* < 0.05 vs. DOTA-NAPamide

Internalization

DOTA-NAP-D-Asp-D-Asp and DOTA-phospho-MSH$_{2-9}$ exhibited excellent internalization profiles. Although the plateau phase was not quite reached for the former, probably because of its lower receptor affinity, the plateau phase was almost reached after 2 h already for DOTA-phospho-MSH$_{2-9}$, indicating that nearly the totality of the peptide was internalized. For DOTA-NAP-D-Asp-D-Asp, this inability to reach the plateau phase may be seen as an issue regarding *in vivo* tumor uptake. For DOTA-phospho-MSH$_{2-9}$, the results exclude internalization of the peptide by tumor cells as a potential issue regarding the *in vivo* tumor uptake, and show that MC1R-downregulation was not retarded by the negatively charged ligand.
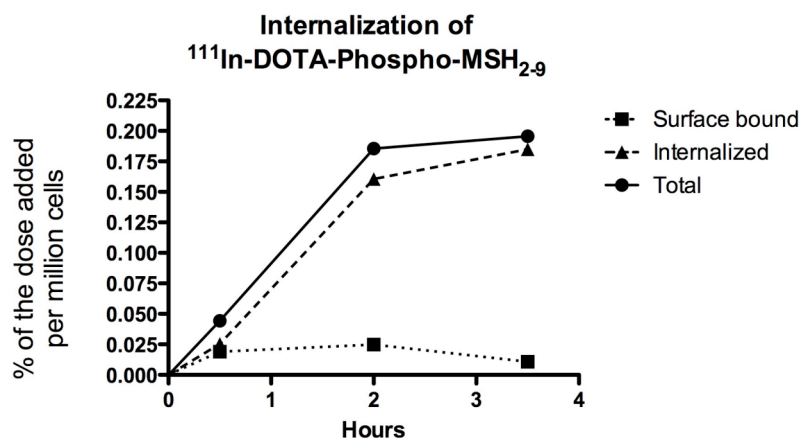
Figure 51: Determination of internalization of DOTA-Phospho-MSH$_{2-9}$ by cultured B16F1 cells.

Biodistribution experiment in tumor-bearing mice

Tissue distributions of the new radiolabeled α-MSH analog and of the reference peptide DOTA-NAPamide are listed in **Table 13**. Tissues, including melanoma tumors, were collected 4 h, 24 h and 48 h after injection of the ^{111}In-labeled analog. Clearance from the blood was fast for both radiopeptides, as almost no radioactivity could be detected after 4 h. DOTA-NAP-D-Asp-D-Asp accumulated in the kidney in a higher extent (25% more) than the reference peptide DOTA-NAPamide, which does not confirm the expected effect of the negative charges. On the other side, the receptor affinity seemed to be lost, as only 1.93 %ID/g accumulated in the tumor 4 h after injection, which is a reduction of 75 % compared to DOTA-NAPamide. Other organs did not accumulate the radioactive tracer at all.

The other peptide studied displayed much more promising data. After 4 h, DOTA-Phospho-MSH$_{2-9}$ accumulated in the tumor to a lesser extent than DOTA-NAPamide did (6.12 ± 0.44 %ID/g vs. 7.77 ± 0.35 %ID/g). This 1.27-fold lower accumulation was compensated for by a much lower uptake of radioactivity by the kidney (2.98 ± 0.20 %ID/g vs. 4.77 ± 0.26 %ID/g), representing a 1.6-fold reduction, and producing the highest tumor-to-kidney ratio at 4 h (2.05) ever observed for a linear peptide. The non-specific uptake by other organs remained comparable to the data obtained for DOTA-NAPamide, thus excluding a switch in the excretion way. Coinjection of 50 μg of α-MSH confirmed that melanoma uptake was an MC1R-mediated process for the α-MSH analog, as it was significantly reduced. An average retention was observed in the tumor, as only 40% of the radioactivity measured after 4 h was found after 24 h, and 17% after 48 h. On the other side, clearance from the kidney appeared to be a slower process. Indeed, 70% and 39% of the radioactivity measured after 4 h were still measured after 24 h and 48 h, respectively. Nevertheless, the difference in uptake observed after 4 h, as can be seen in **Figure 52**, was sufficient to deliver a tumor-to-kidney ratio calculated from the AUC (4-48 h) of 1.42 (**Figure 53**), which is the best ratio observed for a linear radiolabeled α-MSH analog to date. Indeed, DOTA-NAPamide, which was considered as the best linear α-MSH analog, bears a tumor-to-kidney ratio of the AUC (4-48h) of 1.11. Thus, the ratio exhibited by DOTA-phospho-MSH$_{2-9}$ is 28% better than the reference peptide.

Table 13: Tissue distribution, including melanoma tumor, of the negatively charged ^{111}In-labeled α-MSH analogs and DOTA-NAPamide 4, 24 and 48h after injection, expressed in %ID/g of tissue.

Organ	Time (h)	%ID/g of tissue[†]		
		DOTA-NAPamide	DOTA-Phospho-MSH$_{2-9}$	DOTA-NAP-DAsp-DAsp
Blood	4	0.09 ± 0.02	0.02 ± 0.00	0.01 ± 0.00[‡]
	24	0.02 ± 0.00	0.01 ± 0.00	0.01 ± 0.00
	48	0.00 ± 0.00	0.00 ± 0.00	0.01 ± 0.00
Tumor	4	7.77 ± 0.35	6.12 ± 0.44	1.93 ± 0.11[‡]
	24	2.32 ± 0.15	2.42 ± 0.10	0.63 ± 0.03[‡]
	48	1.41 ± 0.12	1.06 ± 0.13	0.23 ± 0.02[‡]
Stomach	4	0.09 ± 0.01	0.17 ± 0.08	0.11 ± 0.02
	24	0.12 ± 0.02	0.16 ± 0.02	0.03 ± 0.00[‡]
	48	0.11 ± 0.05	0.07 ± 0.00	0.02 ± 0.00
Kidney	4	4.77 ± 0.26	2.98 ± 0.20[‡]	5.95 ± 0.85
	24	2.41 ± 0.20	2.09 ± 0.13	4.09 ± 0.16
	48	1.55 ± 0.07	1.16 ± 0.08	2.02 ± 0.08
Liver	4	0.34 ± 0.05	0.20 ± 0.01	0.10 ± 0.00[‡]
	24	0.31 ± 0.02	0.16 ± 0.02[‡]	0.09 ± 0.00[‡]
	48	0.27 ± 0.02	0.12 ± 0.01[‡]	0.07 ± 0.00[‡]
Spleen	4	0.14 ± 0.01	0.11 ± 0.01	0.07 ± 0.00[‡]
	24	0.11 ± 0.01	0.10 ± 0.01	0.07 ± 0.00[‡]
	48	0.10 ± 0.01	0.09 ± 0.01	0.07 ± 0.00
Lung	4	0.08 ± 0.01	0.07 ± 0.02	0.06 ± 0.00
	24	0.05 ± 0.01	0.04 ± 0.00	0.04 ± 0.00
	48	0.03 ± 0.00	0.03 ± 0.00	0.03 ± 0.00
Small Intestine	4	0.07 ± 0.01	0.11 ± 0.03	0.05 ±0.01
	24	0.08 ± 0.01	0.06 ± 0.00	0.04 ± 0.01
	48	0.05 ± 0.01	0.06 ± 0.00	0.03 ± 0.00
Pancreas	4	0.04 ± 0.00	0.05 ± 0.01	0.03 ± 0.00
	24	0.03 ± 0.00	0.03 ± 0.00	0.02 ± 0.00
	48	0.02 ± 0.00	0.03 ± 0.00	0.03 ± 0.00
Heart	4	0.05 ±0.01	0.04 ± 0.00	0.03 ± 0.00
	24	0.03 ± 0.00	0.03 ± 0.00	0.03 ± 0.00
	48	0.01 ± 0.00	0.03 ± 0.00[‡]	0.03 ± 0.00[‡]
Bone	4	0.11 ± 0.02	0.08 ± 0.01	0.07 ± 0.01
	24	0.14 ± 0.02	0.11 ± 0.02	0.06 ± 0.01[‡]
	48	0.05 ± 0.01	0.06 ± 0.01	0.07 ± 0.01
Muscle	4	0.05 ± 0.01	0.02 ± 0.00	0.02 ± 0.00
	24	0.02 ± 0.00	0.02 ± 0.00	0.02 ± 0.00
	48	0.01 ± 0.00	0.02 ± 0.00[‡]	0.03 ± 0.00[‡]
Skin	4	-	0.12 ± 0.03	0.06 ± 0.01
	24	-	0.07 ± 0.02	0.06 ± 0.00
	48	-	0.08 ± 0.02	0.04 ± 0.00[‡]

* Data for DOTA-NAPamide from Froidevaux et al., J Nucl Med (2005) 46, 887-895.

[†] Tissue radioactivity is expressed as means ± SEM (*n*=4-12).
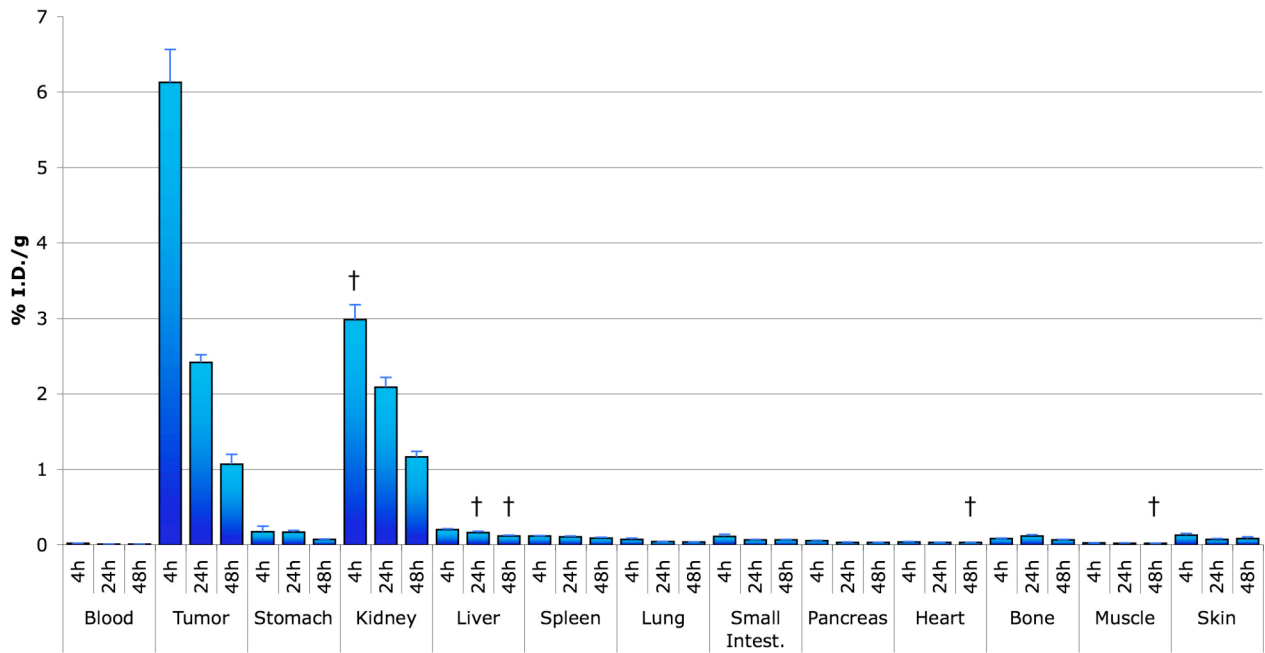
[‡] *P* < 0.05 vs. DOTA-NAPamide.

Figure 52: Tissue distrubution of ^{111}In-labeled DOTA-phospho-MSH$_{2\text{-}9}$ at 4h, 24h and 48h after injection. Results expressed in %ID/g of tissue (means ± SEM), †P<0.05 vs. ^{111}In-DOTA-NAPamide.
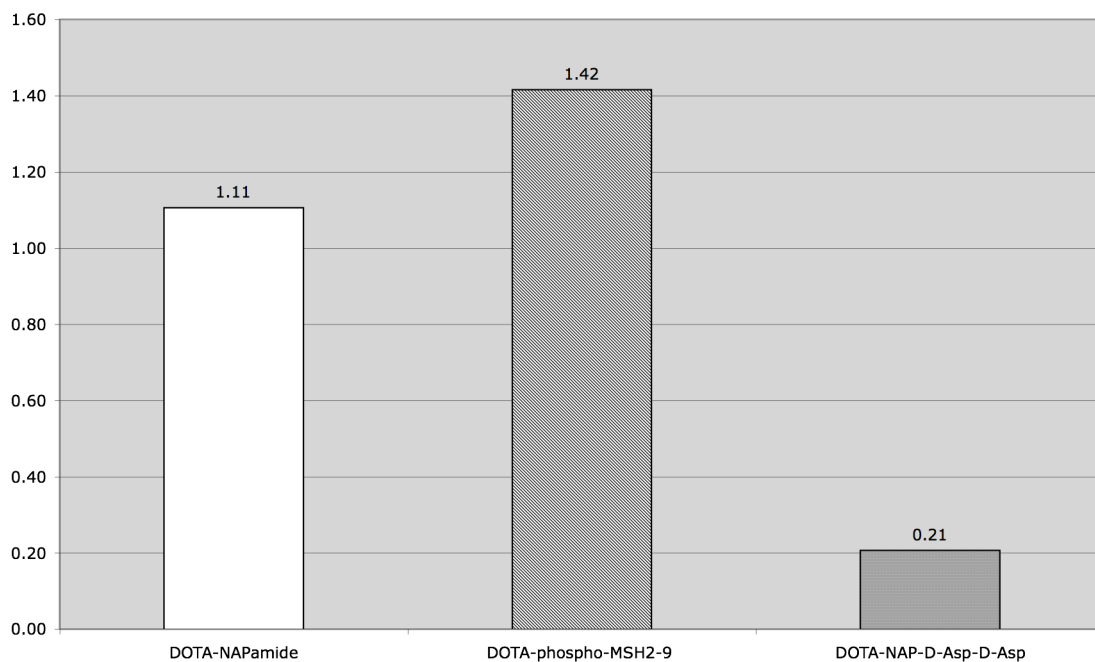
Figure 53: Tumor-to-kidney ratios of ^{111}In-labeled DOTA-phospho-MSH$_{2\text{-}9}$ compared to ^{111}In-labeled DOTA-NAPamide, calculated from the AUC (4-48h).

DISCUSSION

The main goals in the development of new radiolabeled receptor-targeted peptides for applications in nuclear oncology are the maximization of tumor targeting and the minimization of nonreceptor-mediated accumulation. Radiolabeled α-MSH analogs suffer from a high uptake by the kidneys, the main organs responsible for its excretion. In the last years, several studies have shown that the attempts to increase the uptake of radiolabeled α-MSH analogs by the tumor may have reached its limits[25,59,60,110,114,115,203,209]. Therefore, reduction of their kidney uptake has become a crucial step in the further development of these potential tools for melanoma diagnosis and therapy.

Physicochemical properties of the radioactive tracers are determinant for their uptake in excretory organs. Net charge, particularly, seems to have a dramatic impact on the *in vivo* behavior of targeting peptides[7,67,168,181]. Indeed, it has been shown that the surface of tubular cells is negatively charged, involving repulsing electrostatic effects with negatively charged molecules in the luminal part of the proximal tubules[33,78]. Additional observations that coinjection of solutions of basic amino acids such as Lys or Arg significantly reduced the uptake of radiopeptides by the kidney contributed to this theory[114,256]. Indeed, it has been assumed that positively charged amino acids compete with peptides for the charge-dependent uptake by renal tubular cells.

Earlier peptides with a global negative charge were studied in our group and delivered no satisfactory results regarding *in vivo* behavior[115]. One of these peptides carried a succinimidyl group at the C-terminal end of the sequence, and had a global net charge of -1 as well. It delivered a slightly lower kidney uptake than the reference peptide DOTA-NAPamide, but lost its affinity for the tumor *in vivo*. This result, which was in contradiction with the earlier findings mentioned above, suggested that charge localization might be an essential parameter in the quest of improved biodistribution profiles.

The first derivative synthesized during this study bore a -D-Asp-D-Asp ending at its C-terminal end, in order to assess the effect of negative charges at the C-terminus with a peptide more robust than the previously mentioned succinimidyl derivative. The aim of this strategy was to enhance kidney excretion of the Lys(DOTA)-NH$_2$ moiety, presumably a main radioactive metabolite (unpublished observations), by attaching two negative charges supposed to have a repulsive electrostatic interaction with the negatively-charged tubular cells. Receptor affinity was quite poor on both human and murine cells, and these findings were confirmed by biodistribution data. The peptide apparently loses its receptor affinity both *in vitro* and *in vivo* through its modifications. *In vitro*, binding affinities were 10- to 100-fold lower than the reference peptide DOTA-NAP-amide on B16F1 or HBL cells, respectively. *In vivo*, the expected reduction of the kidney uptake could not be observed. Kidney uptake was even slightly higher than that of the reference peptide. Additionally, as expected from the *in vitro* data, tumor uptake was drastically reduced to reach only about one fourth of that of the reference.

To determine the influence of the position of the negative charge, a phosphotyrosine residue was introduced in the sequence in second position, towards the N-terminal end, providing the peptide with a

global net charge of -1. This alteration involved a slight decrease in MC1R affinity (1.68-fold worse than DOTA-NAPamide) in B16F1 cells, but surprisingly did not affect affinity in HBL cells. The position of the additional negative charge was definitely crucial for the pharmacokinetic behavior of α-MSH analogs, as the newly synthesized DOTA-phospho-MSH$_{2-9}$ delivered a significant reduction of the kidney uptake at 4 h (1.6-fold lower than DOTA-NAPamide), without extensively affecting its tumor uptake. This positive impact of the negative charge was reported on the tumor-to-kidney ratio of the AUC (4-48 h), exhibiting a ratio of 1.42, which is 28% better than that of DOTA-NAPamide.

In conclusion, the reduction and above all the adequate positioning of the net charge of peptides has a significant impact on their pharmacokinetics. The influence of this factor on accumulation in MC1R-expressing cells and tissues, however, was not substantial. The *in vitro* affinity of the peptide corresponded to that of DOTA-NAPamide, although slightly lower. This was proven by the biodistribution data, which displayed an average uptake of the negatively charged peptide by the tumor. On the other side, the adequate position of the negative charge on DOTA-Phospho-MSH$_{2-9}$ certainly contributed to the reduction of its renal accumulation. Therefore, it constitutes now the best linear radiolabeled α-MSH analog and the very promising properties it exhibited will certainly be a strong base for further developments in this direction.

6 General discussion and conclusion

During the last two decades, different approaches have been used in an attempt to target melanoma tumor cells. Radiolabeled peptide α-MSH analogs represent one of these approaches and have shown attractive targeting properties. Indeed, on one hand *in vitro* binding affinities on both murine and human cell lines have generally been good and have reached excellence in the last years with IC_{50}s in the (sub-)nanomolar range, which is, *per se*, striking in the world of pharmaceutical drugs. On the other hand, their targeting properties *in vivo* have also improved dramatically, especially in the last decade. Their usefulness has been proven for the targeting of melanoma tumors in pharmacokinetic studies on mice, with interesting tumor-to-non-target-tissue ratios. However, they suffer from a major drawback: their kidney uptake and retention remain relatively high compared to their tumor uptake. Attempts have been made to either increase their uptake by the tumor, or to reduce their uptake by the kidney. Some major advances (replacement of Phe[7] by D-Phe[7], replacement of Met[4] by Nle[4], positioning of DOTA on Lys[11] side chain, etc.) have led to more favorable pharmacokinetical profiles. But if DOTA-NAPamide displays one of the best tumor-to-kidney ratios to date, its profile is still far from satisfying the criteria required for melanoma diagnosis or therapy in humans. Its kidney uptake remains too high, and thus could mask the diagnosis of distant metastases in the renal region, and could irremediably damage the kidney with the higher doses and more harmful radionuclides needed for therapy. Further modifications (localized net charge, cyclization, etc.) have not solved the kidney issue.

The present work was undertaken to determine if new modifications might improve the pharmacokinetical profile of α-MSH analogs. The three major approaches mentioned earlier in this thesis were investigated in a systematical way. First, the derivatives were synthesized, purified and characterized. Then, they were tested *in vitro* against [^{125}I]-NDP-MSH, the well-known high-potency agonist of α-MSH for the MC1R, in competitive binding assays on both murine B16F1 and human HBL cells. They were also tested in cell internalization assays as ^{111}In-labeled peptides, and finally for their biological (melanogenic) activity in melanin assays. The pharmacokinetical profile of the α-MSH analogs was then assessed in *in vivo* biodistribution experiments using melanoma bearing mice.

Firstly, dimeric derivatives were investigated. As mentioned, the idea behind this strategy was to increase the concentration of the binding motif in the vicinity of the receptor in order to ultimately improve the tumor uptake of the peptides *in vivo*. The expected effect could be observed *in vitro* in competitive binding assays, as the binding affinities (IC_{50}) were between 1.75 and 3.37-fold better (murine cells, depending on the peptide) or even 6-fold better (human cells) than those of DOTA-NAPamide, the peptide used for comparison. The biological activity assays (EC_{50}) revealed very similar profiles to DOTA-NAPamide, and internalization assays displayed similarly fast and almost complete uptake of the peptides by the cells.

On the other hand, their *in vivo* pharmacokinetic profiles did not match the encouraging results obtained *in vitro*. Indeed, their kidney uptake dramatically increased to reach values between 25 and 35%ID/g of tissue at 4 h (4.77%ID/g for DOTA-NAPamide). What happened to these peptides in the kidney remains unclear. It may not depend on the position of the chelate, as suggested earlier to inspire the synthesis of the derivative carrying the -Gly-Lys(DOTA) extension, as all three peptides carried the DOTA-moiety at a different position along their sequences and all three displayed the same kind of biodistribution profile. Additionally, the expected effect of dimerization (increasing the number of binding motifs in the vicinity of the target receptor) on tumor uptake was not observed *in vivo*, in contrast to the binding affinities found *in vitro*. Although the tumor uptake of DOTA-diHexa(CN-NC)-amide was quite high (9.08%ID/g), kidney uptake abolished all its benefits. The other two dimeric peptides displayed much lower tumor uptakes than DOTA-NAPamide.

Although new modifications could be adopted, such as variation of the net charge of the peptide or its position along the sequence, insertion of unnatural amino acids in the sequence or synthesis of oligomers for example, it still appears that dimeric derivatives are not the method of choice to improve tumor-to-kidney ratios of radiolabeled α-MSH analogs. Owing to their high receptor affinity, however, they may be useful in pretargeting strategies. Indeed, pretargeting involves the separation of the localization of the tumor, with an anticancer antibody for example, from the subsequent delivery of the imaging or therapeutic radionuclide by peptide haptens. With their excellent binding affinities, the studied dimeric derivatives could serve as "carriers" (for instance, instead of bsMAb (bispecific antibodies) typically used in pretargeting strategies) for other binding motifs, themselves becoming targets for (preferably) bivalent radiolabeled haptens. With pretargeting strategies using bsMAb, tumor-to-non-target-tissue ratios could be dramatically improved. Goldenberg et al. observed much faster blood clearance and measured tumor/blood and tissue ratios often ≥10:1 within 1 h of the radionuclide injection[128]. It is thus reasonable to think that an adaptation of the bsMAb-method to dimeric α-MSH analogs could enhance their pharmacokinetical profiles as well. This approach would be rather complex and time-consuming, but would probably be worth an attempt.

Secondly, glycated derivatives were synthesized and tested. The purpose of glycation was to increase kidney excretion of the radiolabeled peptides thanks to an enhanced hydrophilicity, without reducing their affinity for tumor cells. In *in vitro* competitive binding assays, it was observed that receptor affinity was conserved, with slight variations, compared to the reference peptide DOTA-NAPamide. Indeed, receptor-binding affinities (IC_{50}s) ranged from around 2-fold lower to 3-fold better than the reference peptide (with just one peptide, DOTA-N-NAPamide-Glc, bearing a 3.3-fold lower affinity). It is noteworthy that all glycopeptides displayed competitive binding affinities in the low nanomolar range, thus confirming that glycation does not affect receptor affinity sufficiently to impair binding.

Two main trends were observed in their *in vivo* pharmacokinetical profiles. Glycation at the C-terminal end increased the kidney uptake and above all the retention time (around 100% of the 4 h-values still present after 24h), although tumor uptake and retention remained quite comparable (slightly lower) to those of DOTA-NAPamide. Side-chain glycated peptides displayed similar profiles, with enhanced kidney uptake

and lower tumor uptake than the reference peptide. No extension of the retention time was observed in the kidney for these peptides.

Peptides glycated at their N-terminal end exhibited more interesting profiles. Indeed, although DOTA-Glc-NAPamide displayed a weaker profile (lower tumor uptake and similar uptake in the kidney as in the tumor), DOTA-Mtr-NAPamide and especially DOTA-Gal-NAPamide grabbed our attention. Their profiles were very comparable to the reference DOTA-NAPamide, displaying high tumor uptakes and low kidney uptakes. Analysis of their tumor-to-kidney ratio of the AUC (4-48h) showed all their potential: if DOTA-Mtr-NAPamide was slightly weaker than DOTA-NAPamide (ratio of 0.99 vs. 1.11), DOTA-Gal-NAPamide exhibited a better ratio than the reference, with 1.34. This result, together with the overall analysis of the glycopeptides class, shows that N-terminal glycation is most likely more favorable than glycation at other positions, and that the introduction of a galactose moiety is advantageous over other carbohydrate moieties. From another point of view, this study also confirms previous reports[102,103,237,273,281,301,303,323,324] about the influence that carbohydration can have on pharmacokinetics of peptides. Indeed, dramatic variations were observed, depending on the type of carbohydrate used or its position. Small modifications such as the replacement of a glucose moiety by a galactose readily produce striking effects. The number of potential variations would be infinite, and the lack of methods to precisely forecast the efficiency of new molecules makes the testing of all possibilities unfeasible. Indeed, it was observed in this work that e.g. the results of competitive binding assays did not necessarily correlate with the *in vivo* pharmacokinetical profile of the molecules tested. Additionally, it is ethically and technically definitely not conceivable to test a very large panel of molecules (e.g. synthesized by HTS) in animal experiments. Therefore, the future of glycopeptides should be envisaged with slight modifications of the existing promising peptides, i.e. preferably DOTA-Gal-NAPamide. As the introduction of negative charges in the sequence exhibited very positive effects (see DOTA-phospho-MSH$_{2-9}$), it would be interesting to determine if a synergy between the two methods could be exploited. An attractive candidate would be, for example, a derivative of DOTA-Gal-NAPamide carrying the phosphate group of DOTA-phospho-MSH$_{2-9}$, to investigate if the effect of both modifications on pharmacokinetics is additive.

Further investigations on the effect obtained by attachment of various chemical entities would also be necessary to draw conclusions about structure-activity relationship parameters of radiolabeled α-MSH analogs. It would be interesting to observe the consequences of the substitution of a rather hydrophilic carbohydrate moiety by a lipophilic phenyl or benzyl group, for example. Is the positive effect of galactose in DOTA-Gal-NAPamide only due to the presence at its N-terminus of a sugar and its hydroxyl groups, or could another sterically bulky functional group display the same positive influence on the pharmacokinetic properties of the peptide? A tremendous number of derivations is theoretically mentioned before, it would of course definitively not be possible to test all options, but some preliminary experiments in this direction would certainly be of interest.

Thirdly, two negatively charged peptides were synthesized. The reason for the adoption of this strategy was to enhance kidney excretion of the peptide, thanks to repulsive electrostatic forces between negatively

charged peptides and the negative charges present at the surface of tubular cells, resulting in an enhanced excretion of the tracers in the primary urine and a potential reduction of the kidney uptake. Earlier developments in our group studied the impact of a negative charge localized at the C-terminal end of the peptide, but yielded insufficient biodistribution data. In the peptides tested earlier in our group, the chelate was placed at their N-terminal end. A new peptide was tested that bore the chelate as well as two negatively-charged D-Asp at its C-terminal end, in order to increase kidney excretion of a potential Lys(DOTA)-NH$_2$ metabolite observed previously (unpublished data). While its kidney uptake could not be reduced by this modification, the peptide also lost its affinity to the receptor and displayed a poor tumor uptake *in vivo*. It was suspected that localization of the negative charge was indeed a crucial parameter. Another peptide carrying a phosphotyrosine residue (negatively charged at physiological pH) towards its N-terminus was evaluated. *In vitro* experiments exhibited slightly lower MC1R affinity of DOTA-phospho-MSH$_{2-9}$ than the reference peptide DOTA-NAPamide in murine cells (though still lying in the nanomolar range), but unexpectedly an affinity similar to the reference peptide in human cells. Internalization data showed very good results, with the peptide being almost totally internalized after 2 h. The biodistribution experiment with ^{111}In-labeled DOTA-phospho-MSH$_{2-9}$ displayed very promising results. Indeed, although the tumor uptake was not as high as for some of the peptides (6.12 ± 0.44 vs. 8.30 ± 1.22 for DOTA-Gal-NAPamide), the kidney uptake was much lower (2.98 ± 0.20 vs. 4.43 ± 0.34 for DOTA-Gal-NAPamide), producing a very interesting tumor-to-kidney ratio of the AUC (4-48 h) of 1.42 (1.34 for DOTA-Gal-NAPamide and 1.11 for DOTA-NAPamide). These results really confirmed findings from other groups about the promising effect of negative charges on the pharmacokinetic behavior of such molecules[7,33,67,168,181]. Therefore, it would be relevant to study this approach further, using a systematic modification of the quantity of negative charges and their position along the peptide sequence in order to determine structure-activity relationships. As mentioned in the previous paragraph, introduction of an additional negative charge towards the N-terminus of DOTA-Gal-NAPamide would certainly represent one of the next logical steps in this quest, with regard to combining the results obtained with the two strategies.

We are aware that our studies encompassed a limited panel of derivatives from each type of radiopeptide. The lack of adequate automated cellular assays unfortunately does not allow the development of high-throughput screening methods, and is therefore a limiting factor for the study of further analogs bearing systematic structural modifications. Indeed, as small differences in e.g. the type of sugar coupled to the peptide or the position of a negative charge had such strong influences, testing of a large number of molecules would be necessary. In addition, it was observed that *in vitro* binding affinities were not predictive for the *in vivo* behavior of the peptides, making the step to biodistribution experiments almost mandatory. Nevertheless, some major trends could be observed among the peptides or peptide types developed in this work, providing valuable information for the elucidation of some structural requirements of α-MSH derivatives. These may help to focus upcoming research on precise structural features for further developments in this field. As mentioned, combination of negative charges and sugar moieties may have a synergistic or additive impact on pharmacokinetics. Introduction of more negative charges may contribute to the renal excretion of the radiopharmaceuticals. Replacement of carbohydrates by other non-amino acid functional groups, or new derivatives bearing more non-natural amino acid residues may improve the *in*

vivo behavior of radiolabeled α-MSH analogs. The use of NOTAGA as chelate could constitute another interesting alternative for the improvement of the pharmacokinetical behavior of α-MSH analogs. As mentioned earlier, NOTAGA-coupled peptides such as Tyr[3]-octreotide exhibited enhanced uptake in target tissues and a faster excretion, probably owing to the spacer function of one of its "arms".

The future of α-MSH analogs is still open for optimization and innovations. Future work will certainly have to concentrate on minor modifications, as many investigations about major requirements have been achieved to date. This work hopefully laid a further milestone by investigating some classes of modifications in depth. Their fine-tuning will certainly give birth to new candidates with improved pharmacokinetic profiles and, optimistically, to the valuable diagnostic and therapeutic tools urgently needed in the clinic.

7 References

[1] *Arzneimittel-Kompendium der Schweiz*. (Documed, Basel, 2007).

[2] Abdel-Malek Z., Scott M.C., Suzuki I. et al., The melanocortin-1 receptor is a key regulator of human cutaneous pigmentation, *Pigment cell research / sponsored by the European Society for Pigment Cell Research and the International Pigment Cell Society* **13 Suppl 8** (2000), 156-162.

[3] ACS, American Cancer Society, available at www.cancer.org, 2007.

[4] Adan R.A., Constitutive receptor activity series: endogenous inverse agonists and constitutive receptor activity in the melanocortin system, *Trends in pharmacological sciences* **27** (2006), 183-186.

[5] Agorio C., Schreiber F., Sheppard M. et al., Live attenuated Salmonella as a vector for oral cytokine gene therapy in melanoma, *The journal of gene medicine* **9** (2007), 416-423.

[6] AJCC, American Joint Committee on Cancer, available at http://www.cancerstaging.org, 2007.

[7] Akizawa H., Arano Y., Mifune M. et al., Effect of molecular charges on renal uptake of 111In-DTPA-conjugated peptides, *Nucl Med Biol* **28** (2001), 761-768.

[8] Al-Nahhas A.A., Jafri R.A., Britton K.E. et al., Clinical experience with 99mTc-MAG3, mercaptoacetyltriglycine, and a comparison with 99mTc-DTPA, *Eur J Nucl Med* **14** (1988), 453-462.

[9] Al-Obeidi F., Castrucci A.M., Hadley M.E. et al., Potent and prolonged acting cyclic lactam analogues of alpha-melanotropin: design based on molecular dynamics, *J Med Chem* **32** (1989), 2555-2561.

[10] Al-Obeidi F., Hruby V.J., Hadley M.E. et al., Design, synthesis, and biological activities of a potent and selective alpha-melanotropin antagonist, *Int J Pept Protein Res* **35** (1990), 228-234.

[11] Albert R., Marbach P., Bauer W. et al., SDZ CO 611: a highly potent glycated analog of somatostatin with improved oral activity, *Life Sci* **53** (1993), 517-525.

[12] Ames J.M., Applications of the Maillard reaction in the food industry, *Food Chemistry* **62** (1998), 431-439.

[13] Anderson C.J., Pajeau T.S., Edwards W.B. et al., In vitro and in vivo evaluation of copper-64-octreotide conjugates, *J Nucl Med* **36** (1995), 2315-2325.

[14] Antman K.H., Eilber F.R., and Shiu M.H., Soft tissue sarcomas: current trends in diagnosis and management, *Current problems in cancer* **13** (1989), 337-367.

[15] Arap M.A., Phage display technology - Applications and innovations, *Genetics and Molecular Biology* **28** (2005), 1-9.

[16] Arya P., Barkley A., and Randell K.D., Automated high-throughput synthesis of artificial glycopeptides. Small-molecule probes for chemical glycobiology, *J Comb Chem* **4** (2002), 193-198.

[17] Asa S.L. and Ezzat S., The pathogenesis of pituitary tumours, *Nat Rev Cancer* **2** (2002), 836-849.

[18] Atherton E. and Sheppard R.C., *Solid Phase Synthesis: a Practical Approach.* (Oxford: IRL Press, 1989).

[19] Bagutti C., Stolz B., Albert R. et al., [111In]DTPA-labeled analogues of alpha-MSH for the detection of MSH receptors in vitro and in vivo, *Ann N Y Acad Sci* **680** (1993), 445-447.

[20] Bagutti C., Stolz B., Albert R. et al., [111In]-DTPA-labeled analogues of alpha-melanocyte-stimulating hormone for melanoma targeting: receptor binding in vitro and in vivo, *Int J Cancer* **58** (1994), 749-755.

[21] Bagutti C., Oestreicher M., Siegrist W. et al., alpha-MSH receptor autoradiography on mouse and human melanoma tissue sections and biopsies, *J Recept Signal Transduct Res* **15** (1995), 427-442.

22   Bakker W.H., Albert R., Bruns C. et al., [111In-DTPA-D-Phe1]-octreotide, a potential radiopharmaceutical for imaging of somatostatin receptor-positive tumors: synthesis, radiolabeling and in vitro validation, *Life Sci* **49** (1991), 1583-1591.

23   Bakker W.H., Krenning E.P., Breeman W.A. et al., In vivo use of a radioiodinated somatostatin analogue: dynamics, metabolism, and binding to somatostatin receptor-positive tumors in man, *J Nucl Med* **32** (1991), 1184-1189.

24   Balch C.M., Soong S.J., Gershenwald J.E. et al., Prognostic factors analysis of 17,600 melanoma patients: validation of the American Joint Committee on Cancer melanoma staging system, *J Clin Oncol* **19** (2001), 3622-3634.

25   Bapst J.P., Froidevaux S., Calame M. et al., Dimeric DOTA-alpha-Melanocyte-Stimulating Hormone Analogs: Synthesis and In Vivo Characteristics of Radiopeptides with High In Vitro Activity, *J Recept Signal Transduct Res* **27** (2007), 383-409.

26   Barrett G.C. and Elmore D.T., *Amino Acids and Peptides*. (Cambridge University Press, Cambridge, 2004).

27   Barsh G.S., Pigmentation, pleiotropy, and genetic pathways in humans and mice, *American journal of human genetics* **57** (1995), 743-747.

28   Barsh G.S., The genetics of pigmentation: from fancy genes to complex traits, *Trends Genet* **12** (1996), 299-305.

29   Becker J.C., Kirkwood J.M., Agarwala S.S. et al., Molecularly targeted therapy for melanoma: current reality and future options, *Cancer* **107** (2006), 2317-2327.

30   Behr T.M., Sharkey R.M., Juweid M.E. et al., Reduction of the renal uptake of radiolabeled monoclonal antibody fragments by cationic amino acids and their derivatives, *Cancer Res* **55** (1995), 3825-3834.

31   Behr T.M., Becker W.S., Sharkey R.M. et al., Reduction of renal uptake of monoclonal antibody fragments by amino acid infusion, *J Nucl Med* **37** (1996), 829-833.

32   Behr T.M. and Goldenberg D.M., Improved prospects for cancer therapy with radiolabeled antibody fragments and peptides?, *J Nucl Med* **37** (1996), 834-836.

33   Behr T.M., Goldenberg D.M., and Becker W., Reducing the renal uptake of radiolabeled antibody fragments and peptides for diagnosis and therapy: present status, future prospects and limitations, *Eur J Nucl Med* **25** (1998), 201-212.

34   Bernard B.F., Krenning E.P., Breeman W.A. et al., D-lysine reduction of indium-111 octreotide and yttrium-90 octreotide renal uptake, *J Nucl Med* **38** (1997), 1929-1933.

35   Bertolotto C., Bille K., Ortonne J.P. et al., Regulation of tyrosinase gene expression by cAMP in B16 melanoma cells involves two CATGTG motifs surrounding the TATA box: implication of the microphthalmia gene product, *The Journal of cell biology* **134** (1996), 747-755.

36   Bhardwaj R., Becher E., Mahnke K. et al., Evidence for the differential expression of the functional alpha-melanocyte-stimulating hormone receptor MC-1 on human monocytes, *J Immunol* **158** (1997), 3378-3384.

37   Bodei L., Cremonesi M., Zoboli S. et al., Receptor-mediated radionuclide therapy with 90Y-DOTATOC in association with amino acid infusion: a phase I study, *Eur J Nucl Med Mol Imaging* **30** (2003), 207-216.

38   Bodei L., Cremonesi M., Grana C. et al., Receptor radionuclide therapy with 90Y-[DOTA]0-Tyr3-octreotide (90Y-DOTATOC) in neuroendocrine tumours, *Eur J Nucl Med Mol Imaging* **31** (2004), 1038-1046.

39   Boerman O.C., Oyen W.J., and Corstens F.H., Between the Scylla and Charybdis of peptide radionuclide therapy: hitting the tumor and saving the kidney, *Eur J Nucl Med* **28** (2001), 1447-1449.

40   Bohm M., Schiller M., Stander S. et al., Evidence for expression of melanocortin-1 receptor in human sebocytes in vitro and in situ, *The Journal of investigative dermatology* **118** (2002), 533-539.

41   Bohm M., Eickelmann M., Li Z. et al., Detection of functionally active melanocortin receptors and evidence for an immunoregulatory activity of alpha-melanocyte-stimulating hormone in human dermal papilla cells, *Endocrinology* **146** (2005), 4635-4646.

42   Bohm M., Luger T.A., Tobin D.J. et al., Melanocortin receptor ligands: new horizons for skin biology and clinical dermatology, *The Journal of investigative dermatology* **126** (2006), 1966-1975.

43   Boissy R.E., Sakai C., Zhao H. et al., Human tyrosinase related protein-1 (TRP-1) does not function as a DHICA oxidase activity in contrast to murine TRP-1, *Experimental dermatology* **7** (1998), 198-204.

44   Bolognia J.L. and Pawelek J.M., Biology of hypopigmentation, *Journal of the American Academy of Dermatology* **19** (1988), 217-255.

45   Bolognia J.L., Jorizzo J.L., and Rapini R.P., *Dermatology*. (Mosby, St. Louis, 2003).

46   Breeman W.A., De Jong M., Visser T.J. et al., Optimising conditions for radiolabelling of DOTA-peptides with 90Y, 111In and 177Lu at high specific activities, *Eur J Nucl Med Mol Imaging* **30** (2003), 917-920.

47   Breslow A., Prognostic factors in the treatment of cutaneous melanoma, *Journal of cutaneous pathology* **6** (1979), 208-212.

48   Britz-Cunningham S.H. and Adelstein S.J., Molecular targeting with radionuclides: state of the science, *J Nucl Med* **44** (2003), 1945-1961.

49   Bruns C., Stolz B., Albert R. et al., OctreoScan 111 for imaging of a somatostatin receptor-positive islet cell tumor in rat, *Horm Metab Res Suppl* **27** (1993), 5-11.

50   Burchill S.A., Thody A.J., and Ito S., Melanocyte-stimulating hormone, tyrosinase activity and the regulation of eumelanogenesis and phaeomelanogenesis in the hair follicular melanocytes of the mouse, *The Journal of endocrinology* **109** (1986), 15-21.

51   Busca R., Bertolotto C., Ortonne J.P. et al., Inhibition of the phosphatidylinositol 3-kinase/p70(S6)-kinase pathway induces B16 melanoma cell differentiation, *J Biol Chem* **271** (1996), 31824-31830.

52   Busca R. and Ballotti R., Cyclic AMP a key messenger in the regulation of skin pigmentation, *Pigment cell research / sponsored by the European Society for Pigment Cell Research and the International Pigment Cell Society* **13** (2000), 60-69.

53   Carpino L.A., 1-Hydroxy-7-azabenzotriazole. An Efficient Peptide Coupling Additive, *J Am Chem Soc* **115** (1993), 4397-4398.

54   Castells A. and Rustgi A.K., Tumor Invasion and Metastasis, in *Gastrointestinal Cancers*, edited by A.K. Rustgi and J.M. Crawford (WB Saunders, 2003).

55   Chambers A.F., The metastatic process: basic research and clinical implications, *Oncology research* **11** (1999), 161-168.

56   Chappell M.C., Loh Y.P., and O'Donohue T.L., Evidence for an opiomelanotropin acetyltransferase in the rat pituitary neurointermediate lobe, *Peptides* **3** (1982), 405-410.

57   Cheever M.A. and Chen W., Therapy with cultured T cells: principles revisited, *Immunological reviews* **157** (1997), 177-194.

[58]   Chen J., Cheng Z., Hoffman T.J. et al., Melanoma-targeting properties of (99m)technetium-labeled cyclic alpha-melanocyte-stimulating hormone peptide analogues, *Cancer Res* **60** (2000), 5649-5658.

[59]   Chen J., Cheng Z., Owen N.K. et al., Evaluation of an (111)In-DOTA-rhenium cyclized alpha-MSH analog: a novel cyclic-peptide analog with improved tumor-targeting properties, *J Nucl Med* **42** (2001), 1847-1855.

[60]   Cheng Z., Chen J., Miao Y. et al., Modification of the structure of a metallopeptide: synthesis and biological evaluation of (111)In-labeled DOTA-conjugated rhenium-cyclized alpha-MSH analogues, *J Med Chem* **45** (2002), 3048-3056.

[61]   Cheng Z., Chen J., Quinn T.P. et al., Radioiodination of rhenium cyclized alpha-melanocyte-stimulating hormone resulting in enhanced radioactivity localization and retention in melanoma, *Cancer Res* **64** (2004), 1411-1418.

[62]   Cheng Z., Xiong Z., Subbarayan M. et al., 64Cu-labeled alpha-melanocyte-stimulating hormone analog for microPET imaging of melanocortin 1 receptor expression, *Bioconjug Chem* **18** (2007), 765-772.

[63]   Cheng Z., Zhang L., Graves E. et al., Small-animal PET of melanocortin 1 receptor expression using a 18F-labeled alpha-melanocyte-stimulating hormone analog, *J Nucl Med* **48** (2007), 987-994.

[64]   Chhajlani V. and Wikberg J.E., Molecular cloning and expression of the human melanocyte stimulating hormone receptor cDNA, *FEBS letters* **309** (1992), 417-420.

[65]   Chhajlani V., Xu X., Blauw J. et al., Identification of ligand binding residues in extracellular loops of the melanocortin 1 receptor, *Biochemical and biophysical research communications* **219** (1996), 521-525.

[66]   Chien Y.W., *Transdermal drug delivery and delivery systems*, 2nd ed. (Marcel Dekker, New York, 1992).

[67]   Christensen E.I., Rennke H.G., and Carone F.A., Renal tubular uptake of protein: effect of molecular charge, *Am J Physiol* **244** (1983), F436-441.

[68]   Clark W.H., Jr., From L., Bernardino E.A. et al., The histogenesis and biologic behavior of primary human malignant melanomas of the skin, *Cancer Res* **29** (1969), 705-727.

[69]   Cody W.L., Mahoney M., Knittel J.J. et al., Cyclic melanotropins. 9. 7-D-Phenylalanine analogues of the active-site sequence, *J Med Chem* **28** (1985), 583-588.

[70]   Cybulla M., Weiner S.M., and Otte A., End-stage renal disease after treatment with 90Y-DOTATOC, *Eur J Nucl Med* **28** (2001), 1552-1554.

[71]   D'Amato R.J., Loughnan M.S., Flynn E. et al., Thalidomide is an inhibitor of angiogenesis, *Proc Natl Acad Sci U S A* **91** (1994), 4082-4085.

[72]   Dai D.L., Martinka M., and Li G., Prognostic significance of activated Akt expression in melanoma: a clinicopathologic study of 292 cases, *J Clin Oncol* **23** (2005), 1473-1482.

[73]   Darkes J.M., Plosker G.L., and Jarvis B., Temozolomide: A Review of its Use in the Treatment of Malignant Gliomas, Malignant Melanoma and Other Advanced Cancers., *Am J Cancer* **1** (2002), 55-80.

[74]   De Jong M., Bakker W.H., Breeman W.A. et al., Pre-clinical comparison of [DTPA0] octreotide, [DTPA0,Tyr3] octreotide and [DOTA0,Tyr3] octreotide as carriers for somatostatin receptor-targeted scintigraphy and radionuclide therapy, *Int J Cancer* **75** (1998), 406-411.

[75]   de Looper M. and Bhatia K., Australian health trends 2001*, 2001*, *The Australian Institute of Health and Welfare,* Canberra*.*

[76] De Luca M., Siegrist W., Bondanza S. et al., Alpha melanocyte stimulating hormone (alpha MSH) stimulates normal human melanocyte growth by binding to high-affinity receptors, *J Cell Sci* **105 (Pt 4)** (1993), 1079-1084.

[77] Deakin J.F., Dostrovsky J.O., and Smyth D.G., Influence of N-terminal acetylation and C-terminal proteolysis on the analgesic activity of beta-endorphin, *The Biochemical journal* **189** (1980), 501-506.

[78] Deen W.M., Satvat B., and Jamieson J.M., Theoretical model for glomerular filtration of charged solutes, *Am J Physiol* **238** (1980), F126-139.

[79] Dennis L.K., Analysis of the melanoma epidemic, both apparent and real: data from the 1973 through 1994 surveillance, epidemiology, and end results program registry, *Arch Dermatol* **135** (1999), 275-280.

[80] Diepgen T.L. and Mahler V., The epidemiology of skin cancer, *Br J Dermatol* **146 Suppl 61** (2002), 1-6.

[81] Donatien P.D., Hunt G., Pieron C. et al., The expression of functional MSH receptors on cultured human melanocytes, *Archives of dermatological research* **284** (1992), 424-426.

[82] Dorr R.T., Ertl G., Levine N. et al., Effects of a superpotent melanotropic peptide in combination with solar UV radiation on tanning of the skin in human volunteers, *Arch Dermatol* **140** (2004), 827-835.

[83] Dubin N., Moseson M., and Pasternack B.S., Sun exposure and malignant melanoma among susceptible individuals, *Environmental health perspectives* **81** (1989), 139-151.

[84] Eberle A., Kriwaczek V.M., and Schwyzer R., Hormone--receptor interactions: melanotropic activities of the covalent serum albumin complexes with alpha-melanotropin, alpha-melanotropin fragments, and enkephalin, *FEBS letters* **80** (1977), 246-250.

[85] Eberle A.N., Kriwaczek V.M., and Schwyzer R., Studies on tyrosinase stimulation, binding and degradation of α-MSH interacting with non-synchronized mouse melanoma cells in culture., in *Peptides, Structure and Biological Function.*, edited by E. Gross and J. Meienhofer (Pierce Chemical Corp., Rockford, IL, 1979), pp. 1033-1036.

[86] Eberle A.N., Studies on melanotropin (MSH) receptors of melanophores and melanoma cells, *Biochem Soc Trans* **9** (1981), 37-39.

[87] Eberle A.N., *The Melanotropins: chemistry, physiology and mechanism of action.* (Karger Verlag, Basel, 1988).

[88] Eberle A.N., Proopiomelanocortin and the melanocortin peptides, in *The melanocortin receptors*, edited by R. D. Cone (Humana Press, Totowa, NJ, 2000), pp. 3-67.

[89] Eberle A.N., Froidevaux S., and Siegrist W., Proopiomelanocortin and the melanocortin peptides, in *The melanocortin receptors*, edited by R. D. Cone (Humana Press, Totowa, NJ, 2000), pp. 491-520.

[90] Eberle A.N. and Froidevaux S., Radiolabeled alpha-melanocyte-stimulating hormone analogs for receptor-mediated targeting of melanoma: from tritium to indium, *J Mol Recognit* **16** (2003), 248-254.

[91] Eberle A.N., Mild G., and Froidevaux S., Receptor-mediated tumor targeting with radiopeptides. Part 1. General concepts and methods: applications to somatostatin receptor-expressing tumors, *J Recept Signal Transduct Res* **24** (2004), 319-455.

[92] Eberle A.N. and Beglinger C., Does 177Lu-labeled octreotate improve the rate of remission of endocrine gastroenteropancreatic tumors?, *Nat Clin Pract Endocrinol Metab* **1** (2005), 20-21.

[93] Egleton R.D., Mitchell S.A., Huber J.D. et al., Improved bioavailability to the brain of glycosylated Met-enkephalin analogs, *Brain research* **881** (2000), 37-46.

94   Eisenwiener K.P., Prata M.I., Buschmann I. et al., NODAGATOC, a new chelator-coupled somatostatin analogue labeled with [67/68Ga] and [111In] for SPECT, PET, and targeted therapeutic applications of somatostatin receptor (hsst2) expressing tumors, *Bioconjug Chem* **13** (2002), 530-541.

95   Ell P.J., Jarritt P.H., Costa D.C. et al., Functional imaging of the brain, *Semin Nucl Med* **17** (1987), 214-229.

96   Esser J.P., Krenning E.P., Teunissen J.J. et al., Comparison of [(177)Lu-DOTA(0),Tyr(3)]octreotate and [(177)Lu-DOTA(0),Tyr(3)]octreotide: which peptide is preferable for PRRT?, *Eur J Nucl Med Mol Imaging* **33** (2006), 1346-1351.

97   Evans L.S., Witte P.R., Feldhaus A.L. et al., Expression of chimeric granulocyte-macrophage colony-stimulating factor/interleukin 2 receptors in human cytotoxic T lymphocyte clones results in granulocyte-macrophage colony-stimulating factor-dependent growth, *Human gene therapy* **10** (1999), 1941-1951.

98   Eves P.C., MacNeil S., and Haycock J.W., alpha-Melanocyte stimulating hormone, inflammation and human melanoma, *Peptides* **27** (2006), 444-452.

99   Farmer P.J., Gidanian S., Shahandeh B. et al., Melanin as a target for melanoma chemotherapy: pro-oxidant effect of oxygen and metals on melanoma viability, *Pigment cell research / sponsored by the European Society for Pigment Cell Research and the International Pigment Cell Society* **16** (2003), 273-279.

100   Feuilloley M., Stolz M.B., Delarue C. et al., Structure-activity relationships of monomeric and dimeric synthetic ACTH fragments in perifused frog adrenal slices, *J Steroid Biochem* **35** (1990), 583-592.

101   Fidler I.J., Selection of successive tumour lines for metastasis, *Nat New Biol* **242** (1973), 148-149.

102   Filippi B., Biondi L., Filira F. et al., Synthesis and biological activity of (D)Ala2,Leu5-enkephalins containing hydrophilic or hydrophobic moieties, *Biopolymers* **22** (1983), 575-578.

103   Fisher J.F., Harrison A.W., Bundy G.L. et al., Peptide to glycopeptide: glycosylated oligopeptide renin inhibitors with attenuated in vivo clearance properties, *J Med Chem* **34** (1991), 3140-3143.

104   Fitzpatrick T.B., Szabo G., and Seiji M., Biology of melanin pigmentary system., in *Dermatology in general medicine.*, edited by T.B. Fitzpatrick, A.Z. Eisen, K. Wolff et al. (McGraw-Hill, New York, 1979), Vol. 1, pp. 131-163.

105   Folkman J., Watson K., Ingber D. et al., Induction of angiogenesis during the transition from hyperplasia to neoplasia, *Nature* **339** (1989), 58-61.

106   Frandberg P.A., Doufexis M., Kapas S. et al., Cysteine residues are involved in structure and function of melanocortin 1 receptor: Substitution of a cysteine residue in transmembrane segment two converts an agonist to antagonist, *Biochemical and biophysical research communications* **281** (2001), 851-857.

107   Frantom P.A., Seravalli J., Ragsdale S.W. et al., Reduction and oxidation of the active site iron in tyrosine hydroxylase: kinetics and specificity, *Biochemistry* **45** (2006), 2372-2379.

108   Fritzberg A.R., Abrams P.G., Beaumier P.L. et al., Specific and stable labeling of antibodies with technetium-99m with a diamide dithiolate chelating agent, *Proc Natl Acad Sci U S A* **85** (1988), 4025-4029.

109   Froidevaux S., Heppeler A., Eberle A.N. et al., Preclinical comparison in AR4-2J tumor-bearing mice of four radiolabeled 1,4,7,10-tetraazacyclododecane-1,4,7,10-tetraacetic acid-somatostatin analogs for tumor diagnosis and internal radiotherapy, *Endocrinology* **141** (2000), 3304-3312.

110   Froidevaux S., Calame-Christe M., Tanner H. et al., A novel DOTA-alpha-melanocyte-stimulating hormone analog for metastatic melanoma diagnosis, *J Nucl Med* **43** (2002), 1699-1706.

[111] Froidevaux S. and Eberle A.N., Homologous regulation of melanocortin-1 receptor (MC1R) expression in melanoma tumor cells in vivo, *J Recept Signal Transduct Res* **22** (2002), 111-121.

[112] Froidevaux S. and Eberle A.N., Somatostatin analogs and radiopeptides in cancer therapy, *Biopolymers* **66** (2002), 161-183.

[113] Froidevaux S., Eberle A.N., Christe M. et al., Neuroendocrine tumor targeting: study of novel gallium-labeled somatostatin radiopeptides in a rat pancreatic tumor model, *Int J Cancer* **98** (2002), 930-937.

[114] Froidevaux S., Calame-Christe M., Schuhmacher J. et al., A gallium-labeled DOTA-alpha-melanocyte-stimulating hormone analog for PET imaging of melanoma metastases, *J Nucl Med* **45** (2004), 116-123.

[115] Froidevaux S., Calame-Christe M., Tanner H. et al., Melanoma targeting with DOTA-alpha-melanocyte-stimulating hormone analogs: structural parameters affecting tumor uptake and kidney uptake, *J Nucl Med* **46** (2005), 887-895.

[116] Frolov A., Singer D., and Hoffmann R., Site-specific synthesis of Amadori-modified peptides on solid phase, *J Pept Sci* **12** (2006), 389-395.

[117] Gahl W.A., Potterf B., Durham-Pierre D. et al., Melanosomal tyrosine transport in normal and pink-eyed dilution murine melanocytes, *Pigment cell research / sponsored by the European Society for Pigment Cell Research and the International Pigment Cell Society* **8** (1995), 229-233.

[118] Garbe C., Buttner P., Bertz J. et al., Primary cutaneous melanoma. Identification of prognostic groups and estimation of individual prognosis for 5093 patients, *Cancer* **75** (1995), 2484-2491.

[119] Garbe C., McLeod G.R., and Buettner P.G., Time trends of cutaneous melanoma in Queensland, Australia and Central Europe, *Cancer* **89** (2000), 1269-1278.

[120] Garcia-Borron J.C., Sanchez-Laorden B.L., and Jimenez-Cervantes C., Melanocortin-1 receptor structure and functional regulation, *Pigment cell research / sponsored by the European Society for Pigment Cell Research and the International Pigment Cell Society* **18** (2005), 393-410.

[121] Gerst J.E., Sole J., Hazum E. et al., Identification and characterization of melanotropin binding proteins from M2R melanoma cells by covalent photoaffinity labeling, *Endocrinology* **123** (1988), 1792-1797.

[122] Ghanem G.E., Comunale G., Libert A. et al., Evidence for alpha-melanocyte-stimulating hormone (alpha-MSH) receptors on human malignant melanoma cells, *Int J Cancer* **41** (1988), 248-255.

[123] Giblin M.F., Jurisson S.S., and Quinn T.P., Synthesis and characterization of rhenium-complexed alpha-melanotropin analogs, *Bioconjug Chem* **8** (1997), 347-353.

[124] Giblin M.F., Wang N., Hoffman T.J. et al., Design and characterization of alpha-melanotropin peptide analogs cyclized through rhenium and technetium metal coordination, *Proc Natl Acad Sci U S A* **95** (1998), 12814-12818.

[125] Gibson S., Crosby S.R., Stewart M.F. et al., Differential release of proopiomelanocortin-derived peptides from the human pituitary: evidence from a panel of two-site immunoradiometric assays, *The Journal of clinical endocrinology and metabolism* **78** (1994), 835-841.

[126] Gilbey A.M., Burnett D., Coleman R.E. et al., The detection of circulating breast cancer cells in blood, *Journal of clinical pathology* **57** (2004), 903-911.

[127] Gilchrest B.A., Blog F.B., and Szabo G., Effects of aging and chronic sun exposure on melanocytes in human skin, *The Journal of investigative dermatology* **73** (1979), 141-143.

[128]   Goldenberg D.M., Chatal J.F., Barbet J. et al., Cancer Imaging and Therapy with Bispecific Antibody Pretargeting, *Update Cancer Ther* **2** (2007), 19-31.

[129]   Goodwin D.A., Meares C.F., DeRiemer L.H. et al., Clinical studies with In-111 BLEDTA, a tumor-imaging conjugate of bleomycin with a bifunctional chelating agent, *J Nucl Med* **22** (1981), 787-792.

[130]   Gray-Schopfer V.C., da Rocha Dias S., and Marais R., The role of B-RAF in melanoma, *Cancer metastasis reviews* **24** (2005), 165-183.

[131]   Grunberg J., Novak-Hofer I., Honer M. et al., In vivo evaluation of 177Lu- and 67/64Cu-labeled recombinant fragments of antibody chCE7 for radioimmunotherapy and PET imaging of L1-CAM-positive tumors, *Clin Cancer Res* **11** (2005), 5112-5120.

[132]   Hadley M.E., Sharma S.D., Hruby V.J. et al., Melanotropic peptides for therapeutic and cosmetic tanning of the skin, *Ann N Y Acad Sci* **680** (1993), 424-439.

[133]   Hadley M.E., Hruby V.J., Blanchard J. et al., Discovery and development of novel melanogenic drugs. Melanotan-I and -II, *Pharm Biotechnol* **11** (1998), 575-595.

[134]   Hahn O. and Stadler W., Sorafenib, *Curr Opin Oncol* **18** (2006), 615-621.

[135]   Handl H.L., Vagner J., Han H. et al., Hitting multiple targets with multimeric ligands, *Expert Opin Ther Targets* **8** (2004), 565-586.

[136]   Hara M., Yaar M., and Gilchrest B.A., Endothelin-1 of keratinocyte origin is a mediator of melanocyte dendricity, *The Journal of investigative dermatology* **105** (1995), 744-748.

[137]   Harris M., Monoclonal antibodies as therapeutic agents for cancer, *Lancet Oncol* **5** (2004), 292-302.

[138]   Haskell-Luevano C., Sawyer T.K., Trumpp-Kallmeyer S. et al., Three-dimensional molecular models of the hMC1R melanocortin receptor: complexes with melanotropin peptide agonists, *Drug design and discovery* **14** (1996), 197-211.

[139]   Healy E., Birch-Machin M., and Rees J.L., The Human Melanocortin-1 Receptor, in *The Melanocortin Receptors*, edited by R. D. Cone (Humana Press Inc., Totowa, NJ, 2000), pp. 341-359.

[140]   Hearing V.J., Biochemical control of melanogenesis and melanosomal organization, *The journal of investigative dermatology. Symposium proceedings / the Society for Investigative Dermatology, Inc* **4** (1999), 24-28.

[141]   Hearing V.J., Biogenesis of pigment granules: a sensitive way to regulate melanocyte function, *Journal of dermatological science* **37** (2005), 3-14.

[142]   Hearing V.J., Jr., Ekel T.M., Montague P.M. et al., Mammalian tyrosinase: isolation by a simple new procedure and characterization of its steric requirements for cofactor activity, *Archives of biochemistry and biophysics* **185** (1978), 407-418.

[143]   Helene M., Lake-Bullock V., Bryson J.S. et al., Inhibition of graft-versus-host disease. Use of a T cell-controlled suicide gene, *J Immunol* **158** (1997), 5079-5082.

[144]   Heppeler A., Froidevaux S., Eberle A.N. et al., Receptor targeting for tumor localisation and therapy with radiopeptides, *Curr Med Chem* **7** (2000), 971-994.

[145]   Hill G.J., 2nd, Historic milestones in cancer surgery, *Seminars in oncology* **6** (1979), 409-427.

[146]   Hofmann K., Wingender W., and Finn F.M., Correlation of adrenocorticotropic activity of ACTH analogs with degree of binding to an adrenal cortical particulate preparation, *Proc Natl Acad Sci U S A* **67** (1970), 829-836.

[147] Holbrook K.A., Underwood R.A., Vogel A.M. et al., The appearance, density and distribution of melanocytes in human embryonic and fetal skin revealed by the anti-melanoma monoclonal antibody, HMB-45, *Anatomy and embryology* **180** (1989), 443-455.

[148] Holland J.F. and Frei III E., *Holland-Frei Cancer Medicine*, 6th ed. (BC Decker, Hamilton, Ontario, 2003).

[149] Holst B., Elling C.E., and Schwartz T.W., Metal ion-mediated agonism and agonist enhancement in melanocortin MC1 and MC4 receptors, *J Biol Chem* **277** (2002), 47662-47670.

[150] Horvat S. and Jakas A., Peptide and amino acid glycation: new insights into the Maillard reaction, *J Pept Sci* **10** (2004), 119-137.

[151] Humm J.L. and Chin L.M., A model of cell inactivation by alpha-particle internal emitters, *Radiation research* **134** (1993), 143-150.

[152] Hunt G., Kyne S., Ito S. et al., Eumelanin and phaeomelanin contents of human epidermis and cultured melanocytes, *Pigment cell research / sponsored by the European Society for Pigment Cell Research and the International Pigment Cell Society* **8** (1995), 202-208.

[153] Hynes R.O., Integrins: versatility, modulation, and signaling in cell adhesion, *Cell* **69** (1992), 11-25.

[154] Ichihashi M., Ueda M., Budiyanto A. et al., UV-induced skin damage, *Toxicology* **189** (2003), 21-39.

[155] Imokawa G., Kobayashi T., Miyagishi M. et al., The role of endothelin-1 in epidermal hyperpigmentation and signaling mechanisms of mitogenesis and melanogenesis, *Pigment cell research / sponsored by the European Society for Pigment Cell Research and the International Pigment Cell Society* **10** (1997), 218-228.

[156] Ito S. and Fujita K., Microanalysis of eumelanin and pheomelanin in hair and melanomas by chemical degradation and liquid chromatography, *Analytical biochemistry* **144** (1985), 527-536.

[157] IUPAC, *IUPAC Compendium of Chemical Terminology, Electronic version*, 2nd ed. (1997).

[158] Jang Y.H., Blanco M., Dasgupta S. et al., Mechanism and Energetics for Complexation of 90Y with 1,4,7,10-Tetraazacyclododecane-1,4,7,10-tetraacetic Acid (DOTA), a Model for Cancer Radioimmunotherapy, *J. Am. Chem. Soc.* **121** (1999), 6142-6151.

[159] Jiang J., Sharma S.D., Fink J.L. et al., Melanotropic peptide receptors: membrane markers of human melanoma cells, *Experimental dermatology* **5** (1996), 325-333.

[160] June C.H., Adoptive T cell therapy for cancer in the clinic, *The Journal of clinical investigation* **117** (2007), 1466-1476.

[161] Kapadia D. and Fong L., CTLA-4 blockade: autoimmunity as treatment, *J Clin Oncol* **23** (2005), 8926-8928.

[162] Karasarides M., Chiloeches A., Hayward R. et al., B-RAF is a therapeutic target in melanoma, *Oncogene* **23** (2004), 6292-6298.

[163] Kasper B., D'Hondt V., Vereecken P. et al., Novel treatment strategies for malignant melanoma: a new beginning?, *Critical reviews in oncology/hematology* **62** (2007), 16-22.

[164] Kimelberg H.K., Tracy T.F., Jr., Biddlecome S.M. et al., The effect of entrapment in liposomes on the in vivo distribution of [3H]methotrexate in a primate, *Cancer Res* **36** (1976), 2949-2957.

[165] Klein S., Reuveni H., and Levitzki A., Signal transduction by a nondissociable heterotrimeric yeast G protein, *Proc Natl Acad Sci U S A* **97** (2000), 3219-3223.

[166] Knogler K., Grunberg J., Zimmermann K. et al., Copper-67 radioimmunotherapy and growth inhibition by anti-L1-cell adhesion molecule monoclonal antibodies in a therapy model of ovarian cancer metastasis, *Clin Cancer Res* **13** (2007), 603-611.

[167] Kobayashi T., Urabe K., Winder A. et al., Tyrosinase related protein 1 (TRP1) functions as a DHICA oxidase in melanin biosynthesis, *The EMBO journal* **13** (1994), 5818-5825.

[168] Kok R.J., Haas M., Moolenaar F. et al., Drug delivery to the kidneys and the bladder with the low molecular weight protein lysozyme, *Ren Fail* **20** (1998), 211-217.

[169] Korsmeyer S.J., BCL-2 gene family and the regulation of programmed cell death, *Cancer Res* **59** (1999), 1693s-1700s.

[170] Kozlowski L., Wojtukiewicz M.Z., and Ostrowska H., Cathepsin A activity in primary and metastatic human melanocytic tumors, *Archives of dermatological research* **292** (2000), 68-71.

[171] Kriwaczek V.M., Eberle A.N., Müller M. et al., Tobacco Mosaic Virus as a Carrier for Small Molecules I. The preparation and characterization of a TMV/alpha-melanotropin conjugate., *Helvetica Chimica Acta* **61** (1978), 1232-1240.

[172] Kumar N., Taxol-induced polymerization of purified tubulin. Mechanism of action, *J Biol Chem* **256** (1981), 10435-10441.

[173] Kung H.F., Ohmomo Y., and Kung M.P., Current and future radiopharmaceuticals for brain imaging with single photon emission computed tomography, *Semin Nucl Med* **20** (1990), 290-302.

[174] Kunstfeld R., Wickenhauser G., Michaelis U. et al., Paclitaxel encapsulated in cationic liposomes diminishes tumor angiogenesis and melanoma growth in a "humanized" SCID mouse model, *The Journal of investigative dermatology* **120** (2003), 476-482.

[175] Kurohane K., Namba Y., and Oku N., Liposomes modified with a synthetic Arg-Gly-Asp mimetic inhibit lung metastasis of B16BL6 melanoma cells, *Life Sci* **68** (2000), 273-281.

[176] Kwekkeboom D.J., Teunissen J.J., Bakker W.H. et al., Radiolabeled somatostatin analog [177Lu-DOTA0,Tyr3]octreotate in patients with endocrine gastroenteropancreatic tumors, *J Clin Oncol* **23** (2005), 2754-2762.

[177] Lambert B., Cybulla M., Weiner S.M. et al., Renal toxicity after radionuclide therapy, *Radiation research* **161** (2004), 607-611.

[178] Lamberts S.W., Chayvialle J.A., and Krenning E.P., The visualization of gastroenteropancreatic endocrine tumors, *Metabolism* **41** (1992), 111-115.

[179] Lamberts S.W., Hofland L.J., de Herder W.W. et al., Octreotide and related somatostatin analogs in the diagnosis and treatment of pituitary disease and somatostatin receptor scintigraphy, *Front Neuroendocrinol* **14** (1993), 27-55.

[180] Lande S. and Lerner A.B., The biochemistry of melanotropic agents, *Pharmacological reviews* **19** (1967), 1-20.

[181] Lawrence G.M. and Brewer D.B., Glomerular ultrafiltration and tubular reabsorption of bovine serum albumin and derivatives with increased negative charge in the normal female Wistar rat, *Clin Sci (Lond)* **66** (1984), 47-54.

[182] Leibel R.L., Chung W.K., and Chua S.C., Jr., The molecular genetics of rodent single gene obesities, *J Biol Chem* **272** (1997), 31937-31940.

[183] Lens M.B. and Dawes M., Global perspectives of contemporary epidemiological trends of cutaneous malignant melanoma, *Br J Dermatol* **150** (2004), 179-185.

[184] Lerner A.B. and Fitzpatrick T.B., Biochemistry of melanin formation, *Physiological reviews* **30** (1950), 91-126.

185 Li P. and Xu J.-C., New and Highly Efficient Immonium Type Peptide Coupling Reagents: Synthesis, Mechanism and Application, *Tetrahedron* **56** (2000), 4437-4445.

186 Lin M.S., Goodwin D.A., and Kruse S.L., Bleomycin as a 99mTc carrier in tumor visualization, *J Nucl Med* **15** (1974), 338-342.

187 Ling M.K., Hotta E., Kilianova Z. et al., The melanocortin receptor subtypes in chicken have high preference to ACTH-derived peptides, *British journal of pharmacology* **143** (2004), 626-637.

188 Longstreth J., Cutaneous malignant melanoma and ultraviolet radiation: a review, *Cancer metastasis reviews* **7** (1988), 321-333.

189 Lu D., Willard D., Patel I.R. et al., Agouti protein is an antagonist of the melanocyte-stimulating-hormone receptor, *Nature* **371** (1994), 799-802.

190 Lu D., Vage D.I., and Cone R.D., A ligand-mimetic model for constitutive activation of the melanocortin-1 receptor, *Molecular endocrinology (Baltimore, Md* **12** (1998), 592-604.

191 Luger T.A., Scholzen T., and Grabbe S., The role of alpha-melanocyte-stimulating hormone in cutaneous biology, *The journal of investigative dermatology. Symposium proceedings / the Society for Investigative Dermatology, Inc* **2** (1997), 87-93.

192 Luo Y., Markowitz D., Xiang R. et al., FLK-1-based minigene vaccines induce T cell-mediated suppression of angiogenesis and tumor protective immunity in syngeneic BALB/c mice, *Vaccine* **25** (2007), 1409-1415.

193 Lynch H.T., Frichot B.C., 3rd, and Lynch J.F., Familial atypical multiple mole-melanoma syndrome, *Journal of medical genetics* **15** (1978), 352-356.

194 MacKie R.M., Freudenberger T., and Aitchison T.C., Personal risk-factor chart for cutaneous melanoma, *Lancet* **2** (1989), 487-490.

195 Maillard L.C., Action des acides aminés sur les sucres; Formation des melanoidines par voie méthodique., *Comptes Rendus de l'Académie des Sciences* **154** (1912), 66-68.

196 Mandrika I., Petrovska R., and Wikberg J., Melanocortin receptors form constitutive homo- and heterodimers, *Biochemical and biophysical research communications* **326** (2005), 349-354.

197 Marchitto K.S., Kindsvogel W.R., Beaumier P.L. et al., Characterization of a human-mouse chimeric antibody reactive with a human melanoma associated antigen, *Progress in clinical and biological research* **288** (1989), 101-105.

198 Mariani G., Erba P.A., and Signore A., Receptor-mediated tumor targeting with radiolabeled peptides: there is more to it than somatostatin analogs, *J Nucl Med* **47** (2006), 1904-1907.

199 Mason H.S., The chemistry of melanin. III. Mechanism of the oxidation of dihydroxyphenylalanine by tyrosinase., *J. Biol. Chem.* **172** (1948), 83-99.

200 McQuade P., Miao Y., Yoo J. et al., Imaging of melanoma using 64Cu- and 86Y-DOTA-ReCCMSH(Arg11), a cyclized peptide analogue of alpha-MSH, *J Med Chem* **48** (2005), 2985-2992.

201 Meares C.F. and Wensel T.G., Metal chelates as probes of biological systems, *Acc. Chem. Res.* **17** (1984), 202-209.

202 Miao Y., Owen N.K., Whitener D. et al., In vivo evaluation of 188Re-labeled alpha-melanocyte stimulating hormone peptide analogs for melanoma therapy, *Int J Cancer* **101** (2002), 480-487.

203 Miao Y., Whitener D., Feng W. et al., Evaluation of the human melanoma targeting properties of radiolabeled alpha-melanocyte stimulating hormone peptide analogues, *Bioconjug Chem* **14** (2003), 1177-1184.

[204] Miao Y., Hoffman T.J., and Quinn T.P., Tumor-targeting properties of 90Y- and 177Lu-labeled alpha-melanocyte stimulating hormone peptide analogues in a murine melanoma model, *Nucl Med Biol* **32** (2005), 485-493.

[205] Miao Y., Hylarides M., Fisher D.R. et al., Melanoma therapy via peptide-targeted {alpha}-radiation, *Clin Cancer Res* **11** (2005), 5616-5621.

[206] Miao Y., Owen N.K., Fisher D.R. et al., Therapeutic efficacy of a 188Re-labeled alpha-melanocyte-stimulating hormone peptide analog in murine and human melanoma-bearing mouse models, *J Nucl Med* **46** (2005), 121-129.

[207] Miao Y., Fisher D.R., and Quinn T.P., Reducing renal uptake of (90)Y- and (177)Lu-labeled alpha-melanocyte stimulating hormone peptide analogues, *Nucl Med Biol* **33** (2006), 723-733.

[208] Miao Y., Benwell K., and Quinn T.P., 99mTc- and 111In-labeled alpha-melanocyte-stimulating hormone peptides as imaging probes for primary and pulmonary metastatic melanoma detection, *J Nucl Med* **48** (2007), 73-80.

[209] Miao Y., Gallazzi F., Guo H. et al., 111In-labeled lactam bridge-cyclized alpha-melanocyte stimulating hormone peptide analogues for melanoma imaging, *Bioconjug Chem* **19** (2008), 539-547.

[210] Miller A.J. and Mihm M.C., Jr., Melanoma, *The New England journal of medicine* **355** (2006), 51-65.

[211] Miller M.W., Duhl D.M., Vrieling H. et al., Cloning of the mouse agouti gene predicts a secreted protein ubiquitously expressed in mice carrying the lethal yellow mutation, *Genes & development* **7** (1993), 454-467.

[212] Montalbetti C.A.G.N. and Falque V., Amide bond formation and peptide coupling, *Tetrahedron* **61** (2005), 10827-10852.

[213] Morandini R., Boeynaems J.M., Hedley S.J. et al., Modulation of ICAM-1 expression by alpha-MSH in human melanoma cells and melanocytes, *Journal of cellular physiology* **175** (1998), 276-282.

[214] Mountjoy K.G., Robbins L.S., Mortrud M.T. et al., The cloning of a family of genes that encode the melanocortin receptors, *Science (New York, N.Y* **257** (1992), 1248-1251.

[215] Muceniece R., Mutule I., Mutulis F. et al., Detection of regions in the MC1 receptor of importance for the selectivity of the MC1 receptor super-selective MS04/MS05 peptides, *Biochim Biophys Acta* **1544** (2001), 278-282.

[216] NCI, National Cancer Institute, available at www.cancer.gov, 2007.

[217] NCNN, NCCN Clinical Practice Guidelines in Oncology: Melanoma, 2007, *National Comprehensive Cancer Network.*

[218] Niethammer A.G., Xiang R., Becker J.C. et al., A DNA vaccine against VEGF receptor 2 prevents effective angiogenesis and inhibits tumor growth, *Nature medicine* **8** (2002), 1369-1375.

[219] Nikula T.K., McDevitt M.R., Finn R.D. et al., Alpha-emitting bismuth cyclohexylbenzyl DTPA constructs of recombinant humanized anti-CD33 antibodies: pharmacokinetics, bioactivity, toxicity and chemistry, *J Nucl Med* **40** (1999), 166-176.

[220] Novak-Hofer I., Zimmermann K., Maecke H.R. et al., Tumor uptake and metabolism of copper-67-labeled monoclonal antibody chCE7 in nude mice bearing neuroblastoma xenografts, *J Nucl Med* **38** (1997), 536-544.

[221] Novak-Hofer I. and Schubiger P.A., Copper-67 as a therapeutic nuclide for radioimmunotherapy, *Eur J Nucl Med Mol Imaging* **29** (2002), 821-830.

[222] Okarvi S.M., Peptide-based radiopharmaceuticals: future tools for diagnostic imaging of cancers and other diseases, *Med Res Rev* **24** (2004), 357-397.

[223] Oku N., Tokudome Y., Koike C. et al., Liposomal Arg-Gly-Asp analogs effectively inhibit metastatic B16 melanoma colonization in murine lungs, *Life Sci* **58** (1996), 2263-2270.

[224] Olivares C., Jimenez-Cervantes C., Lozano J.A. et al., The 5,6-dihydroxyindole-2-carboxylic acid (DHICA) oxidase activity of human tyrosinase, *Biochem. J.* **354** (2001), 131-139.

[225] Ollmann M.M., Wilson B.D., Yang Y.K. et al., Antagonism of central melanocortin receptors in vitro and in vivo by agouti-related protein, *Science (New York, N.Y* **278** (1997), 135-138.

[226] Ortonne J.P. and Prota G., Hair melanins and hair color: ultrastructural and biochemical aspects, *The Journal of investigative dermatology* **101** (1993), 82S-89S.

[227] Otte A., Herrmann R., Heppeler A. et al., Yttrium-90 DOTATOC: first clinical results, *Eur J Nucl Med* **26** (1999), 1439-1447.

[228] Paglia P., Medina E., Arioli I. et al., Gene transfer in dendritic cells, induced by oral DNA vaccination with Salmonella typhimurium, results in protective immunity against a murine fibrosarcoma, *Blood* **92** (1998), 3172-3176.

[229] Palczewski K., Kumasaka T., Hori T. et al., Crystal structure of rhodopsin: A G protein-coupled receptor, *Science (New York, N.Y* **289** (2000), 739-745.

[230] Park H.Y., Russakovsky V., Ohno S. et al., The beta isoform of protein kinase C stimulates human melanogenesis by activating tyrosinase in pigment cells, *J Biol Chem* **268** (1993), 11742-11749.

[231] Parker D., Tumour targeting with radiolabeled macrocycle-antibody conjugates, *Chem Soc Rev* **19** (1990), 271-291.

[232] Parkin D.M., Bray F., Ferlay J. et al., Global cancer statistics, 2002, *CA: a cancer journal for clinicians* **55** (2005), 74-108.

[233] Pathak M.A., Jimbow K., and Fitzpatrick T.B., Photobiology of pigment cell., in *Pigment Cell*, edited by M. Seiji (University of Tokyo Press, Tokyo, 1981), pp. 655-670.

[234] Pena C., Stewart J.M., and Goodfriend T.C., A new class of angiotensin inhibitors: N-methylphenylalanine analogs, *Life Sci* **14** (1974), 1331-1336.

[235] Pierce K.L., Premont R.T., and Lefkowitz R.J., Seven-transmembrane receptors, *Nature reviews* **3** (2002), 639-650.

[236] Pierschbacher M.D. and Ruoslahti E., Cell attachment activity of fibronectin can be duplicated by small synthetic fragments of the molecule, *Nature* **309** (1984), 30-33.

[237] Polt R., Porreca F., Szabo L.Z. et al., Glycopeptide enkephalin analogues produce analgesia in mice: evidence for penetration of the blood-brain barrier, *Proc Natl Acad Sci U S A* **91** (1994), 7114-7118.

[238] Poznansky M.J. and Juliano R.L., Biological approaches to the controlled delivery of drugs: a critical review, *Pharmacological reviews* **36** (1984), 277-336.

[239] Prota G. and Nicolaus R.A., On the biogenesis of phaeomelanins., in *Advances in biology of skin*, edited by Montagna W and Hu F (Pergamon Press, Oxford, 1967), Vol. 8, pp. 323-328.

[240] Prusis P., Frandberg P.A., Muceniece R. et al., A three dimensional model for the interaction of MSH with the melanocortin-1 receptor, *Biochemical and biophysical research communications* **210** (1995), 205-210.

[241] Puri N., Gardner J.M., and Brilliant M.H., Aberrant pH of melanosomes in pink-eyed dilution (p) mutant melanocytes, *The Journal of investigative dermatology* **115** (2000), 607-613.

[242] Queensland Melanoma Project, Moles and malignant melanoma: terminology and CLASSIFICATION, *The Medical journal of Australia* **1** (1967), 123-125.

[243] Ramaiah A., Lag kinetics of tyrosinase: its physiological implications, *Indian journal of biochemistry & biophysics* **33** (1996), 349-356.

[244] Ranganathan R.S., Pillai R.K., Raju N. et al., Polymethylated DOTA ligands. 1. Synthesis of rigidified ligands and studies on the effects of alkyl substitution on acid-base properties and conformational mobility, *Inorg Chem* **41** (2002), 6846-6855.

[245] Reid K., Turnley A.M., Maxwell G.D. et al., Multiple roles for endothelin in melanocyte development: regulation of progenitor number and stimulation of differentiation, *Development (Cambridge, England)* **122** (1996), 3911-3919.

[246] Reivich M., Kuhl D., Wolf A. et al., The [18F]fluorodeoxyglucose method for the measurement of local cerebral glucose utilization in man, *Circ Res* **44** (1979), 127-137.

[247] Renn O. and Meares C.F., Large-scale synthesis of the bifunctional chelating agent 2-(p-nitrobenzyl)-1,4,7,10-tetraazacyclododecane-N,N',N'',N'''-tetr aacetic acid, and the determination of its enantiomeric purity by chiral chromatography, *Bioconjug Chem* **3** (1992), 563-569.

[248] Reubi J.C., Neuropeptide receptors in health and disease: the molecular basis for in vivo imaging, *J Nucl Med* **36** (1995), 1825-1835.

[249] Reubi J.C., Peptide receptors as molecular targets for cancer diagnosis and therapy, *Endocr Rev* **24** (2003), 389-427.

[250] Reubi J.C., Somatostatin and other Peptide receptors as tools for tumor diagnosis and treatment, *Neuroendocrinology* **80 Suppl 1** (2004), 51-56.

[251] Reubi J.C., Macke H.R., and Krenning E.P., Candidates for peptide receptor radiotherapy today and in the future, *J Nucl Med* **46 Suppl 1** (2005), 67S-75S.

[252] Rhodes A.R. and Melski J.W., Small congenital nevocellular nevi and the risk of cutaneous melanoma, *The Journal of pediatrics* **100** (1982), 219-224.

[253] Ringholm A., Klovins J., Rudzish R. et al., Pharmacological characterization of loss of function mutations of the human melanocortin 1 receptor that are associated with red hair, *The Journal of investigative dermatology* **123** (2004), 917-923.

[254] Roberts D.W., Newton R.A., Beaumont K.A. et al., Quantitative analysis of MC1R gene expression in human skin cell cultures, *Pigment cell research / sponsored by the European Society for Pigment Cell Research and the International Pigment Cell Society* **19** (2006), 76-89.

[255] Roberts D.W., Newton R.A., and Sturm R.A., MC1R expression in skin: is it confined to melanocytes?, *The Journal of investigative dermatology* **127** (2007), 2472-2473.

[256] Rolleman E.J., Valkema R., de Jong M. et al., Safe and effective inhibition of renal uptake of radiolabelled octreotide by a combination of lysine and arginine, *Eur J Nucl Med Mol Imaging* **30** (2003), 9-15.

[257] Romero-Graillet C., Aberdam E., Clement M. et al., Nitric oxide produced by ultraviolet-irradiated keratinocytes stimulates melanogenesis, *The Journal of clinical investigation* **99** (1997), 635-642.

258   Roscic M. and Horvat S., Transformations of bioactive peptides in the presence of sugars--characterization and stability studies of the adducts generated via the Maillard reaction, *Bioorg Med Chem* **14** (2006), 4933-4943.

259   Rosenkranz C.D., Chiara D., Agorio C. et al., Towards new immunotherapies: targeting recombinant cytokines to the immune system using live attenuated Salmonella, *Vaccine* **21** (2003), 798-801.

260   Rousseau K., Kauser S., Pritchard L.E. et al., Proopiomelanocortin (POMC), the ACTH/melanocortin precursor, is secreted by human epidermal keratinocytes and melanocytes and stimulates melanogenesis, *Faseb J* **21** (2007), 1844-1856.

261   RxList, RxList, available at www.rxlist.com, 2007.

262   Sadler K. and Tam J.P., Peptide dendrimers: applications and synthesis, *J Biotechnol* **90** (2002), 195-229.

263   Sahm U.G., Olivier G.W., Branch S.K. et al., Influence of alpha-MSH terminal amino acids on binding affinity and biological activity in melanoma cells, *Peptides* **15** (1994), 441-446.

264   Salazar-Onfray F., Lopez M., Lundqvist A. et al., Tissue distribution and differential expression of melanocortin 1 receptor, a malignant melanoma marker, *Br J Cancer* **87** (2002), 414-422.

265   Salk D., Technetium-labeled monoclonal antibodies for imaging metastatic melanoma: results of a multicenter clinical study, *Seminars in oncology* **15** (1988), 608-618.

266   Sanz L., Feijoo M., Blanco B. et al., Generation of non-permissive basement membranes by anti-laminin antibody fragments produced by matrix-embedded gene-modified cells, *Cancer Immunol Immunother* **52** (2003), 643-647.

267   Sawyer T.K., Sanfilippo P.J., Hruby V.J. et al., 4-Norleucine, 7-D-phenylalanine-alpha-melanocyte-stimulating hormone: a highly potent alpha-melanotropin with ultralong biological activity, *Proc Natl Acad Sci U S A* **77** (1980), 5754-5758.

268   Schaffer J.V. and Bolognia J.L., The melanocortin-1 receptor: red hair and beyond, *Arch Dermatol* **137** (2001), 1477-1485.

269   Schauer E., Trautinger F., Kock A. et al., Proopiomelanocortin-derived peptides are synthesized and released by human keratinocytes, *The Journal of clinical investigation* **93** (1994), 2258-2262.

270   Schioth H.B., Muceniece R., Wikberg J.E. et al., Characterisation of melanocortin receptor subtypes by radioligand binding analysis, *Eur J Pharmacol* **288** (1995), 311-317.

271   Schioth H.B., Muceniece R., Larsson M. et al., Binding of cyclic and linear MSH core peptides to the melanocortin receptor subtypes, *Eur J Pharmacol* **319** (1997), 369-373.

272   Schmitt-Sody M., Strieth S., Krasnici S. et al., Neovascular targeting therapy: paclitaxel encapsulated in cationic liposomes improves antitumoral efficacy, *Clin Cancer Res* **9** (2003), 2335-2341.

273   Schottelius M., Wester H.J., Reubi J.C. et al., Improvement of pharmacokinetics of radioiodinated Tyr(3)-octreotide by conjugation with carbohydrates, *Bioconjug Chem* **13** (2002), 1021-1030.

274   Schottelius M., Rau F., Reubi J.C. et al., Modulation of pharmacokinetics of radioiodinated sugar-conjugated somatostatin analogues by variation of peptide net charge and carbohydration chemistry, *Bioconjug Chem* **16** (2005), 429-437.

275   Sciagra R., Pellegri M., Pupi A. et al., Prognostic implications of Tc-99m sestamibi viability imaging and subsequent therapeutic strategy in patients with chronic coronary artery disease and left ventricular dysfunction, *J Am Coll Cardiol* **36** (2000), 739-745.

[276]   Searle A.G., An extension series in the mouse, *The Journal of heredity* **59** (1968), 341-342.

[277]   Seftor R.E., Seftor E.A., Kirschmann D.A. et al., Targeting the tumor microenvironment with chemically modified tetracyclines: inhibition of laminin 5 gamma2 chain promigratory fragments and vasculogenic mimicry, *Molecular cancer therapeutics* **1** (2002), 1173-1179.

[278]   Seiberg M., Keratinocyte-melanocyte interactions during melanosome transfer, *Pigment cell research / sponsored by the European Society for Pigment Cell Research and the International Pigment Cell Society* **14** (2001), 236-242.

[279]   Sgadari C., Toschi E., Palladino C. et al., Mechanism of paclitaxel activity in Kaposi's sarcoma, *J Immunol* **165** (2000), 509-517.

[280]   Shibahara S., Tomita Y., Tagami H. et al., Molecular basis for the heterogeneity of human tyrosinase, *The Tohoku journal of experimental medicine* **156** (1988), 403-414.

[281]   Shirota K., Kato Y., Suzuki K. et al., Characterization of novel kidney-specific delivery system using an alkylglucoside vector, *J Pharmacol Exp Ther* **299** (2001), 459-467.

[282]   Shutter J.R., Graham M., Kinsey A.C. et al., Hypothalamic expression of ART, a novel gene related to agouti, is up-regulated in obese and diabetic mutant mice, *Genes & development* **11** (1997), 593-602.

[283]   Siegrist W. and Eberle A.N., In situ melanin assay for MSH using mouse B16 melanoma cells in culture, *Analytical biochemistry* **159** (1986), 191-197.

[284]   Siegrist W., Solca F., Stutz S. et al., Characterization of receptors for alpha-melanocyte-stimulating hormone on human melanoma cells, *Cancer Res* **49** (1989), 6352-6358.

[285]   Siegrist W., Girard J., and Eberle A.N., Quantification of MSH receptors on mouse melanoma tissue by receptor autoradiography, *Journal of receptor research* **11** (1991), 323-331.

[286]   Siegrist W., Bagutti C., Solca F. et al., MSH receptors on mouse and human melanoma cells: receptor identification, analysis and quantification, *Progress in histochemistry and cytochemistry* **26** (1992), 110-118.

[287]   Siegrist W., Stutz S., and Eberle A.N., Homologous and heterologous regulation of alpha-melanocyte-stimulating hormone receptors in human and mouse melanoma cell lines, *Cancer Res* **54** (1994), 2604-2610.

[288]   Siegrist W. and Eberle A.N., Melanocortins and their implication in melanoma, *Trends Endocrinol Metab* **6** (1995), 115-120.

[289]   Sies H., Oxidative stress: oxidants and antioxidants, *Experimental physiology* **82** (1997), 291-295.

[290]   Smith-Jones P.M., Fridrich R., Kaden T.A. et al., Antibody labeling with copper-67 using the bifunctional macrocycle 4-[(1,4,8,11-tetraazacyclotetradec-1-yl)methyl]benzoic acid, *Bioconjug Chem* **2** (1991), 415-421.

[291]   Solca F., Siegrist W., Drozdz R. et al., The receptor for alpha-melanotropin of mouse and human melanoma cells. Application of a potent alpha-melanotropin photoaffinity label, *J Biol Chem* **264** (1989), 14277-14281.

[292]   Solomon E.I., Sundaram U.M., and Machonkin T.E., Multicopper Oxidases and Oxygenases, *Chem. Rev.* **96** (1996), 2563-2606.

[293]   Sosabowsky J., Melendez-Alafort L., and Mather S., Radiolabelling of peptides for diagnosis and therapy of non-oncological diseases, *Q J Nucl Med* **47** (2003), 223-237.

[294]   Sporn M.B. and Liby K.T., Cancer chemoprevention: scientific promise, clinical uncertainty, *Nature clinical practice* **2** (2005), 518-525.

[295]   Steinman R.M., Dendritic cells: understanding immunogenicity, *Eur J Immunol* **37 Suppl 1** (2007), S53-60.

[296] Subramaniam S. and Henderson R., Electron crystallography of bacteriorhodopsin with millisecond time resolution, *Journal of structural biology* **128** (1999), 19-25.

[297] Sun B., Zhang S., Zhang D. et al., Doxycycline influences microcirculation patterns in B16 melanoma, *Experimental biology and medicine (Maywood, N.J* **232** (2007), 1300-1307.

[298] Sundberg M.W., Meares C.F., Goodwin D.A. et al., Chelating agents for the binding of metal ions to macromolecules, *Nature* **250** (1974), 587-588.

[299] Surh Y.J., Cancer chemoprevention with dietary phytochemicals, *Nat Rev Cancer* **3** (2003), 768-780.

[300] Suzuki I., Tada A., Ollmann M.M. et al., Agouti signaling protein inhibits melanogenesis and the response of human melanocytes to alpha-melanotropin, *The Journal of investigative dermatology* **108** (1997), 838-842.

[301] Suzuki K., Ando T., Susaki H. et al., Structural requirements for alkylglycoside-type renal targeting vector, *Pharm Res* **16** (1999), 1026-1034.

[302] Suzuki K., Susaki H., Okuno S. et al., Renal drug targeting using a vector "alkylglycoside", *J Pharmacol Exp Ther* **288** (1999), 57-64.

[303] Suzuki K., Susaki H., Okuno S. et al., Specific renal delivery of sugar-modified low-molecular-weight peptides, *J Pharmacol Exp Ther* **288** (1999), 888-897.

[304] Svenson S. and Tomalia D.A., Dendrimers in biomedical applications--reflections on the field, *Adv Drug Deliv Rev* **57** (2005), 2106-2129.

[305] Takeichi M., Cadherins: a molecular family important in selective cell-cell adhesion, *Annual review of biochemistry* **59** (1990), 237-252.

[306] Temming K., Schiffelers R.M., Molema G. et al., RGD-based strategies for selective delivery of therapeutics and imaging agents to the tumour vasculature, *Drug Resist Updat* **8** (2005), 381-402.

[307] Thody A.J. and Shuster S., Control and function of sebaceous glands, *Physiological reviews* **69** (1989), 383-416.

[308] Tobin D.J. and Bystryn J.C., Different populations of melanocytes are present in hair follicles and epidermis, *Pigment cell research / sponsored by the European Society for Pigment Cell Research and the International Pigment Cell Society* **9** (1996), 304-310.

[309] Torchilin V.P., Recent advances with liposomes as pharmaceutical carriers, *Nat Rev Drug Discov* **4** (2005), 145-160.

[310] Tsatmali M., Graham A., Szatkowski D. et al., alpha-melanocyte-stimulating hormone modulates nitric oxide production in melanocytes, *The Journal of investigative dermatology* **114** (2000), 520-526.

[311] Tsatmali M., Ancans J., and Thody A.J., Melanocyte function and its control by melanocortin peptides, *J Histochem Cytochem* **50** (2002), 125-133.

[312] Untch B.R., Barfield M.E., Bason J. et al., Minimally invasive radio-guided surgery for primary hyperparathyroidism, *Ann Surg Oncol* **14** (2007), 3401-3402.

[313] Urteaga O. and Pack G.T., On the antiquity of melanoma, *Cancer* **19** (1966), 607-610.

[314] Vagner J., Handl H.L., Gillies R.J. et al., Novel targeting strategy based on multimeric ligands for drug delivery and molecular imaging: homooligomers of alpha-MSH, *Bioorg Med Chem Lett* **14** (2004), 211-215.

[315] Valverde P., Healy E., Jackson I. et al., Variants of the melanocyte-stimulating hormone receptor gene are associated with red hair and fair skin in humans, *Nature genetics* **11** (1995), 328-330.

316   van Strien F.J., Galas L., Jenks B.G. et al., Differential acetylation of pro-opiomelanocortin-derived peptides in the pituitary gland of Xenopus laevis in relation to background adaptation, *The Journal of endocrinology* **146** (1995), 159-167.

317   Vertuani S., Angusti A., and Manfredini S., The antioxidants and pro-antioxidants network: an overview, *Current pharmaceutical design* **10** (2004), 1677-1694.

318   Wakamatsu K., Graham A., Cook D. et al., Characterisation of ACTH peptides in human skin and their activation of the melanocortin-1 receptor, *Pigment cell research / sponsored by the European Society for Pigment Cell Research and the International Pigment Cell Society* **10** (1997), 288-297.

319   Waldmann T., ABCs of radioisotopes used for radioimmunotherapy: alpha- and beta-emitters, *Leuk Lymphoma* **44 Suppl 3** (2003), S107-113.

320   Weckbecker G., Raulf F., Stolz B. et al., Somatostatin analogs for diagnosis and treatment of cancer, *Pharmacol Ther* **60** (1993), 245-264.

321   Wei L., Butcher C., Miao Y. et al., Synthesis and biologic evaluation of 64Cu-labeled rhenium-cyclized alpha-MSH peptide analog using a cross-bridged cyclam chelator, *J Nucl Med* **48** (2007), 64-72.

322   Weidner N., Semple J.P., Welch W.R. et al., Tumor angiogenesis and metastasis--correlation in invasive breast carcinoma, *The New England journal of medicine* **324** (1991), 1-8.

323   Wester H.J., Schottelius M., Scheidhauer K. et al., Comparison of radioiodinated TOC, TOCA and Mtr-TOCA: the effect of carbohydration on the pharmacokinetics, *Eur J Nucl Med Mol Imaging* **29** (2002), 28-38.

324   Wester H.J., Schottelius M., Poethko T. et al., Radiolabeled carbohydrated somatostatin analogs: a review of the current status, *Cancer biotherapy & radiopharmaceuticals* **19** (2004), 231-244.

325   Wikberg J.E., Muceniece R., Mandrika I. et al., New aspects on the melanocortins and their receptors, *Pharmacol Res* **42** (2000), 393-420.

326   Wilson B.D., Ollmann M.M., Kang L. et al., Structure and function of ASP, the human homolog of the mouse agouti gene, *Human molecular genetics* **4** (1995), 223-230.

327   World Meteorological Organization, Scientific Assessment of Ozone Depletion: 2006*, 2006, Global Ozone Research and Monitoring Project,* Geneva.

328   Wraight E.P., Bard D.R., Maughan T.S. et al., The use of a chelating derivative of alpha melanocyte stimulating hormone for the clinical imaging of malignant melanoma, *Br J Radiol* **65** (1992), 112-118.

329   Yada Y., Higuchi K., and Imokawa G., Effects of endothelins on signal transduction and proliferation in human melanocytes, *J Biol Chem* **266** (1991), 18352-18357.

330   Yang H. and Kao W.J., Dendrimers for pharmaceutical and biomedical applications, *J Biomater Sci Polym Ed* **17** (2006), 3-19.

331   Yang Y., Dickinson C., Haskell-Luevano C. et al., Molecular basis for the interaction of [Nle4,D-Phe7]melanocyte stimulating hormone with the human melanocortin-1 receptor, *J Biol Chem* **272** (1997), 23000-23010.

332   Yang Y.K., Thompson D.A., Dickinson C.J. et al., Characterization of Agouti-related protein binding to melanocortin receptors, *Molecular endocrinology (Baltimore, Md* **13** (1999), 148-155.

333   Yee C., Thompson J.A., Byrd D. et al., Adoptive T cell therapy using antigen-specific CD8+ T cell clones for the treatment of patients with metastatic melanoma: in vivo persistence, migration, and antitumor effect of transferred T cells, *Proc Natl Acad Sci U S A* **99** (2002), 16168-16173.

[334] Zhang M., Yao Z., Garmestani K. et al., Pretargeting radioimmunotherapy of a murine model of adult T-cell leukemia with the alpha-emitting radionuclide, bismuth 213, *Blood 100* (2002), 208-216.

[335] Zhang S., Zhang D., and Sun B., Vasculogenic mimicry: current status and future prospects, *Cancer letters 254* (2007), 157-164.

[336] Zhou H., Luo Y., Mizutani M. et al., T cell-mediated suppression of angiogenesis results in tumor protective immunity, *Blood 106* (2005), 2026-2032.

[337] Zimmermann A.A. and Becker S.W.J., Precursors of epidermal melanocytes in the Negro fetus., in *Pigment cell biology*, edited by M. Gordon (Academic Press, New York, 1959), pp. 159-170.

Acknowledgments

Steven, my dear friend, we got to know each other through the lab, but actually this was soon forgotten to make place to a true friendship. We went through our thesis together, supporting each other through the ups and downs mentioned above, talking a lot in and outside the lab, did sports together, traveled together, well… the list could go on… You own a very special place in my heart, and hope to keep you as one of my best and closest friends. Steven, "vo Herze dangg scheen!"

My thanks as well to my "Basler" friends, Daniel 1, Daniel 2, Steven, Karin, Cédric, Céline, Morena, Michele and all the ones participating to the crazy "Cargo Bar Mondays". These were great times that allowed to "breathe" a little from the lab. Thanks folks!

I would like to thank my friends back in the Romandie as well. Thank you folks for your support and understanding, and for your true friendship. David, Didier, Sophie et Hervé, merci pour votre amitié!

My very, very, very special thanks go to my family, who not only supported me morally throughout the whole course of my educational career, but also let me feel their love and care. Without you, all this would not have been possible. Thank you soooooo much for your love, for your right words during periods of doubt, for boosting me at some times, for the confidence you placed in me, for your generosity, for all these smiles and gales of laughter at home, and for being as you are… I enjoy every single moment in your company. Maman, Christophe, mon p'tit frère Jonathan, merci pour tout et merci d'être vous!
One thought for you, Dad, who from "up there" probably address me a proud smile… Wish you were here…

Last but not least, I address all my gratitude to Stéphanie, who closely accompanied me during my thesis. You shared my ups and downs, motivated me when needed, and enlightened my life throughout my thesis. Thank you so much for your understanding, as I know it was not easy. Merci…

Curriculum vitae

Jean-Philippe Bapst

Pharmacist

St. Gallerring 50
4055 Basel

jp.bapst@bluewin.ch
P 061 301 52 49
W 061 265 26 08

Born on July 7th 1978
Swiss Nationality

Education and experience

07.2004-07.2008   University Hospital Basel, Basel, Switzerland

PhD studies at the Department of Biomedicine of the University Hospital Basel, Basel, Switzerland, in the lab of Prof. Alex N. Eberle.

"Novel DOTA-α-melanocyte-stimulating hormone analogs for melanoma targeting: the impact of dimerization, carbohydration and negative charges on the in vivo biodistribution."

01.2004-06.2004   Pharmacies Sun Store SA

6 months of full time work experience in various drug stores for the Sun Store Pharmacy Group, managing up to 20 employees.

2000-2003   University of Basel, Basel, Switzerland

Pharmacy studies, 6 semesters, federal pharmacist diploma (M.Sc.).

Diploma thesis in pharmaceutical chemistry (carbohydrate chemistry), Institute for Molecular Pharmacy, University of Basel, in the lab of Prof. Beat Ernst.

"Development of a novel sialyl donor for the synthesis of biologically important sialosides".

1998-2000   University of Fribourg, Fribourg, Switzerland

Pharmacy studies, 4 semesters, propedeutical exams.

1997-1998   University of Lausanne, Lausanne, Switzerland

Geography and informatics, 1 semester.

1994-1997   Collège du Sud, Bulle, Switzerland

High school in D-type (modern languages with Italian), baccalaureate.

Scientific experience

- Synthesis and purification of peptides and glycopeptides.

- HPLC / Mass spectrometry experience for peptide purification and analysis.

- Cell cultures.

- Competitive cell binding assays with ^{125}I, biological activity assays, internalization assays with [111]In.

Biodistribution experiments on mice with [111]In.

- Animal Welfare Course LTK-1 for animal experimentation, with experience.

- Radioactivity safety course for scientists.

- Molecular modeling practical course (poster during studies), University of Basel.

- Optional pharmaceutical technology course during studies (development of a slow-release topical doxycyclin gel), University of Basel.

- "Venture Challenge" course for young entrepreneurship and an introduction to business, by Venturelab (http://www.venturelab.ch), 1 semester at the University of Basel.

Work experience

Various summer jobs (1990-1998) in banking (UBS AG), supermarkets (Coop) and delivery services.

Practical year of the pharmacy studies for drug store "Hardhof-Apotheke" in Basel.

2 years of work experience as an assistant pharmacist on Saturdays and during university breaks for various drug stores (substitution of the pharmacist).

6 months of full time work experience as a pharmacist for various drug stores of the Sun Store Pharmacy Group (2004), managing up to 20 employees.
Since July 2004 still working 2 Saturdays monthly for the Sun Store Pharmacy Group.

Other abilities

Very good computer skills (operating systems, MS Office, ChemDraw, PubMed, Prism, Adobe Photoshop, …) on both Windows and Macintosh operating systems.

Hobbies

Photography, scuba diving, travelling, mountain trekking, snowboarding, badminton, reading, languages.

Languages

French	Mother tongue
English	Written: fluently Spoken: fluently
German	Written: good knowledge Spoken: fluently
Italian	Written: good knowledge Spoken: well
Swiss German	Spoken: fluently

- Language stay in Fenton, Michigan, USA (1995), 3 months. High school lectures.
- Language school in Freiburg im Breisgau, Germany (1998), 3 months.

Academics

Publications

"*Dimeric DOTA-α-melanocyte-stimulating hormone analogs: synthesis and in vivo characteristics of radiopeptides with high in vitro activity.*"
Journal of Receptors and Signal Transduction **27** (2007), 383-409.

Oral presentations

Oncomeeting, internal oncology meeting of the University Hospital Basel, February 2007.

Fall Meeting of the Swiss Chemical Society, Lausanne, Switzerland, September 2007.

IDTM 2007, Intracellular Delivery of Therapeutic Molecules, Grenoble, France, September 2007.

Poster presentations

Melanoma X and The Third Annual International Melanoma Research Congress, Noordwijk, The Netherlands, September 2006.

Bio Valley Life Sciences Week 2006, Basel, Switzerland, October 2006.

Bio Valley Life Sciences Week 2007, Basel, Switzerland, October 2007.

Memberships

Swiss Pharmacists Society.
Swiss Chemical Society (Division of Medicinal Chemistry).
Swiss Young Pharmacists Group, PharmaSuisse.

References

Prof. Dr. Alex N. Eberle, University Hospital Basel, Department of Biomedicine, Endocrinology, Hebelstrasse 20, 4031 Basel (Switzerland).

Mrs Laurence Sottas, pharmacist, Pharmacie du Serpent, Grand-Rue 3, 1630 Bulle (Switzerland).

Mr. Francis Rossier, Vice-Director Pharmacies Sun Store SA, Rue des Jordils 38, 1025 St-Sulpice (Switzerland).